THE
PHYSICAL REVIEW
A journal of experimental and theoretical physics established by E. L. Nichols in 1893

SECOND SERIES, VOL. 69, NOS. 9 AND 10 MAY 1 AND 15, 1946

Cloud-Chamber Photographs of Heavy Particles at High Altitudes

DONALD J. HUGHES
Ryerson Physical Laboratory, University of Chicago, Chicago, Illinois
(Received January 12, 1946)

A series of 5000 cloud-chamber photographs was obtained at an altitude of 15,500 ft., by use of a chamber in a field of 1165 gauss supplied by a permanent magnet. The determination of mass from cloud-chamber photographs of heavily ionizing particles and knock-on electrons is discussed in general and the methods are applied to specific tracks of the present series. It is shown that the errors of mass determination from cloud-chamber data are large but that there is good evidence for a distribution of mesotron masses. The number of slow mesotrons at 15,500 ft. is about equal to the number of slow protons and amounts to 1 percent of the number of fast mesotrons at that altitude. The extremely rapid increase of slow mesotrons with altitude probably means that they are created as such at high altitudes. One photograph, which shows the pair production of low energy mesotrons, is an example of such a process.

I. INTRODUCTION

THE percentage of slow mesotrons in the cosmic radiation at sea level is so low that hundreds of thousands of cloud-chamber photographs must be taken in order to obtain tracks suitable for mass determination. The number of heavily ionizing, slow mesotrons increases rapidly with altitude, however, and the chances of observing them are correspondingly greater. In order to take advantage of this increase with altitude it was decided to take cloud-chamber photographs at as high an altitude as possible during the 1941 South American cosmic-ray expedition of the University of Chicago.

The work was done at the site of the San Cristobal mine of the Cerro de Pasco Corporation near Cerro de Pasco, Peru. A small building with running water and 110-volt a.c. power was available for cloud-chamber work at an altitude of 15,500 ft. The cloud chamber and associated apparatus was the same as that used earlier for underground experiments.[1] The chamber, 20 cm in diameter, was mounted in a permanent magnet which supplied a field of 1165 gauss in the chamber, sufficient to deflect heavily ionizing mesotrons. The entire apparatus was about 700 lb. in weight, completely automatic and easily portable. The chamber was counter-controlled by a variety of counter arrangements during the series; however most of the heavily ionizing tracks occurred independently of the counter control. The apparatus was run for a period of three weeks during July 1941 and about 5000 photographs were made.

Although this same chamber when used underground, or at the surface, did not show a single heavily ionizing particle, a fairly large number were observed at the high altitude. Some of the heavy tracks were discussed qualitatively at the cosmic-ray symposium in Rio de Janeiro of

[1] V. C. Wilson and D. J. Hughes, Phys. Rev. **63**, 161 (1943).

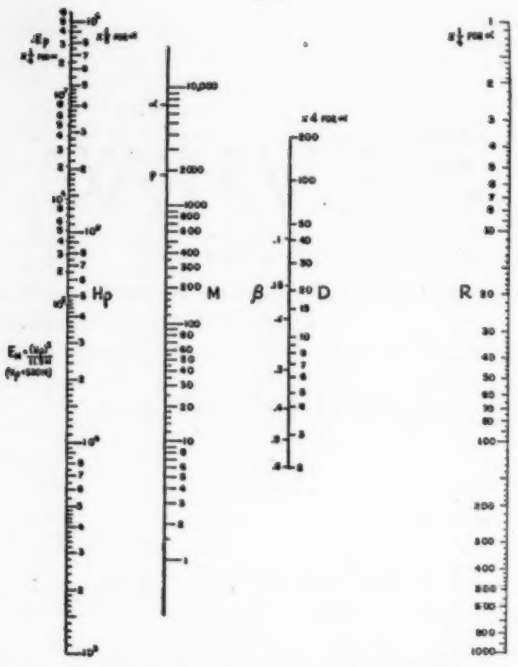

FIG. 1. Nomograph giving magnetic curvature ($H\rho$), velocity (β), density of ionization (D), and range (R) for particles of various masses (M). Any straight line crossing all the scales gives correct values for the above quantities to a few percent.

August 1941,[2] and a photograph of a pair of slow mesotrons has been published.[3] Unfortunately, war research has delayed the publication of a more complete report until the present time. It is felt, however, that even though the material is rather old by now, the part to be reported here is of sufficient interest to merit publication.

II. CLOUD-CHAMBER MASS DETERMINATIONS

Particle masses have usually been determined from cloud-chamber photographs by measuring the range or ionization density together with the magnetic curvature of the tracks. A second method which has not been used widely is to measure the energy of an electron ejected by the particle in an elastic collision (formation of a "knock-on" electron). These two methods will be described in general and illustrated by specific cases from the present work.

A. Mass Determination by Increased Ionization

If a particle has low enough energy so that its velocity is significantly less than that of light ($\beta<1$), then its ionization density increases and its mass may be determined from any two of the three quantities, curvature in a magnetic field, density of ionization, and range. Perhaps the simplest way to picture the dependence of mass on the three quantities is by a nomograph of the type published by Corson and Brode.[4] Such a nomograph is shown in Fig. 1. It is modeled after Corson and Brode's but has been extended to cover all masses from electrons to alphas and also to cover a greater range of $H\rho$ and range values. Any straight line crossing all the scales connects consistent values of $H\rho$ (magnetic field × radius of curvature), density of ionization D (where minimum value for a fast particle = 1), velocity β, and range R (cm of air), for a given mass M (mass of electron = 1). A scale E gives the kinetic energies of protons in electron volts, and if multiplied by $\frac{1}{4}$, the energies for alphas. Energies for other M's can be obtained from the formula shown at the left. The $H\rho$, D, and R scale readings must be multiplied by the factors shown for alphas.

Of course a chart covering such a wide range of variables cannot be precise at all points. It has been designed, however, in such a way that the errors are not excessive for any particular combination of variables. Thus, for protons the range as a function of energy is 9 percent low at 2 cm (by comparison with the curves of Livingston and Bethe[5]), becomes exact at intermediate ranges, and is 9 percent high at 260 cm (the greatest range shown in Livingston and Bethe's curves). For alphas (again by comparison with Livingston and Bethe) the variation is from 12 percent low at about 2 cm to about 4 percent high at 20 cm. For a mesotron of mass 200 the ranges (as a function of $H\rho$) when compared to those given by Rossi and Greisen[6] are high by 10 percent for the shortest ranges, by 5 percent at about 30 cm, and agree at 800 cm. Electron ranges as a function of $H\rho$ from the chart lie within the spread of the experimental determinations of electron ranges from 1 to 100 cm (even though the rule that the straight line on the chart must cross *all* the scales

[2] D. J. Hughes, Acad. Bras. de Ciencias **67** (1941).
[3] D. J. Hughes, Phys. Rev. **60**, 414 (1941).
[4] D. R. Corson and R. B. Brode, Phys. Rev. **53**, 776 (1938).
[5] M. S. Livingston and H. A. Bethe, Rev. Mod. Phys. **9**, 245 (1937).
[6] G. Rossi and K. Greisen, Rev. Mod. Phys. **13**, 240 (1941).

is violated in this case). Although the above errors of the chart are not small, they are smaller in general than the inherent uncertainty of the mass determinations which are discussed below. Figure 1 then turns out to be sufficiently accurate for calculations involving mass determinations from typical cloud-chamber photographs for masses from electrons to alphas, and its use is justified by simplicity.

Range can perhaps be measured most accurately of the above quantities if the particle stops in the gas of the chamber. The density of ionization depends on several variable conditions of the chamber and can only be estimated unless delayed droplet counting is done, and the $H\rho$ value is affected by chamber distortion at high energies and by scattering at low energies. For any measured $H\rho$ value there is always a variation in true radius of curvature due to the spurious radius, ρ_s, caused by scattering which must be added to the uncertainty of measurement of the $H\rho$ value. Williams[7] has given a formula for the average ρ_s which can be reduced to a simple form applicable to the present chamber, and accurate to a few percent for the region covered by Fig. 1. For $H=1165$ gauss, argon gas at a pressure of 80 cm, and a track length of 16 cm we have

$$\rho_s/\rho=15.0\beta, \qquad (1)$$

which shows that for fast particles ρ_s causes a 7 percent error in ρ, and that for $\beta=0.067$ the spurious curvature is equal to the magnetic curvature itself. Thus even though particles of low momentum can have their curvature measured more easily, the error due to scattering will be greater and the accuracy of mass determination actually less for the slower particles.

For a given chamber gas, magnetic field, and particle mass there is a certain curvature value for which the accuracy of mass determination is a maximum. Figure 2 shows the variation in accuracy of mass determination as a function of ρ for the present chamber as a typical example. It is assumed that the error in measuring radius of curvature (due to convection currents, etc.) is equal to a displacement of the center of the track of 0.05 cm, this value being based on tracks measured with no magnetic field in the present chamber. The curves marked "fixed D" show the probable error of the mass values (for an actual mass of 200) which would result when the mass is determined from D (assuming no error in D) and $H\rho$. The curves marked "fixed R" are the probable error when mass is determined from measured R (assuming no error) and $H\rho$. The results were calculated from Fig. 1 and Eq. (1).

It is seen that the accuracy of mass determination is greatest for a radius of curvature of about 125 cm (range of 500 cm) and that it is greater for a determination based on a measured D than on a measured R (assuming no error in measurement of D and R). Even at best, however, the mass would be $200(+50, -32)$. With twice the magnetic field the most accurate point will occur at the same $H\rho$ value (and same range) but the corresponding radius of curvature will be half and the accuracy of mass determination will be doubled. Space does not permit a discussion of the effect of other changes on the accuracy such as the effect of change of chamber gas, change of pressure, use of absorbers in determining R, etc., but they can easily be calculated in a manner similar to that used in calculating Fig. 2. In this connection it is useful to remember that ρ_s/ρ changes very nearly as $l^{\frac{1}{2}}$ (where l is track length), as z^{-1} (z, atomic number of chamber gas), as $p^{-\frac{1}{2}}$ (p, chamber pressure), and as H.

It is obvious that the inherent errors in mass determination with the cloud chamber are large enough so that the errors in the chart of Fig. 1 are much less and its use is justified in such measurements. In the photographs taken in the present

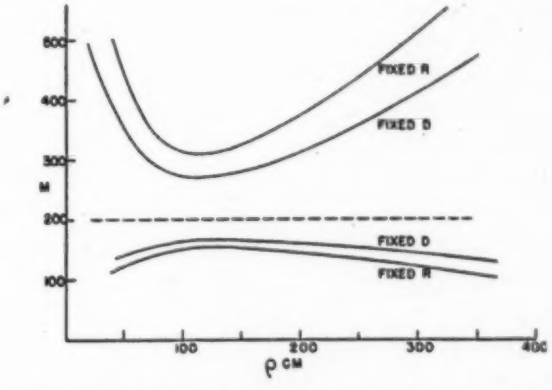

FIG. 2. Variation in measured mesotron mass (M) as a function of radius of curvature for a true mass of 200. Curves labeled "fixed D" refer to measurements based on density of ionization; "fixed R" to those based on range.

[7] E. J. Williams, Phys. Rev. **58**, 292 (1940).

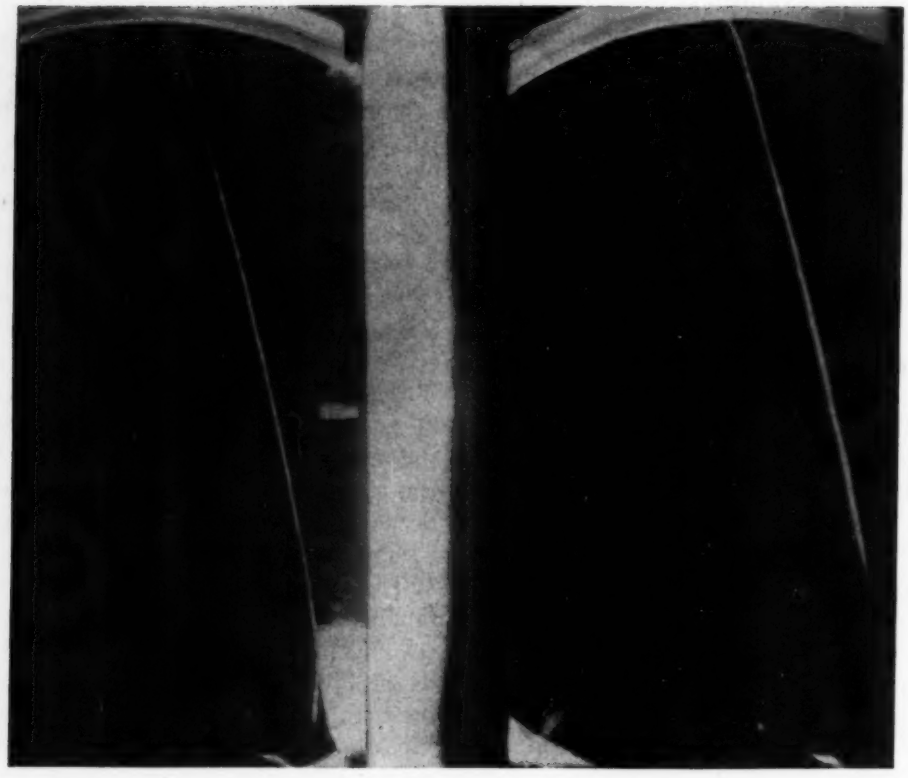

FIG. 3. Stereoscopic views of a positively charged particle whose curvature, density, and range identify it as a proton, of energy about 3 Mev.

series about 50 tracks were observed which ionized heavier than electronic tracks yet showed some curvature in the magnetic field. Some 20 of them were of a quality to justify mass determinations, and several of these tracks will be described here.

Figure 3 is a stereoscopic view of a heavily ionizing particle of positive sign. It is almost exactly in the center of the illuminated portion of the chamber throughout its length and appears to end in the chamber. However, the end of the track is not visible in the right view (obscured by a light baffle) so it is not completely certain that the track does not scatter sharply out of the illumination and pass out of the chamber. The $H\rho$ value measured at the central region (residual range 12 cm) is 1.7×10^5 gauss cm (there is some distortion at the upper rim of the chamber and several scatterings along the track). The ionization is so heavy that discrete blobs of ionization cannot be seen; however, by comparison with slow electrons and fast alphas it is possible to estimate that the density is at least 30 and probably 50–100. Figure 1 shows that the above values of $H\rho$, D, and R are consistent and indicate a mass roughly 1300. Therefore, the particle is probably a proton, and the probable variation in $H\rho$ from Eq. (1) is from 9×10^4 to 10^6. If the values $R=12$, $D=50$–100, and $H\rho=9\times10^4$–10^6 are marked on Fig. 1, it is seen that the particle can certainly be identified as a proton but that its actual mass cannot be precisely determined. Inclusion of the uncertainty in $H\rho$ due to ρ_t increases the uncertainty of the mass determination by a large amount.

The lower track in Fig. 4 is positive (assuming it is moving downward) with an $H\rho$ of 1.05×10^5. It does not ionize as heavily as the proton of Fig. 3 (the discrete blobs are just visible); its density, by comparison with slow electrons, is approximately 10. It does not stop in the chamber so it can be said only that its range is certainly greater than 14 cm air. Figure 1 shows the consistency of the above values with a mass about

250. A mass of 250 then gives a range in $H\rho$ due to ρ_s of 0.82 to 1.46×10^5. This range in $H\rho$ is about the minimum to be expected for the track has a radius of curvature of 90 cm (see Fig. 2) but the corresponding uncertainty in M is from 200 to 350 even if we assume no error in $D=10$. If the D value is between limits of 6 and 15, then the M value will vary even more, from 140 to 440. This track is certainly a mesotron, and of mass about 250, but with a large experimental uncertainty.

As mentioned in the introduction, one photograph of this series has already been published[3] which is quite certainly that of a mesotron pair produced in the material of the cloud chamber. The measurements have now been rechecked with the result that the mass of the right-hand member of the pair has been lowered from 180 to 160 (as judged by $H\rho$ and D) with a range due to uncertainty in curvature and ionization of 120 to 230 for the mass value. The knock-on electron (see below) observed on this track gives a mass value of 190(+85, −50). Combination of the two estimates indicates a mass of 175(+55, −30) for the particle. The mass of the second member of the pair can best be estimated simply by comparison with the first, for its $H\rho$ and D are very nearly the same, thus it seems likely that its mass is also about 175.

Figure 5 shows a track that is heavily ionizing but of unusually great curvature. The heavy verticle white band resulted from a wire in the developing tank which prevented a strip from being completely cleared by the hypo—the complete track in the right-hand view is easily visible on the negative however. The track enters the illumination at the right and stops at the left end which is in the full illumination; it is therefore negative. The $H\rho$ at the center (where the residual range is 1.8 cm of air equivalent) is 4.1×10^3. The track is slightly blurred by age but its ionization density is estimated to be in the range 15 to 40. From Fig. 1 the range and curvature give a surprisingly small mass of 14, which, however, is consistent with the ionization density. If the effect of ρ_s is now calculated, it is found to be so large (because of small $H\rho$ and short track length)

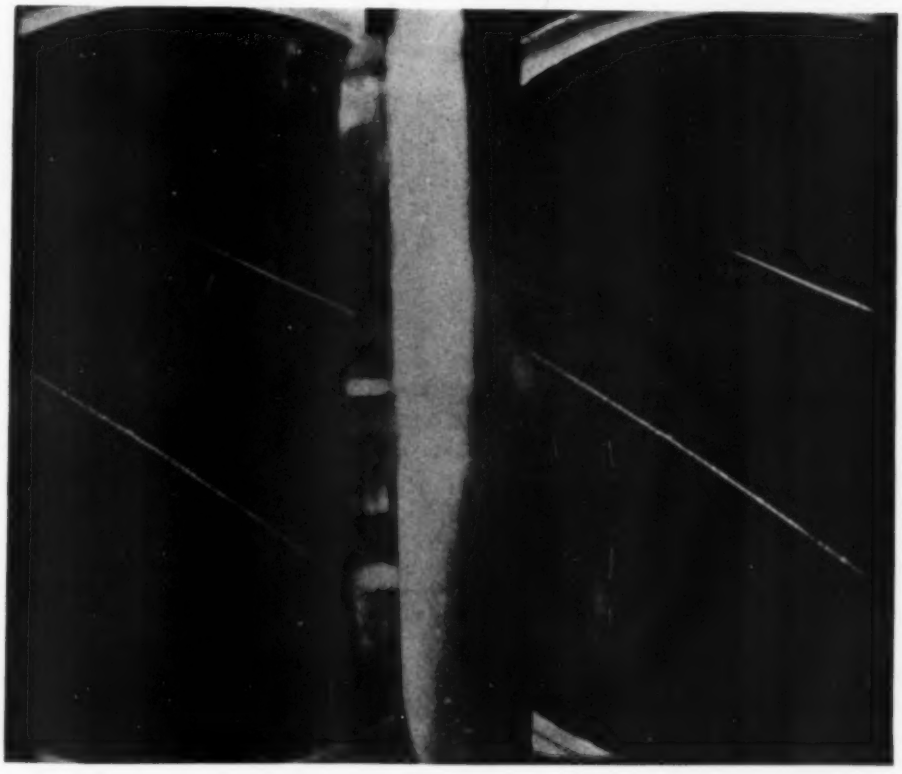

FIG. 4. A positive mesotron of mass approximately 250.

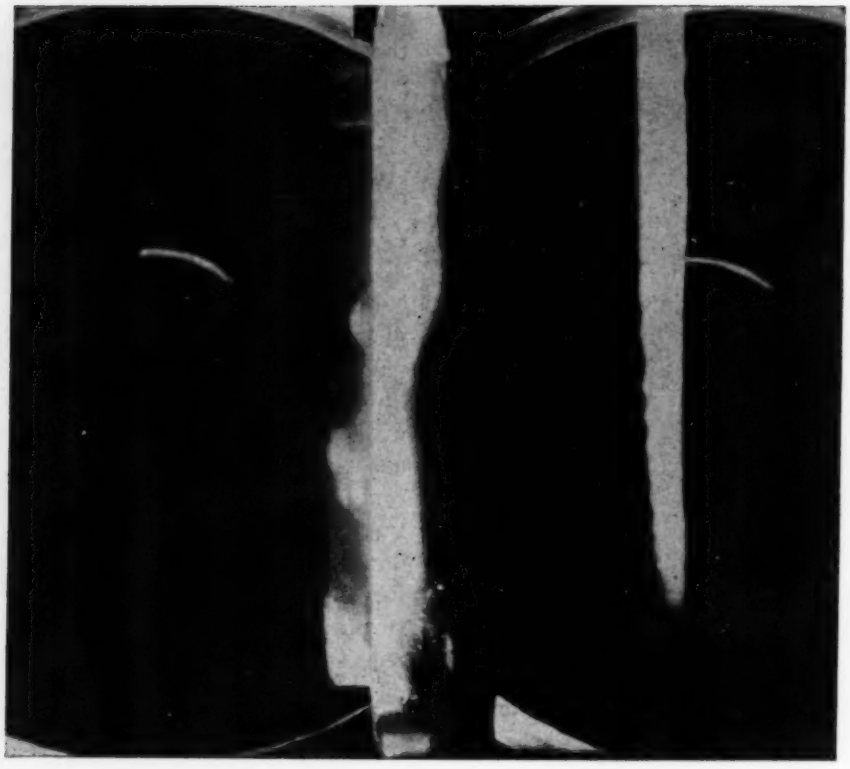

FIG. 5. A negative mesotron whose curvature, density, range, and scattering show that it has an unusually low mass of 30.

that it is necessary to take into account the variation of ρ_s with $H\rho$ and β. When this is done, it is found that all mass values between 6 and 50 could give the observed $H\rho$ and R. However, the ionization density indicates M is at least 10 and probably about 25. The scattering is much less than that of an electron which has a very erratic path when its residual range is 2 cm. As ρ_s for a particle of given range increases with $M^{\frac{1}{2}}$, the latter quantity must be large compared to unity in this case, say at least 5, which would mean an M of at least 25. If all the above values are marked on Fig. 1, it seems that the mass is probably about 30 but definitely in the range 10 to 50.

The heavily ionizing track in the lower left-

TABLE I. Mass determinations from $H\rho$, R, and D.

Number	Sign	$H\rho$	D	R(cm air)	M	Remarks
1 (Fig. 5)	−	4.1×10^3	15–40	1.8	30(+20, −20)	
2	+	3.7×10^4	15–30	13	140(+220, −60)	
3	−	1.03×10^5	4–6	10	175(+55, −30)*	Mesotron pair[a]
4	+	1×10^5	4–6	10	175(+140, −60)	
5 (Fig. 4)	+	1.05×10^5	6–15	20	250(+190, −110)	
6	−	6.4×10^4	20–40	14	250(+380, −100)	
7	+	2.8×10^5	2–4	30	270(+330, −110)	
8	?	$>3\times10^5$	15–30	14	>900	
9	+	2.3×10^5	>20	30	>1100	
10 (Fig. 3)	+	1.7×10^5	50–100	12	1300(+2000, −400)	
11	?	$>2\times10^5$	>40	8	>1200	
12 (Fig. 6)	?	$>10^6$	20–50	14	~10×proton	$Z\sim5$
13	?	$>10^6$	20–50	10	~10×proton	

* Knock-out determination (No. 2 of Table II) included in M value.
[a] See reference 3.

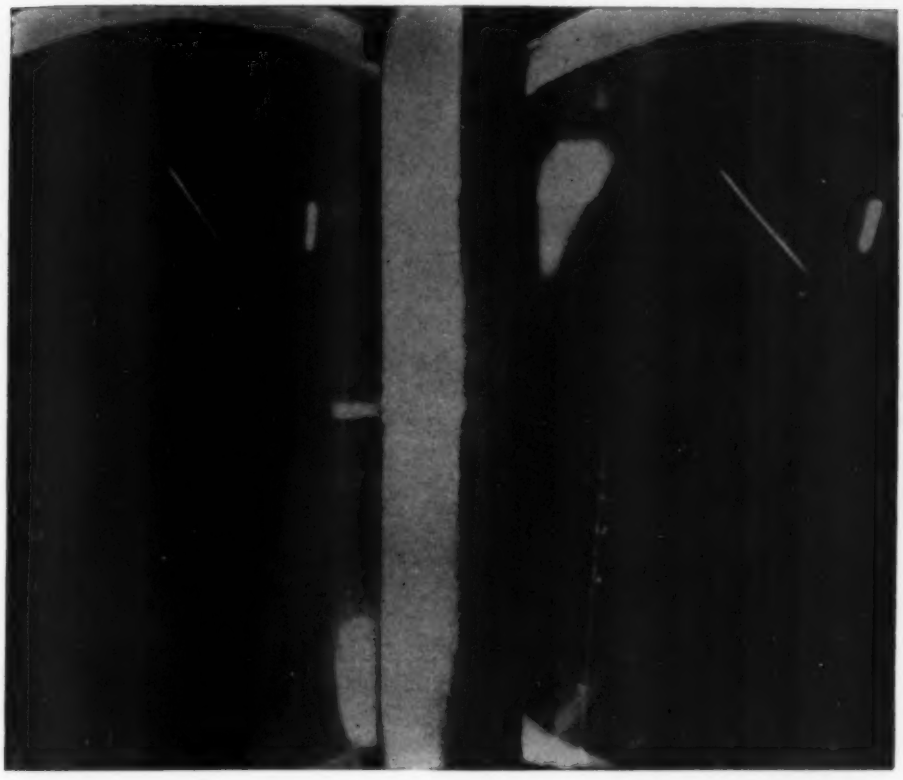

FIG. 6. The track in the lower left corner creates an extremely large number of knock-on electrons. It is identified as a high energy particle of charge about 5.

hand corner of Fig. 6 is unusual in that five knock-on electrons are visible along the illuminated track length of 11 cm air equivalent. The track is sloping so that the upper end is back of the illuminated space and is not visible. The $H\rho$ value is too great to be measured. It has already been found with the present chamber[1] that the number of knock-on electrons per cm track length for fast particles ($\beta=1$) was 6.8×10^{-3}, a value which checked the theoretical estimate. The present track, however, has 0.45 per cm, or 67 times the above value. It is true that the probability of ejection of knock-on electrons increases with decreasing β (as $1/\beta^2$), however, the maximum transferable energy decreases [as $\beta^2/(1-\beta^2)$] and becomes so low for heavily ionizing tracks that knock-ons are not seen as discrete tracks along slow ($\beta<0.1$) mesotron, proton, or alpha tracks. The present track then cannot be a mesotron, proton, or alpha because its large D is inconsistent with the high knock-on energy.

It is possible to reconcile the frequency of knock-ons and large ionization density of the track (which require a low β) with the relatively high knock-on energy (which requires a high β) by assuming that the charge on the particle is high. If β is taken as 0.7 and the particle's charge as 5, then D, which would be 1.5 for $Z=1$ be-

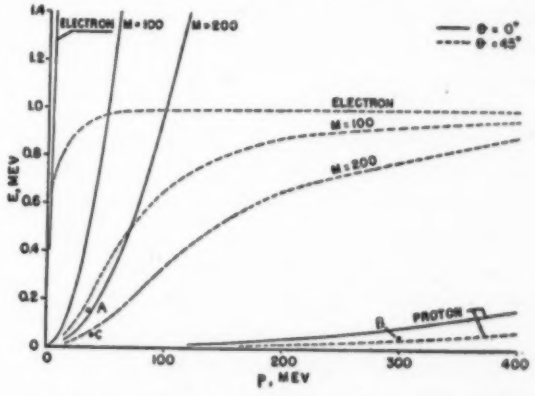

FIG. 7. The energy of knock-on electrons (E) as a function of primary momentum for different primary masses and angles of ejection of knock-ons.

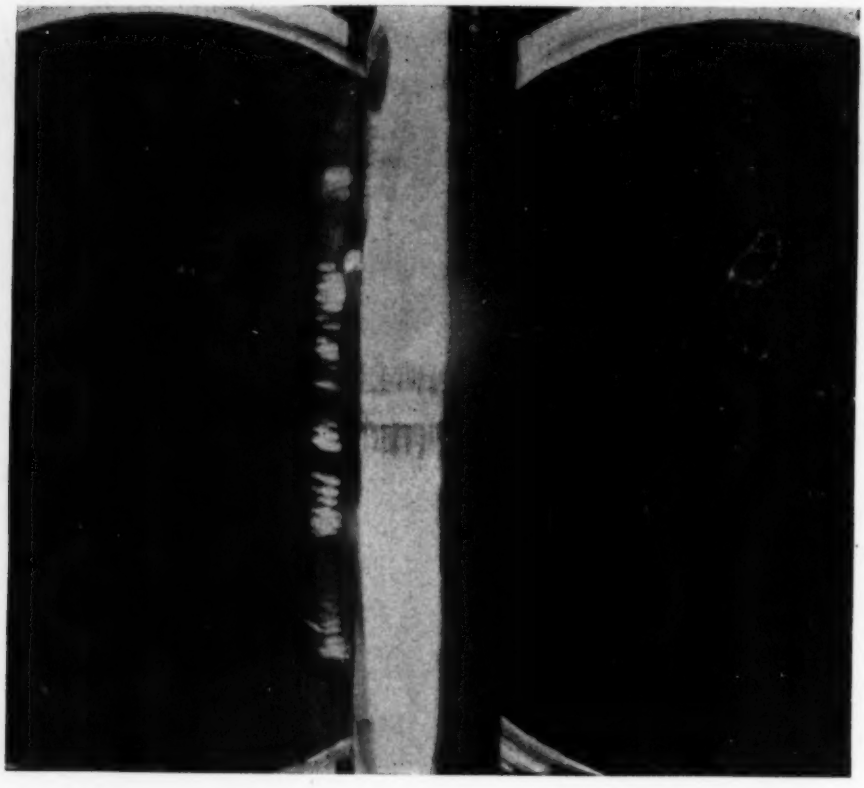

FIG. 8. A mesotron whose mass is estimated as 180 from primary momentum, energy of knock-on electron and angle of ejection of knock-on. The mesotron is not visible beyond the point (center of the chamber) where the knock-on is created.

comes $1.5\times5^2=37$, while the high β value means that the maximum energy transferable to a knock-on is 960 kev and the average observable knock-on energy about 25 kev. The above values for D and knock-on energy agree well with the observed track (average knock-on energy = 15–20 kev, $D=30$–50). The probability of ejection of knock-ons will be $Z^2/\beta^2=50$ times that of fast particles in comparison with the observed 67. The above arguments are independent of the mass of the unknown particle which would presumably be large because of the high Z. Its energy would be about 2×10^8A where A is its atomic weight; thus, if it were a boron 10 nucleus, for instance, it would have an energy of 2000 Mev at which energy it would most certainly have a charge of 5. One other track very similar to that of Fig. 6 was observed during the run and is probably to be interpreted in a similar manner.

Other mass determinations based on $H\rho$, D, and R will not be described in detail but are summarized along with those above in Table I, which will be discussed following the description of the knock-on measurements below.

B. Mass Determination by Knock-On Energy

Although the frequency of occurrence of knock-ons and their energy distribution are independent of the mass of the primary particle (provided the energies are less than the maximum transferable energy), the mass can be obtained for a particular collision if the angle of ejection and energy of the electron as well as primary momentum can be measured. In contrast to the ionization method, the knock-on method can be used where the primary momentum is so high that no increased ionization is exhibited. However, in order to attain accuracy in mass determination the collision must be almost head-on and the primary momentum somewhat low. The formula involved is

$$E=2mc^2\frac{p^2\cos^2\theta}{\{[p^2+(Mmc^2)^2]^{\frac{1}{2}}+mc^2\}^2-p^2\cos^2\theta}, \quad (2)$$

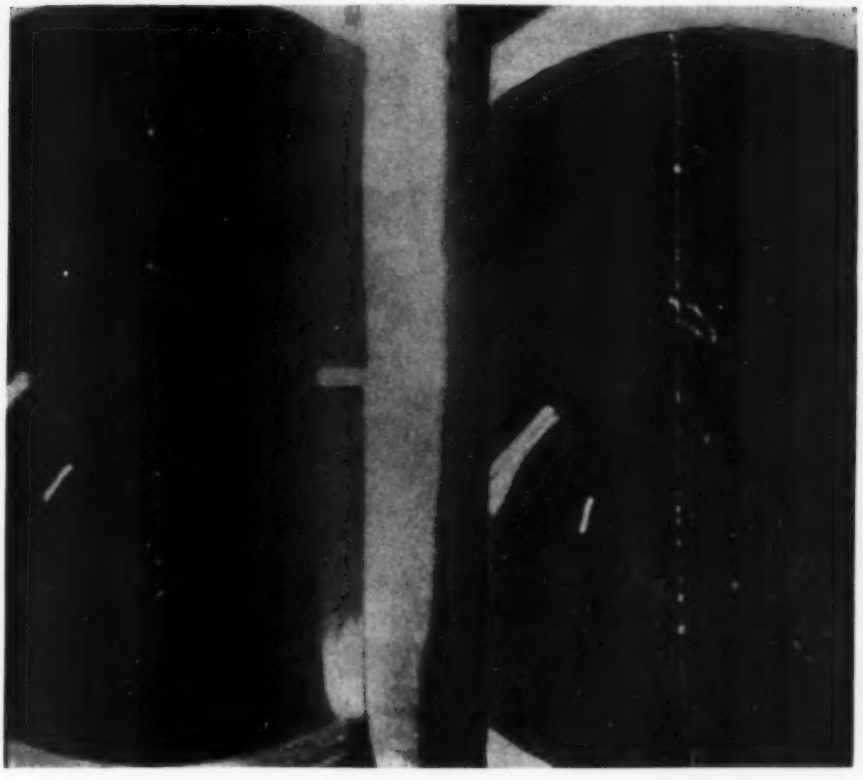

FIG. 9. A low energy knock-on caused by a proton primary.

where E is the knock-on energy, mc^2 the electron rest energy, θ the angle of emission, and p/c the momentum ($p=300H\rho$) of the primary of mass Mm. Figure 7 shows the variation of E with p for different M's and θ's. For $\theta=0$ (head-on collision) mass discrimination is quite good for all values of p; however, such collisions are very rare. For $\theta=45°$ the best p values are about 10^8 ($H\rho=3\times10^5$); at higher momenta electrons cannot be distinguished from mesotrons. For angles greater than 60° the knock-on energies become small as does the accuracy of mass determination.

In Fig. 8 is shown a knock-on from which a mass estimate may be made. The primary passes out of the illumination at about the point where the knock-on is ejected; its $H\rho$ is 1.3×10^5. The angle θ is 18°; hence the collision is nearly head-on ($\cos^2\theta=0.9$). The energy of the knock-on can be obtained by measuring its range in the chamber (30 cm air equivalent) or its $H\rho$ value (1.4×10^3). The range and $H\rho$ values are consistent (Fig. 1) and the energy of the electron is 150 kev. Point A on Fig. 7 corresponds to this knock-on electron, and it is clear that the primary must be a mesotron; Eq. (2) actually gives $M=180$. The principal uncertainty is in the measurement of $H\rho$, which was unfortunately difficult in this case. It leads to an uncertainty in mass of about $(+90, -50)$. A better curvature measurement for this knock-on could give a much better mass determination for the exact θ is not critical and the energy of the electron can be measured accurately.

The knock-on of Fig. 9 is of low energy (50 kev by range) but the primary is of high momentum; because of distortion at the ends only a lower limit of 1.0×10^6 for $H\rho$ can be given. The angle θ is about 50°. The above values are shown in Fig. 7 as B which falls close to the 45° curve for protonic mass, and Eq. (2) gives a lower limit of 1300 for M. The uncertainty in $H\rho$ measurement for this high momentum particle makes exact mass measurement impossible, but the identification as a proton is quite certain. Figure 1 shows that the particle has a velocity low enough so

TABLE II. Mass determinations from knock-on electrons.

Number	Sign	$H\rho$	Electron energy (kev)	θ	M	Remarks
1	−	1.3×10^5	150	18°	180(+90, −50)	
2	−	1.03×10^5	34	50°	190(+85, −50)	Same track as No. 3 of Table I
3	−	3×10^5	130	53°	280(+250, −80)	
4	−	3.6×10^5	300	30°	340(+300, −100)	
5	?	$>1\times10^6$	50	50°	>1300	
6	+	$\sim9\times10^5$	48	45°	~1800	
7	?	$>1\times10^6$	33	40°	>1500	

that the ionization is somewhat greater than unity, about 2–4.

A knock-on due to a mesotron primary obtained in the present series has already been described[8] in connection with a mesotron pair. The electron energy is 34 kev, its angle 50° and the primary $H\rho$ is 1.03×10^5. These values are plotted as C in Fig. 7 and a mesotronic mass of about 200 is indicated. Actual calculation from Eq. (2) if we allow for uncertainty in $H\rho$ due to scattering gives $M=190(+85, -50)$. As discussed in Section II A, the knock-on mass determination for this particle agrees well with that based on the ionization density. Both methods have their main source of inaccuracy in the uncertainty of $H\rho$ which is due, at $H\rho=10^5$, about equally to ρ_s and to experimental error in the actual curvature measurement due to distortion.

The mass determinations from knock-ons discussed above, together with several others from the present series, are summarized in Table II. In general it can be said that the knock-on determinations have no great inherent inaccuracy, but require a higher magnetic field for more precise $H\rho$ measurements in order to utilize the higher momentum tracks which are otherwise suitable for the knock-on method.

III. DISCUSSION OF RESULTS

The 19 tracks of Tables I and II can be divided without much doubt into 10 mesotrons (4+, 6−), 7 protons, and 2 heavier particles. The approximate equality of the number of slow mesotrons and protons means that the area of the mesotron momentum spectrum below 10^8 ev is about equal to that of the proton momentum spectrum below 10^9 ev. The values of the mesotron masses vary from 30 to 340 (plus experimental error). Even though it is true that each mass determination is subject to a large uncertainty it seems difficult to reconcile all the measured mass values with a unique mesotron mass. It is true that most of the values are in the 200 region but track 1 of Table I is very good evidence for the existence of "light mesotrons" of mass much less than the customary 200. Wheeler and Ladenburg[8] in a 1941 review concluded that the experimental evidence at that time was insufficient to "allow a decision of the very important question whether the mass of the meson is unique" but the present results seem to indicate a distribution of mesotron masses.

Most of the tracks of Table I are not those which tripped the counter control of the chamber but simply occurred in the chamber by chance when it expanded. Hence the rate of occurrence, 13 measurable cases in 5000 pictures, refers mainly to the chance rate of occurrence of such tracks in the cloud chamber. If we wish to compare the relative numbers of slow and fast mesotrons, for instance, we must compare the observed heavy tracks with the chance rate for fast mesotrons rather than with the number of fast particles in the chamber, for the latter are counter-controlled. The total "sensitive time" of the cloud chamber for the whole series of pictures can be estimated to be about 450 sec., that is, in addition to the counter control tracks which were observed, all those particles which pass through the chamber in 450 sec. were also observed. The number of fast mesotrons which traverse the chamber can be calculated from the number observed in the experiments of Schein, Jesse, and Wollan[9] at an equal altitude, taking into account

[8] J. A. Wheeler and R. Ladenburg, Phys. Rev. 60, 754 (1941).

[9] M. Schein, W. P. Jesse, and E. O. Wollan, Phys. Rev. 59, 615 (1941).

the geometrical difference between their counter set and the cloud chamber. The result, for mesotrons of range greater than 8-cm lead (i.e., for those above the energy of minimum ionization loss) is that 900 fast mesotrons pass through the chamber in 450 sec. Approximately the same result is obtained from the known rate of occurrence of chance mesotrons in the chamber at sea level (from earlier experiments) and the increase of mesotrons with altitude.[9]

As there were 9 slow mesotrons observed which were not counter-controlled, the ratio of slow (heavily ionizing) mesotrons to fast is 0.01. It is obvious that this ratio is far greater than that at sea-level where, for example, Johnson and Shutt[10] obtained one heavily ionizing particle among 42,000 fast tracks of 50-cm length. Herzog[11] also finds a striking increase of heavily ionizing particles with altitude. He reports that tracks identifiable as slow mesotrons begin to occur at 15,000 ft. and above 25,000 ft. constitute 10 percent of the fast tracks. If it is assumed that the slow mesotrons result only from the slowing down of the fast, then the change of the fast spectrum with altitude could not account for the observed great increase of slow mesotrons with altitude. It seems likely, therefore, that the slow mesotrons observed at high altitudes are created as such and that the process, practically nonexistent at sea level, becomes more and more evident with increasing altitude. The slow mesotron pair[3] photographed during the present experiment is an example of such a process. It is noteworthy, however, that Schein, Jesse, and Wollan[9] found no evidence for slow mesotrons in their flights with thin (4–6 cm) lead absorbers.

It is a pleasure for the writer to acknowledge the inspiring leadership of Dean A. H. Compton during the progress of the above work. The Cerro de Pasco Corporation is to be thanked for the use of many facilities during our stay at San Cristobal and the Academy of Science of Brazil for the cordiality extended to us at the cosmic-ray symposium in Rio De Janeiro, August 3–9, 1941. Mr. Paul Ledig of the Huancayo Observatory and Professor Julio Hubner of San Marcos University were of great assistance during the mountain observations, as were Dr. L. Seren and Mr. E. Strugala of the University of Chicago in the interpretation of the data.

[10] T. H. Johnson and R. P. Shutt, Phys. Rev. **61**, 381 (1942).
[11] G. Herzog, Phys. Rev. **59**, 117 (1941).

Analysis of Cosmic-Ray Fine Structure

Part II. Mexico City Observations

DANA T. WARREN
Municipal University of Omaha, Omaha, Nebraska

(Received February 18, 1946)

The method previously developed has been applied to the preliminary data of Schremp and Baños on the fine structure observed in Mexico City. The nature of the anomalies is quite different from that in Missouri. The irregularity near the zenith has already been discussed, and it is shown that the 36° one cannot be interpreted as due to absorption. The irregularities in the slopes of the curves are extremely puzzling.

IN the first part of this analysis,[1] it was pointed out that the use of a double logarithmic plot has important advantages in picturing the fine structure variations of cosmic-ray intensity as a function of zenith angle. It was there applied as the basis for a least-squares examination of the observations made in Missouri by Cooper[2] and Ribner.[3] The present paper goes on to apply the same method in the analysis of the measurements made in Mexico City by Schremp and Baños.[4] These observations have already been considered[5] from the point of view of their relation to the atom-annihilation theory.[6] Therefore the present discussion will deal mainly with the graphical and analytical presentation of their values. Unfortunately, this cannot be done very completely, since only the preliminary results have been published in the two letters, without any details of apparatus, method of calculation, or probable errors of the individual points.

Figure 1 presents the double logarithmic plot of the Mexico City measurements,[4] as called for in Part I. It presents certain notable features, some of which are also evident in the original j-*vs.*-ζ curves. The most important from the point of view of curve-fitting is the break that occurs in each azimuth at 30° to 36°. Even North is fitted better with two lines. This makes necessary a separate fitting of the lines for low ζ (below 36°) and for high ζ. The constants used for these curves are presented in Table I.[7] The first set of curves given is that selected for Fig. 1 because of least values of Ω.[7] Certain alternatives are also

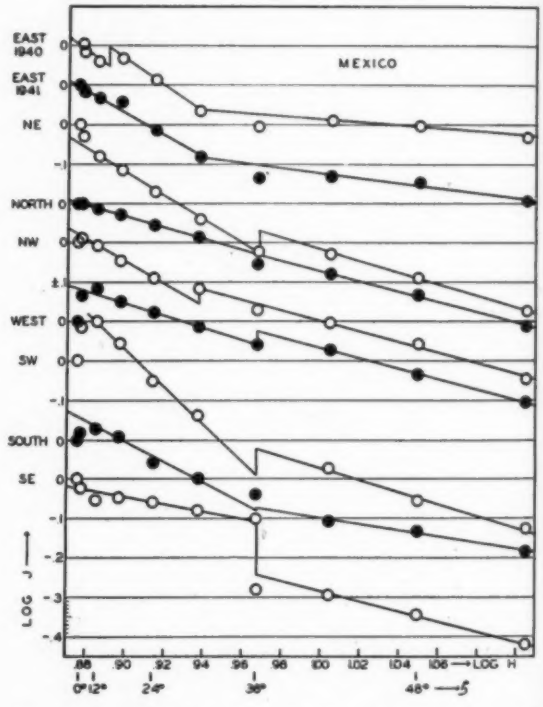

FIG. 1. Logarithmic plot of the cosmic-ray intensities measured at Mexico City by Schremp and Baños. The abscissa is the common logarithm of the atmospheric path length, measured in meters of water. The ordinate is the common logarithm of the relative intensity, normalized to unity at the zenith, scaled from their curves. Note that the eastward curves fall below, the westward curves above the zenith point, for which $\zeta = 0°$.

[1] D. T. Warren, Phys. Rev. **69**, 78, (1946.)
[2] D. M. Cooper, Phys. Rev. **55**, 1272 L (1939); **58**, 288 (1940).
[3] H. S. Ribner, Phys. Rev. **55**, 1271 L (1939); **56**, 1069 (1939).
[4] E. J. Schremp and A. Baños, Phys. Rev. **58**, 662 L (1940); **59**, 614 L (1941).
[5] D. T. Warren, Phys. Rev. **66**, 252 (1944).
[6] R. A. Millikan, H. V. Neber, and W. H. Pickering, Phys. Rev. **61**, 397 (1942); **63**, 234 (1943); **66**, 295 (1944).

[7] Definitions of symbols and formulas used in their computation are the same as those given in the appendix of Part I.

TABLE I. Summary of lines. The table gives the constants of the lines fitted by least squares, in Fig. 1, to the data of Schremp and Baños in Mexico City. For each azimuth α, the constants are given for the two curves fitted. The constant term a is the ordinate corresponding to zenith angle $\zeta = 48°$ (high ζ) or $\log h = 0.926$ (low ζ). b is the slope of the line drawn. Also indicated are the zenith angle values of the points fitted by each curve, and the most probable mean square residual, assuming this to be the true curve, i.e., Ω. The formulas used are given in the appendix to Part I. (See reference 1). The first set of constants for each azimuth is that drawn in Fig. 1. The brackets join different lines having the same slope.

	Lines for low ζ				Lines for high ζ			
α	a	$-b$	ζ's fitted	$\Omega\times10^6$	a	$-b$	ζ's fitted	$\Omega\times10^6$
NW	0.874	2.81	6°, 12, 18, 24	14.5	0.735	1.354	30°, 42, 48, 54	41.5
N	0.928	1.429	0°, 6, 12, 18, 24, 30	2.5	0.763	1.308	42°, 48, 54	15.1
NE	0.797	2.95	12°, 18, 24, 30, 36	13.7	0.611	1.416	42°, 48, 54	9.13
E	0.849	2.76	6°, 12, 24, 30	3.0	0.745	0.649	30°, 42, 48, 54	30.5
SE	0.928	0.879	6°, 18, 24, 30	11.0	0.651	1.254	42°, 48, 54	45.0
S	0.924	2.54	12°, 18, 24, 30	153.0	0.760	0.796	42°, 48, 54	21.0
SW	0.905	4.69	12°, 18, 24, 30	132.5	0.656	1.506	42°, 48, 54	110.0
W	1.003	1.531	18°, 24, 30, 36	1.5	0.868	1.315	42°, 48, 54	9.42
			Alternative choices					
NW					0.735	1.425	42°, 48, 54	61.0
NE					0.609	1.366	30°, 42, 48, 54	16.5
SW					0.659	1.722	30°, 42, 48, 54	235.0
All					0.610 to 0.867	1.208	42°, 48, 54	259.0
All exc. E and S					0.610 to 0.868	1.372	42°, 48, 54	44.8
N	0.930		All except 36°			1.358		7.86
E	0.853	2.84	0°, 6, 12, 18, 24, 30	132.5	0.745	0.641	42°, 48, 54	59.8
E	0.849	2.83	0°, 6, 12, 24, 30	26.3				
E	0.852 / 0.822	3.42	18°, 24, 30 / 0°, 6, 12	51.3				
S	0.935	1.89	6°, 12, 18, 24, 30, 36, 42	226.0				
W	1.004	1.531	6°, 12, 18, 24, 30, 36	99.8				
			From S and B I (1940)					
E	0.820 / 0.868	3.41	0°, 6, 12 / 18°, 24, 30	20.3				
E	0.866	2.49	0°, 6, 12, 24, 30	154.0				

included for comparison, some of them nearly as satisfactory as those adopted. The values of Ω obtained agree reasonably well with the rough average value of $30\text{–}40\times10^{-6}$ calculated from the average probable error quoted for the measurements. Because of the lack of individual probable errors, this is the only test available. As in Missouri, two azimuths show a distinctly poorer agreement.

The azimuthal variation of the constants given in Table I is quite puzzling. The western azimuths show higher intensities than the eastern, due to the bright line[5] of positive particles. But the slopes vary very irregularly and over a very wide range, with little tendency to cluster about 2.3, the high latitude values. For the high ζ lines, it is the constants a that vary unaccountably, while the slopes are comparatively uniform. A direct comparison (incompletely deducible from Table I) showed only a 7 percent increase in Ω when the six concordant azimuths were fitted with a single slope; but E and S are very significantly different, increasing Ω six-fold.

Another consideration that enters in fitting the low ζ lines is also apparent in Fig. 1. Certain points near the zenith form a transition between the higher line from positive primaries in the west and the lower lines to the east, and cannot be fitted to either curve. Since there are no adequate theoretical considerations to determine just how wide this transition zone should be, the only practical course available is to determine this width from these measurements. This might be done more adequately if individual probable errors of the points were available, permitting calculation of chi square. However, only the value of Ω is available as a criterion. The points included in the fitting are listed in Table I, and some of the basis for the adopted selections is given in the "alternative choices." In some cases the comparison is quite conclusive, in others the alternative cannot be certainly excluded.

One of the strangest cases of all occurs in the *E*. This is of particular interest, because of its direct bearing on the question of the reality of a peak of negative particles. The marked difference between the earlier (1940) curve and the later one is very puzzling in this connection. The earlier curve shows very clearly (7.5 to 1) an improvement by using a broken line raised parallel to itself, as by a sharp edge between 12° and 18°. The later curve reverses this appearance and by a factor 17 to 1 indicates a single straight line, with, however, 18° omitted. Since the actual value of Ω is greatly decreased in the later observations (perhaps too greatly), the probability seems greater that the "true" curve does not show a break corresponding to negative particles. The 18° value may be one that was irregularly measured high, such as were also observed in Missouri.[1] Unfortunately, the neighboring azimuths (NE and SE) shed little light on the question, though various extensions of the observations might remedy this situation.

While the anomalies near the zenith are fairly well explained by the Lemaitre-Vallarta theory,[5] the irregularities near 36° are very puzzling. Schremp and Baños attempted to account for them in terms of absorption anomalies, because of their azimuthal symmetry and similarity of path length to the "7° anomaly" in Missouri. However, as pointed out in I, the fact that the intensity actually rises from 36° to 42° in SE and E disproves this. A further difficulty is that, as shown by the knee in intensity at 40° latitude, all primaries incident at Mexico City, and more especially all those showing azimuthal symmetry, penetrate much more air than the 9.3 m of the 36° path to Mexico City. This is also borne out by the low b-values of the high ζ curves, which indicate a considerably higher penetrating power than any obtained in Missouri.

However, no other explanation seems any more satisfactory. The anomaly shows several features and irregularities. In all azimuths the slope changes, mainly to lower values, only very slightly in N and oppositely in SE. The step shown in Fig. 1 in several azimuths depends mainly on the manner in which interpolation is assumed between the measured points. The 36° point does not fit on any of the high ζ curves, but falls below except in S. It fits on the low ζ curves in W and NE, and otherwise is indifferently above or below, mainly according to the value of b. These features do not seem to offer any interpretation of their origin.

This discussion again illustrates the utility of the present method, even where the fine structure anomalies present a quite different appearance from that observed in Part I. Only its compression of scale for low ζ makes it more difficult to picture the outline of the magnetic edge. But the sharpness with which it indicates the breaks, together with their magnitude, constitutes a great advantage of this method. Part of its strength lies also in the fact that the double logarithmic figure leads directly to an analytical expression, no matter what type of anomaly is to be represented. And no previous treatment has permitted any analytic expressions whatever.

A Cloud-Chamber Analysis of Cosmic Rays at 14,120 Ft.

WILSON M. POWELL
Department of Physics, University of California, Berkeley, California
(Received November 12, 1945)

Protons and mesotrons near the end of their ranges are distinguished from each other by a method involving the degree of ionization in the gas of the cloud chamber and the scattering in the lead plates in the chamber. Photographs are shown of the production of protons and mesotrons in the lead by non-ionizing and ionizing radiation. Evidence is presented for the presence of an extremely large number of neutrons. Both neutrons and protons are shown to be secondary particles with a maximum energy near 200 Mev. The conclusion is reached that this maximum energy arises from the large cross section of the atmosphere for the production of pairs of mesotrons. The value of this maximum energy can be used as a measure of the mass of the mesotron. Photographs are shown of cascade showers produced by knock-on electrons, stars produced in the lead and the gas of the chamber, and Auger showers filling the whole chamber.

INTRODUCTION

THE remarkable photographs of G. Herzog and W. H. Bostick[1,2] made with a Wilson cloud chamber between the altitudes of 20,000 and 30,000 feet and the great abundance of slow mesotrons found there both by this method and by Schein, Jesse, and Wollan[3] using counters at still greater heights made it seem advisable to take a large Wilson cloud chamber[4] to the top of Mt. Evans in the summer of 1940 with the hope of discovering the abundance of slow protons and mesotrons and other phenomena occurring there. About 2400 photographs were made, part of them with random expansions and part with counter control. The data obtained were of sufficient value to warrant a second expedition in 1941. This time 20,000 photographs were made of random expansions of the large Wilson cloud chamber, and the two sets of photographs form the subject of this paper.

APPARATUS

Figure 1 shows a side view of the cloud chamber. The front glass Q is 0.5-inch "Tufflex" plate glass. The walls are made of 0.5-inch cold-rolled steel. The lead plates A measure $1\times9.4\times30$ cm. The area photographed was 42 cm high. Compressed air from a paint-sprayer compressor was introduced through six ports, one of which is shown at P. This forced the neoprene diaphragm J against the hole plate K when the chamber was compressed. When expanded, the diaphragm rested against the hole plate D. Nine bolts like those shown at E and F held the plate D in place and permitted the expansion ratio to be adjusted to the proper value. One side of the chamber N was $\frac{3}{8}$-inch "Tufflex." The light entered the chamber through this window and was reflected back by a sheet of chromium plated ferrotype plate on the far side of the chamber. This obviated the necessity for a window and light on the other side. Five lead plates, each one cm thick and spaced six cm apart, traversed the chamber. Small rubber tubes, OO, were placed around the edges making each compartment somewhat airtight. The plates were sheathed in thin chromium-plated ferrotype plates so as to improve the illumination and prevent glare from the surfaces of the lead plates.

The cloud chamber was filled with argon and a small amount of air. The tank argon had been in the tank for more than a year, so that very few alpha-particles from radon appeared in the gas. The liquid was normal propyl alcohol, and no particular precautions were taken about the presence of small amounts of water in the alcohol. Every other one of the lead plates was charged positively to 250 volts, and the rest were at ground potential. The field was removed at the instant of expansion. It was impossible to use any water in the chamber because the insulation of the alternate plates was insufficient.

[1] G. Herzog, Phys. Rev. **57**, 337 (1940).
[2] G. Herzog and W. H. Bostick, Phys. Rev. **58**, 278 (1940).
[3] M. Schein, W. P. Jesse, and E. O. Wollan, Phys. Rev. **57**, 847 (1940).
[4] W. M. Powell, Phys. Rev. **57**, 1061 (1940).

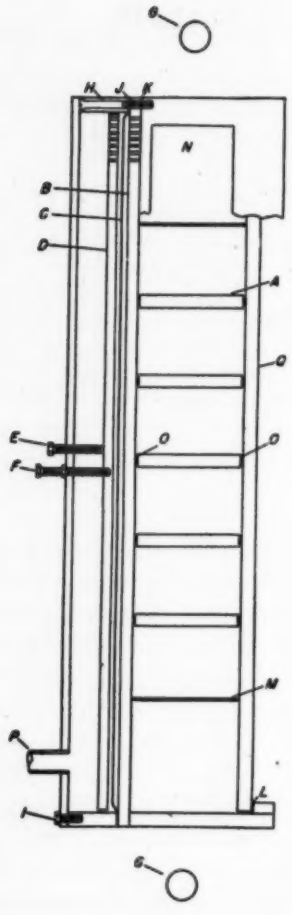

FIG. 1. Cloud chamber.

In 1940 eight coil-coil filament 60-watt, 115-volt clear Westinghouse bulbs with reflectors and condenser lenses were used for illumination. They were run at 240 volts d.c. from 40 second-hand car storage batteries purchased at junk price. The batteries were charged continuously at 125 milliamperes. The lamps were turned on at the moment of expansion and remained on for about 0.1 sec. The camera shutters remained opened continuously. In 1941 an Edgerton "flash lamp" 24 inches long and 0.5 inch in diameter with a cylindrical reflector behind and five double condenser lenses in front formed the source. Horizontal mirrors at the top and the bottom of the lamp-condenser unit gave even illumination at the two ends as well as the middle of the chamber. The lamp was flashed by the discharge of an electrical condenser of 250-microfarad capacity which was kept at 2000 volts by a voltage-controlled rectifier. This light was considerably brighter than the other, and consequently it was possible to use the cheaper DuPont Superior #3 film instead of the Agfa Ultra-Speed film.

The cameras were placed 30 degrees on either side of the normal to the chamber. In 1940 an F number of 3.5 was used for both cameras. In 1941 the camera on the left side nearest the light source used a lens with an F number of 2.5 while the other camera was the same as before.

The counter had a sensitive area of one by eleven inches. Two counters were placed above the chamber and one below, the three being in triple coincidence. In 1940 the cameras were reset by hand. In 1941 everything was operated automatically, and photographs were taken night and day except for about 14 hours during the week. All power was supplied by a 1000-watt 110-volt a.c. gasoline generator.

In 1940 the work was done in the laboratory of the University of Denver and Massachusetts Institute of Technology on the summit of Mt. Evans. In 1941 the apparatus was installed in a house-trailer. The trailer served as living quarters as well as laboratory and could be completely darkened for developing photographs. The walls were of sheet steel which covered the roof except for a small section in the top. Two 30-foot cables were attached to opposite corners of the trailer and buried a foot below ground as a protection from lightning. The generator was outside of the trailer.

DISCUSSION

There are three properties of the cosmic rays which permit identification of the rays with a Wilson cloud chamber containing five lead plates. First, there is the fact that electrons penetrating one cm of lead have a high probability of radiating and producing pairs, whereas protons and mesotrons have a very small probability of producing energetic secondaries. Second, the rate of change of the velocity of protons and mesotrons near the end of their range is quite different, and sufficiently so that they can be distinguished from each other by the appearance of the track just before stopping. Third, the scattering of mesotrons and protons is a function of their momentum and is greater for mesotrons having the same range as protons.

It is generally agreed that the probability of

an electron penetrating a lead plate one cm thick without producing secondaries is small. Owing to the mathematical difficulties encountered in fluctuation problems in shower theory,[5] it has been impossible to calculate this directly. If a particle passes through two or more lead plates without producing secondaries, it is extremely unlikely to be an electron. This criterion is an excellent one for distinguishing between electrons and heavier particles.

The second and third properties can be combined to give a means of distinguishing mesotrons and protons which are near the end of their ranges. All singly charged particles possessing high velocities produce tracks with nearly the same ionization per unit length of track. There is a particular velocity where this ionization reaches a minimum, $I_{\min}$. The ionization I increases quite rapidly as the velocity decreases. For all subsequent calculations the mesotron is assumed to have a mass of 200 times that of the electron.

Figure 2 shows the relative ionization $I/I_{\min}$ of protons and mesotrons plotted against the range in centimeters of lead. A proton with a range of 1.75 cm in lead will have a relative ionization of 3.25. This will be recognizable from inspection alone. Furthermore, when it leaves the next lead plate with a range of 0.75 cm, its relative ionization will be 4.65, and it will appear distinctly heavier than the section of track just above. A proton of shorter range will show a more marked change. A mesotron will have an entirely different appearance. If it has a range of more than 0.2 cm in lead, it will show no appreciable increase in ionization. Mesotrons then can be expected to stop in a lead plate without showing increase in ionization. Some will penetrate the last plate and leave it with less than 0.2 cm range. These will show a heavier track, but there will be no increase in ionization above this plate.

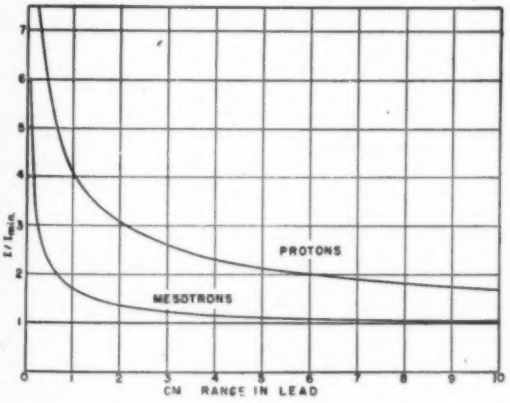

FIG. 2. Relative ionization of protons and mesotrons against range in cm lead.

There are occasions when the illumination of the track above and below a lead plate is not uniform, and there is some doubt about the proper interpretation. It is here where the use of scattering properties comes to the rescue and extends the data for mesotrons to much higher energies. Range and relative ionization were calculated from the paper by J. A. Wheeler and R. Ladenburg.[6]

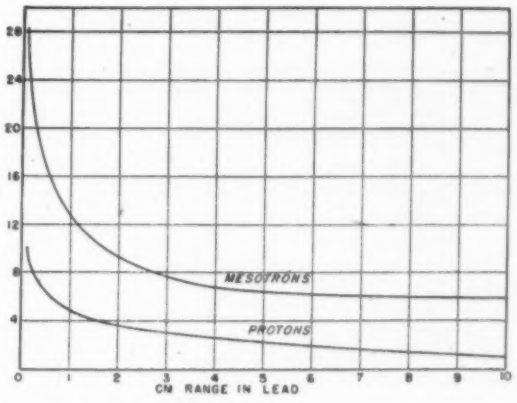

FIG. 3. Average projected angle of scattering in degrees for one cm of lead plotted against the range the particles have in cm of lead on leaving the plate.

IDENTIFICATION OF MESOTRONS AND PROTONS BY THEIR SCATTERING AND IONIZATION

Figure 3 is a graph of the average projected angle in degrees of scattering of mesotrons and protons through one cm of lead against the range in lead possessed by the particle on leaving the lead plate. It is calculated from the expression[7]

$$\tilde{\theta} = (19.5 - 3.1 \log_{10} Z)^{\frac{1}{2}} \frac{600Ze}{\beta E} (Nt)^{\frac{1}{2}}, \qquad (1)$$

where Z is the atomic number of the scatterer, e the charge on the electron, N the number of

[5] B. Rossi and K. Greisen, Rev. Mod. Phys. **13**, 305 (1941).

[6] J. A. Wheeler and R. Ladenburg, Phys. Rev. **60**, 754 (1941).

[7] E. J. Williams, Proc. Roy. Soc. **A169**, 548 (1939).

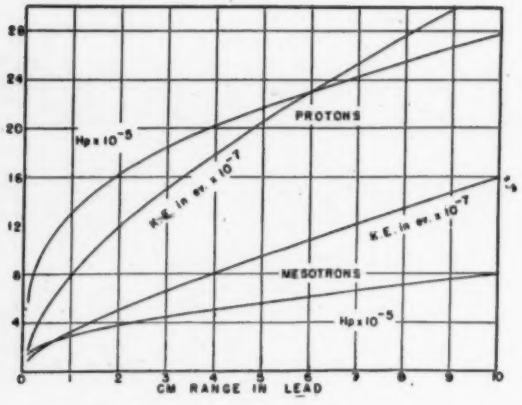

FIG. 4. Kinetic energy and magnetic rigidity ($H\rho$) of protons and neutrons.

atoms per cm³, and t the thickness in cm. This reduces to

$$\bar{\theta}=3\times10^{6}/H\rho\times\beta, \qquad (2)$$

where $H\rho$ is the magnetic rigidity and β is the velocity of the particle divided by the velocity of light.

Figure 4 gives the values of the magnetic rigidity and the kinetic energy for protons and mesotrons as a function of their range in lead.

In calculating the angle of scattering it is necessary to use the average value of the magnetic rigidity for the plate. This is a very uncertain quantity near the end of the range of a particle, owing to the rapid change of $H\rho$. For this reason the plates were divided into sheets one mm thick and the corresponding angles calculated. The angle for a one-cm plate was calculated by taking the square root of the sum of the squares of the ten angles for the corresponding ten sheets. This was done up to a range of 1.5 cm. From there on the average value of the magnetic rigidity is sufficiently definite to permit the use of Eq. (2) directly.

The cameras were situated at 30 degrees on either side of a normal to the chamber. If this angle had been 45 degrees, the angle between the cameras would have been 90 degrees, and the scattering angles observed by each camera would have been independent of each other. As it is, there is a small dependence, but for the sake of argument the two sets of angles are assumed to be independent of each other. If this is assumed, then each traversal gives two observations of the projected angle of scattering. Since there are five lead plates in the chamber, as many as ten angles appear for those rays which penetrate all five plates.

Williams' formula was checked for protons by the following method. Fifteen proton tracks were measured. The particles were identified by the increases in ionization after traversals of the lead plates. All fifteen tracks passed through two plates, seven through three plates, five through four, and two through five. The averages of the angles starting with the plate nearest the end of the range of the particles are 10.1, 5.3, 2.4, 1.1, and 1.2 degrees. This is in reasonably good agreement with the curve for protons. If anything, it indicates that the scattering of protons decreases more rapidly with increase in range than the theory would predict.

Figure 5a shows a proton track. Figure 5b is undoubtedly a mesotron track. It shows no increase in ionization. Therefore, if it were a proton, it would have to have a range greater than 1.75 cm when it leaves the last plate, for otherwise it would show an increase in ionization. The average projected angles p_i for a proton would be less than 3.7, 3.1, 2.7, and 2.4 degrees for the successive traversals, whereas the observed angles Θ_i are very much larger than this. There is a finite chance that a proton would stagger through the lead as shown. This chance can be calculated from the X^2 function where

$$X^2=\frac{2}{\pi}\sum_{i=1}^{n}\theta_i^2/p_i^2.$$

A table for the X^2 function gives the proportion P of protons of range greater than 1.75 cm that will show scattering angles equal to or greater than the observed angles.

The particle in Fig. 5b shows such large scattering angles that the value of P is extremely small. Since other evidence shows that there is an abundance of mesotrons, this small value of P indicates that the particle is *extremely unlikely* to be a proton and therefore must be a mesotron.

METHOD OF COUNTING PICTURES

Since approximately seventeen rays appear in each picture, it is very worth while to use a method which will depend upon counting only conspicuous events. For this reason a basis for

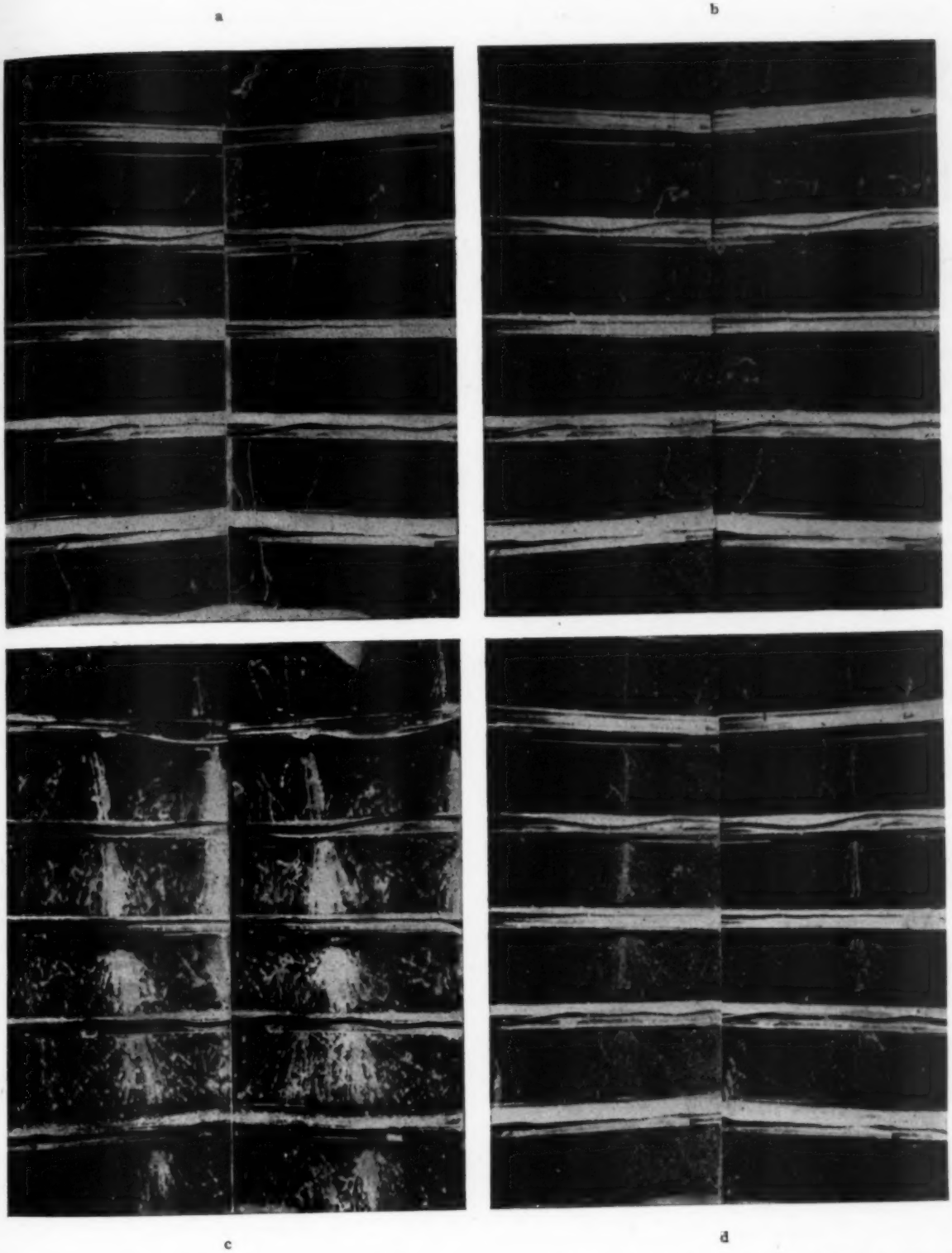

FIG. 5. a. A proton penetrating five plates and showing two increases in ionization at the end. b. A typical mesotron track identified by its large scattering. c. A cascade shower obtained with counter control. d. A cascade shower obtained in a random expansion.

all phenomena was taken as the number of particles penetrating two or more lead plates without producing secondaries. An exception was made to this rule if a particle penetrated two or more plates in a nearly straight line but had a secondary particle appearing with it. The secondary particle was interpreted as a knock-on electron instead of an electron resulting from radiation.

In general the heavy penetrating particles produce tracks showing light ionization. If the cloud chamber was operating poorly or with insufficient illumination, some of these tracks might have been missed while heavily ionizing tracks would continue to be counted. A careful comparison of pictures made with entirely different illuminating systems showed this not to be the case. Runs made in 1940 were compared with pictures made in 1941, and no appreciable difference appears. There is evidence that the sensitive time of the chamber varies from one set of pictures to another. Over a group of 100 pictures made in 1940 the average number of rays excluding the very large showers was 11 per picture. A run of 200 pictures made in 1941 showed an average of 21 rays per picture. This high number does not persist throughout all the 1941 pictures and in some cases drops to values in the neighborhood of six per picture. Nevertheless the relative number of different kinds of events remains unaffected by this change in the sensitive time of the chamber.

PROTONS, MESOTRONS, AND THE DISINTEGRATION ELECTRON

Table I is a collection of data on heavy particles identified by the three methods mentioned above. The top row entitled "Penetrating rays" refers to all rays traversing two or more plates without producing secondaries.[8] Column N_2 gives the percentage of penetrating rays traversing two plates and not more than two plates. Column N_3 gives the percentage of penetrating rays traversing three and not more than three plates, etc. From these values we get a distribution of penetrating particles which in itself means little. However penetrating rays have been chosen as the basis for counting phenomena of all sorts, therefore this analysis is fundamental for what follows. Actually from this analysis it will be shown that the protons in cosmic rays at this altitude are secondaries with a limited range of energy.

[8] See further qualifications above.

TABLE I. Compilation of data.

	Total	N_2	N_3	N_4	N_5	Pen. rays	Pictures
Penetrating rays	6918	51.9	24.1	12.4	11.1	6918	21,885
Mesotrons	312	49	24	17	10	4775	14,525
Mesotrons stopped	53	53	25	9.4		4775	14,525
Mesotrons*	12					4775	14,525
1 plate mesotrons	7					4775	14,525
Heavy I mesotrons	17					4775	14,525
2 plate protons	72	75	19.5	4.1	1.4	4775	14,525
1 plate protons	202					4775	14,525
Scattered rays	738					4775	14,525
Heavy I particles	2984					6918	21,885

* This group of mesotrons showed evidence of the disintegration electron. "Heavy I mesotrons" means mesotrons showing heavy ionization. "Heavy I particles" means tracks showing heavy ionization.

The row in Table I indicated at "2 plate protons" refers to particles identified as protons which penetrate two or more plates. A comparison of the percentages of protons penetrating different numbers of plates with those for penetrating rays or mesotrons shows at once that protons have a limited range. The proportion of protons traversing a few plates is considerably greater while the proportion traversing all five plates is *seven times smaller*. This means that at energies necessary to penetrate five lead plates the energy distribution curve for identifiable protons is falling off very much more rapidly than for all the penetrating rays. The identifiable mesotrons (see "Mesotrons" Table I) do not show this falling off in energy. Their distribution is identical with that of the penetrating rays. Therefore we can state that the protons are dying out at energies around 200 Mev. On the other hand at low energies they are very much more abundant. In the same group of penetrating particles 202 protons were observed which penetrated one plate only. In a group of 100 penetrating particles passing through two or more lead plates, there were 72 particles pene-

trating only one plate which could be interpreted by their lack of scattering and lack of accompanying secondaries as penetrating particles. This proportion is again smaller than that for protons.

This anomalous behavior of the protons is in agreement with the work of G. D. Rochester and M. Bound[9] who found a marked decrease in the number of slow protons at sea level when ten cm of lead were placed over their cloud chamber. They concluded that the protons have a short range less than ten cm of lead and that either more protons are produced in the air outside the chamber than in the lead or that the radiation producing the protons is filtered out by the lead. The fact that equilibrium is not established follows from the observation that only 4.7 percent of the protons are created in the lead plates of the chamber. There is no positive indication that the rest are not created in the walls of the chamber, but this seems unlikely in view of the fact that so much of the available material is concentrated in the lead plates. Furthermore, the creation of slow protons is always accompanied by other penetrating particles when it occurs in the lead, and these would be likely to show up with the protons from the walls. One case of this was observed, and that proton was included in the number created in the chamber. If we include all the penetrating particles created in the chamber with a range of more than one cm of lead and not identifiable as mesotrons, this amounts to only 12.2 percent of those stopped in the chamber. There seems to be no way of looking at the facts which is consistent with the assumption of equilibrium. We are forced to the conclusion that there is a group of protons of energy less than 200 Mev amounting to about 3.3 percent of the penetrating rays and that their number decreases very rapidly with increasing energy.

In this same group of particles there appeared 738 particles which showed at least one scattering angle of more than four degrees. Out of this group 312 particles could be identified as mesotrons by using the X^2 criterion. (Fig. 5b shows a typical scattered mesotron. It passes out of the back of the chamber.) Twenty-four percent of the mesotrons satisfied the condition that P is ten percent. This means that only ten percent of a group of protons which left the last plate with a range of 1.75 cm in lead would give angles equal to or greater than those observed. Because protons were scarce compared to mesotrons, this low value of P means that the particles in this group were very likely to be mesotrons. Thirteen percent of the particles gave a P equal to five percent, and the remaining 63 percent gave a P less than one percent. The distribution of the 312 particles matches that of the penetrating rays within the statistical error (see "Mesotrons," Table I). This indicates that the maximum in the energy distribution curve for mesotrons is well above 200 Mev in line with the majority of the penetrating rays.

Fifty-three mesotrons in this group stopped in the chamber. Ten of these passed through only one plate and identified themselves by large scattering angles and heavy ionization on one side of the plate. When the number of mesotrons which passed through two or more plates and showed heavy ionization were compared with those which failed to show heavy ionization, the proportion showing heavy ionization was found to be 22 percent. This is about the proportion which would be expected. The maximum range for a mesotron leaving a lead plate and showing heavy ionization is approximately 1.75 mm, which would indicate that about 18 percent of the rays stopping should show heavy ionization.

The cloud-chamber technique used here does not permit positive identification of the disintegration electron produced from a decaying mesotron. The following events, however, can be interpreted as mesotron disintegrations though the evidence that they are disintegrations cannot be conclusive.

In eight pictures a thin track appeared at the end of a mesotron track. The thin track was considered not to be the mesotron itself because of the very large angle it made with the mesotron track. In some of these cases the end of the mesotron track showed heavy ionization and then came a thin track at a large angle. Because of the presence of these thin tracks, it is possible to say that there is not negative evidence of the disintegration electron. Figures 6a and b show examples of this. In b the track occurs some

[9] G. D. Rochester and M. Bound, Nature **146**, 745 (1940).

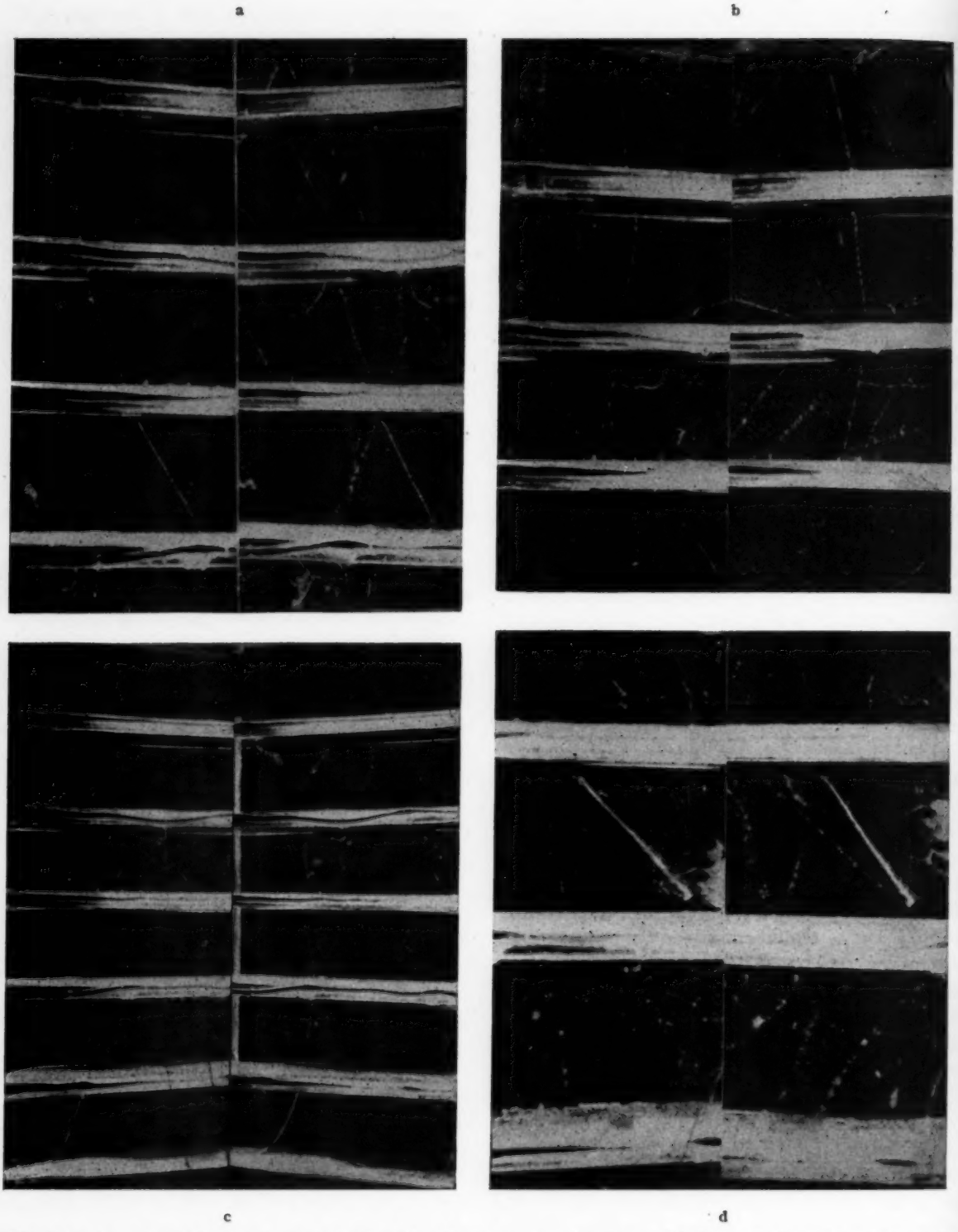

FIG. 6. a. A mesotron showing heavy ionization after the last traversal and a particle below the last plate which can be interpreted as the disintegration electron. b. A mesotron stopping in the bottom plate identified by its stopping and by the delta-ray. The particle going upwards near the end of the mesotron track may be the disintegration electron. c. A mesotron identified by scattering and a single increase ion ionization. d. Probably a mesotron disintegrating in the gas of the chamber and showing the disintegration electron.

distance to the right of the mesotron. The mesotron so near the end of its range could scatter sideways in the lead and then shoot the disintegration electron upwards.

Figure 6d shows a heavy track ending in the gas of the chamber with a thin one leaving the end. This photograph is the nearest approach to a proof of the existence of the disintegration electron that has been obtained with this chamber. It fails to indicate the direction of the particles except for the fact that the end of the heavy track is slightly kinked. This kink would indicate that the particle producing the heavy track stopped or nearly stopped and then produced the electron track. On the other hand, the two particles might have been ejected from an atom excited by a neutron or a photon, or the electron itself might have caused an atom to eject a neutron and the heavy track. The picture of the disintegration electron by E. J. Williams[10] has the same appearance at the end of the heavy track. It must be emphasized that all of the pictures shown here can be interpreted only as negative evidence that there is no disintegration electron.

In a group of 9500 pictures containing 1413 heavy tracks 75 of these heavy tracks ended in the gas of the chamber. These were not alpha-particles. This means that approximately 360 heavy particles stopped in the gas out of the 6918 penetrating particles appearing in the chamber. Figure 6d is the only case of its kind. The extreme scarcity of this phenomenon leads to two possible conclusions. First, that the production of a disintegration electron by a mesotron is very unlikely; second, that most of the particles stopping in the gas are protons. Nothing much can be said about the first, but there are two pieces of evidence which contradict the second. First there is the discovery of D. M. Bose and B. Choudhuri[11] that most of the particles appearing in stars in photographic plates left at altitudes of 12,000 ft. and 14,500 ft. are mesotrons, and second, the fact discussed below that when the reaction is energetic enough for the particles to be identified, there are at least three cases where both protons and mesotrons are produced simultaneously, and at least four cases where a mesotron is created by itself. Of the 52 penetrating particles which passed through two or more plates and were created in the chamber, 8 could be identified as mesotrons, 17 as protons, and the remaining 27 could not be identified. There is one more fact which can be interpreted as an indication that more of these particles are mesotrons. The range of a proton is about ten times greater than the range of a mesotron with the same ionization. This means that mesotrons showing the same ionization as protons are ten times more likely to stop in the gas. Opposing these two arguments there is the fact noted above that the number of slow protons increases very rapidly as their energy decreases. An extrapolation of this behavior to very low energies would indicate that most of the particles in the gas were protons. Then there is the

[10] E. J. Williams, Nature **145**, 102 (1940).
[11] D. M. Bose and B. Choudhuri, Nature **148**, 259 (1941).

TABLE II. Data on heavily ionizing rays.

	Total	Heavy I rays	Per-cent of heavys	S_2	S_3	S_4	S_{5-6-7}	Pene-trating rays	Pic-tures
Heavy I rays	2050	2050	100					4775	14,525
All stars	156	2428		103	27	19	5–1–1	5629	18,909
Air stars	13	2984		6	4	2	1–0–0	6918	21,885
Stars upwards	16	2428		12	3	1	0–0–0	5629	18,909
Heavys in stars	358	2428	14.7					5629	18,909
2 plate protons	72	2050	3.5					4775	14,525
1 plate protons	202	2050	9.8					4775	14,525
Heavy I mesotrons	17	2050	0.8					4775	14,525
Stopped mesotrons	53	2050	2.6					4775	14,525
Alpha-particles	208	2050	10.1					4775	14,525
Unidentified heavy I	1541	2050	75.2					4775	14,525
Single unidentified heavy I	1254	2050	61.2					4775	14,525
Created mesotrons	8	2984	0.29					6918	21,885
Created protons	17	2984	0.63					6918	21,885
Created unidentified penetrating particles	27	2984	1.0					6918	21,885
Total created	52	2984	1.92					6918	21,885
Heavy I particles stopped in gas	75	1413	5.3					3186	9,500

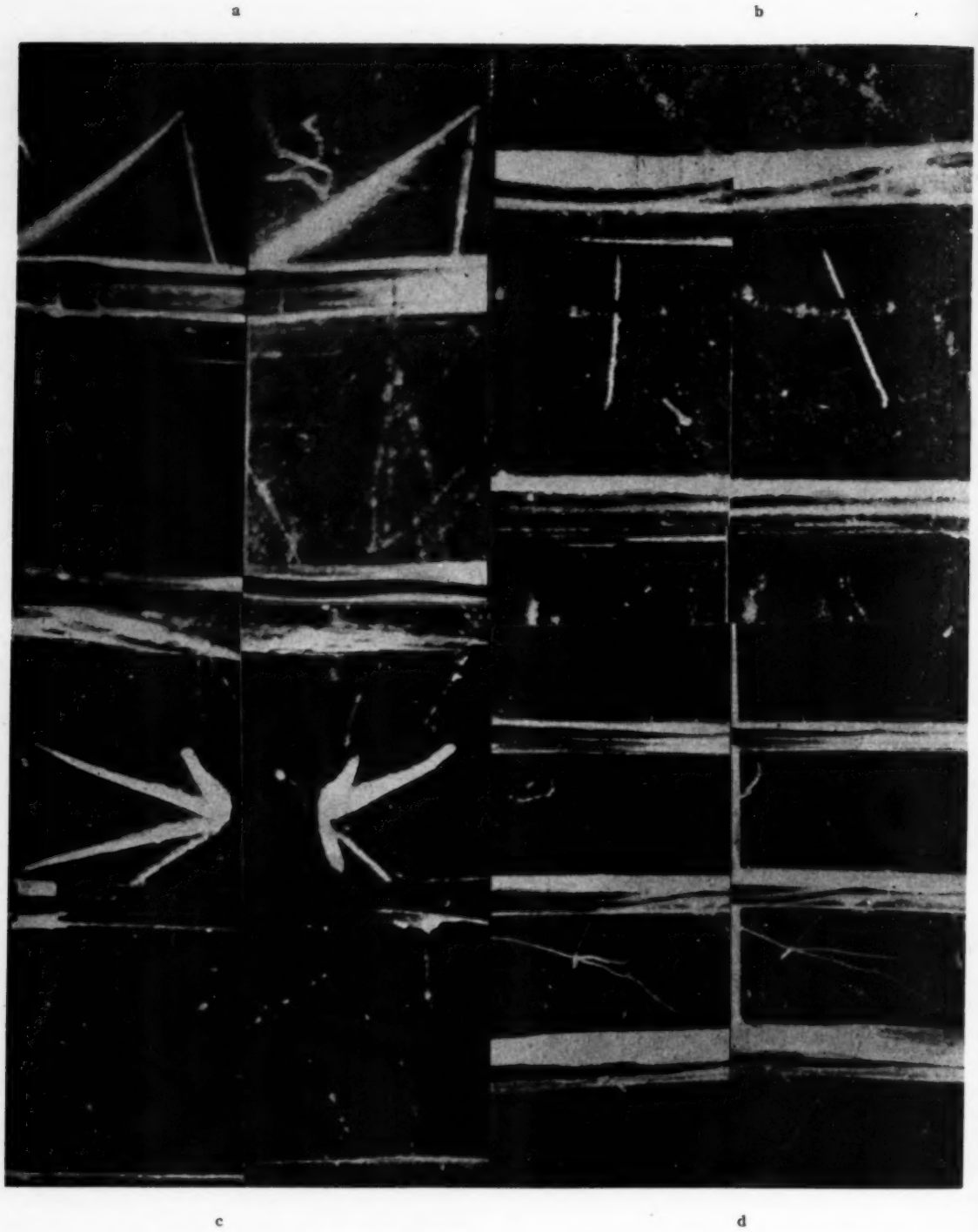

FIG. 7. a. A star in the gas of the chamber showing evidence that the left-hand particle was emitted a few thousandths of a second after the right-hand particle. b. The old horizontal track removed the water vapor from its neighborhood so that a gap appears in the vertical heavy track formed after expansion of the chamber. c. A star in the gas of the chamber showing evidence of neutrons. d. A star in the gas of the chamber with a thin track passing obliquely through the plate just below.

observation of C. D. Anderson and S. H. Neddermeyer[12] that "wherever the direction of the particles is definitely known (as for particles produced by a disintegration occurring inside the chamber), the sense of curvature in the magnetic field is such as to indicate a positive charge." Furthermore, if the assumption is made that the 38 tracks appearing singly in A. and N.'s pictures are going down, then 33 of them are positively charged and five are negatively charged.

In conclusion it can be said that the only strong argument in favor of the slow particles being mesotrons is the one advanced by D. M. S. and B. C. If the particles are all positive and are mesotrons, they are sure to show disintegration electrons. The almost complete absence of the disintegration electron, the increase in the number of protons at low energies, and the strong likelihood that they are all positive give almost overwhelming evidence that the slow particles are protons.

HEAVILY IONIZING RAYS

In a series of 14,525 photographs containing 4775 penetrating particles which pass through two or more plates, there appear 2050 tracks showing heavy ionization. Protons and mesotrons penetrating two or more plates and showing heavy ionization account for 89 of these. The heavy particles can be divided into the following categories (see Table II). Ten percent are alpha-particles, 3.5 percent are protons passing through two or more plates, 9.8 percent are protons passing through only one plate, 0.8 percent are mesotrons passing through one or more plates. This leaves 75 percent of the heavy particles unidentified. The particles in stars coming from either the gas or the lead amount to 14.7 percent. The remaining 61 percent appear singly, starting in the lead and stopping in the next piece of lead or the gas or leaving the chamber. It is open to conjecture as to how many of these are slow mesotrons.

In Table II the columns marked S_2, S_3, etc. give the number of stars with two, three, etc. particles per star. All the stars produced in the gas except the one of five particles appear to be excited by non-ionizing radiation. This star is shown in Fig. 7d. It is probably excited by non-ionizing radiation, but it might be interpreted as being excited by the thin ray passing through the bottom lead plate. This ray is evidently a heavy particle traveling very fast as there is very little scattering in the bottom lead plate. (The reproduction fails to show the thin ray on the far side of the plate.) However, it may perfectly well be coming from the star itself with the star being exited by non-ionizing radiation, as is usually the case.

Two of the stars have the appearance of the one shown in Fig. 5a. A small gap appears at the intersection of the two particles. Figure 7b shows how this might have happened. Here a sharp heavy track evidently laid down after the expansion of the chamber crosses an old diffuse track. The formation of the droplets along the old track robbed the gas of alcohol vapor and heated it with the heat of condensation so that when the vertical track formed conditions for droplet formation were unfavorable at the intersection. The left-hand track in the star appeared first and was followed after a very short time by the right-hand particle. The heavy ionization indicates that the particles were probably alpha-particles.

Photographs similar in appearance to Fig. 7a appear when actinium A is formed and decays in a cloud chamber.[13,14] In W. E. Bennet's paper, Fig. 4b, Plate 1, and in C. T. R. Wilson's paper, Fig. 1, photographs appear which show the gap placed in an exactly similar manner. The mean lifetime of actinium A is 0.0019 sec. In its formation and decay alpha-particles are ejected with ranges longer than the tracks appearing here.

There are difficulties in assuming that actinium A is responsible for these tracks. The argon gas was prepared by distillation from liquid air but had been in its container for over a year. Even if the walls of the chamber were very radioactive, which they do not appear to be, it is difficult to see how enough of the parent gas actinon could leave the walls so as to produce these stars in the middle of the gas. We can conclude that these stars indicate the presence of an atom which may be excited by non-ionizing

[12] C. D. Anderson and S. H. Neddermeyer, Phys. Rev. **50**, 263 (1936).

[13] C. T. R. Wilson, Proc. Camb. Phil. Soc. **21**, 405 (1923).
[14] W. E. Bennet, Proc. Camb. Phil. Soc. **34**, 282 (1938).

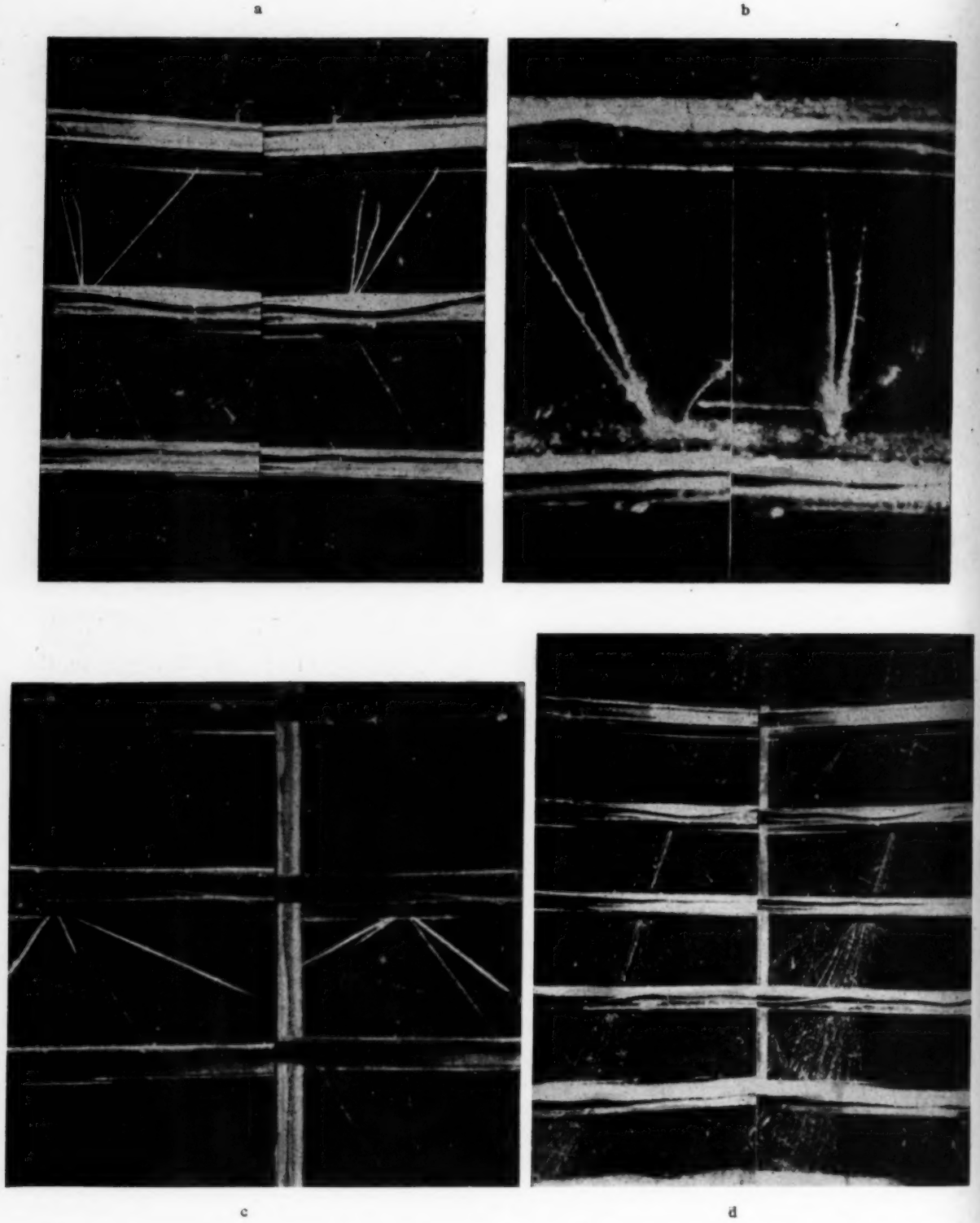

FIG. 8. a. A disintegration in the lead showing no thin tracks. b. A disintegration in the lead. c. A disintegration in the lead. d. A cascade shower produced by a penetrating particle.

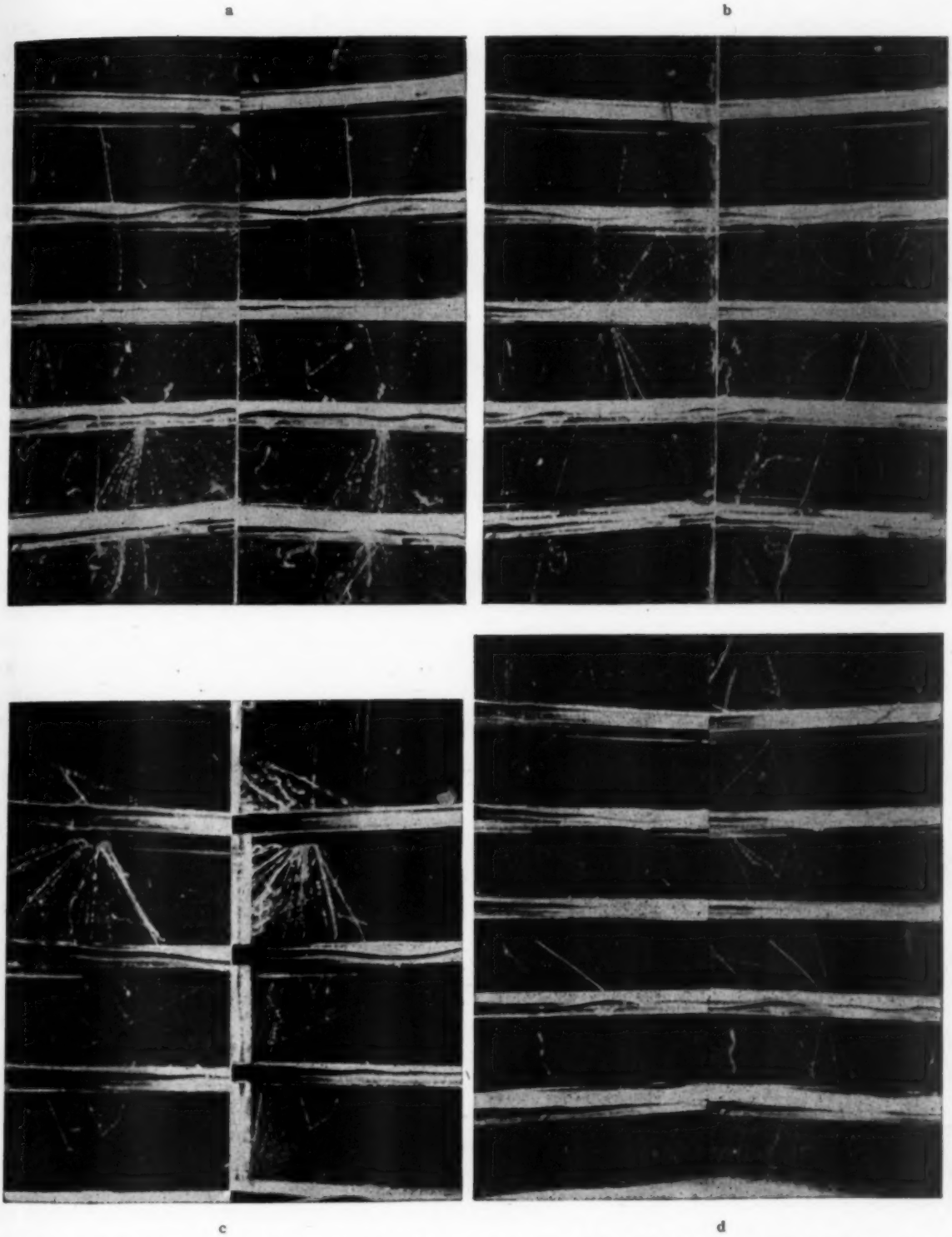

FIG. 9. a. The only case where a heavy particle and a cascade are associated. The right-hand particle above probably initiates the cascade and the particle above to the left which shows by its ionization that it is going up is a proton. b. A penetrating particle produces a proton (lower left) and a particle which may be a mesotron (lower right). c. Two particles enter above and produce one mesotron which penetrates the lower plate, shows scattering and increase in ionization. There are three heavy tracks and at least fifteen thin tracks. d. A penetrating particle produces one heavy track and five thin tracks.

radiation so that it ejects an alpha-particle, has a lifetime in the neighborhood of 0.002 sec., and then ejects another particle.

The four-particle star shown in Fig. 7c on reprojection is found to be going back into the chamber. The star initiates near the middle of the chamber, and two of the particles strike the back of the chamber. One stops in the gas, and one hits the lower lead plate. In order to satisfy the law of the conservation of momentum, it is necessary to assume that neutrons are taking part in this event, either initiating it or pouring out of it or both.

Typical examples of stars originating in the lead plates are shown in Figs. 8a, b, and c. Most of the particles in the stars showed heavy ionization, the number being 358 particles. There were 43 particles accompanying these stars which appeared thin. Not more than one thin track appeared in most stars. No event was called a star if there were no heavy particles in it. Practically all stars were initiated by non-ionizing radiation.

CASCADE SHOWERS PRODUCED BY PENETRATING PARTICLES

There are fifteen cases where cascade showers are produced by penetrating rays. There are five where the penetrating ray traverses one plate, six where it traverses two plates, and four where it traverses three plates. In one case shown in Fig. 9a a proton was ejected upwards and a cascade appeared below. Since there were 19,436 traversals of one cm of lead by penetrating particles which passed through two or more plates the cross section per electron is about 2×10^{-28} cm^2. Figure 8d shows the largest shower produced by a penetrating ray. Its energy is about 1000 Mev. A close inspection of the rays at the top of the picture shows that all but one of the tracks are older (more diffuse) than those appearing in the shower. It seems very unlikely that an electron with sufficient energy to produce this large cascade shower could have passed through the top lead plate without producing secondaries. The particle is undoubtedly heavier than an electron.

PENETRATING PARTICLES PRODUCED BY IONIZING RADIATION

There are twenty-seven events in which penetrating particles are produced by ionizing radiation, and in all cases but one there is no evidence whatsoever that they are associated with cascade showers. The exception to the rule is shown in Fig. 9a. A proton is ejected upwards as is indicated by the increase in ionization of the left-hand ray. The right-hand ray is distorted by turbulence in the chamber but is uniformly thin. It is probably the ray which initiates the cascade shower and the proton. There is always the possibility that any ray appearing above any of these events may be traveling upwards with sufficient velocity to show no change in ionization. It seems to be more likely that the thin particle appearing above is the cause of the event.

Figure 9b shows a penetrating particle which passes through two plates and then produces at least four heavy particles. The lower left-hand one is identifiable as a proton both from its ionization which is obviously heavier than the thin tracks present, and by the delta-ray which indicates a velocity for the particle for which a mesotron would show very large scattering. The long ray on the right side is both thin and scattered. It is probably a mesotron though the scattering is insufficient to determine this with assurance. The two heavy tracks are unidentifiable except for the fact that they must be either either mesotrons or protons.

Figure 9c shows two particles coming into the top plate. Two heavy tracks appear which stop in the next plate. One particle penetrates through two plates and appears heavy under the last plate and markedly scattered. This is a mesotron. Two of the thin tracks can be identified as electrons because of their scattering in the gas. The remainder are probably electrons but might be mesotrons.

In Fig. 9d the penetrating particle is without question coming from above as is indicated by the knock-on electron under the second plate. The heavy particle ejected upwards stops in the gas. The particle starting just above the fourth plate on the left passes down through the fourth and fifth plates and produces a knock-on electron which is the track farthest to the right below the fifth plate. It is just a coincidence that this particle with its knock-on happens to be in the picture. The left-hand particle passing through the fifth plate may very well be a penetrating

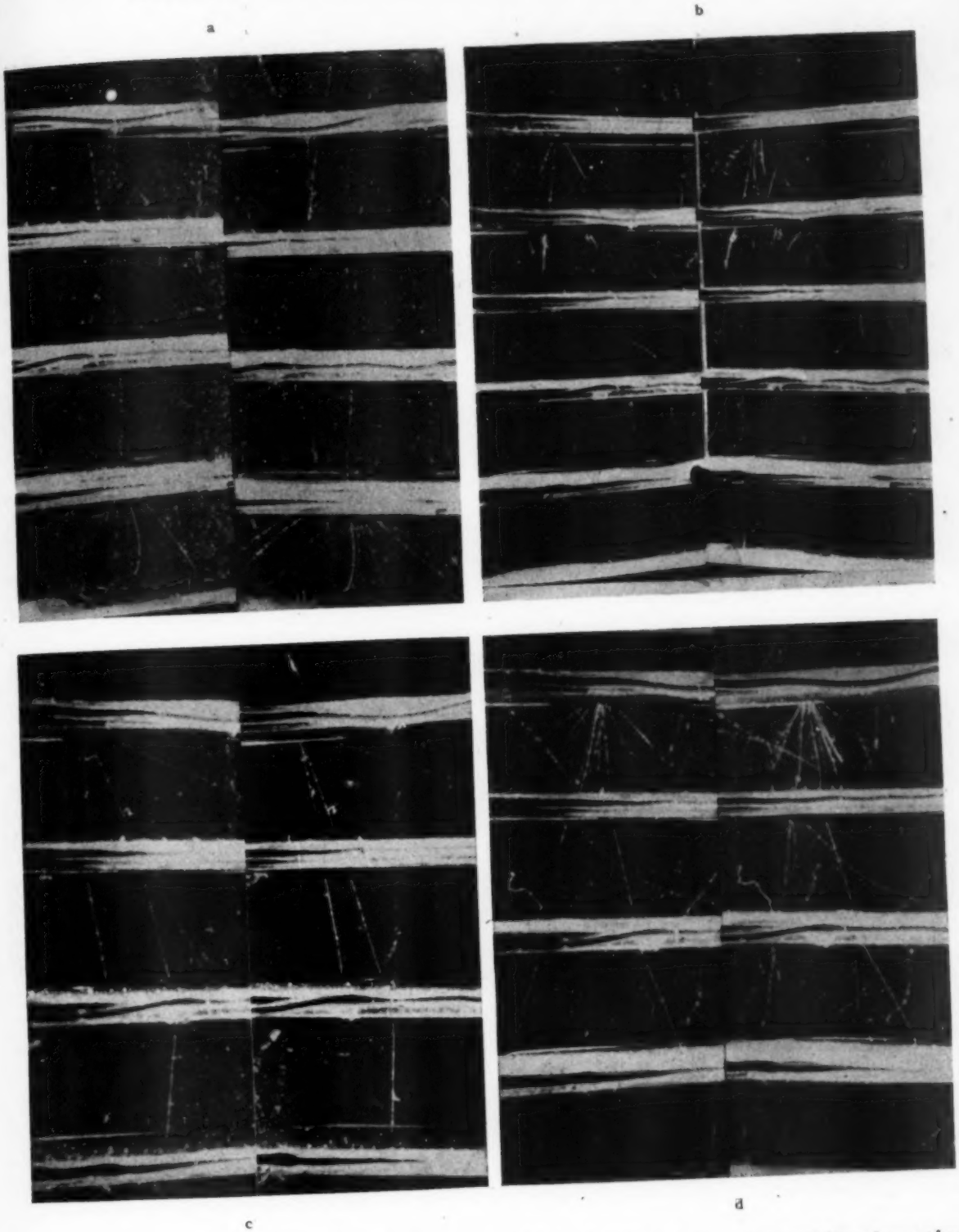

FIG. 10. a. A penetrating particle produces one heavy track and five thin ones. b. A penetrating particle produces at least four heavy particles, one of which is a proton and one a mesotron. c. Non-ionizing radiation produces two protons. d. Non-ionizing radiation produces one proton (lower right) and one mesotron (lower left), the latter stopping in the lead plate.

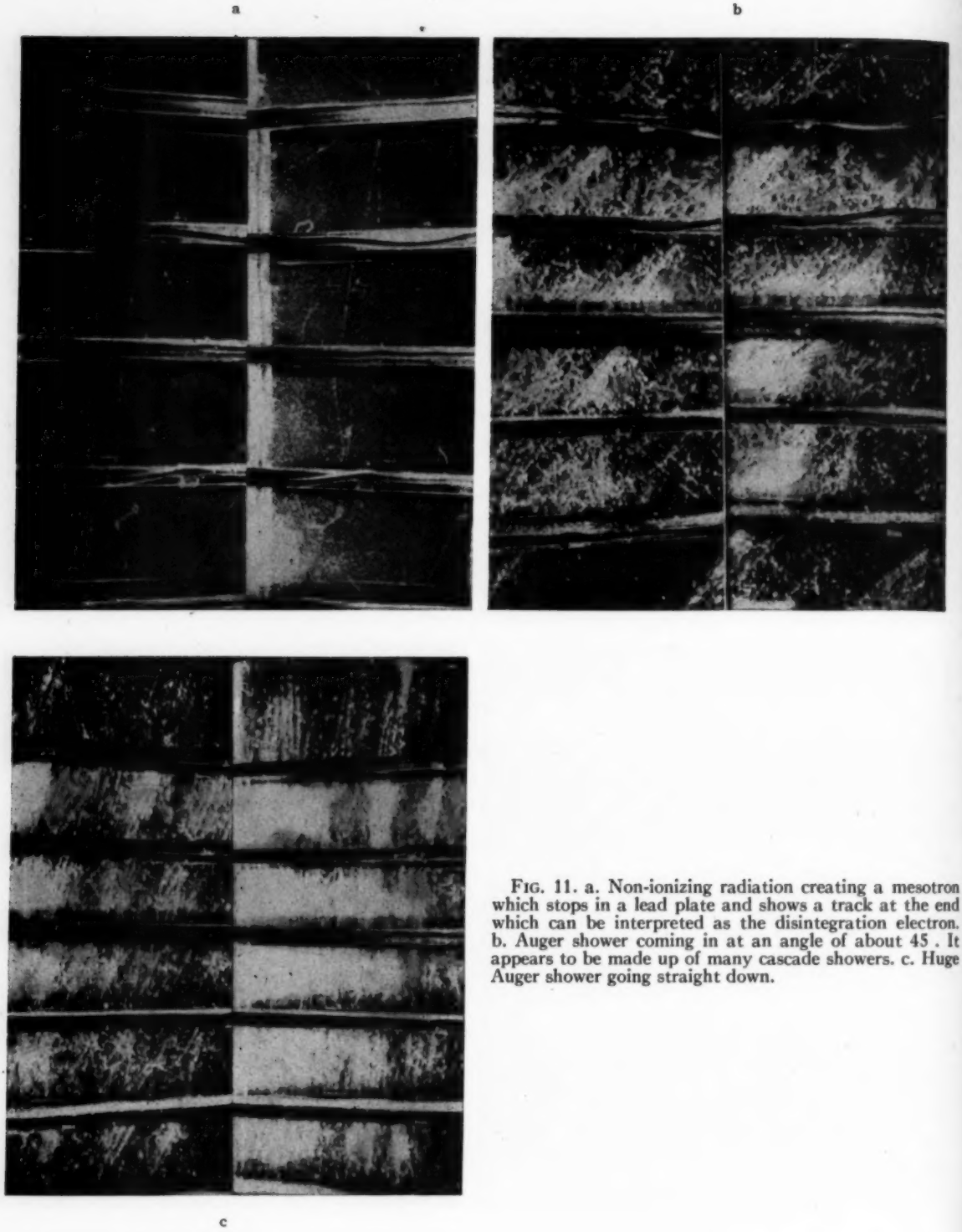

FIG. 11. a. Non-ionizing radiation creating a mesotron which stops in a lead plate and shows a track at the end which can be interpreted as the disintegration electron. b. Auger shower coming in at an angle of about 45 . It appears to be made up of many cascade showers. c. Huge Auger shower going straight down.

particle. It shows some scattering and may be a mesotron.

Figure 10a shows a penetrating particle producing two heavy tracks and a number of thin tracks in the bottom plate. It is not at all unlikely that this event would show other pene-

trating particles if the rays below had had the opportunity to pass through additional pieces of lead.

Figure 10b has appeared before[15] and further study has led to the definite identification of two of the particles. The track which penetrates the second plate and then becomes very thick is without doubt a proton. A study of tracks appearing in the same part of the chamber in other photographs on the same film show that the apparent greater density of the track before it passes through the second plate is real. This alone makes it impossible for the particle to be a mesotron. No additional argument is needed, but the average scattering angle for a mesotron so near the end of its range is very large, and the photograph shows that both scattering angles give an average of only two degrees. The track which penetrates three plates presents scattering angles that only one proton in twenty would show. There is little doubt that this is a mesotron. The particle which penetrates two plates presents angles that only one proton in eight would show. This picture affords unmistakable evidence for the *simultaneous production of mesotrons and protons.* Still another picture appears of this process. The event takes place in front of the chamber, so that it is impossible to identify the incoming ray. A proton penetrates one plate and shows increase of ionization on both sides of the plate. The mesotron penetrates two plates with such large scattering that there is practically no chance that the particle is a proton.

There are altogether 19,438 traversals of the one-cm lead plates by penetrating particles. These 27 cases of the production of heavy particles give a neutron-proton cross section of 1.8×10^{-28} cm^2 for this process. This is of the same order of magnitude as the neutron-proton cross section[16] given by R. P. Shutt of 4×10^{-28} cm^2.

HEAVY PARTICLES PRODUCED BY NON-IONIZING RADIATION

Figure 10c shows the production of two protons by non-ionizing radiation. The upper section of the two proton tracks are obviously heavier than the single track which appears to the right and then between the two tracks. Figure 10d shows another case of the simultaneous production of a mesotron and a proton. The left-hand particle shows small scattering but stops near the middle of the bottom plate. Only a mesotron can do this without showing heavy ionization. The right-hand track is distinctly heavy and also stops in the bottom plate. It is a proton. Still another photograph not reproduced shows two heavy tracks going down and stopping in the next plate while one proton goes up through one plate.

Figure 11a shows a mesotron created in a lead plate. It stops two plates away and a particle comes back from the end. This might very well be the disintegration electron. There are three photographs like this except for the fact that the other two show no disintegration electron. There are four photographs where the appearance is the same except that the particle shows no scattering, and one photograph where only one particle is emitted by the plate. It passes through two plates and then leaves the chamber.

Altogether there are sixteen occasions where a non-ionizing radiation produces penetrating particles which pass through at least one lead plate. Five particles are protons, four are mesotrons, and the remaining eleven particles cannot be identified. This does not count the particles that show heavy ionization but fail to penetrate a plate. Practically all the stars in the gas of the chamber and appearing from the lead are initiated by non-ionizing radiation.

There are six events where it is impossible to determine the type of initiator. Their appearance is essentially similar to those above. Five protons, one mesotron, and five unidentified penetrating particles appear in these.

In all of these events there are seventeen protons, eight mesotrons, and twenty-seven penetrating particles going too fast to be identified. Simultaneous production of mesotrons and protons appears in all three types. Three of the protons are going up. The fact that so many protons are produced in the chamber coupled with the falling off in the number of protons with the number of plates they penetrate indicates again that the protons result from secondaries produced in the atmosphere around the chamber, and that very few, if any, of the primary protons appear in the energy range above 200 Mev.

[15] W. M. Powell, Phys. Rev. **60**, 413 (1941).
[16] R. P. Shutt, Phys. Rev. **61**, 6 (1942).

COUNTER CONTROLLED PHOTOGRAPHS

A total of 1628 pictures were made with counters above and below the chamber. The efficiency of the counters was not known. The counter cylinders were 2.54 cm in diameter and 28 cm long and were placed 80 cm apart above and below the chamber. A third counter was placed between them solely for the purpose of reducing accidental counts. A coincidence occurred once in 45 seconds on the average. Five hundred and ninety-two pictures gave evidence of having been counter-controlled. Of these 411 showed a penetrating particle passing through five plates, 33 showed cascade showers (Fig. 5c), 138 showed numerous thinly scattered particles, and ten showed giant Auger showers two of which passed through the chamber at an angle of about 45 degrees. (Fig. 11b and 3) It is apparent that the Auger showers are made up of huge cascade showers mixed into each other. There is no evidence whatsoever that they include heavily ionizing particles. The confusion is too great to follow through penetrating particles which do not show an increase in ionization. About 100 counter-controlled pictures were made with the counters all above the chamber. In only one case did a ray stop in the chamber.

THE ELECTRON COMPONENT

During 19,438 traversals of the lead plates by penetrating particles 666 electron showers containing more than six particles were observed. These were all random expansions. No large Auger showers were seen in this group.

A careful study was made of the particles appearing between the upper two plates of the chamber. In 200 photographs 985 particles appeared there. If two or more particles started from one point in the lead and failed to penetrate one of the plates or passed out of the chamber they were called electrons. Tracks showing marked scattering in the gas were called electrons. These two classes accounted for 546 particles. There were five knock-on electrons. There were 14 particles which were in groups coming from points in the back or front of the chamber. These were classified as electrons. There were 263 particles which occurred singly and failed to pass through any plates. Fifty-one of these passed through the gas without touching the lead plates. They were unidentified. Seventy-two particles passed through one plate only showing very little scattering and producing no secondaries. Most of these probably were penetrating particles. There were 100 particles which penetrated more than one plate. These were classified as penetrating particles. Of the 710 tracks which could be identified 565, or 80 percent, were electrons. The remainder were heavy particles.

For a cosmic ray to get into this section of the chamber from above it must pass through 1.27 cm of iron and one cm of lead. If we assume that the number of electrons is increased by a factor of ten in passing through the lead and iron, then 29 percent of the incoming rays must be electrons.

A rather surprising discrepancy from theory was found in a comparison of the number of photon-produced and electron-produced pairs. Where theory predicts a ratio of about 1.6 in favor of photon-produced pairs the actual number was 72 photon-produced pairs against 16 electron-produced pairs. J. R. Oppenheimer called attention to the fact that the electrons and photons involved being of low energy it would be expected that the electrons would be absorbed out more readily than the photons because the loss by ionization becomes appreciable. This effect should be less at the top of the chamber and if we compare only those pairs produced in the top lead plate, this is found to be true. There are 30 photons-produced pairs to 10 electron-produced pairs. Agreement with theory is better in the case of three-particle showers. There are 16 photon-produced against 7 electron-produced showers in this group.

NEUTRONS AND THE MASS OF THE MESOTRON

The data given in Table II can be interpreted so as to indicate the presence of a very large number of neutrons. It will be shown that these neutrons have an average energy of 100 Mev, and that probably they have a maximum energy of 200 Mev. It is quite probable that the similarity between this maximum energy of 200 Mev and the mass equivalent of two mesotrons of weight 200 times that of the electron is not fortuitous. This similarity was pointed out by L. W. Alvarez.

Stars arise in the lead and in the gas of the chamber. The particles in the stars frequently come out of one plate and stop in the next. Occasionally a few stop in the gas of the chamber. If the radiation in the chamber has reached equilibrium then the following condition should hold:

$$\frac{\text{Stars produced in the lead}}{\text{Stars produced in the gas}} \geqq \frac{\text{Heavy particles stopped in the lead}}{\text{Heavy particles stopped in the gas}}.$$

Putting in the figures shown in Table II, this becomes

$$\frac{156/5629}{13/6918} \geqq \frac{1338/3186}{75/3186} \quad \text{or} \quad 14.7 \geqq 17.8.$$

This agreement is well within experimental error, so it can be said that equilibrium has been reached.

The average path of a particle in the gas is approximately seven cm, the space between the plates. By multiplying this path length by the ratio above we obtain the average range of a particle in the gas. This amounts to about 120 cm in air. A particle with this range in air would have a kinetic energy of approximately 12 Mev, which agrees closely with the maximum in the energy distribution curve for particles appearing in photographic emulsions left at high altitudes.[17]

It is obvious that many stars are formed inside the lead with insufficient energy to appear in the gas of the chamber. The range of a 12-Mev proton in lead is about 0.02 cm. Since the plates are one cm thick, this means that fifty stars are created inside the lead for one appearing leaving the plates. Now if we assume that it takes about eight Mev to eject a nuclear particle from the nucleus, then one particle would take a total of 20 Mev. The average number of ionizing particles appearing in a star in the gas is three. It is reasonable to assume that one neutron is ejected for every proton. This leaves a total of six particles and a total energy of 120 Mev for the average star. Table II shows one air star of five particles and five stars leaving the lead of five particles. There were no stars of more than seven particles. This is an indication that the maximum energy for stars amounts to about 200 Mev.

Above it was shown very conclusively that the high speed protons had a maximum energy of 200 Mev. This means that the protons are of secondary origin. They would be expected to be in equilibrium. However, the ratio of high speed protons created in the chamber to those stopped instead of being one as it should be for equilibrium is one to twenty. We are forced to conclude that for this group of protons capable of penetrating one or more cm of lead equilibrium is not established.

ENERGY CARRIED BY THE NEUTRONS

Practically all stars are produced by non-ionizing radiation and since they are hardly ever accompanied by cascade showers, it seems reasonable to assume that the producing agent is neutrons. The number of neutrons can be estimated in the following manner. Table II shows 156 stars to occur while there were 5629 penetrating particles. The penetrating particles make slightly more than two traversals each on the average. During each traversal the loss in energy is about 13 Mev. The total energy lost by the penetrating particles is $5{,}629\times2\times13=1.7\times10^5$ Mev. The energy lost by the 156 stars is 156×120 Mev, but we have shown that for one star appearing outside of the lead there are fifty produced inside. Hence this number should be multiplied by fifty giving $156\times50\times120=9.4\times10^5$ Mev as the total energy for all the stars. The remarkable fact appears that the energy used in creating the stars is *five times greater* than the energy lost by the penetrating component in the same amount of material.

THE NUMBER OF NEUTRONS

We are now in a position to estimate the relative number of neutrons present. If we assume that their angular distribution is similar to that for the penetrating particles, then they will traverse two cm of lead on the average. A reasonable assumption for the cross section per lead atom is 3×10^{-24} cm^2. They pass 6×10^{22} lead atoms in penetrating two cm of lead. This means that approximately four out of five neutrons will

[17] A. Widhalm, Zeits. f. Physik **115**, 481 (1940).

pass through the lead without producing a star. The conclusions is that there are $156\times50\times5=3.9\times10^4$ energetic neutrons accompanying 5629 penetrating particles or a ratio of *seven to one* in favor of neutrons.

PROTONS ARE RECOILS FROM NEUTRONS

Above we showed that the high speed protons were of secondary origin and not in equilibrium in the chamber. Inside the chamber there are no very light nuclei except for the small number of protons in the alcohol. The wood of the trailer and the protons in the observer were all available for collision with the abundant energetic neutrons indicated by the presence of the stars. The neutrons transfer their energy without degradation to the protons in the wood of the trailer. One cm of wood in the neighborhood of the chamber would be sufficient to produce the number of fast protons observed. This explanation accounts completely for the lack of equilibrium of the high speed protons found inside the chamber.

THE MASS OF THE MESOTRON

Most of the conclusions drawn in this paper were described in a preliminary letter to the editor in 1942.[18] In a recent discussion of these results L. W. Alvarez pointed out the equality between 200 Mev and the rest mass energy of two mesotrons of mass 200 each. There is little doubt that the mesotrons at this altitude have a mass very close to 200.[19] The explanation of the strong band of secondary neutrons follows directly. Apparently the atmosphere acts as a filter. Neutrons coming down and possessing energies greater than 200 Mev create pairs of mesotrons. If they have insufficient energy to do this, then they come on through and produce the stars and protons described above. An accurate determination of the cut-off with rising energy of the secondary neutrons would yield a minimum value for the mass of the mesotron.

CHANGE OF INTENSITY WITH ALTITUDE

In the 1942 expedition to Mt. Evans[19] the number of heavily ionizing particles was observed to decrease to about half when the apparatus was moved from the peak at 14,100 ft. to Summit Lake at 12,700 ft. This reduction is consistent with the assumption that the particles are produced by the neutrons observed at the summit.

The number of atoms per cm^3 of air at 13,400 ft. is 3×10^9. The average cross section for neutrons in 21 percent oxygen, and 79 percent nitrogen is 8×10^{-25} cm^2 per atom. The intensity I at 12,700 ft. becomes

$$I=I_0(\exp)(-3\times10^{19}\times8\times10^{-25}\times1400\times12\times2.54),$$

where I_0 is the intensity at the summit. The value of the exponent is approximately minus one. The predicted intensity lies between one-half and one-third the intensity at the peak. This agreement is well within the experimental error.

It is apparent that a large increase in the intensity of the neutrons can be expected for a small increase in altitude.

ACKNOWLEDGMENTS

I wish to thank the many organizations and individuals who made this work possible. The continued support of the Rumford Fund of the American Academy of Arts and Sciences was of the greatest help in initiating and sustaining this work. All the preparatory work was done at Kenyon College, Gambier, Ohio. The original grant for construction of the cloud chamber was made by Kenyon College. The Studebaker Corporation through Mr. Paul Hoffman contributed to the first expedition. The late Mr. Wilbur Cummings, trustee of Kenyon College, contributed materially to the initiation of the second expedition. The Fund for Astrophysical Research gave the money for the Edgerton lamp and the power supply. The American Philosophical Society made major contributions toward the second and third[18] expeditions. The Cosmic Ray Committee of the Carnegie Institute of Washington gave the major portion of the funds for the third expedition. Dr. J. A. Fleming's continued interest in this work was of great value before this as well. The John Simon Guggenheim Memorial Fellowship Grant made it possible to carry out the interpretation of the

[18] W. M. Powell, Phys. Rev. **61**, 670 (1942).
[19] C. E. Nielsen and W. M. Powell, Phys. Rev. **63**, 384 (1943).

extensive data in the Department of Physics of the University of California, Berkeley.

Professor R. T. Birge's generous hospitality in extending the facilities of the Department of Physics was of the greatest assistance. Professor R. B. Brode did everything possible to forward the work. Professor J. R. Oppenheimer reviewed much of the data and made many valuable suggestions in its interpretation. Professor Bayes M. Norton of the department of Chemistry at Kenyon College took many of the first photographs made on the mountain.

Two Kenyon students, Richard W. Penn and Henry Meyers, each gave a summer of work on Mt. Evans. Their help was essential to the many things necessary to the success of the expeditions on the mountain. Professor J. C. Stearns, at that time in charge of the laboratory on Mt. Evans, was of great assistance to us while we were on the mountain.

PHYSICAL REVIEW VOLUME 69, NUMBERS 9 AND 10 MAY 1 AND 15, 1946

The Velocity Dependence of the Absorption of Boron for Slow Neutrons

J. H. MANLEY, L. J. HAWORTH, AND E. A. LUEBKE
Department of Physics, University of Illinois, Urbana, Illinois

(Received October 27, 1941)*

Measurements of the slow neutron velocity distribution between 1 and 10 km/sec. from a 14-cm cube of paraffin, with a source of 2.5-Mev neutrons in the center, show the distribution to be approximately Maxwellian with $T=400°K$, but with an excess of fast neutrons for $V>3.5$ km/sec. Similar measurements of the distribution of neutrons transmitted through a boron absorber verify the assumed $1/v$ absorption law in this velocity range.

INTRODUCTION

APPARENTLY a number of physicists[1–4] realized, about 1937, that the development of artificial neutron sources would lead to a method of measuring neutron velocities through modulation of the ion beam producing the neutrons. Previous to these electrical methods a mechanical velocity selector had been used to investigate the neutron distribution from paraffin[5] and the rotating wheel method for checking a $1/v$ absorption law had been applied to boron, cadmium, and silver.[6]

The velocity distribution of slow neutrons has been examined only by the mechanical method and by the electrical method of Fertel, Gibbs, Moon, Thomson, and Wynn-Williams[3] (FGMTW). In neither case was the resolution available particularly high. With a method available for determining velocity distributions, the distribution before and after passing through an absorber or scatterer may be measured and the cross section as a function of neutron velocity found. Only FGMTW have published results on both the distribution and absorption laws, the absorption being in boron. Their results on boron are in disagreement with a $1/v$ variation of cross section which has been assumed for slow neutrons producing an (n, α) reaction in such a light element. The validity of this assumption is of importance since many measurements of neutron energies depend upon it. In addition to the experiment of FGMTW, the rotating disk method has been applied to boron[6] as has been the electrical method of Alvarez.[1] Both indicate a $1/v$ dependence of cross section, but the disk method is not capable of large changes in relative speed and Alvarez assumed thermal equilibrium of the

* This paper was received for publication on the date indicated but was voluntarily withheld from publication until the end of the war.

[1] L. W. Alvarez, Phys. Rev. **54**, 609 (1938).
[2] J. M. W. Milatz and D. Th. J. ter Horst, Physica **5**, 796 (1938).
[3] Fertel, Gibbs, Moon, Thomson, and Wynn-Williams, Proc. Roy. Soc. **175**, 316 (1940).
[4] C. P. Baker and R. F. Bacher, Phys. Rev. **59**, 332 (1941).
[5] G. A. Fink, Phys. Rev. **50**, 738 (1936).
[6] Rasetti, Segre, Fink, Dunning, and Pegram, Phys. Rev. **49**, 104 (1936); Rasetti, Mitchell, Fink, and Pegram, Phys. Rev. **49**, 777 (1936).

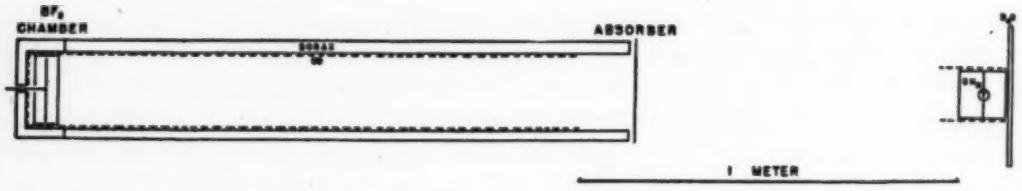

FIG. 1. Arrangement of source, detector, absorbers, and shielding.

neutrons at room temperature which is not justifiable for the small amount of paraffin used.

APPARATUS AND METHOD

The neutron source and circuits for obtaining a sharp neutron burst and the record of time of neutron arrival at a distant detector have been described previously.[7] The detector for these measurements was a parallel plate ionization chamber filled with BF_3 at atmospheric pressure. The chamber was circular, 19 cm in diameter. Positive ions were driven to the collecting electrode by a field of 1000 volts/cm. The sensitive volume of approximately 1100 cm^3 absorbed about 6 percent of the incident neutrons. The arrangement of the chamber, shielding, absorbers, and source is shown in Fig. 1.

In this type of work, it is essential to know of any time delays in the recording of the neutrons. The amplifier itself was first tested by impressing a pulse approximately one microsecond wide on the first grid. This pulse and that from the discriminator output of the amplifier were observed simultaneously on the oscilloscope. No appreciable (much smaller than 5 microseconds) delay was observed. There may be, however, a considerable delay with actual pulses due to possible delays in other parts of the circuit, or in the chamber, as, for example, the finite time of rise of output pulse before the discriminator tube becomes conducting since it must be biased to eliminate amplifier noise. Such delays, together with any involved in the processes inside the paraffin, were studied by determining the number-time distribution when the chamber was placed next to a paraffin block. From these results an over-all delay of about 50 μsec. was observed, an analysis of which is given by the authors.[7]

The shape of the slow neutron burst from the paraffin surface must be known in order to make an accurate velocity analysis. This shape depends on the amount of paraffin present and may be expressed in terms of a half-life for the change of intensity of the emergent neutrons. Measurements of this "source time distribution" were made with a small BF_3 proportional counter very close to the surface of the paraffin block. Figure 2 shows the results, an exponential rise and decay as would be expected from the effects of capture and diffusion in the paraffin. The measured half-life in this case (for a block used in velocity experiments at 250-cm distance) was 50 μsec. As is seen, the delay using the counter is much smaller, amounting to about 8 μsec., attributable to a lag between initiation of the sweep and the incidence of the ion current on the target.[7]

In order to increase the slow neutron intensity for measurements at greater distances a different arrangement was used. The 14-cm cube was surrounded by a large amount of paraffin built up in the form of a howitzer. A large increase in the half-life caused by the much greater amount of

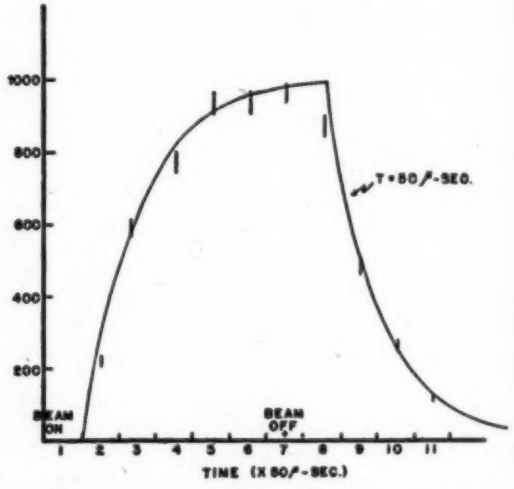

FIG. 2. The slow neutron time distribution from paraffin irradiated by a 325 μsec. fast neutron burst. The half-life for growth or decay is 50 μsec.

[7] L. J. Howorth, J. H. Manley, and E. A. Luebke, Rev. Sci. Inst. 12, 591 (1941).

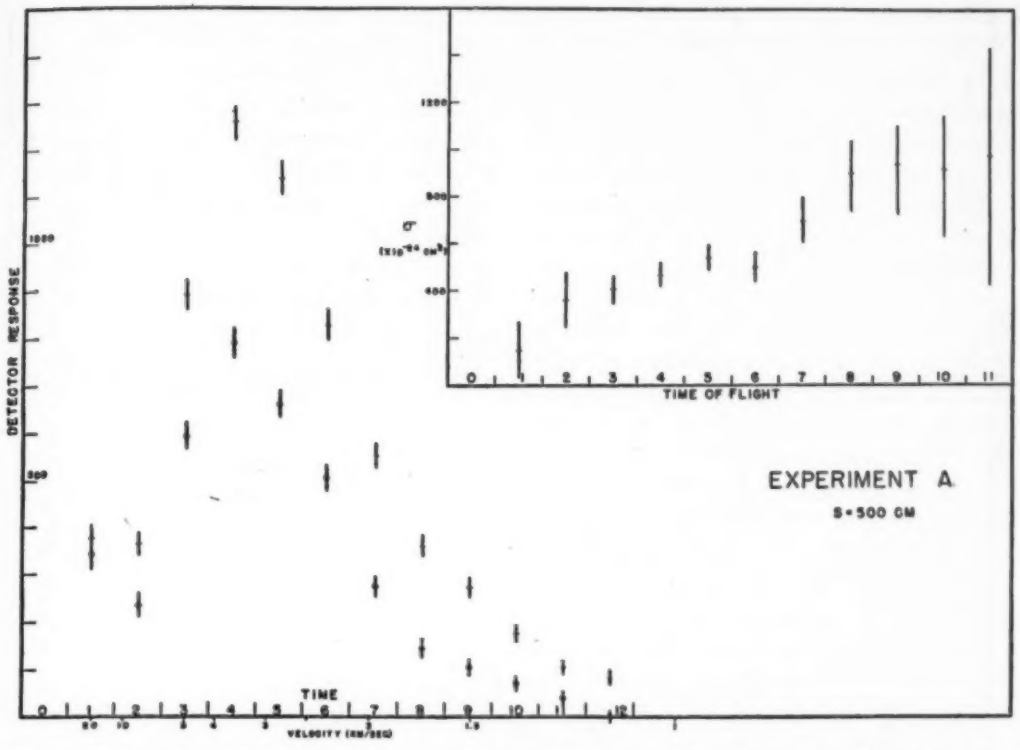

FIG. 3. Neutron time distribution curves, experiment *A*. Bars—without boron absorber; dots—with boron absorber; insert—boron cross section as a function of time of flight.

paraffin was prevented by cadmium sheet so arranged that neutrons slowed to thermal energies in the additional paraffin would be prevented from reaching the inner block. Slightly faster neutrons passing back through the cadmium and subsequently slowed in the small cube contributed to the intensity, but did not greatly increase the half-life since their time spent in the outside paraffin was as fast neutrons. The measured half-life for this arrangement was 90 μsec.

To measure the absorption coefficient of an element for slow neutron absorption, an absorber is required large enough to cover the entrance of the borax tube (Fig. 1) and of a thickness which absorbs about half the neutrons incident on it. The thickness of boron required is the order of 0.02 g/cm^2. Unfortunately it is difficult to produce a uniform, pure boron absorber of this thickness having the necessary mechanical strength. Additional materials must be used and it is desirable that they have a small interaction with slow neutrons. The materials chosen were carbon and aluminum. A space of $\frac{1}{32}$" between two aluminum sheets each $\frac{1}{32}$" thick was filled with a mixture of carbon (Dixon's No. 635 dry graphite) and B_4C (Norton Company.) The mixture was dried by heating in a vacuum and the edges of the absorber were sealed immediately after filling. Based on an analysis of 78.22 percent boron in B_4C (by engineers of the Norton Company) the absorber presented a thickness of 1.03×10^{21} boron atoms per cm^2 to the slow neutron beam.

To eliminate any effect the presence of carbon and aluminum might have on the measured cross section, a "blank" was prepared with the same thickness of carbon and aluminum as in the thin boron absorber. Comparison of measurements with this "blank" and the thin absorber should give an effect due only to the boron. The absorption in the "blank" was found to be less than 5 percent.

The shielding used was not sufficient to eliminate completely the fast neutrons which were scattered from the room. Consequently, in order to be certain that the neutrons measured came directly from the target a thick (0.5 g/cm^2) B_4C and Cd (0.45 g/cm^2) absorber was used to de-

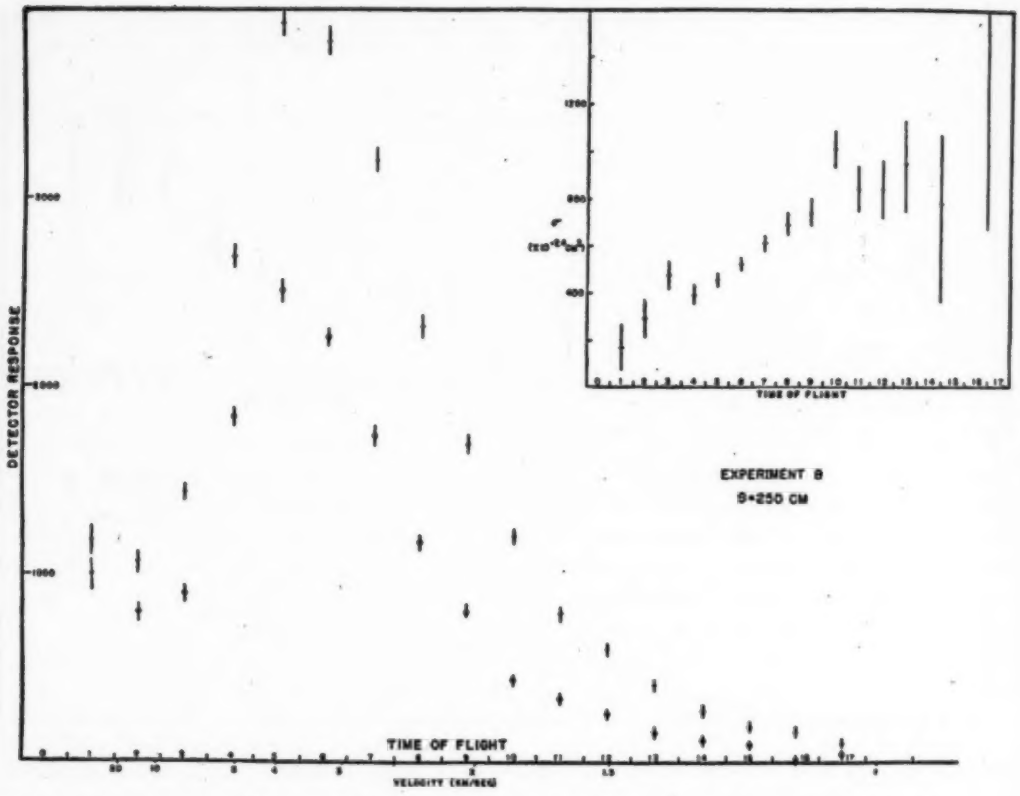

FIG. 4. Neutron time distribution, experiment *B*. Bars—without boron absorber; dots—with boron absorber; insert—boron cross section as a function of the time of flight.

termine this background as a function of time. During the first time interval this fast neutron background was found to be about 40 percent, but it decreased rapidly in successive, later time intervals. It was only 6 percent in the interval corresponding to a velocity of 5 km/sec.

Two complete experiments *A* and *B* were performed. In each case the neutron burst width Δt_1 and the time interval of observation Δt_2 were equal and adjusted to the time of flight, t, so as to give approximately the same resolution, $v/\Delta v$. The time of flight of the slowest neutrons determines the time, τ, between neutron bursts necessary to prevent carry-over of slow neutrons into the fast neutron part of the next cycle. The experiments were performed with the following arrangements in which t and $v/\Delta v$ refer to the slowest neutrons measured, those of approximately 1 km/sec.

	S	$\Delta t_1=\Delta t_2$	t	$v/\Delta v$	τ
A	500 cm	380 μsec.	6000 μsec.	15	6,700 μsec.
B	250 cm	150 μsec.	3000 μsec.	20	4,000 μsec.

It is not possible to specify the resolution accurately because of the effect of the mean life in paraffin. As an indication, since the fast neutron burst time and time of observation were equal, the time of flight divided by the burst time has been taken. This resolution is thus inversely proportional to the velocity of the neutrons being measured.

RESULTS

Figure 3, upper curve, shows the distribution of neutron counts with "blank" absorber N_0 (net) as a function of time interval; lower curve, the distribution with a thin boron absorber N_b (net) as a function of time interval, for experiment *A*. The vertical bars represent standard statistical deviations. The inset is a plot of cross section σ as a function of time interval. Figure 4 is a similar plot for experiment *B*. The velocity scales of the insets were obtained using the average $t=0$ from the center of area of the proper slow neutron time distribution at the source for each

experiment. The observations and results for intervals 1 and 2 in both experiments are not very reliable because of a comparatively low resolution and a large correction for scattered neutrons.

Remembering that the time scale is proportional to $1/v$ it is seen from the insets that, to the approximation involved in using the data directly, the $1/v$ absorption law is verified. Since, however, the method of measurement involved finite time intervals in both the emission and detection processes, more detailed calculations seemed advisable.

Let $M(t)$ be the true time distribution of neutrons arriving at the detector, the spread in time being due only to their velocity. There will also be a time distribution $f(t')$ of the emission of neutrons from the source due to delays in the slowing and escape processes. At a time T, all neutrons emitted at a time t', with a velocity v, such that $T-t'=t=S/v$ will reach the detector and be recorded as a number of counts,

$$R(T)=\int_0^T dt' f(t') M(T-t') D(T-t'), \quad (1)$$

in which $D(T-t')$ is the detector response function. However, the number of counts at the detector is observed during an interval ΔT so the points on the histograms of Figs. 3 and 4 are

$$H(T)=\int_{T-\Delta T/2}^{T+\Delta T/2} dt \int_0^T dt' f(t') M(T-t') D(T-t').$$

It is evident that $M(T-t')$ can be satisfactorily determined only if $f(t')$ is appreciable only at values of $t' \ll T$.

In order to obtain a true representation of the neutron velocity distribution, a curve has been fitted to the experimental points of N_0 (net), Fig. 4, so that the area under the curve over an interval equals the number of counts observed, thus giving $R(T)$. With the observed $f(t')$, a curve $M(t)D(t)$ has been found that satisfies (1). This curve is just the reciprocal velocity distribution seen by the detector as a function of $1/v$. It is replotted in the more usual form in Fig. 5. By anticipating that the thin boron detector obeys the $1/v$ law, we see that $D(t)$ provides just the factor necessary to change from a beam to a density so that Fig. 5 represents the distribution inside a container from which particles are escaping according to the usual kinetic theory picture. It must be recalled that this distribution pertains to neutrons passing through the carbon-aluminum blank. Since the average transmission of this blank over the entire region is more than 95 percent, and it is unlikely that any velocity-dependent interactions confined to a very narrow range exist for these elements, it is assumed that the blank has no effect on the form of the distribution.

Similar analyses were carried out for the distribution transmitted through the thin boron absorber. When the results were applied to the calculation of the cross section, however, no appreciable change was noticeable from the values plotted in the insets of Fig. 4, which indicates that resolution corrections do not affect appreciably the ratio of N_b to N_0. The data of the two experiments are combined in Fig. 6 and shown with the statistical error. This error is largest in the fast neutron end of the observed range due to high background and in the very slow neutron end because of the small number of neutrons of low velocity in the distribution. The results are consistent with the $1/v$ law for boron in this velocity range. From these data the value of K in the law $\sigma_B=K/v$ was found to be approximately 16×10^{-22} cm²-km/sec.

It has been assumed for some time that neutrons slowed by collision in hydrogenous material reach an approximate thermal equilibrium with the material. Indirect measurements of temperature effect and more direct measure-

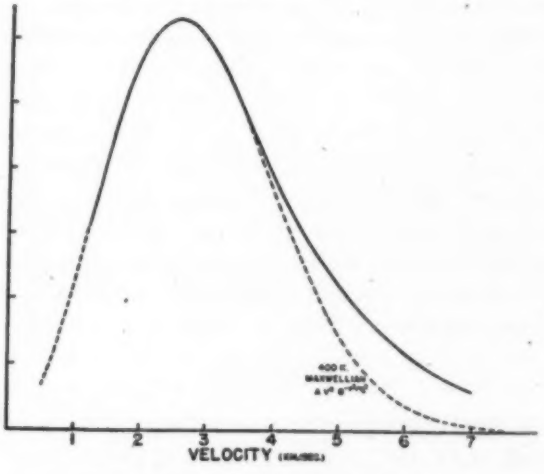

FIG. 5. Neutron velocity distribution.

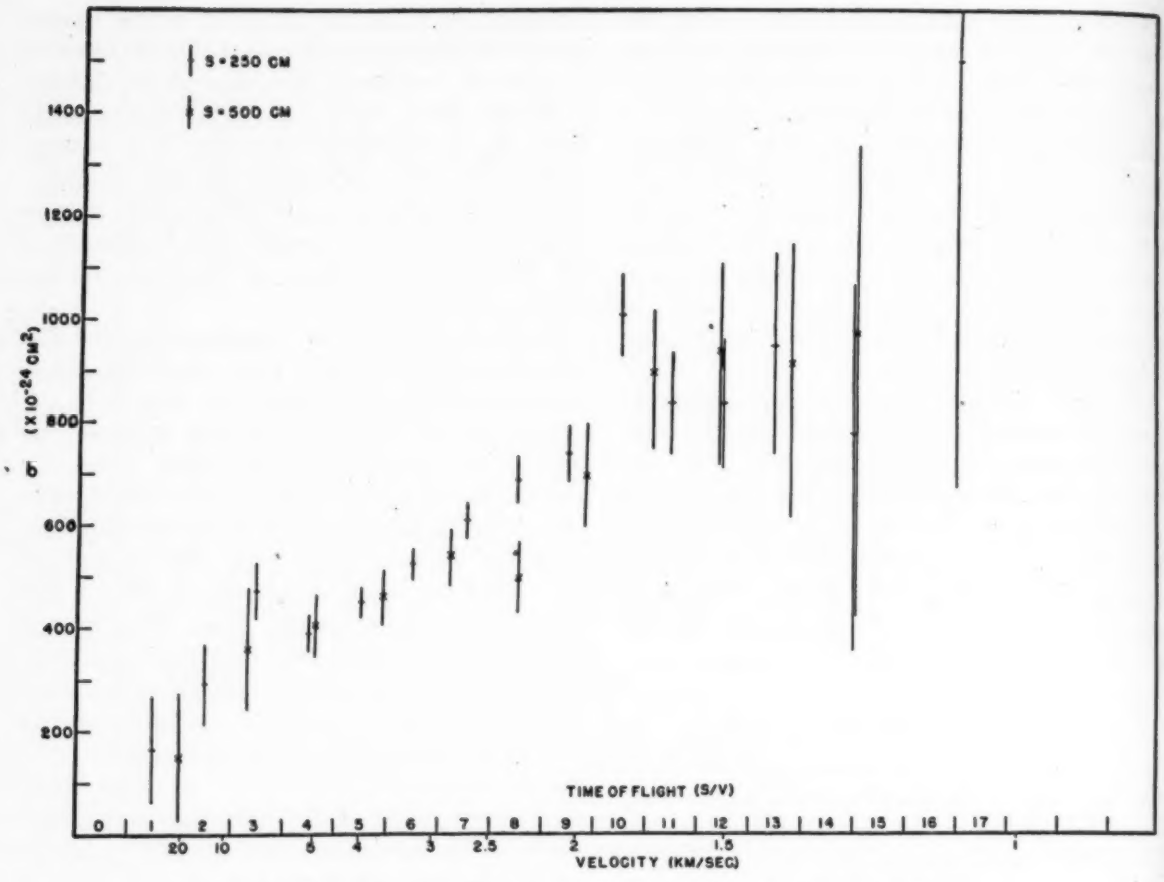

FIG. 6. Composite curve. Boron cross section as a function of time of flight.

ments[3, 5] support this assumption. Although the linear velocity plot of Fig. 5 and variable resolution make portions of the curve less reliable than others, it may still be considered as a fairly good representation of the neutron distribution obtaining to this case. The low velocity portion is most reliable and this was used in determining the temperature of a Maxwellian distribution which would provide the best fit. This is shown by the dotted line of Fig. 5 which is for a temperature of 400°K. The difference between this indicated temperature and that of the paraffin (~300°K) seems to be real, for in experiment *A* with a larger amount of paraffin the indicated temperature was 340°K.

DISCUSSION

Several checks on the results are possible. First of all, the velocity range covered in these experiments includes practically all of the C neutrons as may be seen from the cadmium transmission measurements of Baker and Bacher.[4] A check of the results may be obtained, therefore, by measurement of the C neutron transmission of the absorber used. This was found to be 58 percent in excellent agreement with the ratio $\sum N_b/\sum N_0 = 57.6$ percent obtained from the observations in each time interval. This corresponds to a C neutron cross section for boron of 540×10^{-24} cm². If $\sigma = K/v$ with $K = 16\times10^{-22}$ cm²-km/sec. adequately represents the cross section in this velocity range, the above sum may also be written as $\sum N_0 \exp(-nKx/v)/\sum N_0$. This also has the value 58 percent.

An additional check on K can be obtained from the boron absorption for resonance neutrons, rhodium for example. The data of Goldsmith and Rasetti[8] for the boron absorption coefficient and

[8] H. H. Goldsmith and F. Rasetti, Phys. Rev. **50**, 328 (1936).

the energy of the rhodium resonance, the latter checked by direct velocity measurements,[4] yield $K=10\times10^{-22}$ cm²-km/sec. Other data[9] indicate an even higher value, but all such measurements are subject to corrections which may introduce uncertainties in the absorption coefficient. It is therefore not possible to state the discrepancy is real and that a deviation from the $1/v$ law exists at larger velocities.

The effective thermal energy as would be obtained by the boron method is directly determined from the observed dependence of cross section on velocity. The C neutron transmission of 58 percent would be obtained if all the neutrons had a velocity of approximately 3 km/sec. or an energy of 0.047 ev (1.37 kT for $T=400°$K). This is considerably higher than the usual value from considering the distribution to be Maxwellian.[10]

Our experiments have given direct evidence that the slow neutron distribution from paraffin approximates a Maxwellian distribution with an excess at high velocities. Assignment of a temperature to these neutrons has no very precise meaning, not only because of the departure from an equilibrium distribution, but also because the distribution and "temperature" depend on the amount of slowing material present. Absorption measurements on boron at different neutron velocities have demonstrated the $1/v$ absorption law for this element in the velocity range from 1 to 10 km/sec.

The assistance of Mr. F. B. Berger in part of this work, and a grant from the Graduate School Research Board for equipment, are gratefully acknowledged.

[9] W. J. Horvath and E. O. Salant, Phys. Rev. 59, 154 (1941).

[10] H. A. Bethe, Rev. Mod. Phys. 9, 136 (1937), Fig. 15.

PHYSICAL REVIEW VOLUME 69, NUMBERS 9 AND 10 MAY 1 AND 15, 1946

Capture Cross Sections for Slow Neutrons

J. W. COLTMAN† AND M. GOLDHABER
Department of Physics, University of Illinois, Urbana, Illinois

(Received June 12, 1941)*

A method for measuring capture cross section for slow neutrons has been developed. Neutrons from a Ra-α-Be source are slowed down in a paraffin block containing a cylindrical cavity. A BF_3 detector in the center of the cavity measures the reduction in neutron intensity which results when an element or compound under investigation "suspended" in graphite powder is introduced into the cavity. The arrangement is calibrated with boron. The method has been used to measure the capture cross section of 19 elements. The results are tabulated at the end of the paper.

THERE have been reported recently several investigations of the capture cross sections of various elements for slow neutrons.[1–3] For a considerable number of elements, however, the capture cross sections are still unknown, and in some cases this is due to the fact that they have not been readily measurable by previous methods.

Lapointe and Rasetti have measured the capture cross sections of several elements relative to that of boron by dissolving the substances under investigation in a vessel filled with water in which neutrons were being slowed down, and noting the effect of the solute on the neutron intensity. This method is limited in sensitivity

† Now at the Westinghouse Research Laboratories, Pittsburgh, Pennsylvania.

* This paper was received for publication on the date indicated but was voluntarily withheld from publication until the end of the war.

[1] C. Lapointe and F. Rasetti, Phys. Rev. 58, 554 (1940).

[2] R. D. O'Neal and M. Goldhaber, Phys. Rev. 59, 102 (1941).

[3] F. Rasetti, Phys. Rev. 58, 869 (1940).

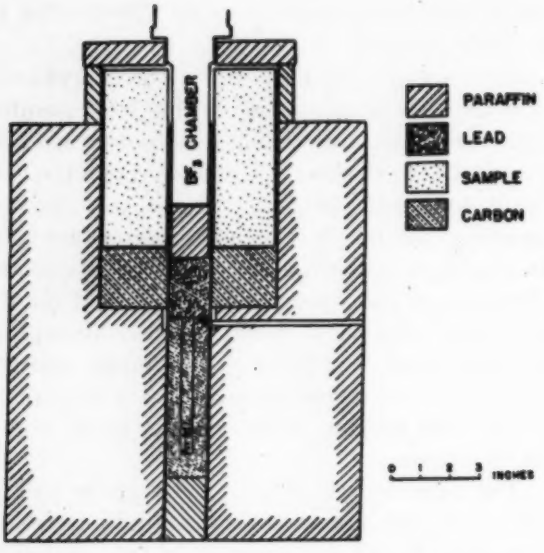

FIG. 1. Apparatus for measuring capture cross sections for slow neutrons.

by the fact that hydrogen has a capture cross section[4] of 0.3×10^{-24} cm². Consequently, cross sections $<1\times10^{-24}$ cm² are difficult to measure reliably. In the method to be described here this limitation is avoided by mixing the samples in powder form with finely divided carbon rather than dissolving them in water. The absorption cross section of carbon is known[4] to be $<0.01\times10^{-24}$ cm².

A drawing of the apparatus used is shown in Fig. 1. Neutrons from a 100-mg Ra-α-Be source were slowed down in a paraffin block containing a cylindrical cavity. The slow neutrons were detected by an ionization chamber filled with one atmosphere of boron trifluoride. The number of counts per minute in the position shown was about 4000. The carbon block beneath the sample can was introduced to help scatter away fast neutrons which might be differently affected by different substances and cause possible errors. More than 99 percent of the neutrons recorded by the BF_3 ionization chamber were found to be C neutrons.

If any absorbing material is placed in the cavity, the neutron intensity will be decreased. Because the neutrons are reflected with a relatively high efficiency at the paraffin boundaries of the cavity, a single neutron on the average traverses the sample can several times. Thus the sensitivity to capture is great, while the sensitivity to scattering is small. If the capture of slow neutrons in carbon is neglected the sensitivity of the arrangement to scattering alone can be determined simply by changing the amount of carbon in the can. This was accomplished by taking advantage of the variation in bulk density of carbon powder with grain size. Two grades of carbon were employed, a 200-mesh graphite flour and a 28–35 mesh petroleum coke. The bulk density of the graphite flour could also be changed 20 percent or more by compression. In this way the reduction in neutron intensity due to scattering was found to be approximately linear up to a carbon density of about 1 g/cm³. The decrease in intensity for 100 g of carbon in the sample can of 2.5 liter volume was found to be 6 percent of the initial intensity.

The sensitivity of the arrangement to absorption was measured by mixing weighed amounts of boron carbide with the carbon. A calibration curve was obtained by plotting the ratio of the count with the boron mixture to the count with pure carbon against the number of grams of boron in the can. This curve was approximately linear in the range investigated. A decrease of 10 percent in the counting rate was obtained for 230 milligrams of boron. The absorption sensitivity was practically the same with either 1300 g of graphite or 2250 g of petroleum coke in the can.

It was necessary to use very finely divided boron carbide to avoid "non-linear" absorption in a single grain, since the mean free path of a slow neutron in boron carbide is about 0.013 cm, and appreciable errors may be introduced unless the grain diameter is much smaller than this length. The 800-mesh boron carbide used showed some tendency to form lumps, even after careful drying, and it was found desirable to mix by hand the weighed sample of boron carbide with a small quantity of silicic acid, a fine white powder in which aggregations of the black B_4C could be readily distinguished and crushed to form an even gray mixture. The whole was then mixed with the carbon in a small machine.

The boron carbide used was a sample which had been analyzed and yielded 78.13 percent boron, very close to the theoretical value ex-

[4] O. R. Frisch, H. v. Halban, and J. Koch, Proc. Danske Vid. Sels. 15, 10 (1938).

pected from the formula B_4C. Capture cross sections were measured in the following way. A known amount of the element under investigation, or of a suitable chemical compound, was mixed well with carbon, and the counting rate determined with the mixture in the sample can. The ratio r of this counting rate to that of a "carbon equivalent of the same scattering power" was taken as a measure of the absorption. The "carbon equivalent" was calculated from the scattering cross section of the element under investigation. This cross section was either taken from previous work[5] and assigned an error of ±10 percent, or measured to about this accuracy by a determination of the total cross section of the sample used. This was particularly necessary whenever it was suspected that the samples contained sufficient water to have an appreciable effect on the scattering due to the large scattering cross section of hydrogen.

Following the procedure of Lapointe and Rasetti[1] a capture cross section $\sigma_B = 600 \times 10^{-24}$ cm² was assumed for boron.

If a ratio r is found for N atoms of a substance of unknown cross section σ in the mixture, we can calculate σ from the equation $N\sigma = N_B\sigma_B$ where N_B is the number of boron atoms which yield the same reduction r in the counting rate (as read off from the calibration curve). This procedure is meaningful only if we assume that the substance investigated follows the same absorption law for slow neutron capture as boron ($1/v$ law), and that the angular distribution of the scattered neutrons is the same for the substance and carbon. As mentioned previously, it also neglects fast neutron effects. It is probable that systematic errors of this kind were small in all the cases investigated here. All measurements were made relative to a standard sample of pure carbon to avoid errors due to gradual changes in the chamber sensitivity over long periods of time. Alternate readings on the mixture and standard were taken every twenty minutes or so. No fluctuations in the counting rate greater than statistical were apparent.

The results obtained are summarized in Table I. The errors given in the table are due to statistical errors in the counting rates and to errors in the scattering cross sections used to calculate the scattering correction.

TABLE I. Capture cross sections for slow neutrons.

Element	Compound	Weight of sample gm	Gm of carbon, equiv. in scattering to mixture	Counting rate relative to that for carbon equiv. (r)	σ $\times 10^{24}$ cm^{-2}
$_{11}$Na	NaF	469	1150	0.952	0.47 ± 0.04
$_{12}$Mg	Mg	359	1197	0.961	0.27 ± 0.02
$_{13}$Al	Al	888	1282	0.944	0.19 ± 0.01
$_{16}$S	S	1302	2216	0.850	0.35 ± 0.03
$_{17}$Cl	NaCl	26.3	2250	0.884	29 ± 2
$_{20}$Ca	CaF_2	1470	1305	0.937	0.37 ± 0.04
$_{22}$Ti	TiO_2	192	1273	0.892	5.2 ± 0.3
$_{24}$Cr	Cr_2O_3	467	1244	0.874	2.5 ± 0.05
$_{25}$Mn	Mn or MnO_2	average of 8 measurements			10.7 ± 0.2
$_{26}$Fe	Fe_2O_3	426	2349	0.907	2.05 ± 0.15
$_{28}$Ni	Ni_2O_3	150	2185	0.909	5.6 ± 0.5
$_{29}$Cu	CuO	454	2310	0.840	3.4 ± 0.3
$_{30}$Zn	Zn	673	1312	0.915	0.92 ± 0.06
$_{38}$Sr	$SrCO_3$	480	1108	0.960	1.3 ± 0.1
$_{42}$Mo	MoO_3	897	1313	0.880	2.3 ± 0.05
$_{50}$Sn	Sn	878	1303	0.963	0.53 ± 0.05
$_{51}$Sb	Sb	239	1322	0.916	4.8 ± 0.3
$_{56}$Ba	BaO	456	1220	0.964	1.3 ± 0.1
$_{82}$Pb	Pb_3O_4	1986	1327	0.981	0.23 ± 0.06

[5] M. Goldhaber and Briggs, Proc. Roy. Soc. 162, 127 (1937).

The Scattering of Neutrons by Magnesium†

R. N. LITTLE,* R. W. LONG,** AND C. E. MANDEVILLE***
The Rice Institute, Houston, Texas

(Received August 17, 1944)††

2.5-Mev neutrons from the D on D reaction were scattered through magnesium. Energies of the scattered neutrons were measured in a cloud chamber. The neutron energy spectrum showed that Mg has its lowest excited level at 1.30 Mev above the ground state. Approximate values of the elastic and inelastic scattering cross section were calculated as 1.6×10^{-24} and 0.6×10^{-24} cm², respectively.

INTRODUCTION

THE energy distribution of 2.50-Mev neutrons after scattering by magnesium has been determined. The method used was similar to that used for the scattering of neutrons by lead.[1] The inelastically scattered neutrons form a group with mean energy about 1.08 Mev.

APPARATUS

The neutrons used in the experiment were the 2.5-Mev neutrons from 0.1-Mev deuterons on a thick deuterium target in the form of heavy paraffin. The 0.1-Mev deuterons were accelerated by a Cockcroft-Walton voltage doubler and rectifier. The ion source was similar to one described by Finkelstein.[2] A vertical section of the ion source and the accelerating tube is shown in Fig. 1. In normal operation the potential drop, V_1, from the gas chamber, C, to the filament, B, was 300 volts. C and the metal cylinder D, which rests on the first accelerating electrode E, were kept at the same potential. A vertical magnetic field of 400 oersteds (at the center) was maintained along the axis of the ion source by a Helmholtz coil arrangement. The filament was a platinum ribbon $\frac{1}{8}$ inch wide, coated with a mixture of barium and strontium oxides and gave an electron emission of about 100 milliamperes at 300 volts. This voltage was not enough to produce a saturation current. The filament required 18 amperes at 4 volts for heating. Since the neutron detecting apparatus was a cloud chamber, the deuteron beam was

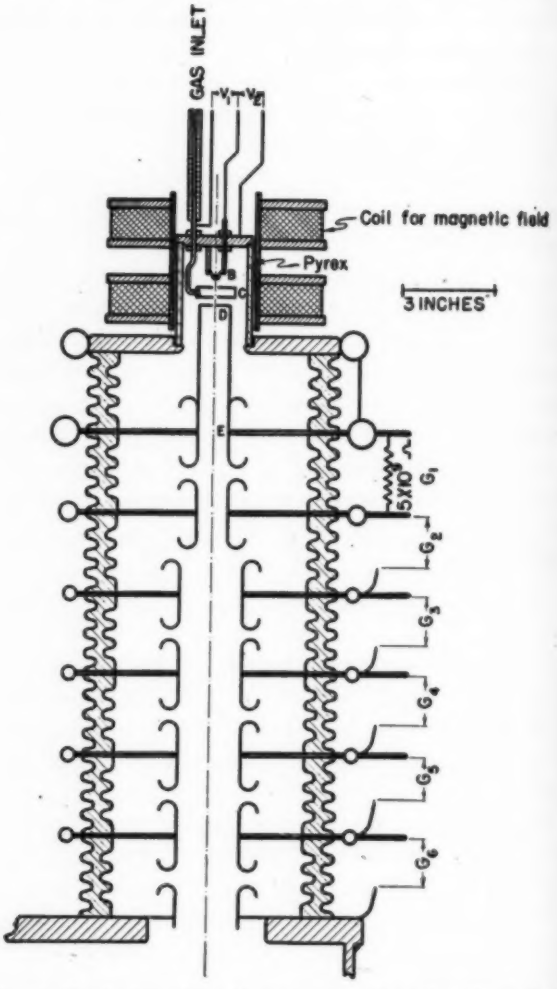

FIG. 1. Vertical section of ion source and accelerating tube.

† This paper represents a report on work submitted to the faculty of The Rice Institute in partial fulfillment of the requirements for the degree of Doctor of Philosophy for R. N. Little.

* Now at the University of Texas.

** Now with the Humble Oil and Refining Company, Houston, Texas.

*** At present at The Bartol Research Foundation of the Franklin Institute, Swarthmore, Pennsylvania.

†† This paper was received for publication on the date indicated but was voluntarily withheld from publication until the end of the war.

[1] H. F. Dunlap and R. N. Little, Phys. Rev. **60**, 693 (1941).

[2] A. T. Finkelstein, Rev. Sci. Inst. **11**, 94 (1940).

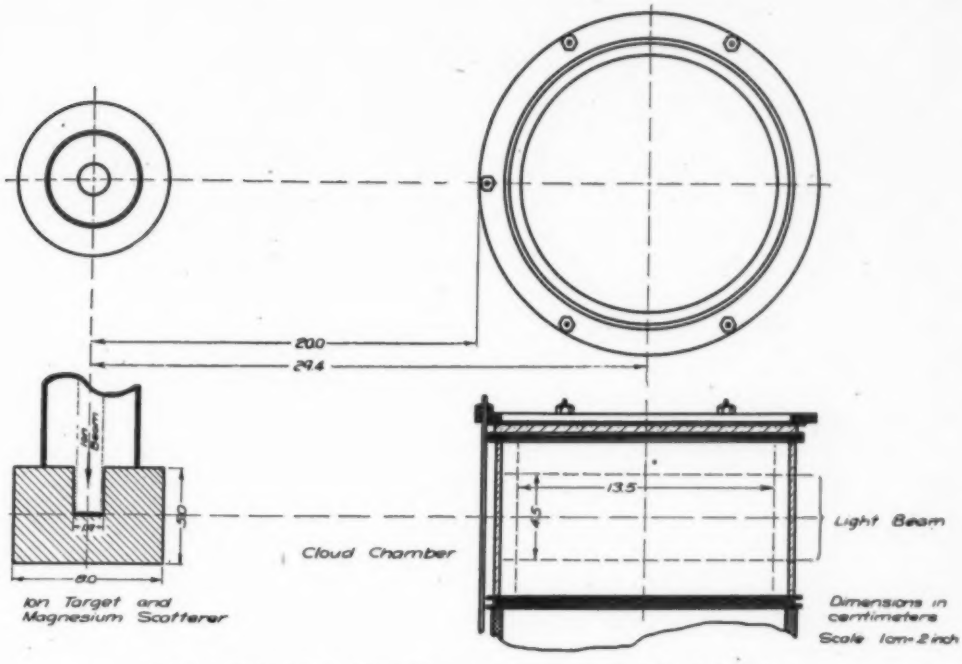

FIG. 2. Relative positions of target, scatterer, and cloud chamber.

wanted only at intervals, and the whole apparatus was controlled by an automatic timing system. The quantities which were operated intermittently to get a beam of short duration were the deuterium flow, the accelerating potential V_1 between filament and box C in the ion source, and the magnetic field. The ion source magnetic field could be left on continuously, but it was found that the deuteron current increased very much for stronger fields and a current was used in the coils which would have given overheating on continuous operation. The deuteron beam hitting the target measured between the limits of 350 to 550 microamperes.

The relative positions of the target, magnesium scatterer, and cloud chamber are shown in Fig. 2. The deuteron beam is directed vertically downward on a thick target of heavy paraffin at the center of a cylinder of magnesium. The scatterer has an average radial thickness from the center of the target of 3.88 cm.

The neutrons were detected by means of proton recoils in a cloud chamber containing ethane at atmospheric pressure as a gas and a mixture of four parts ethyl alcohol to one part water. The stopping power of this combination was found to be 1.43 by calibration with polonium alpha-particles. About 8000 stereoscopic photographs of the expansions were taken and in these pictures there were 863 tracks within 10° of a radial line from the neutron source. Both the spatial orientations and recoil track lengths were observed by reprojection of the photographs through the same camera lens system. These recoil track lengths were then used to calculate the energies of the neutrons observed.

RESULTS

The 863 recoils were grouped in length intervals of 4 mm and a tabulation made of number per interval as a function of the mean range of the intervals. Since the cloud chamber is a detector of finite extent, the probability of observation of complete tracks is greater for short recoil tracks than for long recoil tracks. A correction to compensate for this error factor was made by use of the formula

$$P=[\pi r^2-L(r^2-L^2/4)^{\frac{1}{2}}-2r^2\sin^{-1}(L/2r)]/\pi r^2,$$

where P is the ratio of the volume in which tracks of length L may start in the chamber and lie completely within the chamber to the total volume of the chamber. The radius of the chamber is r.

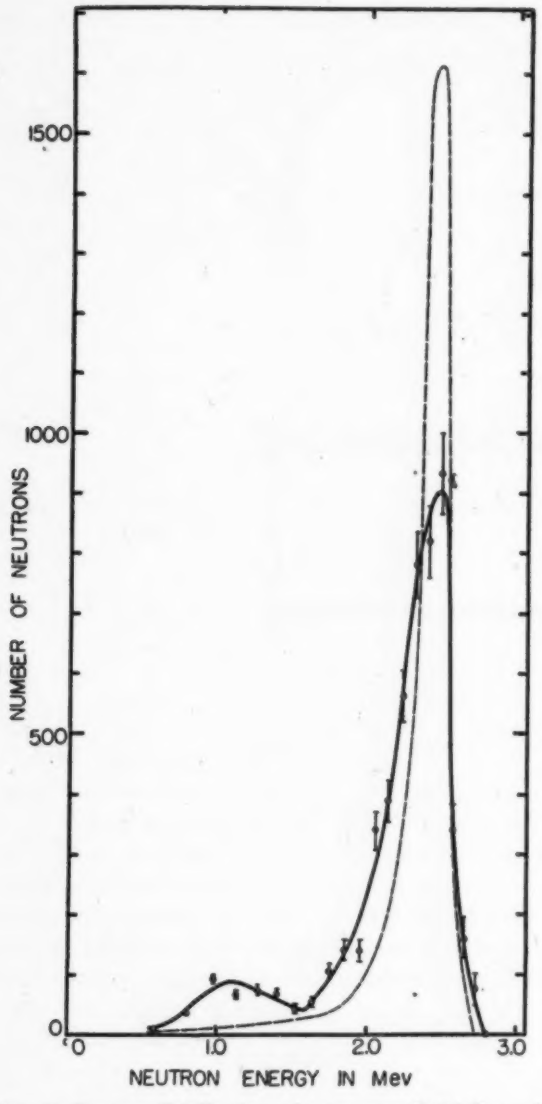

FIG. 3. Energy distribution of neutrons. Solid line with magnesium scatterer; dotted line with no scatterer.

The ranges are converted to energies by the range energy relations given by Bethe and Livingston.[3] Since each ordinate thus calculated did not cover an equal energy interval, each ordinate was divided by the width of the energy interval associated with it. A further correction for variation of neutron proton collision cross section with energy was made by means of relations given by Kittel and Breit.[4] Thus, the area under the curve drawn through the new ordinates between E_1 and E_2 represents the total number of tracks between E_1 and E_2. The curve for the 863 tracks corrected in this manner is shown in Fig. 3 as a solid line. The probable error, e, shown on an observed ordinate was calculated by means of the formula $e=0.67(n)^{\frac{1}{2}}$ where n is the number of observed tracks for that ordinate. Also plotted in Fig. 3 is a curve for the distribution of neutron energies with no scatterer. These data are shown by a dotted curve and were taken by Dunlap and Little in a previous experiment.[5] This latter curve was normalized to make the areas of the two curves equal above $E=1.55$ Mev.

There are two features of the solid curve for scattered neutrons. First, there is a group composed of neutrons direct from the source and neutrons which have been elastically scattered. This group has a most probable energy of 2.46 Mev, but its average energy is 2.36 Mev since the shape of the peak is distorted because of the presence of the elastically scattered neutrons. Second, there is a group composed of inelastically scattered neutrons with a most probable energy of 1.08 Mev. The difference between the average energy 2.36 Mev and the most probable energy 1.08 Mev is not equal to the excitation energy of the first level. Measuring proton recoils with an angle α of the forward direction introduces a difference between the most probable proton recoil energy and the mean neutron energy of $E\alpha^2/2$ where E is the most probable proton recoil energy.[6] This correction brings the mean energy of the inelastic group to 1.09 Mev and the average energy of the elastic and unscattered group to 2.40 Mev. The difference of these two energies still does not give the excitation energy because the recoil nucleus in each case has a different energy. The recoil nucleus energy is given by

$$MV^2/2=m/M(mv^2/2),$$

hence for the inelastic scattering the recoil nucleus has 0.04-Mev energy. The total kinetic energy, E, appearing with the inelastically scattered neutron is 1.13 Mev. A magnesium nucleus which has emitted a neutron of 2.40 Mev energy has a recoil energy of 0.10 Mev. However, in the group which has average energy 2.40

[3] M. S. Livingston and H. A. Bethe, Rev. Mod. Phys. **9**, 268 (1937).
[4] C. Kittel and G. Breit, Phys. Rev. **56**, 747 (1939).
[5] H. F. Dunlap and R. N. Little, Phys. Rev. **60**, 693 (1941).
[6] See reference 3, page 290.

Mev only 1000 in 3830 have been elastically scattered; hence the average recoil nucleus energy for the group as a whole is 0.03 Mev. This makes the average total energy, E^*, appearing with a neutron of the elastically scattered or unscattered group 2.43 Mev. The difference between these two total energies, E^*-E, then gives the excitation energy as 1.30 Mev. This value is to be compared with

1.37 Mev[7]
1.32 Mev[8]

from proton scattering experiments and with the energy differences

1.49 Mev[9]
1.55 Mev[10]
1.46 Mev[11]
1.38 Mev[12]
1.38 Mev[13]
1.31 Mev[14]

which were obtained from gamma-ray measurements.

Comparison of the scattered and unscattered curves (solid and dotted curves) in Fig. 3 also gives an approximate value for the elastic and inelastic scattering cross sections. The curves were normalized to have equal area for energies above 1.55 Mev since this was thought to be an upper bound on the inelastically scattered neutrons and a lower bound on the direct or elastically scattered neutrons. The area then included beneath both curves represents the number of neutrons direct from the source, whereas the number under either curve not included by the other represents the number of elastically scattered neutrons. The neutrons scattered from magnesium can thus be separated into three groups (I, E, D) of inelastically scattered neutrons, elastically scattered neutrons, and neutrons direct from the source with relative numbers.

$$1:E:D=415:1000:2830.$$

From the relations

$$I=N_0[1-\exp(-k_i nx)], \tag{1}$$

$$E=N_0[1-\exp(-k_E nx)], \tag{2}$$

$$N_0=I+E+D, \tag{3}$$

where x is the thickness of magnesium traversed in cm (3.88 cm) and n is the number of magnesium atoms per cc, the two scattering cross sections k_i and K_e can be calculated. These formulae are only approximate, for (1) and (2) assume that the cross sections are small, i.e., that the presence of the two competing scattering mechanisms does not materially affect the number of neutrons available to either scattering mechanism, and (3) assumes that as many neutrons are scattered into the detector by the scattering material which lies outside the solid angle subtended by the detector as are scattered out by the scattering material which lies within the solid angle.

On these assumptions the calculation gives

$$k_i=0.6\times10^{-24}\ \text{cm}^2,$$

$$k_E=1.6\times10^{-24}\ \text{cm}^2,$$

with a ratio

$$k_E/k_i=2.6.$$

In addition to the obvious inaccuracies in the method for resolving the direct and elastically scattered group, it should be pointed out that the correction factors are more critical for the cross section calculation than for the determination of the excited energy level. As can be seen from the probable errors on the solid curve in Fig. 3, the correction factors are larger for the higher energies. If these were in error, the effect on the location of the most probable energy would be very small, whereas a comparison of the heights of two peaks on the curve would be more greatly affected.

In conclusion, we wish to thank Professor H. A. Wilson, Professor C. W. Heaps, and Dr. W. E. Bennett for their interest and suggestions in this work.

[7] T. R. Wilkins, Phys. Rev. **60**, 365 (1941).
[8] R. H. Dicke and John Marshall, Jr., Phys. Rev. **63**, 86 (1943).
[9] C. Kikuchi *et al.*, Proc. Phys. Math. Soc. Japan **21**, 260 (1939).
[10] C. Kikuchi *et al.*, Proc. Phys. Math. Soc. Japan **21**, 381 (1939).
[11] Curran, Dee, and Strothers, Proc. Roy. Soc. **A175**, 546 (1940).
[12] J. Itoh, Proc. Phys. Math. Soc. Japan **23**, 605 (1941).
[13] Elliott, Deutsch, and Roberts, Phys. Rev. **61**, 99 (1942).
[14] C. E. Mandeville, Phys. Rev. **62**, 309 (1942).

The Yield Function and Angular Distribution of the D+D Neutrons

W. E. BENNETT, C. E. MANDEVILLE, AND H. T. RICHARDS
The Rice Institute, Houston, Texas

(Received September 18, 1942)*

The thin target yield of neutrons from the D+D reaction has been measured for deuteron energies 0.5–1.8 Mev. The neutron yield in the forward direction increases smoothly throughout the interval, but the yield at 80° to the bombarding beam remains almost constant. Values of A in the expression $(1+A\cos^2\theta)$ representing the angular distribution of the neutrons in the c.g. system are calculated from the yield data and plotted as a function of voltage. A is found to increase from 1.8 at 0.5 Mev deuteron energy to 3.4 at 1.8 Mev.

THE yield of neutrons from the D+D reaction has been measured at low voltages in a number of experiments. The yield curve was extended to 300 kev by Roberts[1] and to 1 Mev by Amaldi, Hafstad, and Tuve.[2] Thick targets were used in both experiments. Thin target yields can be calculated from the thick target data, as was done by Reddemann,[3] by differentiating the curve and correcting for variation of the rate of energy loss of the deuterons in the target material. The results are less accurate than thin target data taken directly.

Closely connected with the measurement of the number of neutrons from the D+D reaction is the variation of yield with angle. For example, the results of Roberts were taken in the forward direction, but they could be corrected to give total neutron yields if the variation of angular asymmetry with voltage were known. Kempton, Browne, and Maasdorp[4] have shown that in the center of gravity coordinate system the yield at low voltages in the forward direction is $\frac{3}{2}$ the yield at 90° to the bombarding beam. At higher bombarding voltages this ratio increases. Richards[5] found the yield at 0° to be 2.8 times the yield at 90° for a bombarding voltage of 0.7 Mev.

The production of protons by the D+D reaction is believed to be a very similar process to the production of neutrons.[6] The absolute yields of the two kinds of particles are approximately the same.[7] The variation of yield with voltage is very similar,[1] and the angular asymmetry is the same at corresponding voltages.[4] It has been shown[8,9] that the angular distribution of protons can be represented by the expression $(1+A\cos^2\theta)$, where θ is the angle in the coordinate system in which the center of gravity is at rest and A is a constant which may, however, vary with voltage. A has been found to increase with voltage up to 400 kev.[10] It is highly probable that the angular distribution of neutrons can be represented by the same expression.

Myers[6] has obtained a theoretical value for A which is in reasonable agreement with the experimental values at 100 kev. The agreement confirms the view that the intermediate nucleus formed by the coalesence of two deuterons is in a P state. Feenberg[11] has given reasons to expect an excited P state of the alpha-particle at about the dissociation energy.

The present experiment was undertaken to measure the variation of the yield of neutrons with bombarding voltage when thin targets were used. It was also desired to measure the dependence of the angular asymmetry upon voltage. Such measurements might be expected to give evidence of excited states in the alpha-particle, particularly of the level predicted by Feenberg.[11]

* This paper was received for publication on the date indicated but was voluntarily withheld from publication until the end of the war.

[1] R. B. Roberts, Phys. Rev. **51**, 810 (1937).
[2] E. Amaldi, L. R. Hafstad, and M. A. Tuve, Phys. Rev. **51**, 896 (1937).
[3] H. Reddemann, Zeits. f. Physik **110**, 373 (1938).
[4] A. E. Kempton, B. C. Browne, and R. Maasdorp, Proc. Roy. Soc. **A157**, 386 (1936).
[5] H. T. Richards, Phys. Rev. **60**, 167A (1941).
[6] R. B. Myers, Phys. Rev. **54**, 361 (1938).
[7] R. Ladenburg and M. H. Kanner, Phys. Rev. **52**, 911 (1937).
[8] R. O. Haxby, J. S. Allen, and J. H. Williams, Phys. Rev. **55**, 140 (1939).
[9] H. Neuert, Ann. d. Physik **36**, 437 (1939).
[10] R. D. Huntoon, A. Ellett, D. S. Bayley, and J. A. Van Allen, Phys. Rev. **58**, 97 (1940).
[11] E. Feenberg, Phys. Rev. **49**, 328 (1936).

EXPERIMENTAL ARRANGEMENT

The Rice Institute pressure Van de Graaff electrostatic generator was used to obtain beams of deuterons up to 2.2 Mev in energy. The accelerating voltage was measured by an electrostatic voltmeter, the measurements being reproducible to one-half of one percent. The voltmeter was calibrated against the Wisconsin voltage measurements from the published values[12] of the gamma-ray resonances of fluorine bombarded by protons, particularly the resonance at 1.363 Mev. The atomic beam was deflected through 90° in the magnetic analyzer in such a way that the target and detecting devices were shielded from radiation from the high voltage apparatus by a concrete wall one foot thick. A schematic diagram of this arrangement is shown in Fig. 1 of a previous paper.[13] The deuteron beam on the target was measured by a current integrator of the neon discharge type.[14]

The target was deuterium gas. The gas chamber is illustrated in Fig. 1. It was 2.6 cm deep and was separated from the vacuum system by an aluminum foil. The deuteron beam was reduced in energy by passing through this foil which was 1.40 mg/cm² in thickness. It was supported by microphone screening with a transmission coefficient of 20 percent.

A Wulf bifilar type electroscope was used to detect neutrons by measuring the ionization produced in methane by recoil protons. The electroscope was cylindrical in shape, 3 in. inside diameter and 4 in. long. Its walls were of one-half inch thick iron. The two silvered quartz fibers were 0.01 mm in diameter, and they were repelled by charging them to 360 volts. The electric field was, therefore, not great enough to collect ions very efficiently except in the immediate neighborhood of the fibers. This restriction of the sensitive region meant that neutrons were measured at fairly sharply defined angles since the electroscope fibers were 16.6 cm from the center of the gas target. Wall effects in the neutron detector were eliminated by filling the electroscope with 300 lb. pressure of methane (13 percent ethane). The resultant stopping power limited the range of the highest energy recoil protons to 1.7 cm which range was less than the distance from the wall to the most sensitive region.

There may be some question as to whether the ionization currents as measured in the electroscope were proportional to the actual ionization when the conditions were so far from saturation. The electroscope was checked with two radium sources and the extreme variation from linearity was less than 5 percent over the range used. Should it be worse for ionization by protons, the chief effect would be to make our values for angular asymmetry slightly too small.

RESULTS

Ionization was measured as a function of voltage at 0° and at 80° to the direction of the bombarding beam. In both directions the distance from the middle of the gas chamber to the near wall of the electroscope was 11.57 cm. Measurements were taken at 80° instead of 90° so that the correction to 90° in the center of gravity coordinate system would be small.

The aluminum foil and the carbon deposited on the foil and in the microphone screening gave a considerable yield of neutrons when bombarded by deuterons. To correct for this, a definite procedure was adopted. Deuterium gas was let into the target chamber and its pressure was read on a Bourdon gauge. Several measurements were made of the total ionization during bombardment. The gas was then pumped out, and the background was measured immediately. The net effect was divided by the pressure of deuterium.

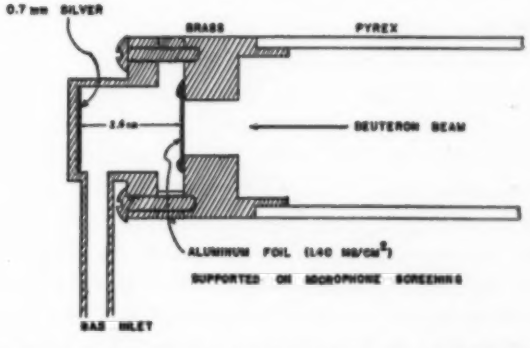

FIG. 1. Diagram of the deuterium gas target. The neutron detector was 16.6 cm from the middle of the gas chamber.

[12] E. J. Bernet, R. G. Herb, and D. B. Parkinson, Phys. Rev. **54**, 398 (1938).
[13] W. E. Bennett, T. W. Bonner, E. Hudspeth, H. T. Richards, and B. E. Watt, Phys. Rev. **59**, 781 (1941).
[14] B. E. Watt, Rev. Sci. Inst. **12**, 362 (1941).

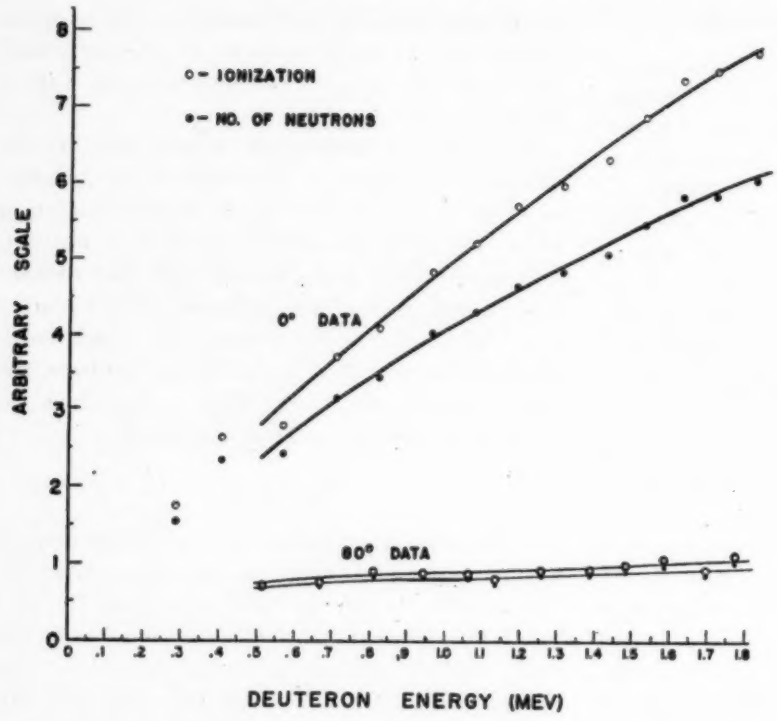

FIG. 2. Experimental yield data. The open circles refer to the ionization produced by recoil protons in a methane filled electroscope. The solid circles represent the number of neutrons per unit solid angle in room coordinates. The number of neutrons was obtained by dividing the ionization effects by the neutron energy and then correcting for the $n-p$ scattering cross section. The deuteron energy is the mean energy of the beam in the gas target.

Pressures of the order of 10 inches of mercury were used in taking the 0° data and the low energy data at 80°. At higher voltages the target thickness was made twice as great to increase the effect from deuterium as compared to the background. The high background was the chief limitation on the accuracy of the results, since at 0° it became equal to the effect from deuterium at the highest voltages, and at 80° it became three times greater. However, the results are believed to be accurate to 2 percent at 0° and to 5 percent at 80°. This mean error was estimated from the reproducibility of several values which were repeated a number of times. All points were checked at least once.

The deuterium gas supplied by the Stuart Oxygen Company was known not to be pure; when it was used in an ion source, the proton beam was of the order of 10 percent of the deuteron beam. Its density was found to be 6 percent higher than expected for pure gas. If the heavy impurity was air, it amounted to 2 percent by volume. A gas analysis showed the presence of oxygen and nitrogen in the proportions of air and amounting to 3 percent by volume. The neutron yield from atmospheric air was 9.5 times the yield from a corresponding pressure of deuterium at 80° and 1.7-Mev bombarding energy. To eliminate this large source of error, the deuterium gas was purified by passing it over hot magnesium on the way to the target chamber. To verify that the air was removed quantitatively, additional air was introduced, and its removal was checked on the electroscope. No magnesium was used when the 0° data were obtained, but measurements were taken at several voltages with air in the target chamber, and the 0° data were corrected on the basis of 2.5 percent air in our deuterium. These corrections amounted to less than 4 percent.

The final results for ionization as a function of voltage are plotted in Fig. 2. The voltage recorded is the mean energy of the deuteron beam as it passed through the deuterium gas of the target. This was obtained from the accelerating voltage by subtracting the loss of energy of the deuterons in the aluminum foil and half the energy loss in the deuterium target. The range-energy relation for protons in aluminum obtained by Parkinson, Herb, Bellamy, and Hudson[15] was used with the usual assumption that a deuteron has twice the range of a proton of half the energy. The stopping

[15] D. B. Parkinson, R. G. Herb, J. C. Bellamy, and C. M. Hudson, Phys. Rev. **52**, 75 (1937).

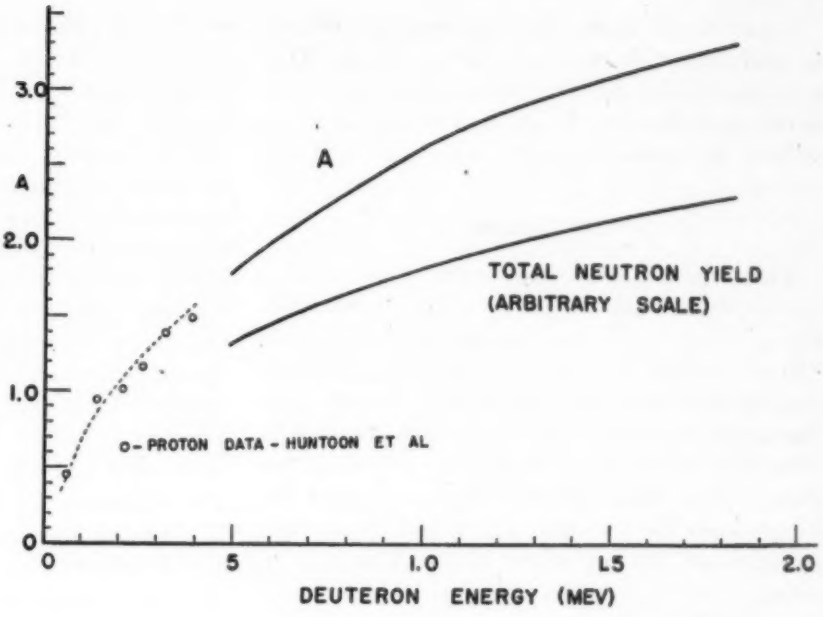

FIG. 3. Variation with voltage of the asymmetry in angular distribution of the neutrons. A is the coefficient of the $\cos^2\theta$ term in the expression for the angular distribution of the neutrons in the c.g. system: $N(\theta)=B(1+A\cos^2\theta)$. The total neutron yield is calculated from the yield at 0° on the assumption that the angular distribution of the neutrons is given by the above expression.

power of deuterium was taken from the data for hydrogen given by Livingston and Bethe.[16]

Figure 2 also shows the yield of neutrons as a function of voltage. To obtain this, the amount of ionization was divided by the energy of a neutron from the D+D reaction at the appropriate voltage and angle, and by the cross section for collision between a neutron of that energy and a hydrogen nucleus. The simplest expression[17] for the cross section (but with $\epsilon'=0.12$ Mev) was considered adequate over the limited range used. The neutron yield given in Fig. 2 will be useful in other experiments where the D+D reaction is used as a thin target source of neutrons.

The yield of neutrons at 80° is so small that an appreciable part of the measured yield might be neutrons produced in the forward and backward direction but scattered toward the electroscope by materials in the room. To check this, the inverse square law was tested in the 80° direction and the result showed that 95 percent of the net effect in the electroscope was produced by radiation from the target itself.

If the angular distribution of neutrons in the center of gravity coordinate system is represented by the expression $B(1+A\cos^2\theta)$, then it is possible to calculate A as a function of voltage from the smoothed curves given in Fig. 2. The neutron yields were first transformed into the center of gravity coordinate system by multiplying by the ratio of the solid angle in the c.g. system to the solid angle in room coordinates,

$$\frac{\sin\theta' d\theta'}{\sin\theta d\theta}=\frac{E_d^{\frac{1}{2}}\cos\theta[6Q+3E_d-E_d\sin^2\theta]^{\frac{1}{2}}+3Q+2E_d-E_d\sin^2\theta}{[\frac{3}{2}(Q+\frac{1}{2}E_d)(6Q+3E_d-E_d\sin^2\theta)]^{\frac{1}{2}}},$$

where θ' and θ refer to the angle in the c.g. system and room coordinates respectively, E_d is the energy of the bombarding deuterons, and $Q=3.31$ Mev.[18] The angle zero is the same in both coordinate systems but the angle 80° in room coordinates becomes an angle in the c.g. system which is a function of bombarding voltage,

$$\cos\theta'=\frac{V_n\cos\theta-\frac{1}{2}E_d^{\frac{1}{2}}}{[\frac{3}{2}(Q+\frac{1}{2}E_d)]^{\frac{1}{2}}},$$

where V_n is the velocity of the neutron in room coordinates. Figure 3 shows the values of A thus calculated from the neutron yield curves of Fig. 2. For comparison the values of A for protons[10] are plotted on the same figure.

[16] M. S. Livingston and H. A. Bethe, Rev. Mod. Phys. **9**, 274 (1937).
[17] H. A. Bethe and R. F. Bacher, Rev. Mod. Phys. **8**, 117 (1937).
[18] T. W. Bonner, Phys. Rev. **59**, 237 (1941).

Figure 3 also shows the total neutron yield on an arbitrary scale as a function of voltage. This was obtained by dividing the neutron yield at 0° in the c.g. system by $(1+A/3)$. The total neutron yield is, of course, the same in either coordinate system.

DISCUSSION

The targets in these experiments were "thin." For the 0° data the loss of energy by the deuteron beam in passing through the target varied from 230 kev at 0.56 Mev deuteron energy to 110 kev at 1.83 Mev deuteron energy. For the 80° data the target thickness varied from 320 kev at 0.52 Mev deuteron energy to 180 kev at 1.83 deuteron energy. The aluminum foil which separated the target from the vacuum system had an average thickness of 260 kev at the highest bombarding energy and was of course thicker at lower energies. These thin foils are known to be rather non-uniform; it was, in fact, difficult to find a square centimeter of it which did not have visible holes. This non-uniformity made the incident beam heterogeneous in energy and added quite appreciably to the effective thickness of the target at low energies. For this reason, points below 0.5 Mev on the 80° data were thrown out because they were apt to be low if the yield at 80° turns sharply down at lower voltages.

Reddemann's calculations[3] of the thin target yields from the thick target data of Amaldi, Hafstad, and Tuve[2] do not agree with our results. He finds that the yield is constant or decreases slightly with increase of voltage between 0.5 and 1.0 Mev while we find a 40 percent increase in total yield. This difference is not in the right direction to be caused by the non-spherically symmetric distribution of thermal neutrons in the water tank used by Amaldi, Hafstad, and Tuve. However, the discrepancy could be caused by rather small experimental errors in the thick target curve, and it is probable that calculations of the type performed by Reddemann are not justified by the accuracy of the data.

The smooth juncture of the values of A for protons and for neutrons, shown on Fig. 3, is further evidence that these two particles are produced in similar processes. The early conclusion[4] that A for neutrons was not a function of voltage led to theoretical difficulties outlined by Schiff[19] which are now clearly removed. We can conclude that the yield curve for the D+D reaction gives evidence concerning a P state of the alpha-particle. The middle of the resonance seems to be at higher bombarding energies than we have attained, but the total yield and the value of A seem to be approaching a maximum. The maximum value of A would be greater than 3.5 and this does not agree with the values 1 and 21/13 calculated by Myers[6] for states $J=1$ and $J=2$ of the compound nucleus. The disagreement could be connected with a breakdown of the Bohr picture for a nucleus containing only four particles. The breadth of the resonance estimated from our curve would not be less than 1.5 Mev in the c.g. system and the half-life of the intermediate nucleus must therefore be less than 4×10^{-22} sec. This is only twice as great as the time required for the emerging neutron to travel across the compound nucleus. If there is much sharing of energy between the particles, it must again be rather quickly concentrated on one particle.

ACKNOWLEDGMENTS

We are indebted to Professor T. W. Bonner and Mr. Bob E. Watt who collaborated in the early part of this experiment. We wish also to thank Professor H. A. Wilson for helpful discussions, and Dr. K. C. ten Brink of the Department of Chemistry for performing the analysis of the deuterium gas.

[19] L. I. Schiff, Phys. Rev. **51**, 783 (1937).

On the Theory of the Slowing Down of Neutrons in Heavy Substances[1]

G. PLACZEK
Cornell University, Ithaca, New York
(Received July 31, 1940)*

The rigorous solution of the integral equation for the stationary energy distribution in the case of slowing down without capture is given. Its relation to the average energy loss is discussed (Sections 1, 2). In Section 3, the problem of mixtures is treated. It is shown, in particular, that for mixtures of a light and a heavy substance concentrations exist for which the energy distribution is at the beginning entirely determined by the energy loss in the heavy substance and at the end by the energy loss in the light substance. The effects of capture are discussed in Sections 4–6. It is shown that the solution assumes a simpler form if the ratio of the mean free paths for scattering and capture varies slowly over energy regions of the order of the average energy loss. The case of $1/v$—capture is treated in detail (Section 5); rapidly varying capture is discussed in Section 6. In Section 7, a simplified treatment, based on the concept of neutron age, is given, and its limitations are discussed. Section 8 contains the discussion of the effects of the chemical binding on the energy distribution. An expression for the mean square distance of diffusion and its mass dependence is derived (Section 9).

THE process of slowing down neutrons by elastic collisions has been studied chiefly in hydrogeneous substances[2–4] where the protons, because of their large scattering cross section, are the chief agents for slowing down. However, for a number of problems, such as the production of small energy changes for the investigation of nuclear energy levels,[5–7] as well as the study of the diffusion in the atmosphere of neutrons, produced by the cosmic radiation,[8] the knowledge of the energy distribution of neutrons slowed down by collisions with nuclei of higher mass is essential. An expression for the distribution in energy of neutrons which have suffered a given number of collisions has been given by Condon and Breit.[9] In the present paper the derivation of the general energy distribution with and without capture will be attempted.

1. The Integral Equation of the Slowing Down Process

We consider a homogeneous medium of infinite extension in which per second Q neutrons of energy E_0 are produced. The energy of these neutrons is changed by collisions. We ask for the stationary energy distribution. So long as we are not interested in the spatial distribution of the neutrons, the distribution of the sources in space is immaterial. We will first suppose that no capture of neutrons occurs. If we measure the energy by $x=E_0/E$, and use for convenience a logarithmic energy scale, we may write for the number of neutrons between $\log x$ and $\log x+d(\log x)$:

$$\rho(x)dx/x=Q[l(v)/v]K(x)dx/x. \qquad (1)$$

Introduction of the quantity $K(x)$ defined by Eq. (1) considerably simplifies the following analysis. In (1), v represents velocity; $l(v)$, mean free path for scattering. $l(v)/v$ is the lifetime of a neutron of velocity v against a scattering collision. The quantity $K(x)(dx/x)$ represents the average number of collisions a neutron experiences in the interval between $\log x$ and $\log x+d\log x$.

We further denote by $k(x, x')dx/x$ the chance that a neutron shall be in the interval dx after one collision, if its energy before the collision was E_0/x'. The function $k(x, x')dx/x$ will depend on the interaction. For its integral we have

$$\int_0^\infty k(x, x')dx/x=1.$$

* This paper was received for publication on the date indicated but was voluntarily withheld from publication until the end of the war.

[1] Part of the results has been presented at the 1939 Washington meeting of the American Physical Society, cf. Phys. Rev. 55, 1130 (1939).

[2] E. Amaldi and E. Fermi, Phys. Rev. 50, 899 (1936).

[3] E. Fermi, *Zeeman Verhandelingen* (s-Gravenhage, M. Nijhoff, 1935), p. 128.

[4] E. Fermi, Ricerca Scient. [2] 7, 13 (1936).

[5] B. Pontecorvo and G. C. Wick, Ricerca Scient. [1] 7, 134, 220 (1936).

[6] E. Fermi and F. Rasetti, Ricerca Scient. 9, 472 (1938).

[7] J. Hornborstel and F. A. Valente, Phys. Rev. 55, 108 (1939).

[8] H. A. Bethe, S. A. Korff, and G. Placzek, Phys. Rev. 57, 573 (1940).

[9] E. U. Condon and G. Breit, Phys. Rev. 49, 229 (1936).

Under stationary conditions the number of collisions in an interval dx/x must be equal to the number of collisions which bring a neutron into this interval. The number of collisions which bring a neutron from the interval dx'/x' into the interval dx/x is

$$K(x')k(x, x')(dx/x)(dx'/x').$$

Therefore we get as condition for a stationary distribution:

$$K(x)=k(x, 1)+\int_0^\infty K(x')k(x, x')dx'/x'. \quad (2)$$

The first term on the right-hand side takes care of the neutrons which reach the interval dx/x directly in one collision from the source.

If the collision is always connected with a loss in energy, we may narrow the limits of the integral in (2), writing

$$K(x)=k(x, 1)+\int_1^x K(x')k(x, x')dx'/x'. \quad (2a)$$

If capture occurs, it has to be accounted for by multiplying the collision function $k(x, x')$ with the relative probability of scattering, *viz.*, $f(x')=l(x')/l_s(x')$, where l is the total mean free path (for capture and scattering) and l_s the mean free path for scattering alone:

$$K(x)=f(1)k(x, 1)+\int_1^x f(x')K(x')k(x, x')dx'/x'. \quad (3)$$

$K(x)dx/x$ remains the average number of collisions in the interval dx/x, which may now be of either the scattering or capturing type. (1) remains unchanged if we understand by l the total mean free path.

I. SLOWING DOWN WITHOUT CAPTURE

2. Substances Containing a Single Type of Nuclei Only

(A) *Protons*

If the neutron energy is large compared to the vibration quanta of bound protons ($\sim\frac{1}{3}$ ev) the protons can be considered free and at rest. In this case the energy distribution after one collision is constant in the energy scale, which gives:

$$k(x, x')=\begin{cases} x'/x & \text{for } x>x' \\ 0 & \text{for } x<x', \end{cases} \quad (4)$$

so that (2a) becomes:

$$K(x)=\frac{1}{x}\left\{1+\int_1^x K(x')dx'\right\}. \quad (5)$$

(5) is solved by $K(x)=1$, which, introduced into (1), gives Fermi's[7, 8] well-known result.

(B) *Nuclei of Atomic Weight M*

For free nuclei initially at rest and an angular distribution of the scattered neutrons spherical in the center of gravity system, the energy distribution after one collision is again constant in the energy scale, but extends now only from E_0 to pE_0, where

$$p=(M-1/M+1)^2. \quad (6)$$

This gives

$$k(x, x')=\begin{cases} \dfrac{1}{1-p}\dfrac{x'}{x} & \text{for } px<x'<x \\ 0 & \text{for } x'/p<x \text{ and } x'>x, \end{cases} \quad (7)$$

and

$$K(x)=\frac{1}{(1-p)x}\left\{1+\int_1^x K(x')dx'\right\} \quad \text{for } 1<x<p^{-1}, \quad (8a)$$

$$K(x)=\frac{1}{(1-p)x}\int_{px}^x K(x')dx' \quad \text{for } x>p^{-1}. \quad (8b)$$

(8a) can be solved directly; its solution is

$$K_0(x)=\frac{1}{1-p}x^{p/(1-p)}. \quad (9)$$

The solution of (8b) is a function of x which is equal to its own mean value in the interval between px and x. If (8b) were valid for all values of x, its only solution would obviously be $K=\text{const}$. We shall see in the following that this is the asymptotic solution of (8b) for large x. Furthermore, we see from (8a, b) that K is discontinuous for $x=p^{-1}$; indeed we have

$$K_1(p^{-1})-K_0(p^{-1})=-p/(1-p)$$

and hence from (9):

$$K_1(p^{-1})=\frac{p}{1-p}(p^{-1/(1-p)}-1). \quad (10)$$

The physical meaning of this discontinuity is, of course, that for values of x larger than p^{-1} the

neutrons can no longer enter the energy interval directly from the source.

In order to solve (8b), we shall make use of a substitution which will map the region of the variable x between 1 and ∞ on the interval between 1 and $1/p$. We call $K_n(x)$ the solution of (8b) for values of $p^{-n} \leqslant x \leqslant p^{-(n+1)}$, introduce the variable

$$z = \frac{p^{1/(1-p)}}{1-p} \log p^n x \tag{11}$$

which varies between $z=0$ for $x=p^{-n}$ and

$$z = p^{1/(1-p)} \log p^{-1/(1-p)} = \zeta \tag{11a}$$

for $x=p^{-(n+1)}$, and put

$$K_n(x) = K_0(x) J_n(z). \tag{12}$$

Substituting (11) and (12) into (8b) we get

$$J_n(z) = J_n(0) - \int_0^z J_{n-1}(z')dz' \quad \text{for } n>0, \qquad J_0(z) = 1 \tag{13}$$

and by recurrent application of (13)

$$J_n(z) = \sum_{m=0}^{n} J_{n-m}(0) \frac{(-z)^m}{m!}. \tag{14}$$

(14) expresses the value of the function we look for in terms of its values at the edges of the intervals. We have now to determine the latter values. We see from (8a, b) that K is continuous except for $x=p^{-1}$. Hence we have

$$J_n(0) = J_{n-1}(\zeta) \quad \text{for } n>1, \tag{15}$$

and because of (10)

$$J_1(0) = J_0(\zeta) - p^{1/(1-p)} = 1 - p^{1/(1-p)}. \tag{16}$$

We write now (14) for $z=\zeta$ and introduce (15) into it. This gives

$$J_{n-1}(\zeta) = J_n(0) = \sum_{m=0}^{n-1} J_{n-m-1}(0) \frac{(-\zeta)^m}{m!} \quad \text{for } n>1. \tag{17}$$

From (16) and (17) we can now determine $J_n(0)$ by iteration. The result is

$$J_n(0) = A_n(\zeta) - p^{1/(1-p)} A_{n-1}(\zeta), \tag{18}$$

$$A_n(\zeta) = \sum_{m=0}^{n-1} (m-n)^m \frac{\zeta^m}{m!}, \qquad A_0(\zeta) = 1, \quad A_{-1}(\zeta) = 0. \tag{18a}$$

Equation (18) together with (14), (13), and (9) contains the complete solution of the integral Eq. (8a, b). We shall first investigate its asymptotic behavior. As shown in Appendix I, the polynomial $A_n(\zeta)$ has for large n the asymptotic value

$$A_{n\,as}(\zeta) = \frac{v_1^n}{1+\log v_1} + \frac{v_2^n}{1+\log v_2}, \tag{19}$$

where v_1 and v_2 are the two roots of the equation

$$-v \log v = \zeta, \tag{20}$$

which for $\zeta \to 0$ go to 0 and 1, respectively. From the definition (11a) of ζ, we see that

$$v_1 = p^{1/(1-p)}. \tag{21}$$

Now we have to find v_2. In general, it is not easy to find v_2 from v_1 (see Section 3). In the present case, however, it is possible. The result is:

$$v_2 = p^{p/(1-p)}. \tag{22}$$

From (21) and (22) one also gets the relation

$$v_2 = v_1/p = v_1^p. \tag{23}$$

We can now find the asymptotic value for the polynomial $J_n(0)$. From (18), (19), and (21) we have, taking also (23) into account:

$$J_{n\,as}(0) = \frac{1-p}{1+\log v_2} v_2^n. \tag{24}$$

The term with v_1 has dropped out. In order to find $J_{n\,as}(z)$ we may introduce (24) into (14) and replace the upper limit n of the sum in (14) by infinity. This gives:

$$J_{n\,as}(z) = \frac{1-p}{1+\log v_2} v_2^n \exp(-z/v_2), \tag{25}$$

and, by making use of the definition (11) of z and of the relation (23)

$$J_{n\,as} = \frac{1-p}{1+\log v_2} x^{-p/(1-p)}. \tag{26}$$

Now we can find the asymptotic expression for K by simply putting (26) and (9) into (12). We get at once:

$$K_{as} = \frac{1}{1+\log v_2} = \frac{1}{1+[p/(1-p)]\log p}. \tag{27}$$

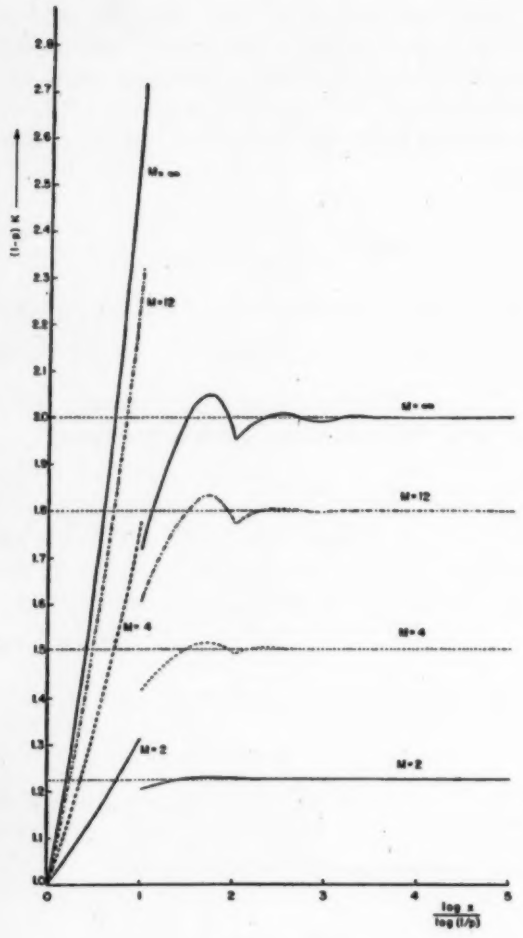

FIG. 1.

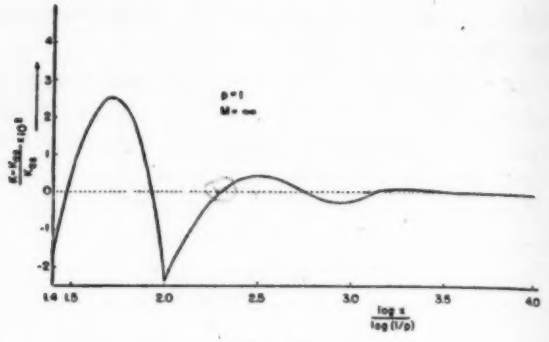

FIG. 2.

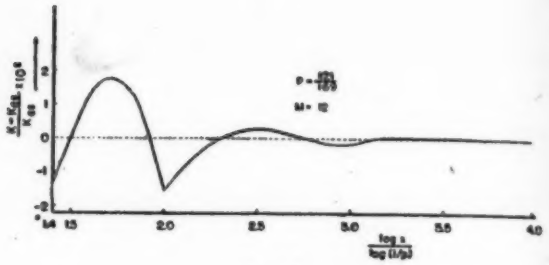

FIG. 3.

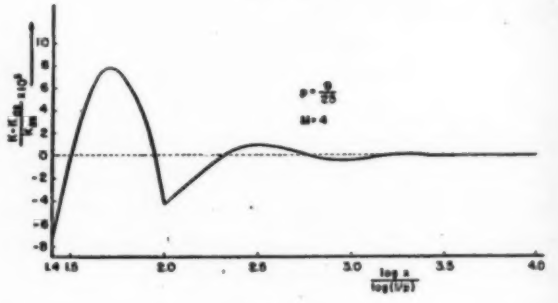

FIG. 4.

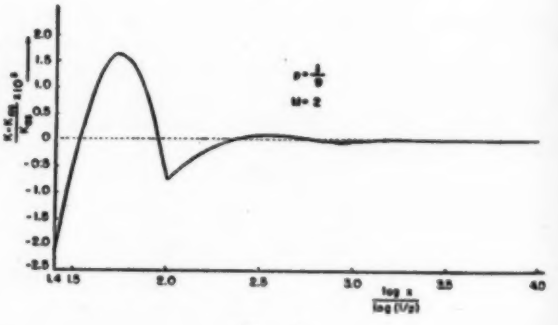

FIG. 5.

So K_{as} is a constant. Its physical significance is very simple: it is the reciprocal mean logarithmic energy loss in one collision.[10]

This means simply that the average number of collisions $K(x)dx/x$ in a given energy interval is asymptotically equal to the logarithmic width dx/x of that interval by the logarithmic width of the interval which is in the average traversed by one collision.

In order to see the dependence on M in a convenient direct way, the following expansion is useful:

$$K_{as}=\frac{1}{1+[p/(1-p)]\log p}=\frac{M}{2}+\frac{1}{3}+\frac{1}{18M}\left(1+\frac{16}{15M}+\frac{8}{45M^2}+\cdots\right). \quad (27a)$$

[10] The mean logarithmic energy loss in one collision is given by

$$(\log x)_{As}=\int_1^p (\log x')k(x',1)\frac{dx'}{x'}$$
$$=\frac{1}{1-p}\int_1^{1/p}\log x'dx'=1+[p/(1-p)]\log p. \quad (28)$$

TABLE I. The values of K for the extrema between $y=0$ and $y=4$.

M	K	$\delta(y)\cdot 10^3$								
∞	$M/2$	−500	359	−141	25.4	−23.8	4.36	−2.74	0.83	−0.41
12	6.3384	−444	290	−108	17.8	−15.6	2.64	−1.55	0.44	−0.19
4	2.3513	−335	180	−58.6	7.95	−6.03	0.82	−0.43	0.10	−0.04
2	1.3787	−184	74	−16.7	1.63	−0.91	0.088	−0.034	0.0053	−0.001
$y(M=2)$		0		1	1.75	2.00	2.54	2.95	3.36	3.81
$y(M=\infty)$		0		1	1.72	2.00	2.50	2.94	3.31	3.78

From this expansion it is seen that $K_{aa}\approx\frac{1}{2}M+\frac{1}{3}$ is a good approximation already for moderate values of M. Indeed, even for $M=2$ the error is only 3.3 percent.

If we want to assume that K is asymptotically equal to a constant, then the value of the constant can be found by simpler ways. As shown in Appendix II, the integral equation (8a, b) can be transformed into the equivalent form

$$K(x)=\frac{1}{1-p}\left\{1+p\int_1^x K(x')\frac{dx'}{x'}\right\} \quad \text{for } px<1, \tag{29a}$$

$$K(x)=1+\frac{p}{1-p}\int_{px}^{x} K(x')\frac{dx'}{x'} \quad \text{for } px>1. \tag{29b}$$

Putting K in (29b) equal to the constant K_{aa}, we find at once (27).[11] The behavior of the complete solution and the way in which the constant asymptotic value of K is reached is shown in Figs. 1–5, which give K as a function of $y=\log x/\log(1/p)$. This measure of the energy gives, for different masses, equal extensions to the maximal energy regions which may be traversed in one collision. As we have seen already, K is discontinuous for $x=1/p$, i.e., $y=1$. Therefore, as can be shown from (13), its nth derivative is discontinuous for $x=p^{-n}$ or $y=n$.

Figure 1 gives $(1-p)K$ as function of y for $y=0$ to $y=4$ for the masses $M=\infty$, 12, 4, and 2. K first rises according to (9), drops discontinuously at $y=1$, goes on rising to a maximum, reaches a minimum with discontinuous tangent at $y=2$, and approaches with oscillations of rapidly decreasing amplitudes the asymptotic constant value K_{aa}. The oscillations can be better seen from Figs. 2–5, where the relative deviation from the asymptotic value, i.e., $(K-K_{aa})/K_{aa}$ is plotted on an enlarged scale for the same masses for $y=1$ to $y=4$. Table I gives numerical values for the extreme deviations of K from its asymptotic value. The first two columns give the masses and K_{aa}, and the following 9 columns show the relative deviation from the asymptotic value:

$$\delta(y)\cdot 10^3=(K-K_{aa})/K_{aa}\cdot 10^3$$

for $y=0$, 1, and all the following extrema up to $y=4$. The values of y at which K is extreme are only slightly different for different masses; they are given in the last two rows for $M=2$ and $M=\infty$ only. (Table I.)

It is seen that the deviations are smaller for light nuclei. It must, however, be remembered that the maximum energy loss in one collision is smaller for heavy nuclei, so that the deviations, if plotted in the energy scale, extend farther for light nuclei. For a heavy nucleus K varies in the first interval by a factor e, but the interval comprises only the region between E_0 and $E_0[1-(4/M)]$, while e.g., for deuterium, the variation in the first interval is only 37 percent, but the interval extends from E to $E/9$. Since one has experimentally always to do with neutrons of a certain width in initial energy, the deviations of K from the constant value will, in general, be directly observable for light nuclei only. However, the importance of these variations lies not so much in the direct effects near E_0 but rather in the fact that they will start anew from every point where capture becomes important.

[11] Formally equivalent to this derivation is the following one: The number of neutrons going per second from the region $x<x_0$ to the region $x>x_0$ must be equal to the number produced per second, i.e., to Q. This gives:

$$\frac{1}{1-p}\int_{x_0}^{x_0/p}\frac{dx}{x^2}\int_{px}^{x_0}K(x')dx'=1, \tag{30}$$

from which again (27) results by putting $K=K_{aa}$. Equation (30) can, of course, also be obtained from the integral equation by using together both forms (8b) and (29b).

3. Mixtures

If the medium in which the neutrons are slowed down contains nuclei of different atomic weights M_s, the energy distribution after one collision [cf. (7)] will be determined by the function:

$$k(x, x') = \mu\left(\frac{x'}{x}\right)\frac{x'}{x}\sum_s \frac{c_s(x')}{1-p_s}\mu\left(\frac{p_s x}{x'}\right). \quad (31)$$

The function $\mu(u)$ is 1 for $u<1$, 0 for $u>1$ and discontinuous for $u=1$. $c_s(x')=l(x')/l_s(x')$, where $l(x')$ is the total mean free path and $l_s(x')$ the mean free path for scattering at a nucleus of type s. c_s is a measure of the concentration, $\sum_s c_s=1$. Introducing the kernel (31) into the general Eq. (2), we get:

$$xK(x) = \sum_s \frac{1}{1-p_s}\left\{c_s(1)\mu(p_s x) + \int_{\lambda(p_s x)}^{x} c_s(x')K(x')dx'\right\}, \quad (32)$$

where

$$\lambda(u) = \mu(u) + u\{1-\mu(u)\} = \begin{cases} 1 & \text{for } u<1 \\ u & \text{for } u>1. \end{cases} \quad (33)$$

As in the discussion of Eq. (3), we see that $K(x)$ is discontinuous at all the points $x=p_s^{-1}$, the discontinuity being

$$K_+(p_s^{-1}) - K_-(p_s^{-1}) = -\frac{c_s(1)p_s}{1-p_s}. \quad (34)$$

If we arrange the quantities p_s according to their magnitude, calling the largest of them p_1, then in the interval $1<x<p_1^{-1}$ Eq. (32) becomes

$$xK(x) = \sum_s \frac{1}{1-p_s}\left\{c_s(1) + \int_1^x c_s(x')K(x')dx'\right\}. \quad (35)$$

This equation is solved by

$$K(x) = \sum_s \frac{c_s(1)}{1-p_s}\exp\left\{\sum_s \frac{p_s}{1-p_s}\int_1^x c_s(x')\frac{dx'}{x'}\right\}. \quad (36)$$

From this solution we can proceed to construct the complete solution in a manner similar to, though more complicated than, the treatment of the case of a single substance. We shall do this later for a significant particular case, and shall now derive the asymptotic solution.

We use the fact, that, as shown in Appendix II, Eq. (32) may be transformed into

$$K(x) = 1 + \sum_s \frac{p_s}{1-p_s}\left\{c_s(1)\mu(p_s x) + \int_{\lambda(p_s x)}^{x} c_s(x')K(x')\frac{dx'}{x'}\right\}. \quad (37)$$

For $x>p_k^{-1}$ (p_k denoting the smallest p), (37) reads:[12]

$$K(x) = 1 + \sum_s \frac{p_s}{1-p_s}\int_{p_s x}^{x} c_s(x')K(x')\frac{dx'}{x'}. \quad (38)$$

If all the mean free paths are constant or vary all in the same way with energy, the c_s are constants. In this case, (38) is again asymptotically solved by a constant K_∞, for which we find from (38) (with constant c_s):

$$K_\infty = \left[1 + \sum_s \frac{c_s p_s}{1-p_s}\log p_s\right]^{-1}. \quad (39)$$

As can be easily checked this constant is again equal to the reciprocal average logarithmic energy loss in one collision. For variable mean free path it is easily seen that (39), with the c_s depending on x, is a good approximation provided the quantities c_s vary slowly enough with energy, so that the variation of (39) in a region of the extension of the average logarithmic energy loss is small.

We now derive the complete solution for the special case of a mixture of hydrogen with another substance, the concentration of which, in the above mentioned units, we denote by c. If the mean free paths are constant, the equation for this case becomes [cf. (32)]:

$$xK(x) = \left(1+\frac{cp}{1-p}\right)\left\{1+\int_1^x K(x')dx'\right\} \quad \text{for } px<1. \quad (40a),$$

$$xK(x) = \frac{c}{1-p}\int_{px}^{x} K(x')dx + (1-c)\left\{1+\int_1^x K(x')dx'\right\} \quad \text{for } px>1. \quad (40b)$$

[12] If hydrogen ($p=0$) is present in the mixture, this region does not exist, but since the term referring to hydrogen in the sum in Eq. (37) drops out because of the p in the numerator, (38) is equally valid in this case for $x>p_{k-1}^{-1}$.

The equivalent form (37) of these equations is:

$$K(x)=\begin{cases}\left(1+\dfrac{cp}{1-p}\right)\left\{1+\displaystyle\int_1^x K(x')\frac{dx'}{x'}\right\} & px<1 \quad (41a)\\ 1+\dfrac{cp}{1-p}\displaystyle\int_{px}^x K(x')\frac{dx'}{x'} & px>1. \quad (41b)\end{cases}$$

The solution of (40a) or (41a) is according to (36):

$$K_0(x)=\left(1+\frac{cp}{1-p}\right)x^{cp/(1-p)}. \quad (42)$$

If we denote again by $K_n(x)$ the solution for $p^{-n}<x<p^{-n+1}$, the substitution

$$K_n(x)=K_0(x)G_n(u), \quad (43)$$

$$u=cv_2^{c-1}z \quad (43a)$$

[for z see Eq. (11)], where u runs from 0 to

$$\xi=cv_2^{c-1}\zeta, \quad (44)$$

leads to

$$G_n(u)=\sum_{m=0}^{n} G_{n-m}(0)\frac{(-u)^m}{m!}, \quad (45)$$

$$G_n(0)=A_n(\xi)-\frac{cpv_2^c}{1-p-cp}A_{n-1}(\xi), \quad (46)$$

where the polynomial A is defined by (18a). While (45) is identical with the corresponding Eq. (14) for the polynomials $J_n(z)$, (46) differs from (18) by the different variable (ξ instead of ζ) and the different factor of A_{n-1}. The latter arises from the fact that the discontinuity at $x=p^{-1}$ has now a different magnitude. The solution $K_n(x)$ is again an oscillating function. We introduce into (46) the asymptotic expression (19) for the A_n:

$$A_{n\,as}(\xi)=\frac{{s_1}^n}{1+\log s_1}+\frac{{s_2}^n}{1+\log s_2}, \quad (47)$$

where s_1 and s_2 are now the solutions of

$$-s\log s=\xi \quad (48)$$

which for $\xi\to 0$ go to 0 and 1, respectively.

Introducing (47) into (46), we have

$$G_{n\,as}(0)=\frac{{s_2}^n}{1+\log s_2}\frac{1-p}{1-p+cp}+\frac{{s_1}^n}{1+\log s_1}\left(1-\frac{cp}{1-p+cp}\frac{s_2}{s_1}\right) \quad (49)$$

and, using (43), (43a), (42), and (6),

$$K_{as}(p^{-n})=\frac{1}{1+\log s_2}+\frac{(s_1/s_2)^n}{1+\log s_1}\times\left\{1+\frac{cp}{1-p}\left(1-\frac{s_2}{s_1}\right)\right\}. \quad (50)$$

Now we have to find the solutions $s_{1,2}$ of Eq. (48). From (20), (22), and (44) we see that

$$s_2=v_2^c=p^{cp/(1-p)}, \quad (51)$$

but, in contrast to the previous case, it now does not seem possible to express the other solution s_1 as a function of p and c in closed form.

However, part of the discussion can be done without explicit knowledge of s_1. We put

$$\frac{s_1}{s_2}=\frac{\log s_2}{\log s_1}=p^{\epsilon}. \quad (52)$$

Hence

$$\log s_1=p^{-\epsilon}\log s_2=\log s_2+\epsilon\log p. \quad (53)$$

This gives, if we insert the value of s_2 from (51) and put $p^{-1}=q$:

$$\frac{q^{\epsilon}-1}{q-1}=\frac{\epsilon}{c}. \quad (54)$$

Equation (54) has only one solution $\epsilon\geqslant 1$. For $c=0$, $\epsilon=\infty$; for $c=1$, $\epsilon=1$.

Introduction of (53) and (54) into (49) and (50) gives

$$G_{n\,as}(0)=\frac{1-p}{1-p+cp}\left\{\frac{{s_2}^n}{1+\log s_2}+\frac{(1-\epsilon){s_1}^n}{1+\log s_1}\right\}, \quad (49a)$$

$$K_{n\,as}(q^n)=\frac{1}{1+\log s_2}+\frac{(\epsilon-1)q^{-n\epsilon}}{\epsilon\log q-\log s_2-1} \quad (50a)$$

and, using (49a), (43), (43a), (45), (51), (53), (54):

$$K_{as}(x)=\frac{1}{1-\dfrac{c}{q-1}\log q}+\frac{(\epsilon-1)x^{-\epsilon}}{\left(\epsilon-\dfrac{c}{q-1}\right)(\log q)-1}. \quad (55)$$

From (54) it can be proved that the factor of $x^{-\epsilon}$ in (55) is always positive. Hence, K_{as} decreases with increasing x and goes finally over into the

constant K_∞, given by the first term of (55) in agreement with the general expression (39). Various expansions for ϵ can be derived from (54) for various cases. In particular, for $1-c=c_2\ll 1$, $1-p=\alpha\ll 1$, one finds:

$$\epsilon-1=\frac{2c_2}{\alpha}\{1+O(\alpha)+O(c_2)\}. \tag{56}$$

Equation (55) then becomes

$$K_{as}(x)=\frac{1}{\alpha/2+c_2+O(\alpha_1{}^2c_2{}^2,\ \alpha c_2)} + \frac{2c_2x^{-[1+(2c_2/\alpha)]}(1+O(\alpha,\ c_2)}{\alpha\{\alpha/2+c_2+O(\alpha^2,\ c_2{}^2,\ \alpha c_2)\}}. \tag{57}$$

Since $\alpha\ll 1$, we can apply this asymptotic expression for K already for values of x not noticeably different from one. Therefore, we can interpret (57) in the following way: K first reaches very rapidly the value $K_{as}(1)=2/\alpha$, which is the final value if no hydrogen were present. With increasing x, the influence of hydrogen comes into play and K decreases until it finally reaches the constant value given by the first term of (57), i.e., the reciprocal mean logarithmic energy loss of a neutron in the mixture. This variation of K is especially important in the case $c_2\gg\alpha/2$, for which there is a considerable difference between the energy loss in the pure heavy substance and in the mixture, since the latter is entirely due to hydrogen. (57) here becomes

$$K_{as}=\frac{1}{c_2}+\left(\frac{2}{\alpha}-\frac{1}{c_2}\right)x^{-[1+(2c_2/\alpha)]}. \tag{57a}$$

At the beginning the neutron density is here entirely determined by the heavy substance, at the end, entirely by hydrogen.[13] The transition takes place for $x_0\approx(2c_2/\alpha)\exp[\alpha/2c_2]$, or in numbers n of intervals: $n_0\approx(1/2c_2)\log(2c_1/\alpha)$, which is always a large number when the above approximation is valid. Moreover, as one can see from (32) to (36), the function K will in the first intervals, where it is still oscillating, be exactly identical with the function for the pure heavy substance, as shown in Figs. 1 and 2, and the transition to the entirely different final value will only start long after the oscillations have died down.

In the more general case that c_2 is no longer small compared to one the transition will take place earlier, but, in order that K should be determined by hydrogen from the very beginning, it is necessary, as we can see from (42), that $1-c_2=c\ll\alpha$, while for K to be determined by hydrogen only in the end it is, of course, sufficient that the mean energy loss in the mixture is the same as in hydrogen, *viz.*, $c_2\gg\alpha/2$. In the opposite case $c_2\ll\alpha/2$, (57) becomes

$$K_{as}=\frac{2}{\alpha}\left\{1+\frac{2c_2}{\alpha}(x^{-[1+(2c_2/\alpha)]}-1)\right\} \tag{57b}$$

and the deviation from the case of the pure heavy substance is small throughout.[14]

The effects discussed here may be considered as characteristic in general for the slowing down process in a mixture of a light and a heavy substance.

II. SLOWING DOWN WITH CAPTURE

4. The Equations

Putting (7) into (3), we have

$$K(x)=\frac{1}{(1-p)x}\left\{f(1)+\int_1^x f(x')K(x')dx'\right\}, \qquad px<1 \tag{59a}$$

$$K(x)=\frac{1}{(1-p)x}\int_{px}^x f(x')K(x')dx', \qquad px>1. \tag{59b}$$

The equivalent transformed equations are (cf. Appendix II):

$$K(x)=\frac{1}{1-p}\left\{1-g(1)+\int_1^x(p-g(x'))K(x')\frac{dx'}{x'}\right\}, \qquad px<1 \tag{60a}$$

[13] It is to be remembered that the neutron density is $Q(l/v)K(x)dx/x$, where $l=c_2l_H$ is the average mean free path, so that the factor c_2 drops out.

[14] This case requires some attention in connection with the treatment of capture. We consider the integral $\int_1^x K(x')dx'$ which enters into Eq. (40b). Writing

$$K(x)=K_\infty+M(x)$$

we find from (57b)

$$\int_1^\infty M(x)dx=2/\alpha; \tag{58}$$

c_2 has dropped out. In spite of this, (58) is *not* valid for $c_2=0$. This can be easily seen by noticing that the second part of (57b) contains c_2 as factor and therefore vanishes throughout for $c_2=0$. Actually, the integral (58) in this case is of the order $-\frac{1}{2}$ because of the contributions of the first intervals where the asymptotic expression (57b) is not yet applicable.

$$K(x)=1-g(1)-\int_1^x g(x')K(x')\frac{dx'}{x'}$$
$$+\frac{p}{1-p}\int_{px}^x f(x')K(x')\frac{dx'}{x'},\quad px>1 \quad (60b)$$

where $g(x)=1-f(x)=1-l(x)/l_s(x)$. The solution of (59a) or (60a) is:

$$K(x)=\frac{f(1)}{1-p}x^{p/(1-p)}$$
$$\times\exp\left[-\frac{1}{1-p}\int_1^x g(x')\frac{dx'}{x'}\right]. \quad (61)$$

For hydrogen ($p=0$) (59a) is valid everywhere, and therefore the complete solution in this case reduces to

$$K(x)=f(1)\exp\left[-\int_1^x g(x')\frac{dx'}{x'}\right], \quad (61a)$$

which is in accordance with Fermi's[3] result.

The solution in the region $px>1$ can in principle be found by repeated integration from (61), in the fashion of Section 2. This procedure has, however, only limited interest since in most of the practical cases the capture sets in only for energies considerably lower than the initial energy. Therefore, it is sufficient to investigate how the *asymptotic* solution of the equation without capture is modified by the capture. This is done by considering (59b) and (60b) valid for all values of x. The methods of solution will be different according as the variation of g in one interval is slow or rapid.

Before entering into these methods, it will be useful to discuss Eq. (60b) somewhat more closely. Multiplying (60b) with

$$a=1+p\log p/(1-p)$$

the average logarithmic energy loss in one collision, we have

$$S(x)=aP(x)+\frac{p}{1-p}\int_{px}^x f(x')S(x')\frac{dx'}{x'}, \quad (62)$$

where

$$S(x)=aK(x)$$

is the ratio between K and the asymptotic solution of the equation without capture (see (27)) and gives thus the relative reduction of K by the capture, and

$$P(x)=1-g(1)-\int_1^x g(x')K(x')\frac{dx'}{x'}$$

is the probability that the neutron is not captured below x.

Adding $p\log p/1-p$ to both sides of (62) and dividing by a, we obtain

$$S(x)=P(x)$$
$$+\frac{p}{(1-p)a}\int_{px}^x\{f(x')S(x')-S(x)\}\frac{dx'}{x'}. \quad (63)$$

In the presence of the second term in (63) consists the essential difference between the mechanism of capture in heavy substances and in hydrogen, for which it is zero. It is of special importance if the capture is large, or small but rapidly varying, in which cases it entirely modifies the solution. Its physical meaning is that the effect of capture occurring at a point x_1 on the value of S at a point x_2 depends on the distance between these points. This may be understood by first considering the case in which the total change of S in the region considered is small. In this case all the capturing points may be considered as independent sources of neutrons taken away of amount $g(x_1)(dx_1/x_1)$, the change in S due to every point x, will then be given by the initial solution of the equation without capture and thus exhibit considerable variations, as shown in Fig. 1, which will extend a few intervals beyond x_1. If the total change is no longer small, these variations will in turn influence each other.

If capture occurs only above a certain energy, S will approach a constant value a few intervals below this energy, whereupon the second term in (63) will vanish, so that the value of the constant is given by

$$S=P=1-\frac{1}{a}\int g(x')S(x')\frac{dx'}{x'}. \quad (64)$$

If the change in S is small, we may replace $S(x')$ in the integral by one and have

$$S=1-\frac{1}{a}\int g(x')\frac{dx'}{x'}. \quad (64a)$$

If the capture occurs in a number of discrete regions, separated by regions without capture as may be the case with absorption lines, we may

apply (64a) for every region separately, writing

$$S_k - S_{k-1} = \frac{S_k}{a} \int_k g(x') \frac{dx'}{x'}, \tag{64b}$$

where S_k is the value of S before entering the capturing region k and the integral has to be taken over this region. From (64b) we may find the final S even if the total change in S is large, provided the changes due to every single region are small.

5. Slowly Varying Capture

We first consider the case of constant capture. Here, the assumption that the capture vanishes in the first intervals is not valid. However, it can be easily seen that the solution obtained by considering (59b) and (60b) valid everywhere will differ from the asymptotic solution of (59a, b) only by a constant factor. If we use the homogeneous form (59b) of the equation, the solution will contain anyhow an undetermined constant factor, which, besides, is immaterial for the following. (59b) with constant f

$$S(x) = \frac{f}{(1-p)x} \int_{px}^{x} S(x')dx' \tag{65}$$

is solved by

$$S(x) = Cx^{-\nu_0}, \tag{66}$$

where C and ν_0 are constants.

Putting (66) into (65), we obtain the following equation for ν_0:

$$\frac{1}{f} = \frac{p^{1-\nu_0} - 1}{(1-p)(\nu_0 - 1)}. \tag{67}$$

Equation (67), which is similar to (54), has only one solution $\nu_0 \geqslant 0$. For $f=1$, $\nu_0 = 0$, for $f=0$, $\nu_0 = \infty$. Of the various possible expansions for ν_0, the following is of particular physical interest.

The right side of (67) can be written as an integral, as follows:

$$\frac{1}{f} = \frac{1}{1-p} \int_p^1 y^{-\nu_0} dy. \tag{67a}$$

Putting now

$$y^{-\nu_0} = \sum_{s=0}^{\infty} \frac{(-\nu_0 \log y)^s}{s!},$$

we obtain the following expansion of $1/f$ in powers of ν_0:

$$\frac{1}{f} = \sum_{s=0}^{\infty} \frac{a_s \nu_0^s}{s!},$$

$$a_s = \frac{(-1)^s}{1-p} \int_p^1 (\log y)^s dy = s! \left\{ 1 - \frac{1}{q-1} \sum_{m=1}^{s} \frac{(\log q)^m}{m!} \right\}. \tag{68}$$

It is easily seen (cf. (28)) that the coefficients a_s are the average $s-t$ powers of the logarithmic energy loss in one collision.

Now we put

$$b_s = \frac{a_s}{s!} = 1 - \frac{1}{q-1} \sum_{m=1}^{s} \frac{(\log q)^m}{m!},$$

$$w = \frac{1}{f} - 1 = \frac{g}{f} = \frac{l_s}{l_c}$$

and have

$$w = \sum_{s=1}^{\infty} b_s \nu_0^s.$$

Reverting this series, we obtain:

$$\nu_0 = \frac{w}{a} \left\{ 1 - \frac{b_2}{a^2} w + \frac{2b_2 - b_3 a}{a^4} w^2 - \frac{b_4 a^2 - 5b_3 b_2 a + 5b_2^3}{a^6} w^3 + \cdots \right\}. \tag{69}$$

The coefficients of the powers of w in the brackets of (69) are of the order of one. They are exactly one in the case of hydrogen, since for this case (cf. (61a)) $\nu_0 = g = w/(1+w)$. For large masses, $1-p = \alpha \ll 1$, we have, as is best directly seen from the integral in (68), $b_s = \alpha^s/(s+1)!$, which makes the coefficients in (69) 1, 2/3, 5/9, 34/135, etc. Thus the expansion (69) will always rapidly converge if $w \ll 1$. Breaking off at the term S will give an approximately correct result for S if $(w^{s+2}/a) \log x \ll 1$.

It is now of interest to calculate the second term in (63) for constant capture. Introducing (66) into the integral and using (67), one obtains

$$P(x) = gS(x)/\nu_0 a. \tag{70}$$

Thus $S(x) - P(x)$ is small compared to $P(x)$ if g or w is small. For large w, however, $\nu_0 a/g$ is large and the second term $S-P$ will be even large compared to P.

We now consider the case of slowly variable capture. Neglecting the variation of f in one interval, we have

$$d \log S/d \log x = \nu_0(x),$$

$\nu_0(x)$ being determined by (67). According to our assumption there is no capture in the first intervals, hence $S(1)=1$ and consequently

$$S(x)=\exp\left[-\int_1^x \nu_0(x')\frac{dx'}{x'}\right]. \tag{71}$$

If, in particular, w is small throughout, we may use the expansion (69) for ν_0. Its first term will be sufficient if

$$\int_1^x w^2(x')dx'/x' \ll a.$$

This condition is for small a, i.e., large masses, perfectly compatible with the first term being large compared to one, *viz.*,

$$\int_1^x w(x')dx'/x' \gg a.$$

Thus, for large masses and small w, the expression

$$S(x)=\exp\left[-(1/a)\int_1^x w(x')dx'/x'\right] \tag{71a}$$

will have a wide range of validity. We now may improve (71) by correcting for the neglected variation of f within one interval. Differentiating (60b), and putting

$$d \log S/d \log x = \nu(x)$$

we obtain

$$\nu(x)=1-\frac{f(x)}{1-p}\left\{1-p\frac{K(px)f(px)}{K(x)f(x)}\right\}. \tag{72}$$

Putting

$$\nu=\nu_0+\nu_1,$$

where ν_0 is given by (6) and ν_1 is the correction term to be determined, we develop f and ν in the interval:

$$\frac{f(px)}{f(x)}\approx 1-\log q\frac{d \log f(x)}{d \log x}, \tag{73}$$

$$\frac{K(px)}{K(x)}=\exp\int_{px}^{x}\nu(x')\frac{dx'}{x'}\approx\exp\left\{\nu(x)\log q-\frac{d\nu(x)}{d \log x}\frac{(\log q)^2}{2}\right\}$$

$$\approx\exp\left\{(\nu_0+\nu_1)\log q-\frac{d\nu_0}{d \log x}\frac{(\log q)^2}{2}\right\}\approx q^{\nu_0}\left\{1+\nu_1 \log q-\frac{d\nu_0}{d \log x}\frac{(\log q)^2}{2}\right\}, \tag{74}$$

where we have replaced $d\nu/d \log x$ by $d\nu_0/d \log x$ and assumed that

$$\nu_1-\frac{\log q}{2}\frac{d\nu_0}{d \log x}\ll 1.$$

Introducing (73) and (74) into (71) and using (67), we obtain finally

$$\nu_1=-\frac{\mu}{1-\mu}\frac{d}{d \log x}\left(\log f+\nu_0\frac{\log q}{2}\right), \tag{75}$$

where

$$\mu=\frac{fq^{\nu_0-1}}{1-p}\log q$$

which by (67) goes over into

$$\mu=\left(\nu_0+\frac{p-g}{1-p}\right)\log q. \tag{76}$$

If $\alpha\ll 1$, $g\ll 1$, (75) reduces to

$$\nu_1=-\tfrac{1}{3}dg/d \log x. \tag{75a}$$

An example for slowly varying capture is the case of the mean free path for scattering being constant and the mean free path for capture proportional to the velocity ($1/v$ law for the capture cross section). This makes

$$w=(x/x_c)^{\frac{1}{2}}, \tag{77}$$

where x_c is a constant. Thus we may use w as a measure of the energy, putting $S(x)=\varphi(w)$, and have for the solution:

$$\varphi(w)=\exp\left[-2\int_0^w\{\nu_0(w')+\nu_1(w')\}\frac{dw'}{w'}\right], \tag{78}$$

where ν_0 and ν_1 are given by (67), (69), and (75). We may do still a little better, since it is here possible to take the variations of the capture within one interval not only approximately but exactly into account. For this purpose we introduce (77) into (59b), which gives the equation

$$w^2\varphi(w)=\frac{2}{1-r^2}\int_{rw}^{w}\frac{w'\varphi(w')}{1+w'}dw', \tag{79}$$

where

$$r=p^2=(M-1)/(M+1).$$

We now expand $\varphi(w)$ in powers of w

$$w^2\varphi(w)=\sum_{s=0}^{\infty}\beta_s w^s, \quad \beta_0=1 \tag{80}$$

and introduce this expansion into both sides of (79). Comparison of the coefficients of equal powers of w on both sides gives after some calculation

$$\beta_s=(-1)^s\lambda_s\prod_{k=1}^{s}(1-\lambda_k)^{-1}, \tag{81}$$

where

$$\lambda_s=\frac{2}{s+2}\frac{1-r^{s+2}}{1-r^2}.$$

The expansion (80), (81) is of some use for small masses. For larger masses, however, the coefficients β_s increase rapidly with increasing s, and in the limit of $\alpha\to 0$ one finds

$$\beta_s=\frac{(-1)^s}{s!}\left(\frac{\alpha}{2}\right)^s,$$

so that

$$\lim_{\alpha\to 0}\varphi(w)=e^{-4w/\alpha}.$$

For large masses, therefore, an expansion of $\log\varphi$ rather than φ will be useful, as is already suggested by (78) with (69). Its coefficients can be determined by introducing it into (79) or also by rearranging (80). One finds

$$\varphi(w)=\exp\left\{-\frac{2}{1-r}\left[\frac{1+r+r^2}{1+2r}w-\frac{1+3r+2r^3}{2(1+2r)^2}w^2-\cdots\right]\right\}. \tag{82}$$

The coefficients of (82) are very near to the coefficients obtained by the approximate treatment, which result from putting (69) and (75) into (78). This may be seen by expanding both in powers of α or $1/M$.

It will now be of interest to compare the effects of 1/v-capture in light and heavy slowing down agents. As in the discussion of (71), we see that the higher terms in (82) will in the case of large masses only come into play at energies for which already most of the neutrons have been captured. Expressing r by M, we have

$$\varphi(w)=\exp\left[-(M+\tfrac{1}{3})w+v\tfrac{1}{3}Mw^2\right], \tag{83}$$

where terms of the order w^2 and Mw^3 have been neglected.

For hydrogen, on the other hand, we have from (61a) and (77)

$$\varphi(w)=1/(1+w)^2. \tag{84}$$

Going over to the neutron density as given by (1), and denoting by $\psi(v)$ the neutron density in the velocity scale we have

$$\psi(v)dv=-\rho(x)\frac{dx}{x}=\frac{2Ql}{a}\varphi(w)\frac{dv}{v^2}=\frac{2Ql_s}{a(1+w)}\varphi(w)\frac{dv}{v^2}. \tag{85}$$

Putting $w=v_c/v$, where v_c is the velocity at which the mean free paths for scattering and capture become equal, we obtain for large M, using (27a):

$$\psi(v)dv=Ql_s(M+\tfrac{2}{3})\times\exp\left[-\left(M+\frac{4}{3}\right)\frac{v_c}{v}+\frac{1}{3}M\left(\frac{v_c}{v}\right)^2\right] \tag{86}$$

and for hydrogen

$$\psi(v)dv=\frac{2Ql_s v dv}{(v+v_c)^3}; \tag{87}$$

$\psi(v)$ has a maximum which lies for hydrogen at $v=(v_c/2)$ and for large M at about $v=(2/M)v_c$. It also may be noted from (86) and (87) that the neutron density in the energy scale has no maximum in the case of hydrogen, while for larger M a maximum occurs at about $(3/M)^2E_c$. In connection with the fact, that the capture in heavy substances already comes into play for energies at which σ_c is of the order of σ_s/M rather than of the order σ_s as in hydrogen, it has been proposed[1] to use slowing down experiments in heavy materials for the detection and measurement of small capture cross sections. It may further be noted that the low energy cut-off is for large M considerably sharper than for hydrogen, which opens experimental possibilities of a different kind. By slowing neutrons down in a heavy substance containing a small and variable admixed amount of boron or another element with $1/v$ capture, it may be possible to produce a continuous neutron spectrum with variable lower limit, which would be

very useful for the analysis of nuclear energy levels. While this method is not in principle different from the usual boron absorption method of neutron spectroscopy, it is not subject to the well-known difficulties which make the analysis of boron absorption data impracticable as soon as thicker layers have to be employed.

6. Rapidly Varying Capture

If f does no longer vary slowly within one interval, the treatment of the preceding section will not hold. In this case it is necessary to solve the equations rigorously. This is not difficult, if the occurrence of capture is limited to one or even a few intervals. Assuming that the capture is negligible for $x<x_0$, we have for the region $x_0<x<x_0/p$:

$$S(x)=\frac{1}{(1-p)x}\int_{x_0}^{x}f(x')S(x')dx', \qquad (88)$$

with

$$S(x_0)=1.$$

(88) can be solved by differentiation with the result:

$$S(x)=e^{\chi(x)}\left\{1-\frac{p}{1-p}\int_{x_0}^{x}e^{-\chi(x')}\frac{dx'}{x'}\right\},$$
$$\chi(x)=\frac{1}{1-p}\left\{p\log\frac{x}{x_0}-\int_{x_0}^{x}g(x')\frac{dx'}{x'}\right\}. \qquad (89)$$

It can be shown from (89) that the solution for rapidly varying g differs from the case of slowly varying g even if $g\ll 1$. The solution in the following intervals $((x_0/p)<x<(x_0/p^2)$, etc.) can be found from (89) by successive integrations. After the capturing region has been passed, S will be subject to fluctuations and finally tend to a constant value, which, with the help of (64), may be derived directly from the solution in the capturing region without explicit knowledge of S in the fluctuating region in between.

A case of rapidly varying g is the capture by absorption lines. Its discussion will be given in a separate paper.

7. A Simplified Treatment and Its Limitations

We shall now illustrate some of the results obtained above by comparing the actual slowing down mechanism with a simpler idealized one. If the loss in energy, which takes place in jumps of different magnitude occurring at different times, were instead continuous, the velocity of a neutron would be a function of its age. (Actually, to every age corresponds a velocity distribution and *vice versa*; these distributions can, at least for constant mean free path, be explicitly derived, the velocity spread for any given age being of the order v_H for hydrogen and of the order $v_H/\sqrt{M}$ for large masses.[15] We find the relation between velocity and age by putting the relative change in velocity dv/v equal to one-half of the average logarithmic energy loss a in one collision times the probability that a collision occurs, which is

$$[v/l_s(v)]dt: \quad dv/v=-\tfrac{1}{2}avdt/l_s(v),$$
$$dt=-(2/a)l_s(v)dv/v^2. \qquad (90)$$

We now ask for the number $N(t)dt$ of neutrons of age between t and $t+dt$. If no capture occurs, all ages are equally probable, and $N(t)$ is therefore equal to Q, the number of neutrons produced per second. Including capture, we have obviously:

$$N(t)dt=Q\exp\left[-\int_0^t\frac{dt'}{\tau_c(t')}\right]dt, \qquad (91)$$

where $\tau_c=[l_c(v)/v]$ is the lifetime of the neutron against capture, which is in general a function of velocity. We now obtain at once the velocity distribution by introducing (90) into (91):

$$\psi(v)dv=-N(t)dt=\frac{2Ql_s(v)}{a}$$
$$\times\exp\left[-\frac{2}{a}\int_v^{v_0}w(v')\frac{dv'}{v'}\right]\frac{dv}{v^2}, \qquad (92)$$

where l_s/l_c has again been denoted by w. (92) is identical with Eq. (71a) except for a factor $l_s/l=1+w$. For large M this factor is of no importance, so that the simplified treatment will here be justified under the conditions of validity of (71a), *viz.*, w slowly varying and

$$\int_v^{v_0}w^2(v')\frac{dv'}{v'}\ll\frac{a}{2},$$

which is also rather obvious from the assumptions. For hydrogen, on the other hand, the changes of the neutron distribution caused by capture may be given wrongly by (92) even if they are small, as is the case for $1/v$ capture,

[15] G. Placzek, Phys. Rev. (to appear later).

where the change of ψ by the capture is in first approximation $-3w\psi$, while (92) gives $-2w\psi$. This is connected with the fact that the velocity spread for any given age in hydrogen is larger than in heavy substances.

8. Modifications at High and Low Energies

Our results will break down at high and low energies because of changes in the mechanism of the collision. As soon as the neutron energy exceeds the energy of the first excited level of the nucleus in question, inelastic collisions will occur, which make the slowing down much more rapid. Another, less important, effect at high energies is the deviation of the angular distribution from spherical symmetry in the center of gravity system. This effect may occur as soon as the neutron wave-length becomes of the order of nuclear dimensions and may change somewhat the collision function $k(x, x')$.

At low energies the collision function will be modified by the chemical binding as soon as the energy transfer to a free nucleus in one collision becomes of the order of the vibration quanta, thus, for large M: $E \sim \frac{1}{2}M\hbar\omega$. These energies are of the order of several volts for heavy substances.

While the binding completely changes the collision function for $E < \frac{1}{2}M\hbar\omega$, it will not affect the average energy loss unless the energy itself becomes of the order of the vibration frequencies.[16] This may be seen from a schematic example. We consider the collision of a neutron with a particle of atomic weight $M \ll 1$, elastically bound in an isotropic field of force of vibration frequency ω, and being in the ground state $n=0$ before the collision. We assume the neutron energy E to be large compared to $\hbar\omega$, but small compared to $\frac{1}{2}M\hbar\omega$.

For this case the cross sections σ_{0n} for the transition $0 \rightarrow n$, which can be found from the theory of the scattering of neutrons by bound protons,[17] reduce to

$$\sigma_{0n} = \sigma_f \cdot \frac{1}{(n+1)!}\left(\frac{4E}{\hbar\omega}\right)^n, \tag{93}$$

where σ_f is the cross section for a fixed nucleus, which for large M is not appreciably different from the cross section of the free nucleus. Only the transitions $0 \rightarrow 0$ and $0 \rightarrow 1$ are of importance, and hence the energy loss is given by

$$\hbar\omega\sigma_{01}/\sigma_f = 2E/M. \tag{94}$$

Thus, instead of frequent small losses of maximum amount $4E/M$ we have a rare large loss of amount $\hbar\omega$, the average remaining $2E/M$.

The formulae for the energy distribution will therefore remain valid down to energies of the order of the vibration quanta if the capture is small and slowly varying within regions of the order of the vibration quanta so that only the average energy loss matters. In the opposite case, however, the deviations will come into play already for energies of the order $M/2$ times the vibration quanta. This effect may play a role in the study of absorption lines.

9. Spatial Distribution

The spatial distribution may be characterized by the average square distance of diffusion $(r^2)_{\text{Av}}$ as a function of initial and final energy. Generalizing the standard treatment as given by Fermi[4] and Bethe,[18] one finds

$$(r^2)_{\text{Av}}(x) = 2\int_1^x \frac{l_s^2(x')K(x')}{1-(\cos\vartheta)_{\text{Av}}}\frac{dx}{x'}, \tag{95}$$

where ϑ is the scattering angle in the system of the observer. Equation (95) is valid if $\log x$ is large compared to the average logarithmic energy loss and l_s varies slowly within regions of the order of the latter. The denominator contains the effect of the angular assymetry of the scattering in the system of the observer. In our case the scattering is isotropic in the center of gravity system. Therefore we have

$$(\cos\vartheta)_{\text{Av}} = \tfrac{1}{2}\int_{-1}^{1} \cos\vartheta\, d\cos\theta, \tag{96}$$

where θ is the scattering angle in the center of gravity system. We now express $\cos\vartheta$ by $\cos\theta$:

$$\cos\vartheta = \frac{1+M\cos\theta}{(1+M^2+M\cos\theta)}. \tag{97}$$

Integrating (96) with (97), one finds

$$(\cos\vartheta)_{\text{Av}} = 2/3M. \tag{98}$$

[16] I am indebted to Professor H. A. Bethe for pointing this out to me.

[17] N. Arley, Kgl. Danske. Vid. Sels. Medd. **16**, 1 (1938).

[18] H. A. Bethe, Rev. Mod. Phys. **9**, 69 (1937).

Putting for K the inverse average logarithmic energy loss and using (98), we write (95) in the form:

$$(r^2)_{Av}(x)=C\int_1^x l_s^2(x')\frac{dx'}{x'},$$

$$C=\frac{2}{\left(1+\frac{p}{1-p}\log p\right)\left(1-\frac{2}{3M}\right)}. \tag{99}$$

For $M=1$,

$$C=6 \tag{99a}$$

which gives the well-known formula for hydrogen; for $M=2$

$$C=4.1. \tag{99b}$$

The decrease is caused by the diminuition of the forward asymmetry of scattering, which in this case overcompensates the change in energy loss. For $M>2$, C increases again and becomes for $M\gg 1$

$$C=M+4/3. \tag{99c}$$

For mixtures, (99) becomes (notations of Section 3):

$$(r^2)_{Av}(x)=2\int_1^x \frac{l_s^2(x')}{\left(1+\sum_k \frac{c_k(x')p_k}{1-p_k}\log p_k\right)\left(1-\frac{2}{3}\sum_k \frac{c_k(x')}{M_k}\right)}\frac{dx'}{x'}. \tag{100}$$

This gives for air[8] $C=15.6$ and 15.8 for low and high energies, respectively. From (99) it may be seen that the effectiveness of hydrogen in slowing down the neutrons in a small space is caused by its exceptionally large scattering cross section rather than to its small mass. If its mass were 2 or 4, the distance required for slowing down would be even smaller.

It remains now to discuss the capture in mixtures, which presents many interesting features and is also of practical importance. The treatment will be given in another connection. It has already been shown in Section 3 that in mixtures of a heavy and a light substance there are for certain concentrations enormous deviations from the asymptotic value of K, which extend over many intervals. Without entering into details, it may therefore be concluded already that in such cases the mutual correlation of the effects of capture occurring at different energies will be of primary importance and act over distances much wider than for single substances.

It is a pleasure to thank Professor H. A. Bethe for many interesting discussions.

APPENDIX I

Asymptotic Evaluation of $A_n(\zeta)$

We write the polynomial

$$A_n(\zeta)=\sum_{m=0}^{n-1}(m-n)^m\frac{\zeta^m}{m!}$$

as the difference of two infinite series:

$$A_n(\zeta)=T_n(\zeta)-B_n(\zeta), \tag{I1}$$

$$T_n(\zeta)=\sum_{m=0}^{\infty}(m-n)^m\frac{\zeta^m}{m!}, \tag{I1a}$$

$$B_n(\zeta)=\sum_{m=0}^{\infty}\frac{(m\zeta)^{m+n}}{m!}. \tag{I1b}$$

Both series converge if $\zeta<e^{-1}$. $T_n(\zeta)$ can be evaluated rigorously. We put

$$\zeta=-v\log v. \tag{I2}$$

Equation (I2) has two roots v_1 and v_2, which for $\zeta\to 0$ tend to 0 and 1, respectively. Expanding ζ in powers of $\log v_2$ and introducing this expansion into (I1a) one obtains[19]

$$T_n(\zeta)=\frac{v_2^n}{1+\log v_2}. \tag{I3}$$

The series $B_n(\zeta)$ consists of positive terms, which, if n is large, have a sharp maximum. Hence we may get the asymptotic value of $B_n(\zeta)$ for large n by using Stirling's formula and replacing the sum by an integral. Putting

$$1+\frac{m}{n}=y^2,\quad \log\zeta=-(1+\gamma)$$

[19] Polya-Szegö, *Aufgaben und Lehrsatze aus der Analysis* (Verlagsbuchhandlung Julius Springer, Berlin, 1926).

we get

$$B_{n\,as}=\left(\frac{2n}{\pi}\right)^{\frac{1}{2}}\int_1^\infty\{(1-y^{-2})e^{-\gamma}\}^{ny^2}dy,$$
$$=\left(\frac{2n}{\pi}\right)^{\frac{1}{2}}\int_1^\infty e^{F(y)}dy. \tag{I4}$$

The integrand has a sharp maximum, the location of which we determine as follows:

We have

$$F(y)=ny^2\{-\gamma+\log(1-y^{-2})\}. \tag{I5}$$

From $F'(y_M)=0$, we get

$$\frac{1}{y_M^2-1}=-\gamma+\log(1-y_M^{-2}). \tag{I6}$$

Putting

$$\zeta=te^{-t}, \tag{I7}$$

we have

$$-\gamma=1-t+\log t$$

and hence may write (I6):

$$1-t+\log t=1-\frac{y_M^2}{1-y_M^2}+\log\frac{y_M^2}{1-y_M^2}, \tag{I8}$$

from which we get:

$$y_M^2=t/(1-t). \tag{I9}$$

Equation (I7) goes over into (I2) by putting $t=-\log v$ and hence has two solutions $t_1\geqslant 1$ and $t_2\leqslant 1$ which tend to ∞ and 0, respectively, for $\zeta\to 0$. Since $y^2=1+(m/n)$ is positive, we see from (I9) that the solution applying to our case is $t_1=-\log v_1$.

We now evaluate B_n by integration around the maximum:

$$B_{n\,as}(\zeta)=\left(\frac{4n}{-F''(y_M)}\right)^{\frac{1}{2}}\exp[F(y_M)]. \tag{I10}$$

From (I5, 6, 9) we have

$$F(y_M)=\frac{-ny_M^2}{y_M^2-1}=-nt_1,$$
$$F''(y_M)=-4n(t_1-1)^2.$$

Hence we get

$$B_{n\,as}(\zeta)=\frac{\exp(-nt_1)}{t_1-1}=-\frac{{v_1}^n}{1+\log v_1}. \tag{I11}$$

And finally, from (I1, 3, I1):

$$A_{n\,as}(\zeta)=\frac{{v_1}^n}{1+\log v_1}+\frac{{v_2}^n}{1+\log v_2}. \tag{I17}$$

APPENDIX II

Transformation of the Integral Equation

Differentiation of (32) gives

$$xK'(x)=\sum_s\frac{p_s}{1-p_s}\{c_s(x)K(x)$$
$$-(1-\mu(p_sx))c_s(p_sx)K(p_sx)\}. \tag{II1}$$

Equation (II1) is not valid at the points $x=p_s^{-1}$, for which K is discontinuous. K' itself is discontinuous for the points $x=p_s^{-2}$. We multiply with dx/x and integrate from 1 to x, taking the discontinuities into account. The left-hand side gives:

$$\int_1^x K'(x')dx'=K(x)-K(1)$$
$$-\sum_s(1-\mu(p_sx))\{K_+(p_sx)-K_-(p_sx)\}.$$

From (36) we have

$$K(1)=\sum_s\frac{c_s(1)}{1-p_s}.$$

Introducing (34) we get

$$\int_1^x K'(x')dx'=K(x)-1-\sum_s\frac{c_s(1)\mu(p_sx)p_s}{1-p_s}.$$

Integration of the right-hand side of (II1) gives

$$\int_1^x K'(x')dx'=\sum_s\frac{p_s}{1-p_s}\int_{\lambda(p_sx)}^x c_s(x')K(x')\frac{dx'}{x'}.$$

Hence,

$$K(x)=1+\sum_s\frac{p_s}{1-p_s}\left\{c_s(1)\mu(p_sx)\right.$$
$$\left.+\int_{\lambda(p_sx)}^x c_s(x')K(x')\frac{dx'}{x'}\right\}. \tag{II2}$$

If only one type of nucleus is present, this reduces to Eq. (29a, b).

The same transformation, applied to the equation with capture, gives the result:

$$K(x)+\int_1^x g(x')K(x')\frac{dx'}{x'}$$
$$=f(1)+\sum_s\frac{p_s}{1-p_s}\left\{f(1)c_s(1)\mu(p_sx)\right.$$
$$\left.+\int_{\lambda(p_sx)}^x f(x')c_s(x')K(x')\frac{dx'}{x'}\right\}. \tag{II3}$$

Partial Separation of the Isotopes of Chlorine by Thermal Diffusion

E. F. SHRADER*
Sloane Physics Laboratory, Yale University, New Haven, Connecticut
(Received December 11, 1942)†

The Clusius-Dickel isotope separator has been modified to allow larger scale separation of the isotopes of chlorine. The modified separator employs two coaxial Pyrex glass cylinders. A special design was necessary to allow for the heating and the resulting thermal expansion of the inner cylinder. The operation of the separator compares favorably with the operation predicted by the theory of Furry, Jones, and Onsager. The degree of isotope separation was determined directly by mass-spectrographic and spectrographic analyses. The concentration of Cl^{37} was also determined by measuring the amount of induced radioactivity resulting from deuteron bombardment of the sample to be analyzed. Sufficient chlorine gas containing 45 percent Cl^{37} was obtained for the determination by spectrographic means of the nuclear spin of Cl^{37}.

1. INTRODUCTION

THE phenomenon of thermal diffusion in which a concentration gradient is set up in a mixture of gases in the presence of a temperature gradient was first discovered by Enskog[1] in 1911 and independently by Chapman[2] in 1917. Clusius and Dickel[3] using a combination of thermal diffusion and fractionation have achieved great success in the separation of chlorine and neon into their isotopic components. Their apparatus consisted of a heated wire along the axis of a long vertical hollow tube into which was placed the gas whose isotopic components were to be separated. The combination of thermal diffusion and convective currents increased greatly the small separation produced by the temperature gradient alone. In general the light component goes to the hot wall and collects at the top while the heavy component collects at the bottom of the column.

The theory of thermal diffusion as applied to isotope separation of an element with two isotopes has been fully developed by Furry, Jones, and Onsager[4] for the case of a temperature gradient produced between two vertical plane walls at different temperatures. Corrections to the cylindrical case have been made by Furry and Jones.[5]

The separating power of such a thermal diffusion column is called the separation factor of the column which is independent of the relative proportion of the constituents of the gas to be separated. It is defined as

$$S=\frac{k_1(1-c_1)}{c_1(1-k_1)}=\exp(4A_D l),$$

where C_1 is the initial concentration of component 1 and k_1 is its final equilibrium concentration at the other end of the column. Then $1-C_1$ and $1-k_1$ are the concentrations of component 2 at each end of the column. S may be obtained from the dimensions of the column and the physical properties of the gas; l is the effective length of the column; and

$$A_D=\frac{A}{(1-K_D/K)},$$

where

$$A=\frac{63}{4}\frac{\alpha\eta D}{\rho g w^4}f\left(\frac{\Delta T}{T}\right)$$

and

$$\frac{K_D}{K}=1890(T_1^2+T_1T_2+T_2^2)\left(\frac{D\eta}{w^3\rho g\Delta T}\right)^2.$$

The notation used is:

T_2, T_1 the temperatures of the hot and cold walls, $\Delta T=T_2-T_1$,
$2w$ equals the distance between walls,
D is the coefficient of ordinary diffusion,
ρ is the density of the gas,
η is the viscosity,
g is the acceleration of gravity,
$f(\Delta T/T)=1.016$ for $T_2=2T_1$, and
$f(\Delta T/T)=1.039$ for $T_2=3T_1$.

* Now on leave from the Case School of Applied Science, Cleveland, Ohio and at Clinton Laboratories, Monsanto Chemical Company, Knoxville, Tennessee.

† This paper was received for publication on the date indicated but was voluntarily withheld from publication until the end of the war.

[1] D. Enskog, Physik. Zeits. **12**, 56 and 533 (1911).
[2] S. Chapman, Phil. Trans. **A217**, 184 (1917).
[3] K. Clusius and G. Dickel, Zeits. f. physik. Chemie **B44**, 397–473 (1939).
[4] W. H. Furry, R. C. Jones, and L. Onsager, Phys. Rev. **57**, 1083 (1939).
[5] W. H. Furry and R. C. Jones, Phys. Rev. **57**, 561A (1940).

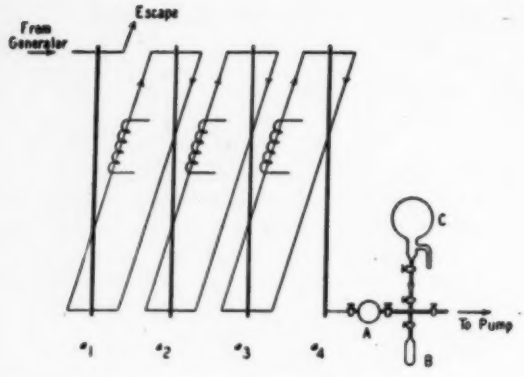

FIG. 1. Experimental arrangement.

For the case of rigid elastic spheres as applied to isotopic constituents Enskog's and Chapman's results reduce to

$$D_T/D=k_T=\alpha C_1C_2$$

where D_T is the coefficient of thermal diffusion and

$$\alpha=0.35(m_2-m_1)/(m_2+m_1),$$

the m's being the relative masses of the two constituents.

The coefficient of thermal diffusion vanishes for Maxwellian molecules. For molecules such that the forces vary as an inverse power of the separation which is less than five the lighter molecules accumulate in the colder part of the gas. Actual molecules in general lie between the case of hard spheres and Maxwellian molecules. The ratio, R_T, of α for hard spheres for which it is a maximum, to α for actual molecules has been calculated by Jones[6] and by Brown[7] on the basis of various molecular models. These values of R_T run from less than 0.10 for HCl and Cl_2 to over 0.6 for neon and the other noble gases.

2. EXPERIMENTAL

The experimental arrangement is shown in Fig. 1. The separation column consists of four stages which are convectively coupled together as shown. The first stage consists of two concentric glass Pyrex tubes, 1.3 and 2.2 cm in diameter. The inner cylinder is heated to 370°C by a spiral Nichrome ribbon heater while the outer cylinder is kept at room temperature by means of tap water flowing through the condensor surrounding the column. This stage is 3.5 m in over-all length with a gap space of 4.5 mm.

The construction of the three very effective last stages is shown in Figs. 2 and 3. The diameters of the two concentric tubes are 0.6 cm and 1.55 cm giving a gap space of 4.75 mm. The inner cylinder is heated to 375°C by a twenty-mil tungsten wire heated to incandescence which is suspended along the axis of the inner tube. The differential expansion of the tubes is taken up by a sylphon bellows prepared inside with Bakelite varnish to withstand the action of the corrosive HCl gas.

The HCl gas used in the separation was prepared by dropping chemically pure concentrated hydrochloric acid into concentrated sulphuric acid. The rate of production of the hydrogen chloride gas was governed by a dropping funnel equipped with a capillary tip. The gas was dried by passing it through, first, a tube containing glass wool, and second, through a sulphuric drying tower. The tower was double, allowing the gas to go either way thus preventing the possibility of blowing the acid back through the system. It is important to have pure and dry HCl since both Cl_2 and the associated molecule formed of HCl and H_2O will go to the "heavy" end of the tube and interrupt its action. A flow of 250 cm³ an hour of HCl through the "light"

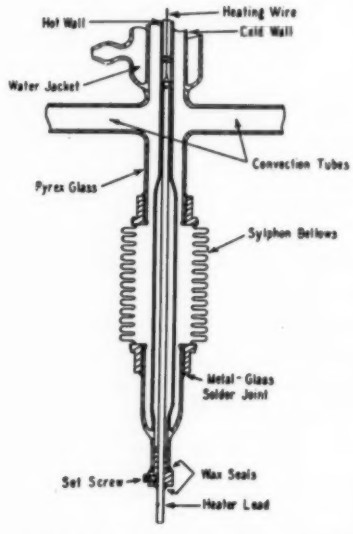

FIG. 2. Detail of lower end of last three stages.

[6] R. C. Jones, Phys. Rev. 58, 111 (1940).
[7] Harrison Brown, Phys. Rev. 57, 242L (1940).

end was maintained to insure that the gas at that point did not become enriched in the light isotope.

A 20-cm³ container placed between two stopcocks placed at the heavy end of the column allowed 20-cm³ portions of the enriched HCl to be removed from the column without disturbing the equilibrium since the effective end volume of the tube is around 100 cm³. The gas thus withdrawn could then be frozen down by the use of liquid air into appropriate containers for testing and further use. When the HCl was not needed in gaseous form, it was allowed to condense on ice at liquid air temperature.

The column was placed in operation by first evacuating it and then filling it to slightly over atmospheric pressure with gas from the generator. The tubes were then heated and the column allowed to come to equilibrium for 20 days without withdrawal of gas. After this time a total of 600 cm³ of gas were withdrawn in 100-cm³ portions over a period of 18 days. The column was then allowed to run for an additional ten days after which four 100-cm³ portions were withdrawn at intervals of five days. Satisfactory proton bombardment analyses were obtained of each of these latter samples. The total gas withdrawn was made into one portion and converted into Cl_2 by oxidation of NaCl by means of MnO_2 and concentrated H_2SO_4. The chlorine formed was used for spectroscopic studies.

3. ANALYSES

When chlorine is bombarded with deuterons there results a radioactive product whose half-life is 37 minutes. It has been established that the radioactive product is Cl^{38} from the reaction

$$Cl^{37}+H^2 \rightarrow Cl^{38*}+H'.^8$$

Two equal portions of HCl gas, one being a normal sample and the other being an enriched sample, were given equal deuteron bombardments from the 28″ Sloane Laboratory cyclotron. The resulting radioactivity was measured by means of a calibrated Lauritson electroscope. The relative strengths of the two samples gives the relative concentration of Cl^{37}. A five-minute bombardment of 2 cm³ of HCl at atmospheric pressure by a 0.5-microampere beam of 3.2 Mev deuterons was quite sufficient for measurement.

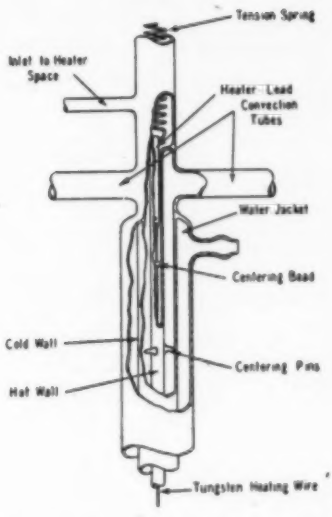

FIG. 3. Detail of upper end of last three stages.

Analyses of three of the last 100-cm³ portions of HCl gas withdrawn gave an average concentration of 53.3 percent Cl^{37}.

If an atomic mixture consists of two isotopes, the relative abundance of various diatomic molecules which can be formed is given by the expression

$$(C_1a+C_2b)^2=C_1^2aa+2C_1C_2ab+C_2^2bb,$$

where a and b represent the two isotopes and C_1 and C_2 their relative abundances hence

$$\frac{I_{aa}}{I_{bb}}=\frac{C_1^2}{C_2} \quad \text{or} \quad \frac{C_1}{C_2}=\left(\frac{I_{aa}}{I_{bb}}\right)^{\frac{1}{2}},$$

where I_{aa} and I_{bb} are the intensities of lines due to the molecules aa and bb in the spectrum of the diatomic molecules.

A spectroscopic determination of the isotope abundance was made from the absorption spectrum of Cl_2 obtained from the total operation of the column. This determination showed a trifle over 45 percent of Cl^{37} present as compared to 24.28 percent of Cl^{37} in normal Cl_2.

4. DISCUSSION OF RESULTS

It is now a well-known fact that any degree of isotopic purity may be obtained if one is willing to build a thermal diffusion column that is long

[8] E. F. Shrader and E. Pollard Phys. Rev. 59, 277–280 (1941).

enough. There is also sufficient evidence that the relatively simple theory outlined by Furry, Jones, and Onsager is fairly adequate in predicting the performance of such a column. Therefore, the main emphasis in this work was put on the production of a large amount of chlorine enriched in the heavy isotope for later spectroscopic study. In spite of the fact that the column was not run in a manner which best permitted a comparison with the theoretical predictions, it is interesting to make this comparison on the basis of the data available.

Column No. 1 was studied independently before the construction of the later column. After allowing the column to come to equilibrium a mass-spectroscopic analysis was made of a sample through the courtesy of Professor Urey of Columbia University. This analysis showed a concentration of 28.3 percent of Cl^{37} as compared to the original 24.28 percent Cl^{37}. This gives 1.18 as the maximum separation factor of the column.

The proton bombardment analyses of these last three samples taken show an average concentration of 53.3 percent Cl^{37}. This is with a transport of 0.80 cm^3/hr., S.T.P., of HCl with the assumption, of course, that a state of quasi-equilibrium has been established. For the last three columns, therefore, the separation factor is 2.89, or 1.42 for a single stage. For continuous operation with a transport $\tau = nH$ Furry, Jones, and Onsager give for the case of C_1 between 0.3 and 0.7 that

$$k - C_1^0 = (1 - \exp[-4_n A_d I])/4n.$$

From the transport the separation factor for true equilibrium may be obtained. This raises the separation factor for each of the columns to 1.45.

Before any calculations as to separation factors can be made a suitable value of R_t must be found. Brown calculates, from viscosity data, a value of $R_t = 0.12$ for chlorine, while Jones does not give any value, but indicates that it is small. For the purpose of this calculation a value of $R_t = 0.10$ was chosen.

For column No. 1 the actual performance fell far short of the theoretical predicted performance which was calculated to have a separation factor of 1.70. This fact indicated the necessity that any other columns built should be of different design. The theoretically predicted separation factors of columns No. 2–No. 4 were each 1.46. While it is impossible to compare the theoretically predicted performance with actual performance due to the approximations involved, it may be said that the last three columns outperform column No. 1. This is probably caused by the fact that their construction allows a higher degree of mechanical and temperature symmetry. The peripheral distance enters as the fourth power into the terms giving the remixing due to temperature asymmetry and this is quite important. The calculations show that the value R_t chosen is the right order of magnitude.

In conclusion the author wishes to thank Professor L. Onsager for his valuable suggestions and Professor E. Pollard for his help and advice in making determinations of the isotope concentrations by deuteron bombardment. The author is especially indebted to Professor W. W. Watson for his interest and guidance in this problem.

PHYSICAL REVIEW VOLUME 69, NUMBERS 9 AND 10 MAY 1 AND 15, 1946

Experiments with a Slow Neutron Velocity Spectrometer II*

R. F. BACHER, C. P. BAKER, AND B. D. MCDANIEL
Cornell University, Ithaca, New York

(Received February 23, 1942)**

The apparatus previously used for the determination of neutron energy by time of flight method has been completely rebuilt with a view to increasing the accuracy of measurement as well as the high energy limit. The repetition frequency is obtained from a series of relaxation oscillators and a 50-kc oscillator and frequencies of 100, 200, 500, 1000, and 2500 c.p.s. are available. Four detector channels have been built so that neutrons in four different time of flight groups can be counted simultaneously. When used with the highest repetition frequency, this decreases the time to obtain data by a factor of 24 and has thus made the present experiments feasible with the small Cornell cyclotron. The study of the transmission of Ag with a 1.35-g/cm² absorber shows a single strong resonance at 5.8 ev. A re-examination of In with considerably higher resolution than was previously used shows a single resonance at about 1.35 ev. The effective mean life of neutrons in several different sources was examined and a thin paraffin source with Cd backing devised for measurements in the thermal region. The absorption of B has been examined and found to be proportional to $1/v$ within the limits of error of the experiment, from 0.028 to 50 ev. An experiment to determine the B cross section of the Cd stopped neutrons gave 540×10^{-24} cm². The B absorption curve shows that the cross section of thermal neutrons (0.025 ev) is 708×10^{-24} cm². It is concluded that the effective energy of the Cd stopped neutrons is not that of kT at thermal energy, for the geometry used, but is 0.041 ev. This conclusion is confirmed by the measured resonances in Ag and In which are higher than the values obtained by the boron absorption method. Correction of these values, as measured by Horvath and Salant (reference 4) for the effective energy of the Cd stopped neutrons, leads to 1.32 ev for In and 5.2 ev for Ag, in agreement with the present results. It is concluded that resonances measured by the boron absorption method are in error by an amount which depends upon the geometry of the experiment, and are probably too low by a factor of $0.041/0.025 = 1.64$.

IN order to extend the range of the equipment[1] previously developed to determine neutron energy from time of flight, the apparatus has been completely rebuilt. Since the previous equipment was able to detect only very low resonances, it appeared that an extension of the energy range and greater resolution were desirable to study neutron transmission characteristics and to obtain more information about resonance absorption.

In addition to higher timing accuracy and the possibility of greater resolution, it appeared necessary to decrease the time required to obtain data. The time required in the region of 1 ev was already excessive, and with higher resolution would be expected to be longer. Accordingly, three new features were incorporated in the equipment: (1) a finer and more accurate subdivision of the cycle of operation, (2) a range of frequencies of the fundamental cycle so that it might be possible to increase the intensity by increasing the frequency to the limit determined by the overlapping of cycles at the detector, and (3) the possibility of recording data in several different time of flight intervals simultaneously.

APPARATUS

A schematic diagram of the measuring equipment is shown in Fig. 1. All frequencies are controlled from a 50-kc oscillator, and the repetition frequencies are obtained from relaxation oscil-

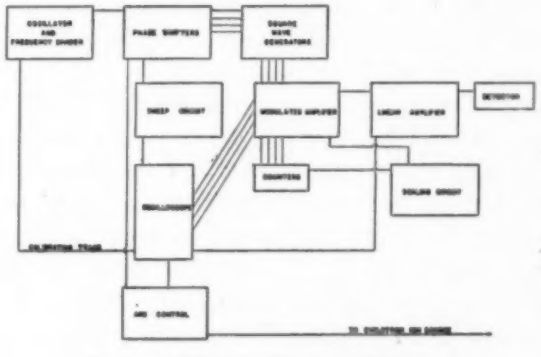

FIG. 1. Schematic diagram of neutron velocity spectrometer.

* Some of the observations reported in this paper have been considerably extended since its preparation. It is hoped that the somewhat more precise and detailed results of these experiments will be reported in the near future.

** This paper was received for publication on the date indicated but was voluntarily withheld from publication until the end of the war.

[1] C. P. Baker and R. F. Bacher, Phys. Rev. 59, 332 (1941).

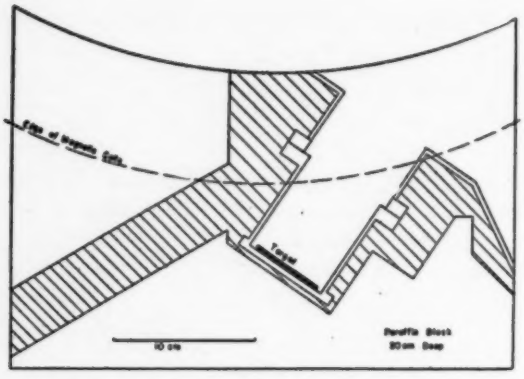

FIG. 2. Central section plan of paraffin block source and cyclotron target.

lators. These feed into a bank of six phase shifters, four of which control the square wave generators which work into the modulated amplifier to govern the "on" time of the detecting channels. Another phase shifter controls a special sweep circuit providing for large expansion, and all time comparisons are made and checked with a 50-kc calibrating trace directly on the oscilloscope face. The last phase shifter adjusts the arc control.

The oscillator and frequency divider was a primary oscillator working at 50 kc and four frequency division stages composed of thyratron relaxation oscillators. By proper tuning of the relaxation oscillators to lock in with the primary oscillator and with each other, a repetition frequency of 100, 200, 500, 1000, or 2500 c.p.s. could be obtained for use as a modulation frequency. The primary oscillator or any of the relaxation oscillators could be used as a calibrating wave and furnished a convenient subdivision of the cycle. A small oscilloscope was provided to observe and check the operation of this system, the saw-tooth wave form of the relaxation oscillators making the patterns very easy to recognize. Since it was possible to obtain any desired frequency with no stage differing by more than a factor of five from its driving stage, very little difficulty with stability was found. The frequency of the primary oscillator was checked and reset from time to time by comparison of one of the lower frequencies with a 1000-cycle fork although it was never found to differ from its previous setting by as much as one percent.

The phase shifter consisted of a filter to provide sinusoidal wave form and a resistance and capacity to produce a 90° phase shift. The two signals 90° out of phase were impressed on the grids of six twin triodes in parallel. The output of each member of the twin was fed into a mixing circuit, and the proper combination of the two signals made it possible to obtain a wave of any desired phase. It was arranged so that the manipulation of two variable resistors gave a smooth continuous 360°-phase shift. The outputs of these mixing circuits were used to control the timing of the production and detection and observation of the neutrons.

The arc control made use of two FG67 thyratrons which controlled the voltage on the arc type ion source in the cyclotron. One tube was placed in series with the arc to turn it on and the other in parallel to turn it off by short circuiting. A considerable amount of redesign on this circuit from that used in the previous work was necessary, both because of the higher frequencies required and because of the low power electronic source of the repetition frequency instead of an a.c. motor generator supply. Tubes with a short de-ionization time were necessary, and type FG67 was found to be most satisfactory from this standpoint but required much more grid power than the FG57's formerly used. Each tube consequently required a power amplifier. Difficulty was also experienced in extinguishing the tubes after their cycle of operation since the power supplied to the arc came from a d.c. motor generator set. Some method of interrupting the current through the tubes for at least 100 μsec. must be provided. After several unsuccessful attempts to do this with other thyratrons, a bank of power tubes was placed in series with the motor generator. At the lower frequencies this method was not necessary, but at 2500 cycles no simpler method was found.

The modulated amplifier was very little changed from the one previously described except for the inclusion of four channels instead of one and for the particular care taken to obtain speed of response. The first tube was a thyratron discriminator which flashed for all neutrons detected, and which was fed into the scaler and into the four modulated channels. A modulated channel consisted of an amplifier tube whose

control grid was actuated by the neutron pulse and whose screen grid was actuated by a square wave generator which determined the open time of the tube. Output circuits were provided to drive the counters. The square wave generators were almost identical with that previously described except for a modification in the phasing and grid driving. The waves were quite accurately square, the voltage rising or falling within 0.5 μsec. The square pulse could be varied in width from 1 μsec. at 2500 cycles (a little more at lower frequencies) to a quarter of a cycle.

A new linear amplifier was constructed with special consideration for stability and speed of response. The gain per stage had to be sacrificed on both of these counts so that seven stages were necessary. Small time constants and negative feedback were incorporated, and to reduce the difficulties introduced by the unavoidable shunt capacity of the cable connecting the amplifier proper with the ionization chamber, two stages of amplification preceded this cable.

Tests on resolution were made using two of the square wave generators. With two pulses of 5 μsec. duration and 15 μsec. separation center to center impressed on the grid of the first tube, two completely separated pulses could be observed at the output. With 10 μsec. separation the pulses were not completely resolved, but the voltage fell to half maximum between pulses. The over-all time lag of the apparatus, including lags in production and acceleration of the deuterons in the cyclotron and in collection of ionization in the detector, was measured by the method previously described[1] and found to be 19 μsec. Subsequent improvements have been made during the course of the experiments, the shortest lag so far produced being 8.5 μsec. This compares to a time lag of 35 μsec. in the earlier apparatus.

EXPERIMENTAL PROCEDURE

The general arrangement of the equipment with the cyclotron was essentially the same as that previously shown. The cyclotron chamber has been rotated about 30°, making the target somewhat more centrally located. The geometry of the paraffin block surrounding the B target which is shown in Fig. 2 was also changed to keep the face perpendicular to the line to the ionization chamber. The face dimensions were approximately 20×35 cm².

In order to cut down the fast neutron background, about 10 cm of paraffin was placed around the collimating tube holding the ionization chamber. Figure 3 shows the fraction of fast neutrons as a function of time. These measurements were taken with about 10 cm of paraffin, Cd, and a thick B_4C absorber in front of the collimator. For time of flight experiments, carried out at 3 meters, the background is 3 percent or less for energies of 19 ev or below.

A hydrogen-filled ionization chamber was used to determine how accurately the production and detection of neutrons was controlled under actual experimental conditions. This chamber was sensitive only to fast neutrons so that times of flight and scattering difficulties did not enter, and the time distribution of proton recoils gave an accurate indication of the time of production of neutrons. The duration of the neutron burst was measured in the following manner: the square pulse controlling the ion source was adjusted for 10 μsec. width, and the square pulse controlling detection was made very long (120 μsec.) and initially completely overlapping the time of production. The start of the detector "on" time was then made later and later in the cycle so that it overlapped the time of production by smaller and smaller amounts. This procedure is similar to that used for the previously described time lag measurement.[1]

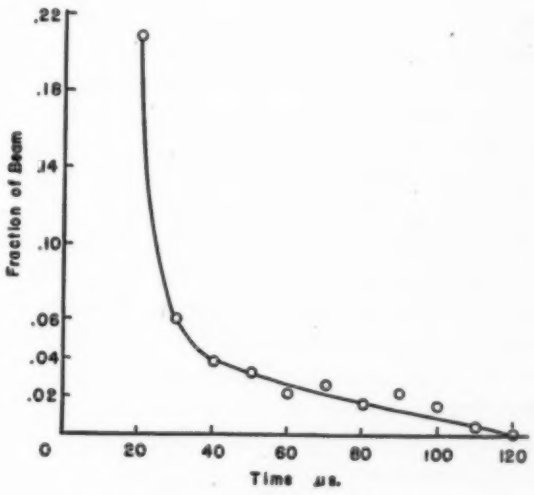

FIG. 3. Fraction of counts due to fast neutrons plotted against time of observation.

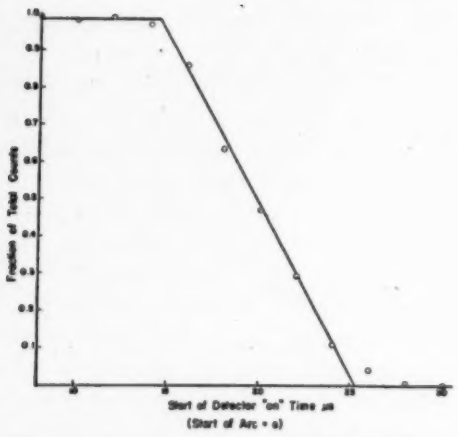

FIG. 4. Relative counts observed with hydrogen-filled ionization chamber plotted against the difference in time setting of the start of the burst and the start of the detector "on" time.

One would expect the counting rate to be constant as long as there is complete overlap and a linear decrease until there is no overlap so that the duration of the linear decrease is a measure of the duration of the burst. Figure 4 shows the counting rate plotted against the difference in time between the settings of the start of the burst and the start of the detector "on" time. The counting rate is seen to be constant until 14.5 μsec. and then to decrease until 25.2 μsec., showing an "on" time of the source of 10.7 μsec. There is evidence for a small tail as a few neutrons were recorded after production had presumably stopped. This amounts to about 4 percent of the maximum intensity about 2 μsec. later, and less than 1 percent 6 μsec. later. The magnitude of this tail was found to be insensitive to changes in gas pressure, filament temperature, or arc voltage. The fact that the start of the decrease occurs at 14.5 μsec. indicates an over-all time lag of this amount.

The detector was measured in a similar way, and the sensitivity was found to be 3 μsec. longer than the duration indicated by the setting of the controlling square wave, although otherwise well behaved, having no observable tailing effects. The extra 3 μsec. was found to be due to the smearing of a pulse in the modulated amplifier which should have been of very short duration. This pulse has now been sharpened, but unfortunately the difficulty was not discovered until after the measurements described here were made. The effect of this broadening is to increase the resolution width by 3 μsec. and to decrease the mean time of flight associated with an observation or the distance between the centers of the "on" times by half this amount. For the data taken at three meters this means a change in resolution of 1 μsec. and a change of 0.5 μsec. in the time of flight in the plots on the one meter time of flight axis and was neglected.

RESULTS

A. Silver

The experiments on Ag were carried out at a repetition frequency of 2500 c.p.s. and with a Cd absorber 0.45 g/cm² thick in front of the collimator to absorb the low energy neutrons which would otherwise appear in succeeding cycles. The time of flight spectrum of the source as measured with the chamber and Cd absorber is shown in Fig. 5. The number of counts per unit total is plotted against time of flight and the number of neutrons per time of flight interval is nearly constant except where the Cd begins to cut off.

The results of a series of three separate runs on a 1.35-g/cm² thick Ag absorber have been collected and the relative transmission plotted against time of flight for 1 meter in Fig. 6. The circles with a cross in them represent data from a preliminary run taken at 2 m with 20 μsec. "on" time for source and detector. These data were taken with the same amplifier used in the previous work.[1] The open circles represent data taken at 3 m with the same equipment and "on" times. The heavy circles represent data taken at 3 m at the same resolution with the new linear

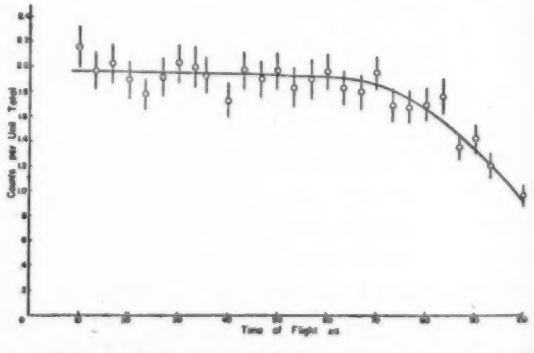

FIG. 5. Time of flight spectrum (in μsec./meter) of paraffin block source measured through a 0.45-g/cm² Cd filter.

amplifier described briefly above. While the settings were the same, these points do not have the same abscissae as the open circles because of the different measured time lag with the new amplifier. The vertical lines indicate the probable errors from the number of counts. Measurements of the over-all transmission were made in the 3-m runs, and these two measurements were averaged. This over-all transmission was used in the way previously described[1] to obtain the transmission curve. The preliminary data were adjusted to the same over-all transmission and are included here mainly to show that the data repeat with a different path length. Since the timing errors can hardly depend on the path length, this provides a check.

The datum representing transmission at a given time of flight actually represents a time of flight band due to the resolving power of the apparatus. Since the "on" times of source and detector are each 20 μsec., the data taken at 3 m include for a particular point no neutrons whose velocity is 6.7 μsec./meter different from that indicated for the point. The distribution function is triangular[1] and is such that 0.75 of the neutrons have velocities between those of the two adjacent points.

The most prominent feature of the transmission curve is the strong absorption which appears to be just below the point at 5.8 ev. While there seems to be some evidence for a lower transmission at about 1.5 and 0.78 ev, the interpretation of these dips as resonances is very doubtful, and they are not included in the curve. The data

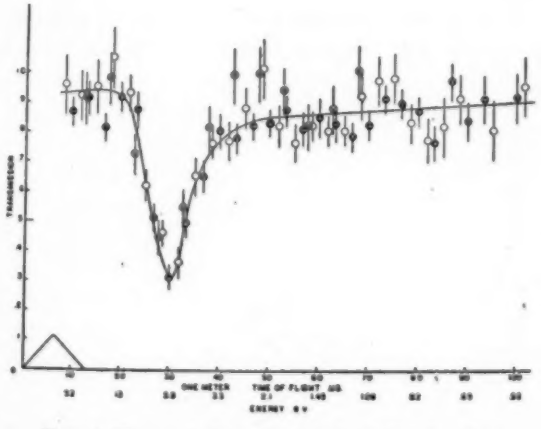

FIG. 6. Transmission of 1.35-g/cm² Ag absorber plotted against time of flight for 1 meter.

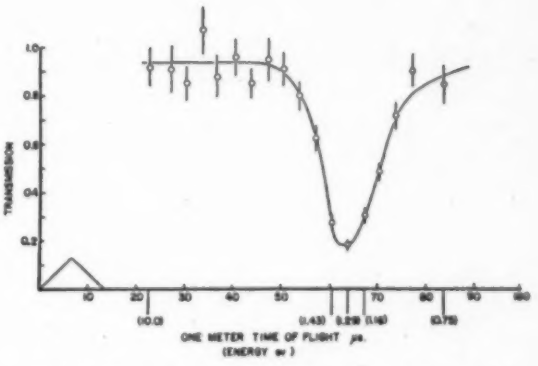

FIG. 7. Transmission of 0.169-g/cm² In absorber plotted against time of flight for 1 meter.

show a transmission of about 0.3 at the resonance minimum. In order to give a transmission of 0.25 at 30 μsec. and 0.5 at the adjacent points, it takes nearly complete absorption between 4.7 and 7.3 ev with the resolution of the apparatus considered. Such strong absorption over a wide band is to be expected with the thick absorber used.

B. Indium

Further experiments were made on indium in order to establish more accurately the energy of the resonance. The previous measurements[1] showed a transmission minimum slightly above 1.0 ev. This measurement was made with much poorer resolution than it has since been found possible to use and serves mainly to demonstrate the effect of this resonance. Because of the considerable effect of resolution, low precision, and background corrections involved it is not considered a reliable measure of the resonance energy.

The present measurements of the transmission of indium were made at a distance of 3 m with "on" times of source and detector of 20 μsec. using an absorber of 0.169 g/cm² and covered the energy region from 10 to 0.75 ev (23 to 84 μsec./m). The results are plotted in Fig. 7. The vertical lines indicate the probable error in the transmission measurements, and the isosceles triangle shows the resolution function, or spread in time of flight to which the apparatus was sensitive. The fast neutron background was not significant in the region studied. It is evident that between 0.75 ev and 10 ev there is only one strong resonance, and it occurs in the neigh-

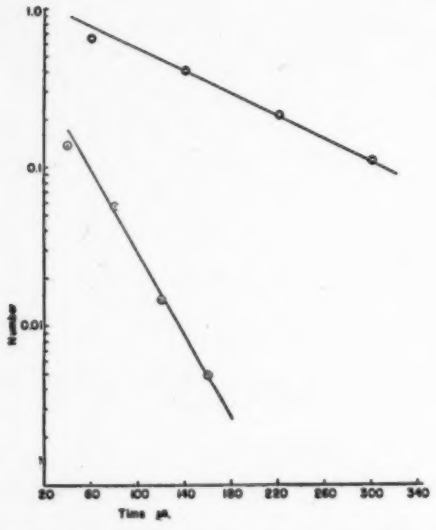

FIG. 8. Relative number of neutrons plotted against time after neutron burst for paraffin block source (upper curve) and tray (lower curve).

borhood of 1.3 ev. This shows a much better resolution of the resonance than the previous measurement even though the thickness of the absorber is less.

While no effort has been made to find the shape of a resonance which could produce the observed curve with the resolution used, it seems probable that there must be a region of negligible transmission of approximately 5 to 10 μsec. in width, or several tenths of a volt, showing that the exact position of the resonance is still masked by the resolution and by the thickness of the absorber. An investigation of the effect of resolution on certain sample transmission curves calculated from the Breit-Wigner one-level formula shows that both of these effects make the resonance appear at a lower energy than its actual value.

A further measurement was made with a thinner absorber (0.051 g/cm²) and higher resolution which indicated that the energy lies between 1.29 and 1.43 ev probably at or above 1.35 ev. More complete measurements on indium are in progress making use of a wide range of thickness, and until these are complete no attempt will be made to determine the shape of the level.

C. Effective Mean Life

It was known from the previous measurements that the time of arrival of *thermal* neutrons at the detector is not a good measure of their time of flight because of the relatively long mean life in the paraffin. Unless precautions are taken to reduce this effect the results of time of flight measurements are uncertain below 0.2 ev and probably quite untrustworthy below 0.1 ev. A method of controlling the effective mean life was devised which made use of a change in the source geometry.

The face of the paraffin block was covered with a sheet of cadmium 43×43 cm and 0.45 g/cm² in thickness. This absorbed all thermal neutrons emitted, but allowed neutrons of somewhat higher energy to penetrate. Thermal neutrons were regenerated in a thin (1.6-cm) layer of paraffin 38×38 cm placed in front of this cadmium. The whole assembly is referred to as the tray. It was anticipated that the effective mean life in this thin layer would be considerably reduced by diffusion out of the paraffin.

The effective mean life was measured by placing the face of the ionization chamber against the source and measuring the time dependence of the emission of neutrons after the burst. The results of the measurements are shown in Fig. 8. The "on" times of both source and detector were 40 μsec., and the relative number of neutrons recorded in the various time intervals are plotted on a logarithmic axis. The upper curve is for the paraffin block shown in Fig. 2, and shows an effective mean life of 123 μsec. The lower curve is for the same block with the tray in front, and shows an effective mean life of 33 μsec. This geometry was used for all work below 0.5 ev.

It was found possible to control the effective mean life by another and possibly more satis-

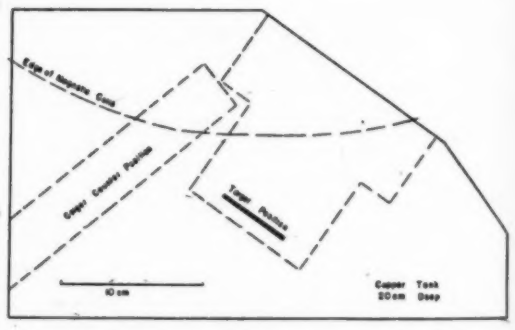

FIG. 9. Central section plan of copper water tank source and cyclotron target.

factory method.[2] The source was surrounded by a copper water tank of a shape similar to the paraffin block and shown in Fig. 9. The effective mean life was measured in the same way with water and with various strengths of B_2O_3 solution. The results showed a life of 107 μsec. for tap water, 70 μsec. for a solution of 1.8 g/liter B_2O_3, and was reduced to 43 μsec. for a solution of 7.3 g/liter B_2O_3. The volume of the tank was 11 liters. It is realized that a measurement of the true mean life could be made with a detector placed in the middle of the source and with a different timing scheme, but the purpose of these measurements was to measure the effective mean life of the neutrons arriving at an external detector in order to evaluate the results of time of flight measurements.

D. Boron

The absorption of boron in the form of B_4C absorbers has been investigated from 0.028 ev to about 50 ev (1-m time of flight 430 μsec. to 10 μsec.). The B_4C absorbers[3] were made in flat bottomed Al cups by dusting the powder from a height of about 5 ft. The powder rained into the cup which was filled with ether and a small amount of celluloid dissolved in acetone to act as binder. The amount of celluloid remaining in the absorber after evaporation was obtained for each absorber and varied from about 2 percent by weight for the thinnest absorber to 0.2 percent for the thickest absorber. The thicknesses of B were corrected for this known amount of binder. Since the resulting absorber was a rather compact cake, the thickness was determined by cutting out the material around the edge to give a circular disk which still adhered to the Al, and the thickness in g/cm² was obtained from the size and the known weights before and after making the absorber.

Five B_4C absorbers were used in the experiments containing 0.273, 0.1197, 0.0585, 0.0487, and 0.0318 g/cm² B. Experiments with the two thicker absorbers were carried out using the paraffin block source shown in Fig. 2, and with a distance of 3 m between source and detector.

[2] This was suggested by E. Fermi.

[3] The B_4C was obtained from the Norton Company and is reported to be sufficiently pure B_4C that the percentage of boron was computed from the atomic weights giving 78.3 percent B by weight.

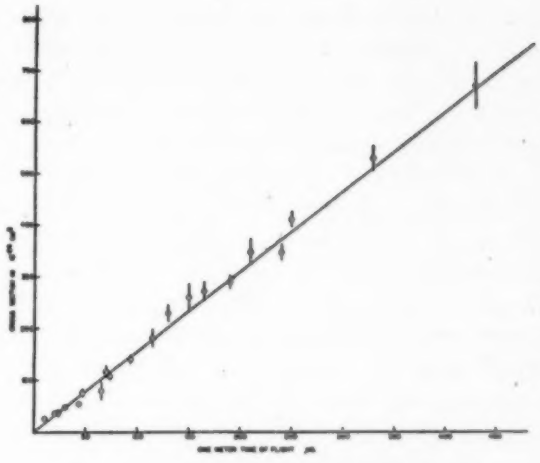

FIG. 10. Boron cross section plotted against time of flight for 1 meter.

The source and detector were "on" for 20 μsec. each. The repetition frequency was 2,500 c.p.s., and a Cd absorber 0.9 g/cm² was used as a screen.

For the three thinner absorbers the repetition rate was 500 c.p.s. with "on" times of 50 μsec. for the 0.0487-g/cm² absorber, and 80 μsec. for the other two absorbers. The distance of source to detector of 2 m was used for these three absorbers. At the lower recurrence rate used, it was necessary to investigate the effect of neutrons appearing in succeeding cycles (recycling) by some measurements at still lower frequency. With the usual source it was found that there was a very considerable effect. This was decreased by the use of the tray previously described to cut down the mean life in the source and by the introduction of a thin B_4C screen containing 0.0205 g/cm² of B. Without the screen there was still an appreciable recycling, but with the screen the effect was indistinguishable from background.

The collected results of the absorption measurements on B are shown in Fig. 10 where the B cross section is plotted against $1/v$ in μsec./meter. Within the accuracy of the data the points fit a straight line. The straight line shown was fitted by least squares methods, the vertical lines representing probable errors from the number of counts taken. The slope of the straight line is $(1.55\pm0.035)\times10^{-24}$ cm²/μsec., and the intercept is $(-0.5\pm2.1)\times10^{-24}$ cm². The one point at 43 μsec. is rather far off the curve, and in fact makes half the contribution of the sum

of the squares of the residuals. Omitting this point the slope remains unchanged, and the intercept is increased to $(+4.4\pm1.4)\times10^{-24}$ cm². A negative intercept has no physical significance, and indeed a small positive intercept is to be expected due to the scattering cross section.

A further experiment with boron was carried out to determine the cross section in boron of the neutrons emitted from the paraffin block source stopped in thick Cd. No timing arrangements were used for this experiment, and the experiments are subject to errors in stability of the source which do not appear for the time of flight experiments. The geometry of the experiment was essentially that described above for the B measurements at 2 m except for the removal of the tray in front of the source and of the B_4C screen. In addition to the brass face of the ionization chamber there was a 20-mil piece of copper for electrical shielding in the beam path. An examination of a piece of brass of the same thickness as the ionization chamber face and a piece of 20-mil Cu showed that its transmission for the Cd stopped and transmitted neutrons was within the accuracy of the experiment the same. The Cd absorber used was 0.90 g/cm². Further experiments were also carried out with the tray source described previously, but with the geometry otherwise the same.

The results are summarized in Table I for the three different B absorbers which were used. The third column gives the absorber thickness, the fourth the observed transmission, and the fifth the cross section of the Cd stopped neutrons obtained. The cross sections have been used with the curve of Fig. 10 to obtain the corresponding time of flight, from which the effective energy given in the last column can be obtained.

The effective energy of the Cd stopped neutrons is nearly twice that expected on the basis of thermal equilibrium. With the large paraffin block this seemed so unusual that the measurements were scrutinized very carefully but repeated experiments gave essentially the same results. This difference will be discussed later. It will also be noticed that there is a gradual increase in σ for the thinner absorbers, which might be expected if there were a filtering or "hardening" action of the absorber. The experiments with the thinner source show a higher effective energy which might be expected from the thinner paraffin. They also show a much greater dependence of the effective energy on absorber thickness, associated possibly with a more inhomogeneous source.

TABLE I. Summary of B absorption measurements of the Cd stopped neutrons emitted by two different sources.

Source	Measurements	Absorber thickness g/cm²	Transmission	$\sigma(B)$ Cd stopped neutrons cm²×10⁻²⁴	τ time of flight μsec.	E effective energy ev
Paraffin block	3	0.0487	0.242	519	334	0.047
Paraffin block	3	0.0318	0.388	531	342	0.045
Paraffin block	1	0.0205	0.539	540	348	0.043
1.6-cm paraffin over Cd	1	0.0487	0.319	418	270	0.072
	1	0.0318	0.435	466	301	0.058
	1	0.0205	0.550	522	337	0.046

DISCUSSION OF RESULTS

The results in boron show that within the accuracy of the experiments, the cross section is proportional to $1/v$ from 0.028 to 50 ev. The cross section attributed to neutrons of thermal energy (0.025 ev) is 708×10^{-24} cm², which is considerably greater than the values usually quoted for the so-called C group neutrons (those absorbed in thick Cd) which are usually referred to as thermal neutrons. The measurements of Horvath and Salant[4] give an absorption coefficient for the C group neutrons of $K=30.2\pm0.03$, which gives a cross section $\sigma=539\times10^{-24}$ cm². The strong difference in the measured cross sections suggests that the neutrons emitted with the relatively small amount of paraffin usually used may not have the expected thermal distribution. This may be due to the effect of the leaking out of neutrons at the sides of the slowing down material.

The measurement of the cross section of the C neutrons in B was made in the untimed experiments previously described using various B absorbers. The paraffin block source which was used was designed to be as nearly as practicable like a Fermi cylinder[4] with the source located near the top. If the cross sections obtained from the measurements with the three different absorbers are plotted against absorber thickness, a straight line is obtained, and if extrapolated to zero absorber thickness this line gives a cross section of 552×10^{-24} cm² or an absorption co-

[4] W. J. Horvath and E. O. Salant, Phys. Rev. 59, 154 (1941).

efficient of 31.0 cm²/g. The thinnest absorber used gave 54 percent transmission, and this leads to a cross section of 540×10^{-24} cm² (Table I). This is in close agreement with the measurements of Horvath and Salant[4] with somewhat the same geometrical arrangement. There appears, therefore, to be no disagreement on these absorption measurements.

The cross section of 552×10^{-24} cm² above gives from the plot of Fig. 10 an effective energy of the Cd stopped neutrons of 0.041 ev. In the determination of resonance energies by the boron absorption method,[5] this energy is assumed to be that of thermal neutrons and the ratio of the boron absorption coefficient of the C group neutrons to that of the resonance group used to multiply the assumed thermal energy to obtain the desired resonance energy. The conclusions arrived at here indicate that the resonance energies thus obtained by the boron method are in error by an amount which depends upon the geometry of the experiment. For the Fermi geometry the energies so obtained should be raised by a factor $0.041/(kT)=0.041/0.025=1.64$. It should be pointed out that the determination of this factor depends upon the untimed experiments and may, therefore, be subject to certain small errors arising from the steadiness of the source.

The measurements of the Ag and In resonances provide a strong check on the above conclusions. In Ag the most prominent feature of the observed neutron absorption spectrum (Fig. 6) is the resonance at 5.8 ev. This resonance shows very strong absorption and must be correlated with the A group in Ag. The careful boron absorption measurements of Horvath and Salant[4] using a Fermi cylinder give a resonance energy for the A group of 3.3 ev. This value is in violent disagreement with the resonance energy observed by these time of flight experiments, but if the value obtained by the boron absorption method is multiplied by the correction factor,[6] the resonance energy as obtained is 5.2 ev which agrees fairly well.

For In the measurements of Horvath and Salant yield a resonance energy of 0.84 ev for the 54-min. period. The present measurements show only one resonance and that at 1.35 ev. With the same correction factor the value of Horvath and Salant becomes 1.32, which agrees very well. This agreement must depend to a considerable extent on the rough similarity of geometry.

These results lead to the inescapable conclusion that with the geometrical arrangements used in the past, the C group neutrons are not of thermal energy. Resonance energies determined by the boron absorption method which assume that the C group neutrons have thermal energy are incorrect. The correction factor for the geometry used here is 1.64, but this factor will depend on the experimental arrangements.

Early experiments[7] with a mechanical velocity selector indicated that the velocity distribution of the C group neutrons observed from a paraffin block or howitzer source was such that agreement between the expected and observed distribution was obtained if it is assumed that the emitted neutrons have a Maxwell distribution at room temperature. This result now appears to be in disagreement with the present work. The disagreement is possibly caused by the fact that the mechanical velocity selector experiments were of necessity carried out with very poor resolution. It seems difficult, therefore, to consider the disagreement serious.

The earlier experiments also showed that when the source was cooled, the emitted distribution shifted toward lower velocity. Furthermore it was shown in experiments by Fink[7] that the cross section of various elements except Cd increase when the source is cooled, in agreement with the increased activity also observed. This definitely shows the presence of some neutrons in thermal equilibrium, and this qualitative conclusion does not disagree with the present results.

The authors are indebted to the Research Corporation for a grant which made this work possible.

[5] H. Bethe, Rev. Mod. Phys. 9, 134 (1937).
[6] Here 1.57 since Horvath and Salant use $kT=0.026$ ev.

[7] J. R. Dunning, G. B. Pegram, G. A. Fink, D. P. Mitchell, and E. Segrè, Phys. Rev. 48, 704 (1935); G. A. Fink, Phys. Rev. 50, 738 (1936).

Experiments on the Elastic Single Scattering of Electrons by Nuclei*, **

R. J. VAN DE GRAAFF, W. W. BUECHNER, AND H. FESHBACH
Massachusetts Institute of Technology, Cambridge, Massachusetts

(Received November 30, 1945)

Experiments on the elastic single scattering of electrons by nuclei are described, the measurements extending over a range of voltages, angles, atomic numbers, and foil thicknesses. Observations were made at a number of voltages from 1.27 to 2.27 Mev and at angles from 20 degrees to 50 degrees on both sides of the incident electron beam. The scattering foils were aluminum, copper, silver, platinum, and gold, the atomic numbers thus varying from 13 to 79. When the foil thickness exceeded that for a "thin" target, a correction was made for multiple scattering. The use of an accurately focused homogeneous beam of electrons from an electrostatic generator made possible clear-cut control of the basic experimental variables. The experimental method was designed to minimize the effect of x-ray background, etc. The present results are in close agreement with the relativistic theory of electron scattering, as developed by Mott, over the entire range of the experimental variables except for the case of 2.27-Mev electrons on aluminum. Excepting only this case, the average of all the ratios of experimental result to theoretical prediction is 1.01 with a standard deviation of 0.06. This is in marked contrast with most of the previous work in this field where results have been widely divergent. The results of this paper, combined with spectroscopic data, extend the range of validity of the Coulomb law of attraction between electron and nucleus in close to the surface of the nucleus. The measurements of the scattering of 2.27-Mev electrons by aluminum will be repeated as soon as circumstances permit, as these results now indicate for the larger angles an interesting divergence from theory.

INTRODUCTION

SINCE the scattering of fast electrons offers the most direct method for determining experimentally the forces between electrons and nuclei at close distances of approach, a large number of researches have been performed in this field. As has been frequently pointed out,[1] the results have been widely divergent, various values having been reported for the ratio of the experimentally observed scattering to that predicted by the theory of Mott. In fact the values found for this ratio range from 0.15 to 100. Much of this spread may be accounted for by the experimental limitations associated with the inhomogeneity in energy and low intensity of the beta-ray sources usually employed. Recently, however, the availability of high speed electron beams of high intensity and accurately known and controllable energy has made possible an approach under clear-cut experimental conditions.

In the experiments described in detail below, a narrow parallel beam of electrons homogeneous in energy was made to fall on a thin target foil whose atomic number, thickness, and orientation with respect to the beam could be readily changed. The voltage of the electron beam could be read on a meter and easily varied. The detecting ionization chamber was arranged so that it could be calibrated to measure only the electrons elastically scattered by nuclei at a given angle, being at the same time shielded from those electrons which were either scattered by other electrons or inelastically scattered by nuclei. The effect of the x-ray background on the ionization chamber was substantially eliminated by means of a null arrangement.

EXPERIMENTAL METHOD

Scattering Chamber

Certain essential features of the scattering chamber are shown schematically in Fig. 1. The electron beam was produced by a high voltage electrostatic installation described elsewhere.[2] The beam as it descended from the accelerating tube was accurately parallel and somewhat larger than $\frac{1}{4}$ inch in diameter. The $\frac{1}{4}$-inch hole in the

* Because of circumstances associated with the national emergency, the preparation of this paper for publication has been considerably delayed. The scattering apparatus was dismantled at the termination of the experimental work in August, 1941.

** An abstract of this paper was presented on November 30, 1945 at the St. Louis meeting of the American Physical Society.

[1] For example, see the summaries in the following papers: F. C. Champion, *Reports on Progress in Physics* (1938), Vol. 5, p. 348; W. Bosshard and P. Scherrer, Helv. Phys. Acta 14, 85 (1941); R. B. Randels, K. T. Chao, and H. R. Crane, Phys. Rev. 68, 64 (1945).

[2] L. C. Van Atta, D. L. Northrup, R. J. Van de Graaff, and C. M. Van Atta, Rev. Sci. Inst. 12, 534 (1941).

beryllium diaphragm[3] shown in Fig. 1 was used to define the beam more precisely. The effect of electrons scattered by the beryllium was minimized by placing an aluminum diaphragm with a $\frac{5}{16}$-inch hole at the entrance to the chamber as shown in Fig. 1. To check the definition and the accurate vertical alignment of the beam passing through the chamber, an insulated aluminum diaphragm having a $\frac{5}{16}$-inch hole was located at the exit of the chamber. The beam then continued downward into a Faraday cage. The vacuum maintained in the chamber was of the order of 10^{-5} mm of mercury so that gas scattering was negligible.

The scattering chamber was in the form of a hollow cylinder of welded steel 12 inches in diameter and 8 inches deep. One end was removable, being bolted on and sealed by means of a lead gasket. The target foils were mounted around the rim of an insulated aluminum disk. The disk in turn was mounted in such a way that any particular foil could be accurately placed in the center of the chamber and tipped at any angle about a horizontal axis passing through this center. This was accomplished by a simple arrangement consisting of a detent mechanism and two concentric shafts passing out through the lid of the chamber. The shafts pass through a region filled with a thick stopcock grease under pressure, thus affording a reliably vacuum-tight joint.

Collector Assembly

The collector assembly for measuring the electrons scattered at a given angle θ is shown in outline in Fig. 1 and in detail in Fig. 2. In order to conveniently and accurately control the angle θ, the collector assembly was mounted on a large disk fastened to the end of a hollow horizontal shaft passing out through the fixed end of the scattering chamber. The axis of this shaft was accurately in line with the horizontal axis of the chamber. The joint between shaft and chamber was made vacuum tight by a pressure grease seal. To the outer end of the shaft was fastened an accurate worm gear, 7.5 inches in diameter and having 360 teeth.[4] This was driven by a small worm mounted on the shaft of a Selsyn motor which could be remotely controlled. Thus, from the main control station, the angle θ could be quickly changed and reset to within the order of one minute of arc.

The design and essential arrangement of the collecting assembly can be seen in Fig. 2. The scattered electrons were measured by an ionization chamber which could be reached only by the electrons passing through the three diaphragms in front of the chamber. The diaphragm nearest the ionization chamber defined the small solid angle of the cone of electrons received from the foil. The other two diaphragms shield the ionization chamber from the stray electrons which may be initially scattered from the foil and subse-

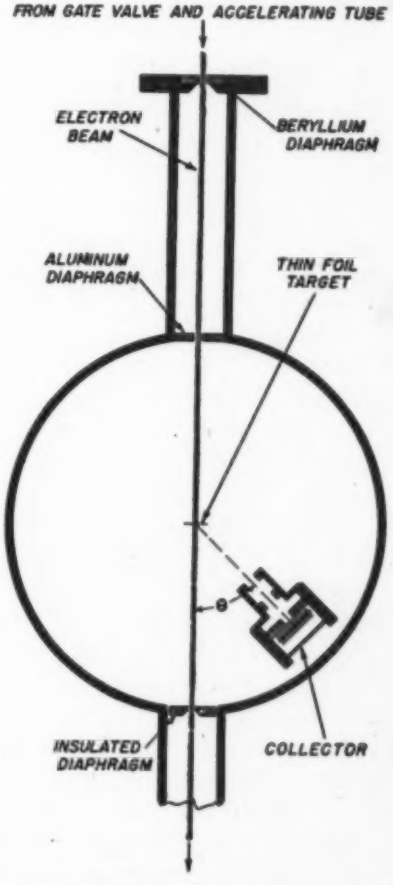

FIG. 1. Schematic diagram of scattering chamber.

[3] The beryllium disk was very kindly made for this purpose by Professor John Wulff of the Department of Metallurgy of Massachusetts Institute of Technology.

[4] It is a pleasure to acknowledge the valuable help of Mr. Walter H. Kallenbach in the construction of the worm gear drive and the steel scattering chamber.

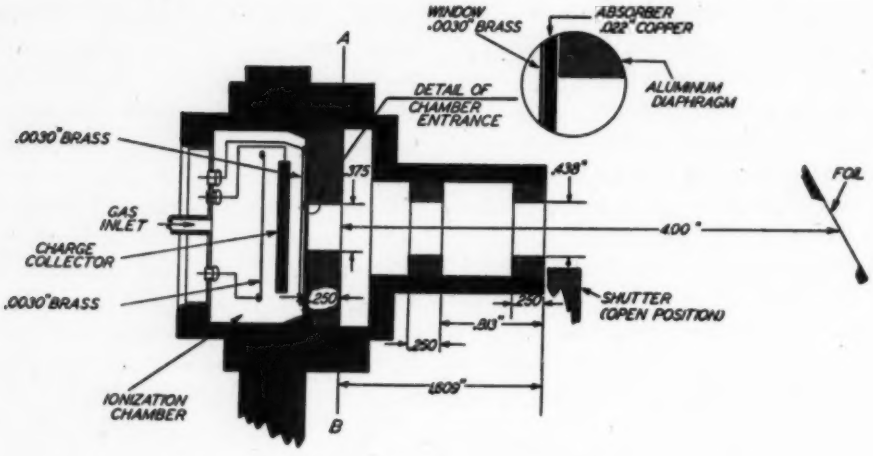

FIG. 2. Details of ionization chamber.

quently scattered back towards the ionization chamber by the walls of the scattering chamber.

Ionization Chamber

The ionization chamber was especially designed to minimize x-ray background. This background is produced principally by electrons scattered by the foil and subsequently striking the walls of the scattering chamber. The presence of such background is difficult to eliminate since it is so intimately associated with the scattering by the foil. The background due to the relatively weak x-radiation from the top beryllium diaphragm was substantially eliminated by lead packed around the neck of the scattering chamber. The ionization chamber was filled with air at atmospheric pressure which was maintained by a gas inlet tube connected to the outer atmosphere through the large hollow shaft supporting the collector assembly. The electrical leads for the ionization chamber were brought out through the shaft in a similar manner. The charge collector was a brass disk, 2 mm thick, sandwiched between the two thin brass disks as shown. The charge collector was at approximately zero potential while one disk was at approximately 1000 volts positive and the other at about 1000 volts negative. The background due to x-rays could be balanced out with this arrangement by suitably adjusting the potentials of the thin plates so that the collector current was zero when no electrons were entering the chamber. The scattered electrons entering the chamber produce a full net ionization current since they only pass through the half of the chamber nearest the foil. The scattered electrons could be prevented from entering the chamber by means of a remotely controlled shutter shown in Fig. 2, sufficiently thick to stop the electrons but small enough so its relatively slight shift in position did not appreciably change the x-ray background. The null ionization chamber with shutter proved very useful, since without means for measuring and minimizing the background considerable errors might have been made, particularly at the larger angles.

Another type of undesirable background might be owing to electrons which have been scattered from the primary beam and have suffered a loss in energy. This loss might be caused by inelastic nuclear scattering, to ionization losses, to electron-electron scattering, or to combinations of these three mechanisms. Such electrons can be screened from the ionization chamber by placing an absorber between it and the last diaphragm as is shown in Fig. 2. The absorber used in these measurements was of a thickness corresponding to slightly less than the range of 1.27-Mev electrons, the voltage used in the initial series of experiments.

Calibration of Ionization Chamber

In order to determine the ratio of the ionization currents observed to the current actually carried into the ionization chamber by the elastically scattered electrons, the following calibration

scheme was used. The collector assembly was rotated so that there was no foil or other obstruction in the path of the primary electron beam. The beam thus passed cleanly through the diaphragm system into the ionization chamber and produced an ionization current. The ratio between this current and the primary beam current which produced it gives the desired calibration factor for that particular voltage and absorber. The primary beam was then measured after swinging the collecting system clear of the beam, which then passed cleanly through the lower diaphragm shown in Fig. 1, and impinged on the beryllium bottom of the insulated Faraday cage mentioned previously. The potential across the ionization chamber was sufficient to insure saturation for all currents measured by the chamber.

Experimental Procedure

In making a series of measurements at a particular voltage and with a particular foil, the following procedure was used. First, the alignment of the chamber was checked. Secondly, after adjustment of the beam current to a suitably low value the ionization chamber was calibrated according to the method described above. The beam current was then increased to a value suitable for scattering experiments, the desired foil interposed and tipped to an angle appropriate to the scattering angle. At a given angle θ, the shutter was closed and the ionization chamber balanced. The shutter was then removed from the path of the scattered electrons and the ionization current observed. At the end of a run, both the beam current and the calibration of the ionization chamber were checked. During the course of a run, the total current to the scattering chamber was read continuously.

Runs were made at voltages 1.27, 1.81, 2.00, 2.27 Mev. At each voltage observations were in general made on foils of aluminum, copper, silver, platinum, and gold covering a range in atomic number from 13 to 79. The thickness of the foils ranged from approximately 0.0001 inch to 0.001 inch. The angular range covered in these experiments varied from 20° to 50° on each side of the beam. The beam currents ranged from about 2 microamperes to 100 microamperes, the ionization current due to scattered electrons from about 0.002 microampere to 0.3 microampere. The calibration currents used varied from about 0.5 microampere to 1 microampere. The calibration factor, ionization current/calibration current, varied from about 1 to 15.

The voltage was measured by a generating voltmeter which was calibrated both by the use of the threshold voltages of the photo-disintegration of deuterium and beryllium as well as by the more usual extrapolation methods. The voltage was known to within one percent and was kept steady to within that value. Calculations based on the analysis supplied by the manufacturers indicated that any errors due to impurities of the foils were inappreciable. Foil thicknesses were measured, in general, by weighing and by an optical lever method.[5] These determined the thickness to approximately one percent. The angle θ could be set by the remote control mechanism to within approximately one minute of arc. The beam current was measured by a microammeter to within an accuracy of 1 percent. The calibration and ionization current were measured by a sensitive galvanometer generally to within 1 percent, although for the lowest currents the error was somewhat greater.

Corrections and Possible Errors

In order to compare the experimental results with theoretical predictions it is necessary to consider the possibility of corrections for the finite beam diameter, finite solid angle subtended by the ionization chamber, the alignment of the scattering chamber, and the possible lack of symmetry of the beam. In addition, corrections must be considered for multiple and inelastic scattering.

The effect of a finite beam width of $\frac{1}{4}$ inch and finite size window of the ionization chamber was evaluated by use of the Mott formula. The effect was calculated to be less than 1 percent. Although the beam was approximately aligned with the scattering chamber as described above, there was no way of ensuring that the center of the beam as it passed through the aligning diaphragms corresponded exactly with the centers of these diaphragms. Assymmetry in this respect would result in unequal reading of the scattered current for angles of $+\theta$ and $-\theta$ particularly since the

[5] We are indebted to Mr. E. N. Strait for making these measurements.

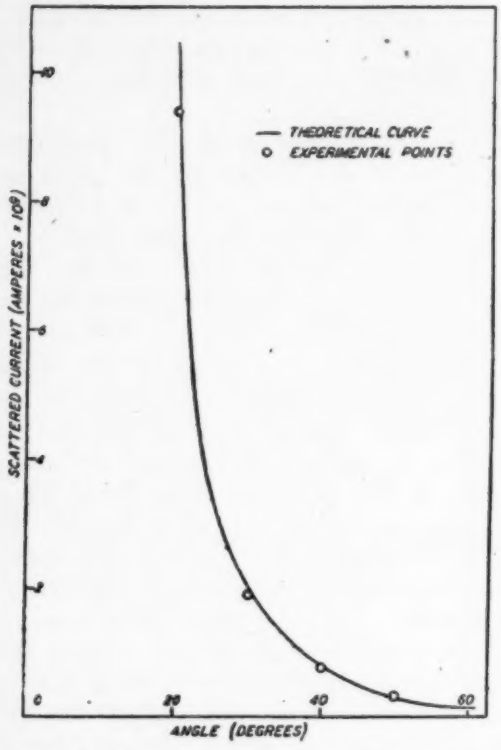

FIG. 3. Plot of scattered current *vs.* angle for aluminum at 2.00 Mev.

scattering in this angular range varies approximately with the inverse fourth power of the angle θ. A difference in the readings at plus and minus θ was actually observed. This was corrected for theoretically, using the Mott formula. It was found that a good measure of the scattering at angle θ could be found by taking the arithmetical mean of the arithmetical and geometrical means of the readings at $+\theta$ and $-\theta$. If these two means, the geometrical and the arithmetical, do not differ very much, this result is more than sufficiently precise. For the cases which occurred in the measurements reported in this paper, the error introduced by this assumption is about 1 percent.

The window to the ionization chamber was taken to be the 0.375″ hole in the plane AB, shown in Fig. 2. The solid angle corresponding to this window is 6.94×10^{-3} steradian. The effective size of the window may be somewhat reduced from this value because a few of the electrons passing through this window will strike the sides of the cylindrical hole of the diaphragm at a glancing angle. A fraction of these electrons will be lost by absorption in the aluminum, although the majority will probably be scattered into the ionization chamber. However, an effect counterbalancing this occurs because some of the electrons striking the aluminum just outside the circumference of the window may be scattered into the ionization chamber. It is estimated that these counterbalancing errors are of the same order and that their difference is small enough to be neglected.

A possible source of error in measurements of this kind is the inclusion of electron-electron scattering along with nuclear scattering. To check the order of magnitude of this scattering experimentally, the net current to a foil through which the primary beam was passing was measured. An aluminum foil was used. The ratio of electron-electron scattering to nuclear scattering will be less for other foils since they are of higher atomic number. With a suitable arrangement of bias potentials to eliminate low energy secondary electrons, it was found that the total number of extra electrons emitted in all directions from the foil due to electron-electron impacts was of the order of a few percent. This in accordance with the theoretical expectations.[6] Since electron-electron scattering involves an energy loss, only a small fraction of such scattered electrons could penetrate the absorber and enter the ionization chamber. Thus, there is both theoretical and experimental evidence that the error due to electron-electron scattering was considerably less than 1 percent.

Another possible source of error is the inclusion of inelastic nuclear scattering along with the elastic nuclear scatterings. Since the general theory of x-ray production in this energy range appears to be in general agreement with experiment,[7] the theory was used to calculate the amount of expected inelastic nuclear scattering.[8] The effect appears to be negligible under the conditions of these experiments. Moreover, the use of the absorber, as mentioned above, afforded an additional experimental precaution.

The thickness of the foils was chosen so as to

[6] Möller, Ann. d. Physik **14**, 568 (1932).
[7] A. A. Petrauskas, L. C. Van Atta, and F. E. Myers, Phys. Rev. **63**, 389 (1943).
[8] N. F. Mott, Proc. Camb. Phil. Soc. **27**, 255 (1931).

satisfy Wentzel's criterion and thus minimize the effect of multiple scattering. As is well known, Wentzel's criterion is rough and a correction of the data for possible multiple scattering still has to be applied. The procedure followed here was suggested by Saunderson and Duffendack.[9] This makes use of the results of Chase and Cox[10] giving the plural scattering error at angle θ as

$$\langle\theta^2\rangle_{Av}[\csc^2(\theta/2)-\tfrac{1}{2}],$$

where the average is taken with respect to the actual scattering distribution. This average has been computed by Goudsmit and Saunderson,[11] thus making it possible to evaluate the effect of multiple scattering. It should be mentioned here that this procedure, based on a statistical approach, is not completely accurate for the plural scattering of importance in these experiments.

Possibility of such corrections for multiple scattering was considered for all points reported here. Many of the points required no correction, although in one instance the correction ran as high as 20 percent. In certain cases where the foils were sufficiently thin, the observed scattering was accurately proportional to thickness, thus affording direct experimental evidence of true single scattering.

COMPARISON OF THEORY AND EXPERIMENT

Comparison of the results, after correction, was made to the predictions of Mott[12] based on the Dirac theory of the electron. If f is the ratio of the scattered current to incident current, the theory predicts for small atomic numbers, high incident velocities, and small solid angle that

$$f=nt\Omega\left(\frac{Ze^2}{2mc^2}\right)^2\frac{1-\beta^2}{\beta^4}\times\csc^4\frac{\theta}{2}\left[1-\beta^2\sin^2\frac{\theta}{2}+\frac{Z\pi\beta}{137}\cos^2\frac{\theta}{2}\sin\frac{\theta}{2}\right],$$

where n = number of atoms per unit volume; t = thickness of foil; Ω = solid angle subtended at foil by ionization chamber; Z = atomic number; β = velocity of electron divided by velocity of light; and θ = angle of scattering. This formula is not correct for high Z, even at these voltages, as has been shown by the calculations of Bartlett and Watson[13] for gold. However, their results indicate that the deviation of the exact calculation from the Mott formula is small within the angular range of these experiments except for gold and platinum. We have, therefore, used the above formula for aluminum, copper, and silver, whereas we used Bartlett and Watson's result for gold and platinum.

In Fig. 3 we have plotted f_{theo} and f_{exp} as a function of the angle θ for 2-Mev electrons incident on aluminum. This indicates the range and the rapidity of variation with angle in that range over which measurements were taken. This method of comparison is, however, not a very sensitive one for showing variations from theoretical predictions. We have, therefore, computed the ratio f_{exp}/f_{theo}. These results are given in Table I and plotted in Figs. 4 and 5. In the latter, the abscissa is the distance of closest distance of

TABLE I. Ratios of the experimental results to the theoretical predictions. Only those points have been included for which observations were made on both sides of the beam and for which the multiple scattering correction did not exceed 20 percent.

Energy (Mev)	20°	30°	40°	50°
		Nucleus: aluminum		
1.49		1.01	0.97	1.04
1.81		1.02	0.96	0.97
2.00		0.95	0.97	1.02
2.27	1.11	1.26	1.52	1.64
		Nucleus: copper		
1.49		0.97	0.88	1.12
1.81		0.96	1.09	1.07
2.00		1.05	0.96	0.96
2.27		1.15	1.06	
		Nucleus: silver		
1.27			0.93	
1.49		0.97	1.03	1.02
1.81		0.97	1.02	1.03
2.00		1.01	1.06	1.07
		Nucleus: gold and platinum		
1.49				1.08
1.81				1.09
2.00			1.10	1.00

[9] J. L. Saunderson and O. S. Duffendack, Phys. Rev. **60**, 190 (1941).
[10] C. T. Chase and R. T. Cox, Phys. Rev. **58**, 243 (1940).
[11] S. Goudsmit and J. L. Saunderson, Phys. Rev. **57**, 24 (1940).
[12] N. F. Mott, Proc. Roy. Soc. London **A124**, 425 (1929); **135**, 429 (1931). See also P. Urban, Zeits. f. Physik **119**, 67 (1942). The correction given by Urban to the Mott formula is negligible in the angular and voltage range occurring in these measurements.
[13] J. H. Bartlett and R. E. Watson, Proc. Am. Acad. Art Sci. **74**, 53 (1940).

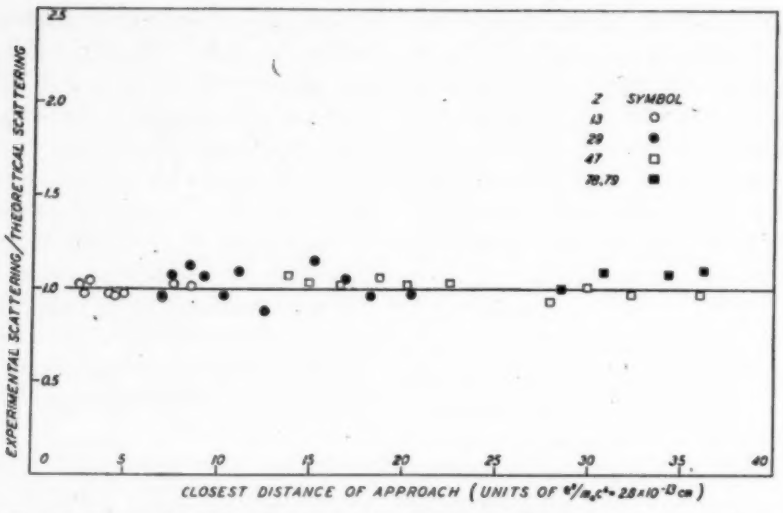

FIG. 4. Comparison of experimental results with theory (except for 2.27-Mev electrons on aluminum).

approach to the nucleus. The closest distance of approach is given by the formula

$$\frac{R}{(e^2/mc^2)}=Z\frac{\epsilon}{\epsilon^2-1}\left[\left\{\frac{1}{\epsilon^2}+A(\theta)\right\}^{\frac{1}{2}}-1\right],$$

$$A(\theta)=\cot^2\frac{\theta}{2}+2\beta^2\ln\sin\frac{\theta}{2}+\frac{2Z\pi\beta}{137}\left(\sin\frac{\theta}{2}+\csc\frac{\theta}{2}-2\right),$$

where ϵ is the total energy of the electron in units of its rest mass.

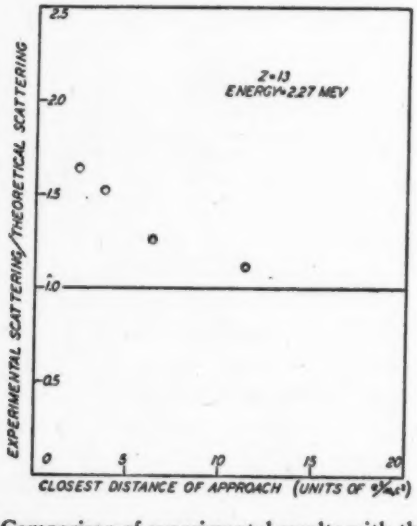

FIG. 5. Comparison of experimental results with theory for 2.27-Mev electrons on aluminum.

No undue importance should be attached to this choice of scattering parameter, especially since the distance of closest approach is much smaller than the wave-length and from the point of view of the uncertainty principle not very meaningful. However, it is a practical method in this angular and voltage range, for the comparison of different experiments involving different voltages, nuclei and scattering angles.

DISCUSSION

As can be seen in Figs. 4 and 5, the present results are in close agreement with the relativistic theory of electron scattering, as developed by Mott, over the entire range of the experimental variables except for the case of 2.27-Mev electrons on aluminum. Excepting only this case, the average of all the ratios of experimental result to theoretical prediction is 1.01 with a standard deviation of 0.06.

The points shown in Fig. 5, corresponding to 2.27-Mev electrons on aluminum, indicate a systematic departure from theory which increases with an increasing scattering angle. This group of points was taken under the same general experimental conditions as the points in Fig. 4. For example, copper points were taken at these angles and at the same voltage, and are in agreement with the Mott formula. Because the wave-length of the electrons is very much larger than the radius of the aluminum nucleus, these

points would require a radical departure of the force between electron and the aluminum nucleus from the Coulomb force. Moreover, it would have to be energy dependent and Z dependent in order to be consistent with the agreement of aluminum points at 2.00 Mev and copper points at 2.27 Mev with the Mott formula. Unfortunately, the data for aluminum at 2.27 Mev were among the last taken before research of this type was interrupted by the war. These measurements with aluminum will be repeated as soon as circumstances permit as they now indicate for the larger angles an interesting divergence from theory.

ACKNOWLEDGMENTS

It is a pleasure to thank Professor F. E. Myers, then on leave from New York University, for preliminary calculations of the Mott formula and Wentzel's criterion and also for his work on the design of the scattering chamber. We are particularly grateful to Mr. Anthony Sperduto for his many important contributions in carrying out the various experimental techniques involved in this work. Mr. Howard Rowland rendered valuable assistance particularly in making experimental observations. Mr. E. A. Burrill, Jr. helped in the computations and analysis of the experimental data. We wish to thank Professor C. F. Squire for his valuable help during the period in which the experimental observations were made. In connection with the construction of the apparatus used in these experiments, we acknowledge with pleasure the able help of Mr. E. W. Nickerson in charge of the shop of the High Voltage Laboratory.

We are glad to have this opportunity to express our great appreciation to the Research Corporation and to the Carnegie Corporation of New York for their generous grants made in support of this work.

PHYSICAL REVIEW VOLUME 69, NUMBERS 9 AND 10 MAY 1 AND 15, 1946

Isotope Separation by Thermal Diffusion: The Cylindrical Case

W. H. Furry and R. Clark Jones*
Research Laboratory of Physics, Harvard University, Cambridge, Massachusetts

(Received December 26, 1940)†

All of the theoretical treatments of the thermal separation column published up to the present time have been restricted by the assumption that the column consists of two parallel plane walls, one hot and the other cold. Actually, nearly all of the separation columns used in practice consist of two concentric cylinders, the inner cylinder often being simply a hot wire. The theoretical treatment of the plane case which was given by Furry, Jones, and Onsager is here extended to include the cylindrical case. The extension is carried through in general, that is, for a gas whose physical properties are arbitrary functions of the temperature. It is found that the extended treatment is formally very similar to that already given for the plane case. The difficulty of the calculations is enormously increased, however, by the explicit appearance in the characteristic differential equation of the radius as a function of the temperature. The solution is here carried through in detail only for a perfect gas whose viscosity, thermal conductivity, and diffusivity have the same temperature dependences as those of a Maxwellian gas. Exact numerical solutions for a few cases have been obtained, but the computations were so tedious that it was found desirable to develop approximate methods of solution. Two different kinds of approximate solutions are given: a series solution useful when the ratio of radii is not larger than about four or five, and an asymptotic solution valid when the ratio of radii is large, as in the case of the hot-wire types of separation column.

THE theory of the functioning of the new apparatus[1] for isotope separation by thermal diffusion has been investigated by various writers.[2–7] The quantitative agreement between

* National Scholar, Harvard University, at the time this work was done. Now with Polaroid Corporation, Cambridge, Massachusetts.

† This paper was received for publication on the date indicated but was voluntarily withheld from publication until the end of the war.

[1] K. Clusius and G. Dickel, Naturwiss. **26**, 546 (L) (1938); Zeits. f. physik. Chemie **B44**, 397 (1939).

[2] L. Waldmann, Zeits. f. Physik **114**, 53 (1939).

[3] W. H. Furry, R. Clark Jones, and L. Onsager, Phys. Rev. **55**, 1083 (1939). This will be referred to as FJO.

[4] W. van der Grinten, Naturwiss. **27**, 317 (L) (1939).

[5] P. Debye, Ann. d. Physik **36**, 284 (1939).

[6] J. Bardeen, Phys. Rev. **57**, 35 (1940) (further considerations based on reference 3).

[7] For a general account of the subject, given mostly from

theory and experiment has been found to be reasonably good.[8] It therefore seems worth while to try to improve the theoretical treatment by dispensing with an idealization which has been involved in all of the calculations so far published: namely, the assumption that the processes take place between plane walls. In actual practice one is usually concerned with concentric cylinders. In some cases[9] the radii of the cylinders are so nearly equal that the results for plane walls are fairly accurate; in many cases, however, the inner cylinder is simply a fine wire, and the "plane case" formulas are completely inapplicable.

We shall first show how the formulation in terms of a master function, which was used in FJO, can be extended to the cylindrical case. We then specialize the formulas to the Maxwellian case, in which heat conductivity, viscosity, and diffusivity are proportional to the first, first, and second powers of the absolute temperature, and carry out various specific calculations on this basis.

The present paper is devoted entirely to the task of determining for the cylindrical case the constants H, K_c, and K_d which enter into the transport equation of the thermal separation column.

I. GENERAL FORMULATION

We shall carry through the formulation in strict analogy to the argument in FJO, Eqs. (6)–(26). For convenience of comparison, we shall number the analogous equations here as (106)–(126). The notation is the same, with two exceptions: (a) Instead of the Cartesian coordinate x, we now have the variable r of cylindrical coordinates, the limits being r_1 and r_2; we assume $r_1>r_2$, corresponding to $T_1<T_2$, because we take the inner cylinder to be the hot one. (b) The symbol Q has a different meaning, $2\pi Q$ being the heat flow by conduction per unit length of the cylinders, in cal./cm-sec.

The equations of the temperature field are now

$$2\pi Q=2\pi r\lambda(-dT/dr),$$

$$Q\log(r_1/r_2)=\int_{T_1}^{T_2}\lambda dT, \tag{106}$$

$$(\partial/\partial r)=-(Q/r\lambda)(\partial/\partial T).$$

For $\mathbf{v}$ parallel to z, $\partial v/\partial z=\partial v/\partial\varphi=0$, the hydrodynamical equation in cylindrical coordinates is

$$r^{-1}(\partial/\partial r)r\eta(\partial v/\partial r)=(dp/dz)+\rho g, \tag{107}$$

and substitution from (106) gives

$$(Q^2/\lambda r^2)(d/dT)(\eta/\lambda)(dv/dT)=(dp/dz)+\rho g. \tag{108}$$

The boundary conditions are, as before,

$$v(T_1)=v(T_2)=0. \tag{109}$$

The equation for the flux of species 1 is, of course, just Eq. (10) of FJO:

$$\mathbf{J}_1=\rho[\mathbf{v}c_1+D(-\text{grad } c_1+\alpha c_1c_2\text{ grad log } T)]. \tag{110}$$

(In order that this equation be strictly correct, the density ρ should be considered as the density the gas would have if all of the molecules were of species 1.)

The formulation given in FJO is based on certain simplifying assumptions which are not really essential and the use of which can be avoided by a procedure given by Bardeen.[10] Although the argument of Bardeen can readily be extended to the present case, we shall, for simplicity and brevity, adhere to the procedure of FJO.

We accordingly apply the stationary condition,

$$\text{div } \mathbf{J}_1=0, \tag{111}$$

which, when we use (110) and (106), becomes

$$(\partial/\partial T)(\rho D/\lambda)[(\partial c_1/\partial T)-(\alpha c_1c_2/T)]=(\lambda\rho r^2/Q^2)[v(\partial c_1/\partial z)-D(\partial^2c_1/\partial z^2)]. \tag{112}$$

As in FJO, we omit the term in $(\partial^2c_1/\partial z^2)$; the effect of longitudinal diffusion is of course to be included later in a simpler way. We use, then, the equation

$$(\partial/\partial T)(\rho D/\lambda)[(\partial c_1/\partial T)-(\alpha c_1c_2/T)]=(\lambda\rho r^2/Q^2)v(\partial c_1/\partial z). \tag{112'}$$

---

the theoretical point of view, see R. Clark Jones and W. H. Furry, Rev. Mod. Phys., submitted for publication. This article includes a summary of the results of the present paper.

[8] A. O. Nier, Phys. Rev. **57**, 30 (1940). The calculations made in the present paper show that the agreement is even better than is indicated by Nier.

[9] For example, in the case described in reference 8.

[10] J. Bardeen, Phys. Rev. **58**, 94 (L) (1940). The extension of this argument to the cylindrical case is given essentially by changing the variable x to r and replacing ρ by $r\rho$ throughout.

In terms of the function G defined by

$$(\partial c_1/\partial z)G(z, T) = (r\lambda Q^3/\rho D)J_{1r} \quad (113a)$$

$$= Q^4[(\partial c_1/\partial T) - (\alpha c_1 c_2/T)], \quad (113b)$$

(112′) can be written

$$(\partial/\partial T)(\rho D/\lambda)(\partial c_1/\partial z)G(z, T) = \lambda\rho Q^2 r^2 v(\partial c_1/\partial z). \quad (114)$$

The final assumption made by FJO is that $(\partial^2 c_1/\partial z \partial T) = 0$. By just the same arguments as were used in FJO (Eqs. (15)–(17)), this leads to two consequences: The total transport of gas along the tube is zero, and G is a function of T only. Equation (114) can then be solved for v:

$$v(T) = (1/\lambda\rho Q^2 r^2)(\partial/\partial T)(\rho D G(T)/\lambda). \quad (118)$$

By substitution of (118) in (108) and differentiation with respect to T, we obtain the differential equation for $G(T)$:

$$\frac{d}{dT}\frac{1}{\lambda r^2}\frac{d}{dT}\frac{\eta}{\lambda}\frac{d}{dT}\frac{1}{\lambda\rho r^2}\frac{d}{dT}\left(\frac{\rho D}{\lambda}G(T)\right) = g\frac{d\rho}{dT}. \quad (120)$$

The boundary conditions can readily be obtained from (113a), (109), and (118):

$$G(T_1) = G(T_2) = G'(T_1) = G'(T_2) = 0. \quad (121)$$

We can now obtain the expression for τ_1, the upward transport of species 1. By (106) we have

$$\tau_1 = 2\pi\int_{r_2}^{r_1}\rho c_1 v r dr = (2\pi/Q)\int_{T_1}^{T_2}\rho\lambda c_1 v r^2 dT. \quad (115)$$

Substitutions of (118) in (115) gives

$$\tau_1 = (2\pi/Q^3)\int_{T_1}^{T_2} c_1(d/dT)(\rho D G(T)/\lambda)dT. \quad (122)$$

By partial integration and use of (121) and (113b) we now obtain the transport equation in standard form,

$$\tau_1 = Hc_1c_2 - K_c\partial c_1/\partial z, \quad (123)$$

with coefficients given by

$$H = -(2\pi/Q^3)\int_{T_1}^{T_2}(\rho D\alpha/\lambda T)G(T)dT, \quad (124)$$

and

$$K_c = (2\pi/Q^7)\int_{T_1}^{T_2}(\rho D/\lambda)\{G(T)\}^2 dT. \quad (125)$$

In order to obtain the correct transport equation, we must add to (123) a term which gives the effect of diffusion along the tube, since this effect was omitted when (112) was replaced by (112′). The term required is $-K_d\partial c_1/\partial z$, where

$$K_d = 2\pi\int_{r_2}^{r_1}\rho D r dr.$$

On using (106), we obtain

$$K_d = (2\pi/Q)\int_{T_1}^{T_2}\lambda\rho D r^2 dT. \quad (126)$$

The problem for the cylindrical case has now been given a formulation which is, formally, precisely analogous to that of the plane case. The practical difficulties of solution, however, are enormously increased. This is due to the appearance in the differential equation (120) of the factor r, which must be obtained as a function of T by the integration of Eq. (106). This leads to complicated calculations even when the temperature dependences of the properties of the gas are assumed to be very simple.

II. THE MAXWELLIAN CASE

Formulation in Terms of Dimensionless Quantities

We assume that the quantities

$$(\lambda/T), (\eta/\lambda), (\rho D/\lambda), (\rho T)$$

are all independent of T. From (106) we then obtain by integration

$$2\log r = -(\lambda/QT)T^2 + \text{const.} \quad (1)$$

We now introduce the dimensionless variable t and the dimensionless parameters t_1, t_2:

$$t = (\lambda/QT)^{\frac{1}{2}}T, \quad t_i = (\lambda/QT)^{\frac{1}{2}}T_i. \quad (2)$$

The quantities t_1 and t_2 can be determined from

$$t_2/t_1 = T_2/T_1, \quad (3)$$

$$t_2^2 - t_1^2 = 2\log(r_1/r_2). \quad (4)$$

To save writing we introduce a length r_0, defined by writing (1) in the form

$$r^2 = r_0^2\exp(-t^2). \quad (5)$$

We also introduce a new master function γ which differs from G by a constant factor:

$$G(T) = -(QT/\lambda)^{\frac{1}{2}}(\lambda^4\rho g/\eta D)r_0^4\gamma(t). \quad (6)$$

The differential equation (120) now takes the form

$$\frac{d}{dt}t^{-1}\exp(t^2)\frac{d^2}{dt^2}\exp(t^2)\frac{d\gamma}{dt}=t^{-2}, \tag{7}$$

with the boundary conditions

$$\gamma(t_1)=\gamma(t_2)=\gamma'(t_1)=\gamma'(t_2)=0. \tag{8}$$

The formulas for H, K_c, and K_d reduce to

$$H=2\pi\cdot\{\rho^2g^3/\eta\}\cdot r_0^4\int_{t_1}^{t_2}(\alpha\gamma/t)dt, \tag{9}$$

$$K_c=2\pi\cdot\{\rho^3g^2t^7/\eta^2D\}\cdot r_0^8\int_{t_1}^{t_2}\gamma^2dt, \tag{10}$$

$$K_d=2\pi\{\rho D/t\}\cdot r_0^2\int_{t_1}^{t_2}t^2\exp(-t^2)dt. \tag{11}$$

In these expressions the quantities in curly brackets are independent of the temperature.

The results of the computations may be stated conveniently in terms of the following definitions of dimensionless "shape factors" h, k_c, k_d:

$$H=(2\pi/6!)\{\alpha\rho^2g/\eta\}_1\cdot r_1^4\cdot h, \tag{12}$$

$$K_c=(2\pi/9!)\{\rho^3g^2/\eta^2D\}_1\cdot r_1^8\cdot k_c, \tag{13}$$

$$K_d=2\pi\cdot\{\rho D\}_1\cdot r_1^2k_d, \tag{14}$$

$$h=6!t_1^3\exp(2t_1^2)\int_{t_1}^{t_2}(\alpha/\alpha_1)(\gamma/t)dt, \tag{15}$$

$$k_c=9!t_1^7\exp(4t_1^2)\int_{t_1}^{t_2}\gamma^2dt, \tag{16}$$

$$k_d=t_1^{-1}\exp(t_1^2)\int_{t_1}^{t_2}t^2\exp(-t^2)dt. \tag{17}$$

Here the quantities in curly brackets are not independent of the temperature, and have been given the subscript 1 to indicate that they are to be evaluated at the lower temperature T_1. In the extreme cylindrical case this is the most reasonable simple choice of a temperature characteristic of the gas as a whole, since only a very small part of the gas is at temperatures near T_2. Equation (15) has been written in a form which can be applied when the quantity α varies with the temperature; α_1 is the value of α at the temperature T_1.

The numerical factors in Eqs. (12)–(14) have been chosen to correspond to those in the formulas for the plane case as given by FJO, with the correlations $B\to 2\pi r_1$, $2w\to r_1$.

For the "nearly plane case," r_1/r_2 not very large, it is convenient to define the shape factors h', k_c', k_d':

$$H=(2\pi/6!)\{\alpha\rho^2g/\eta\}\cdot\tfrac{1}{2}(r_1+r_2)(r_1-r_2)^3(2u)^2h', \tag{18}$$

$$K_c=(2\pi/9!)\{\rho^3g^2/\eta^2D\}\cdot\tfrac{1}{2}(r_1+r_2)(r_1-r_2)^7(2u)^2k_c', \tag{19}$$

$$K_d=2\pi\cdot\{\rho D\}\cdot\tfrac{1}{2}(r_1+r_2)(r_1-r_2)\cdot k_d', \tag{20}$$

$$h'=6!\cdot\bar{t}^3\cdot 2[\exp(-\tfrac{1}{2}t_1^2)+\exp(-\tfrac{1}{2}t_2^2)]^{-1}\cdot[\exp(-\tfrac{1}{2}t_1^2)-\exp(-\tfrac{1}{2}t_2^2)]^{-3}\cdot(2u)^{-2}\int_{t_1}^{t_2}(\alpha/\bar{\alpha}_1)(\gamma/t)dt. \tag{21}$$

$$k_c'=9!\cdot\bar{t}^7\cdot 2[\exp(-\tfrac{1}{2}t_1^2)+\exp(-\tfrac{1}{2}t_2^2)]^{-1}\cdot[\exp(-\tfrac{1}{2}t_1^2)-\exp(-\tfrac{1}{2}t_2^2)]^{-7}\cdot(2u)^{-2}\cdot\int_{t_1}^{t_2}\gamma^2dt, \tag{22}$$

$$k_d'=\bar{t}^{-1}\cdot 2[\exp(-t_1^2)-\exp(-t_2^2)]^{-1}\cdot\int_{t_1}^{t_2}t^2\exp(-t^2)dt. \tag{23}$$

Here the quantities in curly brackets are to be evaluated at the arithmetical mean temperature $\bar{T}=(T_2+T_1)/2$. We have used the abbreviations

$$\bar{t}=(t_2+t_1)/2, \tag{24}$$

$$u=(\Delta T/2\bar{T})=(T_2-T_1)/(T_2+T_1)=(t_2-t_1)/(t_2+t_1). \tag{25}$$

In the limit $(r_1-r_2)/r_1\to 0$, the factors h', k_c', k_d' approach limits

$$\begin{aligned} h'&\to f(2u)=1+u^2/7+u^4/21+\cdots,\\ k_c'&\to 1,\\ k_d'&\to 1+u^2/3, \end{aligned} \tag{26}$$

and Eqs. (18)–(20) become identical with the results of FJO for the plane case, with the identifications $B\to\pi(r_1+r_2)$, $2w\to r_1-r_2$. With these identifications, the coefficients of h', k_c', and k_d' in Eqs. (18)–(20) are identical with the $H^{(0)}$, $K_c^{(0)}$, and $K_d^{(0)}$ of reference 7.

Since by (7) and (8), the function γ depends only on t, t_1, and t_2, it follows from (15)–(17) and (21)–(23) that the shape factors h, k_c, and k_d, and h', k_c', k_d' depend only on t_1 and t_2. By writing

Eqs. (3) and (4) in the form

$$t_1^2=\frac{2\log(r_1/r_2)}{(T_2/T_1)^2-1}, \tag{3'}$$

$$t_2^2=\frac{2\log(r_1/r_2)}{1-(T_1/T_2)^2}, \tag{4'}$$

it is evident that t_1 and t_2 are in turn functions only of the two ratios r_1/r_2 and T_2/T_1. *The shape factors are therefore functions only of the two numbers* r_1/r_2 *and* T_2/T_1. Our problem is to determine the values of the shape factors for any given values of these two ratios. This is done by computing the shape factors as functions of the convenient dimensionless parameters t_1 and t_2, whose values are related to those of r_1/r_2 and T_2/T_1 by (3') and (4').

The Formal Expression for the Master Function

In order to obtain the solution of (7) which satisfies (8), we must obtain a particular integral of (7) and four linearly independent integrals of the homogeneous equation

$$\frac{d}{dt}t^{-1}\exp(t^2)\frac{d^2}{dt^2}\exp(t^2)\frac{dz}{dt}=0. \tag{7'}$$

We denote the particular integral by y, and, since $z=$*constant* obviously satisfies (7'), we may denote the integrals of (7') by u, v, w, 1. The solution of (7) which satisfies (8) is then

$$\gamma=\epsilon/\delta, \tag{27}$$

where

$$\epsilon=\begin{vmatrix} y & u & v & w & 1\\ y_1 & u_1 & v_1 & w_1 & 1\\ y_2 & u_2 & v_2 & w_2 & 1\\ y_1' & u_1' & v_1' & w_1' & 0\\ y_2' & u_2' & v_2' & w_2' & 0 \end{vmatrix}, \tag{28}$$

$$\delta=\text{cofactor of } y \text{ in } \epsilon. \tag{29}$$

Here the prime means differentiation with respect to t, and subscripts 1, 2 indicate that the function is evaluated at t_1, t_2, respectively. (The use of u as one of the integrals of (7') should not be confused with the use of the same symbol as the parameter defined by (25).)

In carrying out the computation of γ, the determinant (28) may be manipulated in any of the usual ways, and its order may be reduced; but in so doing it is convenient to impose the following conditions: (a) The sign affixed to the resulting determinant must be positive. (b) The function $y(t)$ must occur in only one element, and with coefficient $+1$. Under these conditions one may still use Eq. (27), with δ defined as the cofactor of the element which contains $y(t)$.

The functions y, u, v, w can all be expressed in terms of exponentials and error functions. For shortness and flexibility we shall introduce the following special notations:

$$e=\exp(-t^2),\quad e_i=\exp(-t_i^2),\quad (i=1,2), \tag{30}$$

$$f=\int^t \exp(-x^2)dx,$$

$$f_i=\int^{t_i} \exp(-x^2)dx,\quad (i=1,2), \tag{31}$$

$$g=\int^t \exp(-2x^2)dx,$$

$$g_i=\int^{t_i} \exp(-2x^2)dx,\quad (i=1,2). \tag{32}$$

The lower limits are left unspecified, but are to be the same throughout any expression in which these symbols appear. We also define

$$f_{0t}=\int_0^t \exp(-x^2)dx,$$

$$f_{t\infty}=\int_t^\infty \exp(-x^2)dx,$$

$$f_{12}=\int_{t_1}^{t_2} \exp(-x^2)dx,$$

$$f_{it}=\int_{t_i}^t \exp(-x^2)dx=-f_{ti}, \tag{33}$$

$$f_{0i}=\int_0^{t_i} \exp(-x^2)dx,$$

$$f_{i\infty}=\int_{t_i}^\infty \exp(-x^2)dx,\quad (i=1,2);$$

and g_{0t}, $g_{t\infty}$, etc., are to have corresponding meanings.

A set of solutions suitable for use in (28) is

$$y=\tfrac{1}{2}ef-g;\quad u=f^2;\quad v=f;\quad w=e. \tag{34}$$

Equation (27) holds independently of our choice

of the lower limit of the integrals. We may also replace (34) by a set in which an arbitrary linear combination of u, v, w, 1 is added to y, and in which u, v, w are replaced by any three such linear combinations which, together with 1, make a linearly independent set.

III. THE NEARLY PLANE CASE

We now consider the case in which r_2 is not small compared to r_1, so that the plane case formulas retain the significance of first approximations. The factors h', k_c', k_d' defined in Eqs. (18)–(23) can here be expressed as power series in $\log(r_1/r_2)$, the leading terms being given by (26).

From (3) and (4) we see that if $\log(r_1/r_2)$ is small, and T_2/T_1 is not too close to unity, then t_1, t_2, and, *a fortiori*, t are small numbers. We proceed by expanding γ in ascending powers of these quantities. As a first step it is desirable to choose the set of solutions $y, u, v, w, 1$ in such a way that the first terms in their series expansions are linearly independent, in order to avoid needless complication and heavy cancellation in the calculations. This can be done by considering the equation

$$\frac{d}{dt}t^{-1}\frac{d^3\gamma}{dt^3}=t^{-2}, \tag{35}$$

to which (7) reduces if we set $\exp(t^2)\to 1$. This is, apart, from a constant dimensional factor, the equation for the Maxwellian plane case as used by FJO. For this equation the simplest choice of a set of functions $y, u, v, w, 1$ is obviously

$$\begin{aligned} &y=-t^3/6,\\ &u=t,\quad v=t^2,\quad w=t^4. \end{aligned} \tag{36}$$

We therefore wish to take our set of functions in the forms:

$$\begin{aligned} y&=-(t^3/6)\{1+p_2t^2+p_4t^4+\cdots\},\\ u&=t\{1+a_2t^2+a_4t^4+\cdots\},\\ v&=t^2\{1+b_2t^2+b_4t^4+\cdots\},\\ w&=t^4\{1+d_2t^2+d_4t^4+\cdots\}. \end{aligned} \tag{37}$$

This can be accomplished by setting

$$\begin{aligned} y&=\tfrac{1}{2}f(e+1)-g,\\ u&=f,\\ v&=1-e,\\ w&=6(1-e-f^2). \end{aligned} \tag{38}$$

We then have

$$\begin{aligned} &p_2=-7/10, \quad p_4=3/10, \quad \cdots,\\ &a_2=-1/3, \quad a_4=1/10, \quad \cdots,\\ &b_2=-1/2, \quad b_4=1/6, \quad \cdots,\\ &d_2=13/15, \quad d_4=61/140, \quad \cdots. \end{aligned} \tag{39}$$

Using (37), we can carry out the expansion of the determinants ϵ and δ, defined by (28) and (29), in terms of the quantities:

$$\epsilon(klmn)=\begin{vmatrix} t^k & t^l & t^m & t^n & 1\\ t_1^k & t_1^l & t_1^m & t_1^n & 1\\ t_2^k & t_2^l & t_2^m & t_2^n & 1\\ kt_1^{k-1} & lt_1^{l-1} & mt_1^{m-1} & nt_1^{n-1} & 0\\ kt_2^{k-1} & lt_2^{l-1} & mt_2^{m-1} & nt_2^{n-1} & 0 \end{vmatrix}; \tag{40}$$

$$\delta(lmn)=\begin{vmatrix} t_1^l & t_1^m & t_1^n & 1\\ t_2^l & t_2^m & t_2^n & 1\\ lt_1^{l-1} & mt_1^{m-1} & nt_1^{n-1} & 0\\ lt_2^{l-1} & mt_2^{m-1} & nt_2^{n-1} & 0 \end{vmatrix}. \tag{41}$$

The result is:

$$\begin{aligned} -6\epsilon=&\epsilon(3124)+[d_2\epsilon(3126)+p_2\epsilon(5124)]\\ &+[(a_4-a_2p_2)\epsilon(3524)\\ &+(b_4-b_2d_2)\epsilon(3164)+d_4\epsilon(3128)\\ &+p_4\epsilon(7124)+d_2p_2\epsilon(5126)]+\cdots, \end{aligned} \tag{42}$$

$$\begin{aligned} \delta=&\delta(124)+[a_2\delta(324)+d_2\delta(126)]\\ &+[a_4\delta(524)+a_2d_2\delta(326)\\ &+(b_4-b_2d_2)\delta(164)+d_4\delta(128)]+\cdots. \end{aligned} \tag{43}$$

Here each quantity in square brackets is a homogeneous function of t_1, t_2, t, whose degree exceeds by two that of the preceding quantity.

One can without much effort evaluate those of the determinants (41) which are involved in the three terms written in (43). It is convenient to write the results in the notation introduced in (24), (25):

$$\begin{aligned} &\delta(124)=64\bar{t}^5u^4,\\ &\delta(234)=\bar{t}^2(1-u^2)\delta(124),\\ &\delta(126)=\bar{t}^2(5+3u^2)\delta(124),\\ &\delta(146)=\bar{t}^4(15-2u^2+3u^4)\delta(124),\\ &\delta(128)=2\bar{t}^4(7+14u^2+3u^4)\delta(124),\\ &\delta(245)=\bar{t}^4(5-6u^2+u^4)\delta(124),\\ &\delta(236)=3\bar{t}^4(3-2u^2-u^4)\delta(124). \end{aligned} \tag{44}$$

The calculation of the quantities $\epsilon(klmn)$ is facilitated by the fact that these functions and their first derivatives vanish at $t=t_1$ and $t=t_2$, so that $(t-t_1)^2(t-t_2)^2$ is a factor of $\epsilon(klmn)$. One can see by inspection what powers of t occur and what coefficient t^k has, and this usually suffices to

TABLE I. Series coefficients for the nearly plane case with α = constant.

u	T_2/T_1	f	h_1	h_2	k_{c1}	k_{c2}	k_{d1}	k_{d2}
0.0	1	1	0	−0.174	0	−0.213	0	0
0.1	11/9	1.001	0.101	−0.169	0.172	−0.198	−0.033	−0.0002
0.2	3/2	1.006	0.203	−0.154	0.344	−0.153	−0.066	−0.001
0.3	13/7	1.013	0.307	−0.128	0.516	−0.078	−0.098	−0.002
0.4	7/3	1.024	0.415	−0.092	0.688	+0.028	−0.129	−0.003
0.5	3/1	1.039	0.527	−0.044	0.861	+0.163	−0.158	−0.005
0.6	4/1	1.061	0.648	+0.018	1.033	+0.329	−0.186	−0.007

determine the form of $\epsilon(klmn)$. For example, we see that

$$\epsilon(3126)=\delta(126)\bar{t}^3+l_0+l_1\bar{t}+l_2\bar{t}^2+l_6\bar{t}^6$$
$$=(A\bar{t}^2+B\bar{t}+C)(t-t_1)^2(t-t_2)^2.$$

The requirements that the coefficient of $\bar{t}^3$ be $\delta(126)$ and that the coefficients of $\bar{t}^4$ and $\bar{t}^5$ vanish provide three equations from which A, B, C can be determined.

We shall write the results in terms of the quantities $\bar{t}$ and u, and a variable s:

$$s=(2t-t_2-t_1)/(t_2+t_1);$$
$$t=\bar{t}(1+us),$$
$$(t-t_1)^2(t-t_2)^2=\bar{t}^4u^4(1-s^2)^2, \qquad (45)$$
$$dt=\bar{t}uds,$$
$$t_1\leqslant t\leqslant t_2, \quad -1\leqslant s\leqslant 1.$$

We find:

$$\epsilon(3124)=-\delta(124)(\bar{t}^3u^4/4)(1-s^2)^2,$$
$$\epsilon(3126)=\bar{t}^2(15+2u^2+6us+u^2s^2)\epsilon(3124),$$
$$\epsilon(5124)=\bar{t}^2(-10+2u^2-4us)\epsilon(3124),$$
$$\epsilon(3524)=\bar{t}^4\{-5+6u^2-u^4 -4(1-u^2)us\}\epsilon(3124),$$
$$\epsilon(3164)=\bar{t}^4\{45-24u^2-u^4+12(3-u^2)us +2(3-u^2)u^2s^2\}\epsilon(3124),$$
$$\epsilon(3128)=\bar{t}^4\{70+56u^2+3u^4 +8(7+2u^2)us+2(14+u^2)u^2s^2 +8u^3s^3+u^4s^4\}\epsilon(3124), \qquad (46)$$
$$\epsilon(5126)=\bar{t}^4\{50-10u^2+4u^4 +40us+2(5+u^2)u^2s^2\}\epsilon(3124),$$
$$\epsilon(7124)=\bar{t}^4\{-105-14u^2 +3u^4-4(21+2u^2)us -28u^2s^2-4u^3s^3\}\epsilon(3124).$$

From (27), (42), (43), (39), (44), and (46) we obtain:

$$\gamma=\{\bar{t}^2u^4(1-s^2)^2/24\}\cdot\{1+\bar{t}^2[-2-(u^2/5) -(12us/5)-(13u^2s^2/15)] +\bar{t}^4[2+(4u^2/15)+(139u^4/2100) +(24us/5)+(104u^3s/525)+(24u^2s^2/5) +(239u^4s^2/3150)+(16u^3s^3/7) +(61u^4s^4/140)]+\cdots\}. \qquad (47)$$

The integrals required for h' and k_c' can be evaluated by use of the formulas

$$\int_{-1}^{1}(1-s^2)^2s^n ds$$
$$=\begin{cases}0 \text{ for odd } n,\\ \dfrac{16}{(n+1)(n+3)(n+5)} \text{ for even } n\end{cases} \qquad (48)$$

$$\int_{-1}^{1}(1-s^2)^4s^n ds$$
$$=\begin{cases}0 \text{ for odd } n,\\ \dfrac{768}{(n+1)(n+3)(n+5)(n+7)(n+9)} \text{ for even } n,\end{cases} \qquad (49)$$

and the integration for k_d is of course performed by expanding $\exp(-\bar{t}^2)$ in power series. The other factors occurring in (21)–(23) must also be expressed as power series in $\bar{t}$, and multiplied by the series obtained by integration. The results can then be expressed as power series in $\log(r_1/r_2)$ by using the relation

$$2\bar{t}^2u=\log(r_1/r_2), \qquad (50)$$

which follows from (4), (24), and (25).

We finally obtain the series:

$$h'=h_0(u)+h_1(u)\cdot\ln(r_1/r_2) +h_2(u)\cdot\{\ln(r_1/r_2)\}^2+\cdots, \qquad (51)$$

$$k_c'=1+k_{c1}(u)\cdot\ln(r_1/r_2) +k_{c2}(u)\cdot\{\ln(r_1/r_2)\}^2+\cdots, \qquad (52)$$

$$k_d'=1+(u^2/3)+k_{d1}(u)\cdot\ln(r_1/r_2) +k_{d2}(u)\cdot\{\ln(r_1/r_2)\}^2+\cdots. \qquad (53)$$

For α independent of T we get:

$$h_0(g)=f(2u)=1+0.143u^2+0.048u^4+\cdots,$$
$$h_1(g)=(9u/10)f(2u)+(23/30u)\{f(2u)-1\}$$
$$=1.010u+0.165u^3+0.059u^5+\cdots,$$
$$h_2(g)=\{-(17/60)+(3499/8400)u^2\}f(2u) +\{(23/30u^2)+(53/72)\}\cdot\{f(2u)-1\} -(37/80u^2)\{f(2u)-1-(u^2/7)\} \qquad (54)$$
$$=-0.174+0.496u^2+0.088u^4+\cdots.$$

These coefficients can of course be computed readily enough when α is any polynomial in T, or any power series which converges rapidly in the range in question. For example, for $\alpha \propto T$ we obtain

$$h_0(u)=1,$$
$$h_1(u)=176u/210=0.838u, \qquad (55)$$
$$h_2(u)=-(73/420)+(571/1575)u^2$$
$$=-0.174+0.363u^2.$$

The coefficients which occur in k_c and k_d are

$$\begin{aligned} k_{c1}(u) &= 284u/165 = 1.721u. \\ k_{c2}(u) &= -(703/3300)+(339044/225225)u^2 \\ &= -0.213+1.505u^2, \end{aligned} \tag{56}$$

$$\begin{aligned} k_{d1}(u) &= -(u/3)\{1-(u^2/5)\} \\ &= -0.333u+0.067u^3, \\ k_{d2}(u) &= -(u^2/15)\{(1/3)-(u^2/7)\} \\ &= -0.022u^2+0.010u^4. \end{aligned} \tag{57}$$

The amount of labor required to obtain successive terms in this series formulation increases very rapidly, so that it does not seem worth while to go beyond the terms given here. The three terms we have obtained are presumably adequate at least up to $r_1/r_2=3$; some comparisons with the results of numerical computations from the exact formulas are given later. The radii of convergence of the series of course remain unknown.

Some values of the various coefficients are given in Table I. The quantities h_1 and h_2 are for α independent of temperature. The table is not extended beyond $u=0.6$ because large values of T_2/T_1 are not practicable in the nearly plane case.

IV. SOLUTION BY NUMERICAL INTEGRATION

The integral in Eq. (17) can be expressed easily in terms of known functions. The result is

$$k_d=\tfrac{1}{2}-(t_2/2t_1)\exp(t_1^2-t_2^2)+\tfrac{1}{2}f_{12}. \tag{58}$$

The values of the integrals in (15) and (16) can likewise be worked out, for any chosen simple temperature dependence of α, in terms of exponentials, error functions, and a small number of new functions defined by integrals. Such a formulation would have the aesthetic advantage of involving only the values at t_1 and t_2 of various functions of a single variable. The formulas would, however, be so extremely complicated that the only way to give them any practical meaning would be to carry out a quite tedious process of numerical evaluation for each given pair of values t_1, t_2. Actually the most feasible procedure for determining the behavior of the functions h and k_c seems to be to choose various specific pairs of values of t_1, t_2, plot the function γ for each such pair, and perform numerical integrations *ad hoc* according to (15) and (16). This is essentially what we shall do. In order to carry out such a program with some economy of effort, it is desirable to have available two different algebraic translations of the formula (27) for the function γ.

Formulation with t_1 as Lower Limit of All Integrals

If t_1 is taken as the lower limit of all the integrals used in (31) and (32) to define the symbols used in writing (34), then several elements in the second and fourth rows of the determinant (28) vanish automatically. The evaluation of the determinants ϵ and δ is then not difficult, and one obtains from (27):

$$\gamma=\tfrac{1}{2}(e+e_1)f_{1t}-g_{1t}-Af_{1t}^2+C_1(e_1-e-2t_1f_{1t}), \tag{59}$$

where

$$A=\frac{2f_{12}(t_2e_1-t_1e_2-t_1t_2f_{12})-\tfrac{1}{2}(e_1-e_2)^2-2(t_2-t_1)g_{12}}{2f_{12}\{(t_1+t_2)f_{12}-(e_1-e_2)\}}; \tag{60}$$

$$C_1=\frac{f_{12}(3e_2+e_1+2t_2f_{12})-4g_{12}}{4\{(t_1+t_2)f_{12}-(e_1-e_2)\}}. \tag{61}$$

This formulation is convenient for dealing with a set of cases in which t_1 remains the same.

Formulation with t_2 as Lower Limit

The evaluation of the determinants is of course simplified just as much if t_2 is taken as the lower limit in (31) and (32). For convenience we reverse the limits of all integrals, with corresponding sign changes, in writing the result:

$$\gamma=g_{t2}-\tfrac{1}{2}(e+e_2)f_{t2}-Af_{t2}^2+C_2(2tf_{t2}+e_2-e) \tag{62}$$

where

$$C_2=\frac{f_{12}(3e_1+e_2-2t_1f_{12})-4g_{12}}{4\{(t_1+t_2)f_{12}-(e_1-e_2)\}}. \tag{63}$$

This formulation would be more convenient for dealing with a set of cases in which t_2 remains the same. It can also be used as a starting point in obtaining an approximate solution for cases in which $r_1 \gg r_2$.

The Extreme Cylindrical Case

The parameter t_2 occurs in (62) in two quite different ways: (a) As a factor in certain terms in numerators and denominators; (b) in the exponential e_2 and as a limit of integrals. The limit $(r_2/r_1)\to 0$ corresponds to $t_2\to\infty$; the result of setting $t_2\to\infty$ in (62) is not, however, a very good approximation to any practical case, since $(r_2/r_1)=10^{-3}$ corresponds only to $t_2\sim 4$. A good approximation is rather to be obtained by setting $t_2\to\infty$ only where it occurs as described in (b); we thus set

$$f_{t2}\to f_{t\infty},\quad g_{t2}\to g_{t\infty},\quad e_2\to 0. \tag{64}$$

This procedure introduces errors which are only of order $(r_2/r_1)^2$. The fractional errors in the results are then of order $(r_2/r_1)^2$, unless the terms retained cancel heavily. Strong cancellation will indeed occur for low values of t_2 (less than about 2.5), and in practice this is what limits the application of the formulas obtained by these approximations.

The physical basis for the distinction between the two ways in which t_2 appears is quite simple. The finite radius of the wire affects the values of H, K_c, and K_d: (a) because it exerts a restraining effect on the convection, and (b) because the wire occupies a certain amount of cross-sectional area. The second effect is obviously of the order $(r_2/r_1)^2$, and it is the second effect which we are ignoring in the approximations (64). The terms which we are retaining are inversely proportional to t_2, and therefore depend only logarithmically on r_1/r_2.

We may show by a simple analogy that the restraining effect of the wire on the convection may be expected to depend logarithmically on r_1/r_2. Consider the case of ordinary pressure-driven lamellar flow between two concentric cylinders of radii r_1 and r_2. In the approximation in which we ignore terms of the order $(r_2/r_1)^2$ compared with unity, the total rate of flow F is given by[11]

$$F=F_0\left(1-\frac{1}{\log\,(r_1/r_2)}\right), \tag{65}$$

where F_0 is the rate of flow (given by Poiseuille's formula) for $r_2/r_1=0$. We see from this relation that for a ratio of radii as high as 100, the presence of the wire reduces the flow by 21.7 percent.

When (64) is substituted into (62), (60), and (63), we obtain after some algebraic manipulation the expression

$$\gamma\cong\frac{\gamma_\infty-(\gamma''/t_2)}{1-(\delta''/t_2)}, \tag{66}$$

where

$$\gamma_\infty=g_{t\infty}-\tfrac{1}{2}ef_{t\infty}+(g_{1\infty}+t_1f_{1\infty}{}^2-e_1f_{1\infty})(f_{t\infty}/f_{1\infty})^2 +(\tfrac{3}{2}e_1f_{1\infty}-2g_{1\infty}-t_1f_{1\infty}{}^2)(f_{t\infty}/f_{1\infty}), \tag{67}$$

$$\gamma''=\delta''(g_{t\infty}-\tfrac{1}{2}ef_{t\infty})+(t_1g_{1\infty}-\tfrac{1}{4}e_1{}^2)(f_{t\infty}/f_{1\infty})^2 +(\tfrac{3}{2}e_1f_{1\infty}-2g_{1\infty}-t_1f_{1\infty}{}^2)(e/2f_{1\infty}), \tag{68}$$

$$\delta''=(e_1/f_{1\infty})-t_1. \tag{69}$$

We now make a further approximation similar to those indicated in (64) by replacing t_2 by ∞ as the upper limit of the integrals in (15) and (16). We thus obtain

$$h\cong 6!t_1{}^3\exp\,(2t_1{}^2)\cdot\frac{h_\infty-(h''/t_2)}{1-(\delta''/t_2)}, \tag{70}$$

$$k_c\cong 9!t_1{}^7\exp\,(4t_1{}^2)\cdot\frac{k_\infty-(2k_1''/t_2)+(k_2''/t_2{}^2)}{\{1-(\delta''/t_2)\}^2}, \tag{71}$$

with

$$h_\infty=\int_{t_1}^\infty(\alpha/\alpha_1)(\gamma_\infty/t)dt,$$
$$h''=\int_{t_1}^\infty(\alpha/\alpha_1)(\gamma''/t)dt, \tag{72}$$
$$k_\infty=\int_{t_1}^\infty\gamma_\infty{}^2dt,$$
$$k_1''=\int_{t_1}^\infty\gamma_\infty\gamma''dt, \tag{73}$$
$$k_2''=\int_{t_1}^\infty\gamma''{}^2dt.$$

Equations (67)–(73) express h and k asymptotically in terms of the quantities h_∞, h'', k_∞, k_1'', k_2'', which are functions of t_1 only. The sole dependence on t_2 is that indicated by the explicit appearance of t_2 in (70) and (71).

It is important to remember that (70) and (71) do *not* simply indicate the first terms in power series or asymptotic series in $(1/t_2)$: the error

[11] See, for example, L. Page, *Introduction to Theoretical Physics*, second edition (D. Van Nostrand Company, Inc., New York, 1935), p. 260.

involved in using (70) and (71) is not given by a power of $(1/t_2)$, but is of the order of exp $(-t_2^2)$ $\sim(r_2/r_1)^2$, as we have already discussed in some detail.

The formulas (70) and (71) are adapted, and much more strongly so than (59), to the treatment of sets of cases in which t_1 is held fixed and t_2 is given various values. It is interesting to note what such cases have in common physically. From Eq. (2) we see that if Q and T_1 are given, t_1 is determined. Thus if the outer radius r_1, the lower temperature T_1, and the heat dissipated by conduction per unit length per second, $2\pi Q$, are given, the factors H, K_c, K_d are completely determined by (12)–(14), except for the dependences of the factors h, k_c, k_d on t_2. Any two cases of such a set have the same temperature field throughout the region which is occupied by gas in both cases. The specification of r_2 then fixes the inner boundary of this region and, by (3) and (4), the temperature at this boundary.

In experimental language, one may say that such a set of cases is realized when one has a number of identical outer tubes, maintained at the same temperature, but containing coaxial wires of various sizes, provided that the temperatures of the wires are adjusted so that the heat flow by conduction is the same per unit length in all the tubes.

Numerical Data for Use in the Asymptotic Formulas

The functions γ_∞ and γ'' can be tabulated readily, since excellent tables are available for all the functions involved.[12–14] In order to avoid interpolation, we obtained $f_{t\infty}$ from Burgess's tables[12] and $g_{t\infty}$ from the British Association Tables.[13] The elimination of interpolation in this manner was a considerable saving of time because heavy cancellation made it necessary to obtain numbers from the tables accurate to nine places for the smaller values of t. In the worst case, the use of nine significant figures led to results accurate to three.

In Table II we give the values of γ_∞ and γ'', so that they may be available for numerical use in applying (70) with any specified temperature dependence of α.

In Table III are listed the coefficients (72) and (73), the values h_∞ and h'' being for α independent of temperature.

Comparison of Exact and Approximate Results

The function γ was tabulated for $t_1=\frac{1}{2}$ and several values of t_2, the calculations being based on the exact formula (59). The coefficients h and k_c were then calculated by numerical integration from (15) and (16), for the case $\alpha\equiv\alpha_1$.

The comparison of these exact results with the results obtained from the approximate formulas (70), (71) is given in Table IV. It is seen that the agreement is excellent for $(r_1/r_2)=20$, and is tolerably good even for $(r_1/r_2)=6.5$.

In Table V we compare the exact results with the results obtained from the series expressions (51) and (52) for the nearly plane case; again we take $\alpha\equiv\alpha_1$. The table also shows the comparison between the results obtained from (58) and those from (53), for the shape factor k_d'. The comparison is made in terms of the quantities h', k_c', k_d', which differ from h, k_c, k_d only by easily computed factors (cf. Eqs. (21)–(23) and (15)–(17)). It is seen that the agreement is excellent for $(r_1/r_2)=1.45$, is fairly good for $(r_1/r_2)=2.72$, and is passable even for $(r_1/r_2)=6.5$.

These comparisons indicate that the two types of approximation taken together cover the whole range fairly well.

Tables for the Extreme Cylindrical Case

By using the results given in Table III, we can compute from (70) and (71) the values of h and k_c for a chosen value of $(r_1/r_2)\gg1$ and for certain values of $(T_2/T_1)=(t_2/t_1)$ which are determined by the available values of t_1. By graphical interpolation we can then obtain h and k_c for other values of T_2/T_1. Tables VI and VII were constructed in this way. Table VIII gives the

[12] J. Burgess, Trans. Roy. Soc. Edinburgh **39**, 257 (1899). This article contains tables of $H_1(t)=(2/(\pi)^{\frac{1}{2}})f_{0t}$:

$t=0.000$ to 1.250, interval 0.001, 9 places,
$t=1.000$ to 1.500, 0.001, 15 places,
$t=1.500$ to 3.000, 0.002, 15 places,
$t=3.0$ to 5.0, 0.1, 15 places.

[13] *British Association Mathematical Tables* (Cambridge University Press, London, 1931), Vol. 1. On pp. 60–71 there is a table of $Hh_0(2t)=2g_{t\infty}$:

$2t=-7.0$ to 6.6, 0.1, 10 places.

[14] F. W. Newman, Trans. Camb. Phil. Soc. **13**, 146 (1883). This article contains tables of the descending exponential e^{-x}:

$x=0.000$ to 15.349, 0.001, 12 places.

TABLE II. Values of γ_∞ and γ''.

	$t_1=0.5$		$t_1=0.8$		$t_1=1.0$		$t_1=1.2$	
t	$\gamma_\infty\times10^8$	$\gamma''\times10^8$	$\gamma_\infty\times10^7$	$\gamma''\times10^7$	$\gamma_\infty\times10^7$	$\gamma''\times10^7$	$\gamma_\infty\times10^6$	$\gamma''\times10^6$
0.5	0	0						
0.6	187	283						
0.7	542	835						
0.8	867	1360	0	0				
0.9	1073	1714	465	792				
1.0	1141	1863	1242	2148	0	0		
1.1	1096	1831	1826	3216	155	286		
1.2	975	1672	2078	3731	391	730	0	0
1.3	816	1439	2037	3738	543	1032	450	891
1.4	650	1181	1805	3393	585	1133	1069	2150
1.5	497	931	1486	2866	543	1075	1403	2871
1.6			1153	2288	456	925	1428	2980
1.7	261	523	854	1746	357	742	1256	2678
1.8					264	564	1002	2187
1.9	122	263	418	911	186	410	745	1668
2.0					126	288	524	1207
2.1	52	120	181	423	83	196	353	837
2.3	20	50	71	178	33	83	144	364
2.5	7	19	25	68	12	31	53	142
2.7	2	7	8	24	4	9	18	53
2.9		2	2	8	1	2	6	19
3.1				2			2	6

values of k_d calculated from (58) for the same values of r_1/r_2 and T_2/T_1.

V. DISCUSSION

Behavior of the Transport Coefficients in the Extreme Cylindrical Case

A rather surprising feature of the results given in Tables VI and VII is the great difference between the dependences of H and K_e on T_2/T_1 in the highly cylindrical case and in the plane case. Whereas in the plane case both coefficients increase (as $(\Delta T/\bar{T})^2$) with increasing T_2/T_1, in the highly cylindrical case H is rather insensitive to this ratio and K_e *decreases* strongly as T_2/T_1 increases. This result would hardly be expected without calculation, but it can be made plausible by physical considerations. For high values of T_2, the gas near the hot wire becomes highly conductive of heat and very viscous. This has the effect of reducing the convective flow. Now H depends both on the convective flow, which is decreased, and on the temperature gradient, which is increased. K_e, on the other hand, depends only on the convective flow, and indeed quadratically.

This behavior of H and K_e should be of considerable utility in practice. It seems likely that it depends rather strongly on the temperature dependences of the gas coefficients, and for this reason calculations for other dependences are desirable.

It is probable that the value of H would be rather strongly influenced by any marked temperature dependence which the factor α might have. Since the assumption that α depends on a power of the temperature is quite artificial and probably decidedly lacking in verisimilitude, numerical integrations were not carried through for such cases. Whenever the temperature dependence of α for a given gas may become reasonably well known empirically, it can be used together with the results tabulated in Table II to carry out an *ad hoc* numerical integration for the value of H.

It is easily shown[15] that the effectiveness of a unit length of column is measured by $H^2/(K_e+K_d)$. By adjusting the value of r_1, however, it is always possible to make K_d any specified multiple of K_e. The power efficiency of a column may thus be measured by H^2/K_eQ. For any given gas this ratio is independent of r_1, provided that the temperature T_1 is held constant, as will usually be the case in practice, and is proportional to $h^2t_1^2/k_e$. This factor, which may be considered as a measure of the relative power efficiency, is tabulated in Table IX.

Perhaps the most interesting feature of the

[15] See reference 7, Eq. (333).

TABLE III. Values of h_∞, h'', etc.

t_1	0.5	0.8	1.0	1.2
$h_{\infty\prime\prime}$	0.838×10^{-3}	1.113×10^{-4}	0.2565×10^{-4}	0.5314×10^{-5}
h''	1.409×10^{-3}	2.076×10^{-4}	0.5113×10^{-4}	1.132×10^{-5}
k_{∞}	0.729×10^{-6}	2.178×10^{-8}	0.1575×10^{-8}	0.897×10^{-10}
k_1''	1.221×10^{-6}	4.029×10^{-8}	0.3112×10^{-8}	1.892×10^{-10}
k_2''	2.056×10^{-6}	7.47×10^{-8}	0.6161×10^{-8}	3.995×10^{-10}
δ''	1.3327	1.5070	1.6390	1.7809

TABLE IV. Comparison of exact and approximate results for the extreme cylindrical case with $t_1=\frac{1}{2}$.

t_2	r_1/r_2	h(exact)	h(from (70))	k_c(exact)	k_c(from (71))
3	79.8	0.984×10^{-1}	0.984×10^{-1}	0.356×10^{-2}	0.356×10^{-2}
2.5	20.1	0.875×10^{-1}	0.872×10^{-1}	0.286×10^{-2}	0.287×10^{-2}
2	6.52	0.666×10^{-1}	0.594×10^{-1}	0.170×10^{-2}	0.145×10^{-2}

TABLE V. Comparison of exact and approximate results for the nearly plane case with $t_1=\frac{1}{2}$.

t_2	r_1/r_2	h' (exact)	h' (series)	k_c' (exact)	k_c' (series)	k_d' (exact)	k_d' (series)
1	1.45	1.127	1.127	1.207	1.209	0.996	0.991
1.5	2.72	1.475	1.522	1.964	2.024	0.930	0.919
2	6.52	2.066	2.35	4.02	4.09	0.814	0.745

results tabulated in Table IX is the fact that the entries vary as little as they do. The largest entry is only 1.73 times the smallest. The table further indicates that with a small temperature ratio, the concentric tube type of construction is the more efficient, whereas for gases which permit a large temperature ratio, the hot wire type of construction is more efficient.

Comparison with Experiment

A rather extensive comparison of experiment with the theory presented in this paper, as well as with other aspects of the theory of the separation column, is given in Part IV of reference 7. In particular, we present there a detailed comparison with the results of Clusius and Dickel, of Nier, and of Taylor and Glockler. The agreement is found to be good.

In order to avoid unnecessary duplication of material, we shall present here only the comparison with the experimental work of Nier.[8]

The column used by Nier had the specifications

$$\begin{aligned} &r_1=2.458\text{ cm};\quad r_2=1.746\text{ cm};\\ &T_1=300°\text{K};\quad T_2=573°\text{K};\\ &\log(r_1/r_2)=0.342;\quad u=0.313. \end{aligned} \tag{74}$$

At the mean temperature 436.5°, we find from the recent work of Trautz and Sorg[16] that the coefficient of viscosity of methane is

$$\eta=1.51\times10^{-4}\text{ poise}, \tag{75}$$

and from the same reference we find that at this temperature the coefficient of viscosity varies as $T^{0.78}$. That is to say, the power by which η depends on the temperature is

$$n=0.78. \tag{76}$$

We have further

$$\rho=4.47\times10^{-4}\text{ g/cm}^3 \tag{77}$$

if we consider that methane is chiefly $C^{12}H_4$.

The value of D may now be estimated on the basis of the inverse power model from a formula given by one of the writers.[17] From Eqs. (29) and (31), and Table I of reference 17, we find from (76) that

$$D=1.406\eta/\rho=0.475\text{ cm}^2/\text{sec}. \tag{78}$$

The value of α has been determined experi-

TABLE VI. Values of h with α=constant.

T_2/T_1 \ r_1/r_2	15	25	40	60	100
2	0.059	0.059	—	—	—
3	0.091	0.098	0.100	0.101	0.100
4	0.092	0.103	0.109	0.113	0.116
5	0.075	0.092	0.103	0.108	0.114
6	—	—	0.085	0.093	0.102

TABLE VII. Values of k_c.

T_2/T_1 \ r_1/r_2	15	25	40	60	100
2	0.0144	0.0184	—	—	—
3	0.0095	0.0130	0.0162	0.0183	0.0207
4	0.0045	0.0068	0.0088	0.0105	0.0128
5	0.0022	0.0034	0.0046	0.0056	0.0072
6	—	—	0.0025	0.0031	0.0040

TABLE VIII. Values of k_d.

T_2/T_1 \ r_1/r_2	15	25	40	60	100
2	0.61	0.60	—	—	—
3	0.75	0.73	0.70	0.68	0.67
4	0.91	0.87	0.83	0.81	0.78
5	1.08	1.01	0.97	0.94	0.90
6	—	—	1.11	1.07	1.03

[16] M. Trautz and K. Sorg, Ann. d. Physik **10**, 81 (1931).
[17] R. Clark Jones, Phys. Rev. **58**, 111 (1940).

mentally by Nier,[18] who finds

$$\alpha = 0.0077. \tag{79}$$

These data are all for a pressure of one atmosphere.

Substituting the data (74)–(79) in Eqs. (18)–(20), we find

$$\begin{aligned} H/h' &= 2.585\times10^{-5}\ \text{g/sec.},\\ K_c/k_c' &= 1.041\times10^{-2}\ \text{g-cm/sec.},\\ K_d/k_d' &= 1.997\times10^{-3}\ \text{g-cm/sec.} \end{aligned} \tag{80}$$

Furthermore, we find upon substituting (74) in Eqs. (51)–(57)

$$h' = 1.109; \quad k_c' = 1.176; \quad k_d' = 0.998. \tag{81}$$

Combining (80) and (81), we have finally

$$\begin{aligned} H &= 2.866\times10^{-5}\ \text{g/sec.},\\ K_c &= 1.224\times10^{-2}\ \text{g-cm/sec.},\\ K_d &= 1.992\times10^{-3}\ \text{g-cm/sec.} \end{aligned} \tag{82}$$

On the basis of the transport equation

$$\tau_1 = Hc_1c_2 - (K_c+K_d)(\partial c_1/\partial z), \tag{83}$$

it has been shown by Furry, Jones, and Onsager[3] that the logarithm of the equilibrium separation factor is

$$\log q_e = \frac{HL}{K_c+K_d}, \tag{84}$$

where L is the length of the column. Since it follows directly from (18)–(20) that the coefficients H, K_c, and K_d are proportional, respectively, to the second, fourth, and zeroth power of the pressure, we have from (82) and (84)

$$\log q_e = \frac{1.710/P^2}{1+0.1628/P^4}, \tag{85}$$

where P is measured in atmospheres, and where we use $L = 7.3$ meters.

Nier found that his three experimental points

[18] A. O. Nier, Phys. Rev. **56**, 1009 (1939).

TABLE IX. Values of $h^2l_1^2/k_c$ with α = constant.

T_2/T_1 \ τ_1/τ_2	1	15	25	40	60	100
2	0.46	0.44	0.41	—	—	—
3	0.54	0.59	0.59	0.57	0.57	0.56
4	0.54	0.68	0.67	0.66	0.66	0.64
5	0.51	0.58	0.67	0.71	0.71	0.69
6	0.48	—	—	0.61	0.65	0.68

could be fitted exactly by the formula

$$\log q_e = \frac{1.34/P^2}{1+0.126/P^4}. \tag{86}$$

If we multiply numerator and denominator of this expression by 1.283, we have

$$\log q_e = \frac{1.72_0/P^2}{1.283+0.161_7/P^4}. \tag{87}$$

Comparison of (87) with (85) indicates that the assumption of a parasitic remixing (cf. Eq. (70) of reference 3) given by

$$K_p/K_c = 0.283, \tag{88}$$

leads to a discrepancy between theory and experiment of 0.6 percent. The excellence of this check is of course fortuitous, since the physical constants used are not known to this accuracy; in particular, the probable error in the measurement of α is several percent.

It will be remembered that Nier found a discrepancy of about 10 percent, and a value of K_p/K_c equal to[19] about 0.78. The improved check and the much smaller value of K_p/K_c found in the calculation given here are due primarily to the inclusion of the corrections (81) for the cylindricity of the apparatus, and secondarily, to the use of the better viscosity data of Trautz and Sorg.

[19] Nier actually found $K_p/K_c = 0.63$, but this larger value follows if we match the coefficients of P^{-2} and P^{-4} with equal fractional errors, instead of placing all of the burden on one of them.

Schematic Treatment of Nuclear Resonances

G. BREIT
University of Wisconsin, Madison, Wisconsin
(Received February 20, 1946)

A schematic model of competitive nuclear disintegration processes is examined with special attention to the following features: (*a*) The definition of the compound state in a manner independent of the introduction of a "nuclear radius" into the definition; (*b*) the evaluation of the influence of barrier penetration on the parameters entering the dispersion formulas; (*c*) the comparison of the equivalent disintegration probabilities entering as products in the numerators of the dispersion terms with the resonance widths which occur as coefficients of i in the imaginary part of the denominators in the same formulas. It is found that a definition of the compound state can be given in the case considered without the aid of an arbitrarily assigned nuclear radius. The definition of the compound state is arranged to be such as to be nearly independent of the potential barriers affecting the disintegration products. The damping constants turn out to be expressible primarily through the regular radial functions f and are found to depend also on the irregular functions g, inasmuch as the latter determine the linear combinations with which the different damping integrals denoted by $I_n^{(q)}$ combine to give the damping constants Γ. The cross sections can be expressed in the present model in terms of determinants with a finite number of rows and columns. The answer is also transformed into a "dispersion formula" form and it is found that the relation between the resonance width and the disintegration probabilities can be made to be exact in the "isolated level" form but is only an approximation in the representation of the general case that has been used. At the end of the paper a special case is discussed for which the energy dependence of the answer is worked out in terms of elementary functions rather than infinite series.

1. INTRODUCTION

IT is customary and convenient to represent the energy dependence of nuclear reaction cross sections by means of formulas similar to those in the theory of optical dispersion and often referred to as "dispersion formulas." In the vicinity of sharp and isolated resonance energies there is little doubt concerning the correctness of the usual theoretical interpretation[1] of the experimentally observable quantities such as the resonance widths and the values of cross sections for different processes. The analysis of experimental material in energy regions exposed to the combined influence of several resonances is naturally more difficult and the interpretation of the experimentally obtainable parameters in terms of theoretical concepts of nuclear structure is somewhat less definite. Bethe and Placzek[2] as well as Bethe[3] discuss the problem by means of a definition of the level system of the compound nucleus in terms of a preassigned nuclear radius. While this attack has many virtues when the nuclear radius is known, it is doubtless better to free the theory of this somewhat artificial feature as well as to throw light on the nature of the approximations which have to be made in its applications. The discussion of Kalckar, Oppenheimer, and Serber[4] is concerned primarily with situations in which the partial width is large and makes considerable appeal to the analogy with the optical case. Kapur and Peierls[5] define resonance levels somewhat as in earlier work on one body resonances.[6,7] Their levels depend, however, on an assumed nuclear radius and the formula derived for the cross section by Kapur and Peierls contains a length r_0 which must exceed a certain amount. This length enters not only in the damping constants denoted by them as γ_n but also in the term representing the scattering from a hard sphere which is an integral part of their formula. By increasing r_0, say by a factor 2, one can obviously vary the relative magnitudes of contributions among the terms of their formula by considerable amounts. In close proximity of a sharp resonance this arbitrariness of representation makes little difference because in this case the term with the nearly vanishing

[1] G. Breit and E. Wigner, Phys. Rev. **49**, 519 (1936). N. Bohr, Nature **137**, 344 (1936).
[2] H. A. Bethe and G. Placzek, Phys. Rev. **51**, 450 (1937).
[3] H. A. Bethe, Rev. Mod. Phys. **9**, 71, 101–117 (1937).
[4] F. Kalckar, J. R. Oppenheimer, and R. Serber, Phys. Rev. **52**, 273 (1937).
[5] P. L. Kapur and R. Peierls, Proc. Roy. Soc. **A166**, 277 (1938).
[6] G. Breit, Phys. Rev. **40**, 127 (1932).
[7] G. Breit and F. L. Yost, Phys. Rev. **48**, 203 (1935); A. J. F. Siegert, Phys. Rev. **56**, 750 (1939).

resonance denominator is the important one. The representation of the background with which the contribution of the sharp resonance level combines by interference can be varied considerably, however, on account of the presence of r_0 in their formula. This flexibility of representation constitutes progress in that it shows that the representation of experimental results by a dispersion formula is far from unique. It also raises the question as to whether one can represent the cross sections and wave amplitudes in a form that does not involve the employment of arbitrarily assigned lengths and in which the calculation of the parameters entering the final formula does not involve investigations of roots of transcendental equations in the complex domain.

A limited improvement of the situation can be obtained through the employment of the notion of the collision matrix or scattering matrix[8] which has been introduced by J. A. Wheeler for his discussion of resonating group structure and which can be applied to competitive processes in general. Also if one assumes the general form of dependence of cross sections of competitive processes on energy as being of the form of a resonance term superposed on a constant background, the form of the matrices can be established within certain limits. In addition to the relations which follow from the principle of detailed balance which have been found by Wheeler,[9] one finds as a consequence of the "single resonance+background" assumption that an *exact* relation between disintegration probabilities and resonance width can be established. One also finds that the coefficients of the resonance term can be accurately represented in terms of products of disintegration probabilities. The background matrix is found to be expressible in terms of an arbitrary symmetric unitary matrix.

The considerations just mentioned are only a partial help in the general problem. They say nothing about how the potential barriers around the nucleus are to be taken into account and they are based somewhat too heavily on an assumed approximate form of the answer. The way in which barrier penetration affects the formulas representing the cross sections is not sufficiently clear in other work as well. The result of Kapur and Peierls in the interpretation of Konopinski and Bethe[10] is that one should use

$$\Gamma \propto E^{\frac{1}{2}}G^{-2}$$

in the usual notation. On the other hand, the explicit construction of solutions by means of Green's functions gave[11] for sharp resonance and for an interaction taking place between two particles in a thin spherical shell the result

$$f_k^2(kr_0)/k \propto \Gamma$$

in the notation of the latter reference. For some other limiting forms of the assumed interaction, however, the Green's function construction gave[11] a combined occurrence of the functions f, g.

In order to throw light on the questions raised above, it appeared advisable to work out some schematic representations of competitive disintegration processes in which the bothersome features can be more definitely understood. The present paper gives an account of calculations in which the model of the nucleus is sufficiently simple to allow an explicit solution.

The model used below is very schematic and is not intended to be a faithful representation of a nucleus. It takes account, however, in a qualitative way of the following features of actual nuclear processes:

(a) Competition of alternative modes of disintegration. This competition is reproduced only to the extent of having one or another type of disintegration take place at a time.

(b) Effect of barriers on the disintegration probabilities.

(c) Varying conditions of nuclear level spacings and of resonance widths.

The schematic representation is defective and incomplete in the following respects:

(a) The many body interactions are schematically represented by the processes of disappearance of a particle in the nucleus and subsequent reappearance of the same particle or the birth of another

[8] G. Breit, Phys. Rev. **58**, 1068 (1940).
[9] J. A. Wheeler, Phys. Rev. **52**, 1107 (1937).
[10] E. J. Konopinski and H. A. Bethe, Phys. Rev. **54**, 130 (1938).
[11] G. Breit, Phys. Rev. **58**, 506 (1940).

particle which then escapes from the nucleus. These processes are represented in the equations by the occurrence of interaction energies $H_p(r)$ as is seen in Eq. (2.1). The system is treated as though it were a particle with a many valued spin variable having components $\varphi_1, \varphi_2, \cdots, \varphi_N, \varphi$.

(b) The processes of particle disappearance and rebirth are not as complete and general as one could ask for even in the schematic representation which has been employed. Thus, for instance, the matrix elements H_p are taken to be functions only of the distance r from the center of the nucleus. Also direct conversion of an incident particle into an emergent one is not considered so that transitions in the continuum are not taken care of.

(c) The schematic representation employed here does not take into account recoil effects on the residual system when a particle escapes.

(d) In all of the computations the interaction energies H_p and the eigenfunctions u_n are supposed to be real. The matrix (H_{nm}) of the compound state is as a consequence symmetric while in the general case it should be Hermitean.

(e) The residual system described by Eqs. (2.5) is supposed to have a discrete spectrum and no continuum. It would have been better to consider the case of the continuum as well.

(f) The residual system is supposed to be the same independently of which particle leaves the nucleus. This feature would have been very bad if it were not for the fact that the potential energies of the emerging particles are supposed to be different from each other.

The main outline of the calculation is as follows. With the schematic representation of processes of particle absorption by the nuclear system and subsequent creation of the same or other particles introduced by Eq. (2.1) one obtains in terms of the residual system defined by Eq. (2.5) a representation of the asymptotic forms of the radial functions $\times r$ in a form

$$\varphi_q(r) \sim \delta_{pq} f_q(k_q r) + A_q[g_q(k_q r) + i f_q(k_q r)], \tag{1}$$

where f_q, g_q are the regular and irregular functions in the potential fields appropriate to the different disintegration products. One then finds that the amplitudes A_q which are essentially the elements of the collision matrix can be expressed as

$$A_q = B_{pq}/(w_p D) + i\delta_{pq}, \tag{1.1}$$

where the w_p are defined by Eq. (2.3b) and the determinant D is defined by (3.9a) in terms of quantities $\beta_{qq'}$. The definition of the latter involves two steps:

(a) The introduction of the "compound state" by means of the matrix (H_{nm}) and the formation of the matrix of transformation coefficients a_n^r from the compound state to the residual. By means of these transformation coefficients one forms projections of the damping integrals $I_n^{(q)}$ on to the Hilbert space axes of the compound state and calls these projections σ_q^r. The quantities σ_q^r and the energy levels of the compound state are used for the definition of $\beta_{qq'}$.

In principle the problem is solved by formula (1.1) in which the determinant D and the cofactor of its (p, q) element which is denoted by B_{pq} are formed by the process just described. At this stage the conversion of the answer to a dispersion formula form could be taken up by an expansion of A_q in terms of the zeros of $1/A_q$ by the method of residues. Such an expansion would have much similarity to the procedure of Kapur and Peierls.[5] In order to carry it through, however, one would have to go into the question of the analytic character of the function A_q in the complex plane.

In order to avoid the consideration of questions of the analytic behavior of functions in the complex plane, the transformation of Eq. (1.1) into a dispersion formula form is carried out by expressing the answer in terms of damping constants and resonance energies which themselves depend on the energy. In this respect there is again a similarity to the procedure of Peierls and Kapur. In the present calculation, however, the determination of the damping constants and energy shifts is reduced to the solution of a system of linear equations.

This system of equations is

$$(\mathsf{W}_r - E_j^{(c)})\xi_j^r - i\sum_{r'} S^{rr'}\xi_j^{r'} = 0. \tag{1.2}$$

Here the W_r are the energies of the compound state defined by

$$\sum_m H_{nm} a_m{}^r = \mathsf{W}_r a_n{}^r, \tag{1.3}$$

with

$$H_{nm} = W_n \delta_{nm} - \sum_q w_q J_{nm}{}^{(q)}, \tag{1.3'}$$

where the $J_{nm}{}^{(q)}$ are double integrals defined by (3.5b). The definition of the compound state by means of Eq. (1.3) has no reference to any assumed nuclear radius. It applies even if all interactions extend to ∞.

The quantities $S^{rr'}$ which occur in Eq. (1.2) are obtainable as

$$S^{rr'} = \sum_q w_q \sigma_q{}^r \sigma_q{}^{r'}, \tag{1.4}$$

where

$$\sigma_q{}^r = \sum_n a_n{}^r I_n{}^{(q)}, \tag{1.4'}$$

with the $a_n{}^r$ defined by (1.3) and the orthogonality relations. The $I_n{}^{(q)}$ are damping integrals obtainable from Eq. (3.5a).

The dispersion formula for the cross section is then

$$\sigma_{p\to q} = (2L+1)\frac{\Lambda^2}{\pi}\left|\delta_{pq}\exp\left[-i\delta_p\right]\sin\delta_p + \sum_j \frac{G_{qj}G_{pj}}{E_j{}^R - E - i\sum_q \Gamma_{qj}}\right|^2, \tag{1.5}$$

where

δ_p = phase shift of wave function f_p describing the pth mode of disintegration,
Λ = wave-length of relative motion,
$L\hbar$ = orbital angular momentum of all the particles,
$G_{qj} = w_q{}^{\frac{1}{2}} \sum_r \xi_j{}^r \sigma_q{}^r$,
$\Gamma_{qj} = |G_{qj}|^2 / \sum_r |\xi_j{}^r|^2$,
$E_j{}^R = \sum_r \mathsf{W}_r |\xi_j{}^r|^2 / \sum_r |\xi_j{}^r|^2$,
$E_j{}^c = E_j{}^R - i\sum_q \Gamma_{qj}$.

The validity of (1.5) is predicated on the possibility of expanding B_{pq}/D in partial fractions in terms of the quantity E^c. The variable E^c is a name for the energy E occurring in the form $\mathsf{W}_r - E$ in the quantities $\beta_{qq'}$ which give the elements of the determinant D. The variable E^c is set equal to the energy E at the end of the calculation. By this strategem one can side step questions of the character of the dependence of the quantities $\sigma_q{}^r$ on E. The energy E still enters the quantities $\sigma_q{}^r$ but is treated in this connection only as a parameter.

The form (1.5) is a legitimate one to use whenever the quotient B_{pq}/D can be considered as the limit of the expressions obtained by employing a finite number of terms in the formula (3.8a) for $B_{qq'}$. This corresponds to the successive inclusion of the levels of the compound nucleus. It is assumed that this procedure converges. It is known to converge in some cases. No general proof of convergence is available and general applicability of this part of the paper is not being claimed.

The quantities G_{qj} have essentially the meaning of disintegration probabilities *via* disintegration mode q for the resonance level j. The sum $\sum_q \Gamma_{qj}$ may be called the resonance width of level j. For sharp and widely spaced levels one has the relation

$$\Gamma_{qj} \cong |G_{qj}|^2,$$

which gives a ready interpretation of resonance widths essentially as the sum of disintegration probabilities. It is seen, however, that the factor $\sum_r |\xi_j{}^r|^2$ which represents the ratio of the right to the left side of the above approximate equality interferes with the exactness of the relation. It should be stated that the representation of the cross section in terms of a formula of the dispersion type is not unique once one allows the occurrence of coefficients varying with energy.

In Section 7 a transformation of the form (1.1) is carried out in such a way as to represent conditions in the vicinity of an isolated level. The collision cross section is represented by Eq. (7.91) in which the contributions due to the isolated level combine with potential scattering as well as with a background due to other levels. In this representation the relation between resonance width and the

disintegration probabilities is *exact* as shown by Eq. (7.6b) as well as by general arguments applying to such a representation as previously shown.[8]

In Section 8 the way in which the formulas reduce for "weak coupling" is explained. The levels are now sharp in relation to their spacing and here again the relation between resonance width and the disintegration probabilities is exact. The relation of the "isolated level" form of the answer to the more general dispersion form is reexamined and it is shown how the two give the same results. The conditions for weak coupling are very similar to those in the theory of optical dispersion.[12]

In Section 9 the relation of the methods to the one-body problem is discussed. In Section 10 a solution is described in which the energy dependence of the answer is explicitly described by means of elementary functions.

2. EQUATIONS REPRESENTING THE INTERACTION

The simultaneous equations are taken to be

$$\left[\frac{\hbar^2}{2M}\frac{d^2}{dr^2}+E-V(r)\right]\varphi(r)+\sum_{p=1}^{N}H_p(r)\varphi_p(r)=0, \tag{2.1}$$

$$\left[\frac{\hbar^2}{2M_p}\frac{d^2}{dr^2}+E-V_p(r)\right]\varphi_p(r)+H_p(r)\varphi(r)=0; \quad (p=1, 2, \cdots, N). \tag{2.2}$$

Here:

r = distance of any one of the $N+1$ particles from common center.
$\varphi_p(r)=r\times$radial wave function of the pth particle; $4\pi|\varphi_p(r)|^2dr$ = chance that pth particle is in dr.
M_p = mass of the pth particle.
$V_p(r)$ = potential energy of the pth particle in effective central field acting on it. The centrifugal force term $\hbar^2L(L+1)/(2M_pr^2)$ is supposed to be incorporated in $V_p(r)$.
$\varphi(r)=r\times$radial function of particle representing the residual nucleus.
M = mass of particle representing residual nucleus.
E = energy of system.
$V(r)$ = potential energy of particle representing residual nucleus. The centrifugal term is incorporated in $V(r)$.
$H_p(r)$ = interaction energy of pth particle with residual nucleus at distance r.

It is convenient to introduce the following symbols:

$$E_p=E-V_p(\infty), \tag{2.3}$$

$$k_p=(2M_pE_p)^{\frac{1}{2}}/\hbar, \tag{2.3a}$$

$$w_p=2M_p/(\hbar^2k_p)=2/(\hbar v_p), \tag{2.3b}$$

$$v_p=(2E_p/M_p)^{\frac{1}{2}}. \tag{2.3c}$$

The quantity v_p is the velocity of the pth particle at $r=\infty$. It is assumed that

$$V(\infty)>E, \tag{2.4}$$

so that the equations

$$\left[\frac{\hbar^2}{2M}\frac{d^2}{dr^2}+W_n-V(r)\right]u_n(r)=0 \tag{2.5}$$

have a discrete set of proper values W_n and proper functions $u_n(r)$. The latter will be taken to be real and normalized to unity:

$$u_n^*=u_n; \quad \int_0^\infty u_n^2(r)dr=1. \tag{2.6}$$

[12] V. Weisskopf and E. Wigner, Zeits. f. Physik **63**, 54 (1930); V. Weisskopf, Ann. d. Physik **9**, 23 (1931). For the transition to the case of overlapping levels and the effect of the field on the level system through the damping matrix see G. Breit, Rev. Mod. Phys. **5**, 91 (1933); G. Breit and I. S. Lowen, Phys. Rev. **46**, 590 (1934).

The following remarks should be made concerning the schematic representation of interactions described by Eqs. (2.1), (2.2):

(a) The interactions are such that a particle can disappear. In its place there appears then another particle. One of the particles capable of being removed to infinity can interact in the above manner only with the particle described by the wave function $\varphi(r)$ and potential energy $V(r)$. Direct interaction between particles capable of escape is neglected.

(b) The system described by Eq. (2.5) gives a set of energy levels W_n which will be referred to as the levels of the residual nucleus. This terminology is justified by the fact that if the interaction energies H_p were made to vanish, one would have a possibility of simultaneous existence of escaping particles described by Eqs. (2.2) together with a bound particle described by (2.1). It should be remarked, however, that one would be also justified in referring to the W_n in a certain sense as the levels of a compound nucleus because they are the energy levels of a system which results by allowing one of the particles to become converted into a state $\varphi(r)$ and then severing the interaction.

In the interests of definiteness the levels W_n will be referred to as the levels of the residual nucleus. It will be seen later that another system of levels can be introduced so as to correspond more closely with one's intuitive requirements for the level system of the compound nucleus.

(c) It will be noted that the interaction energies $H_p(r)$ correspond to the creation and disappearance of particles at the same value of r. This feature is introduced into the schematic model in the interests of simplicity.

(d) While the schematic model employed here does not represent an actual many body interaction, it has some of the features which are essential for the representation of resonances in systems containing many particles.

3. SOLUTION OF THE EQUATIONS

The solution of the equations can be expressed in terms of functions $f_p(k_p r)$, $g_p(k_p r)$ having the properties of being solutions of

$$\left[\frac{\hbar^2}{2M_p}\frac{d^2}{dr^2}+E-V_p(r)\right]\{f_p(k_p r), g_p(k_p r)\}=0 \tag{3}$$

normalized so that for $r\to\infty$

$$f_p(k_p r)\sim\sin(k_p r-L\pi/2+\delta_p), \tag{3.1a}$$

$$g_p(k_p r)\sim\cos(k_p r-L\pi/2+\delta_p). \tag{3.1b}$$

One has, therefore,

$$f_p' g_p-f_p g_p'=1. \tag{3.1c}$$

Solutions of the original equations are considered for which the asymptotic forms at $r=\infty$ are

$$\varphi_q\sim\delta_{pq}f_p+A_q(g_q+if_q). \tag{3.2}$$

This choice of the asymptotic form corresponds to there being an incident wave only in the form φ_p, i.e., for particle p. Here δ_{pq} is the Kronecker δ. Straightforward application of the one-dimensional Green's function theory gives

$$\varphi(r)=\textstyle\sum_n a_n u_n(r), \tag{3.3}$$

$$\varphi_q(r)=\delta_{pq}f_p(k_p r)+w_q\textstyle\sum_n a_n\Big\{if_p(k_p r)\int_0^\infty f_p(k_p r')H_p(r')u_n(r')dr'$$

$$+g_p(k_p r)\int_0^r f_p(k_p r')H_p(r')u_n(r')dr'+f_p(k_p r)\int_r^\infty g_p(k_p r')H_p(r')u_n(r')dr'\Big\}, \tag{3.4}$$

where the a_n are determined by the inhomogeneous set of linear equations

$$(E-W_n)a_n+\textstyle\sum_q w_q[iI_n^{(q)}\sum_m I_m^{(q)}a_m+\sum_m J_{nm}^{(q)}a_m]+I_n^{(p)}=0. \tag{3.5}$$

The quantities I, J occurring above are

$$I_n^{(q)}=\int_0^\infty u_n(r)f_q(k_qr)H_q(r)dr, \tag{3.5a}$$

$$J_{nm}^{(q)}=\int_0^\infty dr\cdot g_q(k_qr)H_q(r)\int_0^r f_q(k_qr')H_q(r')[u_m(r)u_n(r')+u_m(r')u_n(r)]dr'. \tag{3.5b}$$

For large r one obtains the asymptotic forms

$$\varphi_q(r)\sim\delta_{pq}f_q(k_qr)+A_q[g_q(k_qr)+if_q(k_qr)], \tag{3.6}$$

where

$$A_q=w_q\textstyle\sum_n a_nI_n^{(q)}. \tag{3.6a}$$

The above system of equations can be simplified through the introduction of properties of a *compound nucleus*. This is accomplished by means of the matrix having elements

$$H_{nm}=W_n\delta_{nm}-\textstyle\sum_q w_qJ_{nm}^{(q)}, \tag{3.7}$$

and the auxiliary set of equations

$$\textstyle\sum_m H_{nm}a_m^r=\mathsf{W}_ra_n^r. \tag{3.7a}$$

The energy levels W_r are the energy levels of the compound nucleus. The matrix (H_{nm}) is symmetric. If the functions $u_n(r)$ were complex rather than real this matrix would be replaced by a Hermitean one. In terms of the a_n^r one has

$$a_m=\textstyle\sum_r c_ra_m^r, \tag{3.7b}$$

and one has the usual orthogonality relations

$$\textstyle\sum_r a_n^ra_m^r=\delta_{nm}\,;\quad \sum_n a_n^ra_n^s=\delta_{rs}. \tag{3.7c}$$

By means of these relations it is found that

$$iA_q/w_q+\textstyle\sum_{q'}\beta_{qq'}A_{q'}=i\beta_{qp}, \tag{3.8}$$

where

$$\beta_{qq'}=\sum_{r'}\frac{\sigma_q^r\sigma_{q'}^r}{\mathsf{W}_r-E},\quad \sigma_q^r=\textstyle\sum_n a_n^rI_n^{(q)}. \tag{3.8a}$$

The reaction is described by a knowledge of the A_q. The system (3.8) contains, therefore, all the results of immediate interest. It determines the A_q as the solution of N inhomogeneous linear equations on the N unknowns A_q. The coefficients in this system of equations are defined by (3.8a) together with the properties of the compound nucleus determined by (3.7) and (3.7a).

The solution of (3.8) can be verified to be

$$A_q=\frac{B_{pq}}{w_pD}+i\delta_{pq}, \tag{3.9}$$

where

$$D=\det|i\delta_{qq'}/w_q+\beta_{qq'}|, \tag{3.9a}$$

and B_{pq} is the cofactor of $\beta_{pq}+i\delta_{pq}/w_q$ in D.

In connection with the above formulas it should be observed that

(a) The functions $f_q(k_qr)$, $g_q(k_qr)$ involve the energy E not only in k_qr but also as another variable or parameter. In order not to complicate the notation this dependence of f_q, g_q on E is not indicated. It is nevertheless a strong dependence in many cases.

(b) The functions f_q, g_q have been introduced with the same value of the orbital angular momentum L for all q.

(c) On account of the dependence of $f_q(k_qr)$ on the energy the quantities $I_n^{(q)}$, $J_{nm}^{(q)}$ are functions of the energy. Consequently the matrix elements H_{nm} depend on the energy E and therefore Eq. (3.7a) gives energy levels of the compound nucleus W_r which themselves depend on the energy E. The

transformation coefficients a_n^r representing the change from the proper function system $u_n(r)$ of the residual nucleus to the system of proper functions of the compound nucleus are also functions of the energy of the system.

(d) It is seen from the above that the dependence of the matrix elements of D on the energy is not only that taking place through the occurrence of E in w_p through E_p and the explicit dependence of $\beta_{qq'}$ on E in the combination $\mathsf{W}_r - E$. In addition W_r and the σ_q^r are seen to be functions of the energy.

(e) The quantities $I_n^{(q)}$ depend markedly on barrier penetration on account of the occurrence of f_q under the integral in (3.5a). On the other hand the quantities $J_{nm}^{(q)}$ contain the combination

$$g_q(k_q r) f_q(k_q r'), \quad (r \geqq r').$$

The barrier penetration factors largely compensate in this combination.

It can in fact be verified that if one adds a very high and wide barrier for values of the radius greater than those corresponding to appreciable values of the $u_n(r)$ then the values of the $J_{nm}^{(q)}$ become independent of the height, width, or location of the barrier.

It is seen that the definition of the compound state by means of the matrix satisfies an essential requirement of lack of strong dependence of the compound state on a potential barrier surrounding the whole nucleus.

(f) It will be noted that the definition of the compound state employed here does not depend on an arbitrary introduction of a nuclear radius. Considerations of properties of explicit solutions of one body systems show that essential features in the relation between the mean life and the resonance width are not reproduced if the nuclear radius is arbitrarily defined. In fact if this is done the probability of the escape of a particle from the nucleus is not estimated correctly because the probability of the particle being in the region of negative kinetic energy should be counted as part of the chance of the particle being in the compound state.

(g) The definition of the compound state employed above does not depend on investigations of the somewhat complicated dependence of f_p, g_p on E for complex values of E. The usefulness of such considerations for radioactive states has been shown by Gamow who did not employ arbitrary nuclear radii in his considerations. In Gamow's paper the problem under discussion was one of very sharp states of long lived natural radioactive nuclei. The dependence on complex E could, therefore, be easily followed. The relation of Gamow's picture to a conservative calculation involving real energies is simple[6,7] and depends only on properties of a Taylor expansion for the coefficients of outgoing and incoming waves. The attempts to formulate along analogous lines a general theory of nuclear resonances which have been made by Peierls and Kapur[5] are naturally more involved because for the general theory it is not sufficient to be concerned with first-order effects of the imaginary part of the energy on the coefficients of outgoing and incoming waves. It may be noted in this connection that Gamow's considerations ended by a complete elimination of the explicit use of complex energies and that these results can be established also without any mention of complex energies.

It is believed, therefore, that the definition of the compound state made in Eqs. (3.7), (3.7a) has advantages of not involving arbitrary nuclear radii or of employing difficult questions of analysis in the investigation of properties of functions in the complex domain. Its main disadvantage is that it is formulated for a special class of systems.

(h) The compound state defined by Eqs. (3.7), (3.7a) could be defined also by asking for a solution of Eqs. (2.1), (2.2) subject to the condition of having the φ_q asymptotic to const. $\times g_q$ at $r = \infty$. For high barriers V_q this condition corresponds to a maximum probability of the particles being inside the nucleus as compared with their density outside. It may be recalled that in the one-body problem[6,7,11] the maximum phase shift is obtained when the wave function has a similar asymptotic behavior and that the resonance width in this case is expressible for sharp resonance in terms of the reciprocal of $\int g^2 dr$, the integral being taken up to a suitable r. It is convenient to have the compound state have the property of becoming the one-body compound state and at the same time to have it defined so as to include the many-body case.

4. COMPLEX ENERGIES AND RELATION OF PROBLEM TO VIBRATION THEORY OF CLASSICAL DYNAMICS

In a sense the solution of the problem is completed by Eq. (3.9). This equation does not show, however, the interference of neighboring levels in an obvious form. In the present paragraph transformations of the answer will be made in terms of the complex roots of the determinant D in such a way as to show the interference of levels. These transformations are suggested by the similarity of (3.9) to formulas in the vibration theory of classical dynamics. In the classical theory of small vibrations the vanishing of the determinant of the associated system of linear equations is the feature characteristic of resonance.

The roots of the determinant D will be introduced here by first assigning a real value to the energy, obtaining in terms of it the $J_{nm}^{(q)}$, H_{nm}, W_n, a_n^r and also the $I_n^{(q)}$ as well as the w_q. These quantities will be regarded as parameters in the determinant D the elements of which are

$$b_{qq'}=\beta_{qq'}+i\delta_{qq'}/w_q. \tag{4}$$

The energy E occurs explicitly in the denominators of the terms representing $\beta_{qq'}$ as a sum by means of formula (3.8a). All considerations concerned with complex values of E made below are carried out by allowing only the E in the combinations W_r-E to take on complex values. This is done only as a helpful mathematical device. The value of E in any physical formula is, of course, real. In order to distinguish the E occurring in the denominators W_r-E in Eq. (3.7a) from the real values of the energy it will be referred to as E^c so as to indicate that it will be allowed to take on complex values. Final formulas will involve the special value of E^c *viz.*, $E^c=E$ where E is the real energy for which the other quantities have been evaluated. In this sense the determinant D will be considered as a function of E^c:

$$D=D(E^c).$$

There is a set of roots of this function which will be distinguished by suffixes j so that

$$D(E_j^c)=0. \tag{4.1}$$

The fractions B_{pq}/D in Eq. (3.9) will now be expressed in terms of these roots. It will be noted that the solutions of

$$\sum_q b_{pq}\bar{y}_q=\bar{z}_p \tag{4.2}$$

are

$$\bar{y}_p=\sum_q B_{pq}\bar{z}_q/D. \tag{4.2a}$$

The Eqs. (4.2) can be rewritten as

$$iy_p+\sum_{q,r} s_p^r s_q^r y_q/(\mathsf{W}_r-E)=z_p, \tag{4.2b}$$

where

$$\bar{y}_p=w_p^{\frac{1}{2}}y_p, \quad s_p^r=w_p^{\frac{1}{2}}\sigma_p^r, \quad z_p=w_p^{\frac{1}{2}}\bar{z}_p. \tag{4.2c}$$

The above equations are now meant to hold for all p. The matrix $(S^{rr'})$ is next introduced by letting

$$S^{rr'}=\sum_p s_p^r s_p^{r'} \tag{4.3}$$

and the Eqs. (4.2b) are multiplied by s_p^r and summed over p. One finds

$$(\mathsf{W}_r-E^c)\xi^r-i\sum_{r'} S^{rr'}\xi^{r'}=X^r, \tag{4.4}$$

where ξ^r is defined by

$$(\mathsf{W}_r-E^c)\xi^r=\sum_q s_q^r y_q=\sum_q \sigma_q^r\bar{y}_q, \tag{4.4a}$$

and

$$iX^r=\sum_p s_p^r z_p. \tag{4.4b}$$

The solution of Eqs. (4.4) can be arranged for by introducing a set of transformation coefficients ξ_j^r by means of the equations

$$(\mathsf{W}_r-E_j^c)\xi_j^r-i\sum_{r'} S^{rr'}\xi_j^{r'}=0. \tag{4.5}$$

These equations introduce also a set of complex numbers E_j^c which may be termed the complex eigenvalues of the problem. If $E^c=E_j^c$ then it is possible to satisfy (4.4) with all $X^r=0$. But if all $X^r=0$ then (4.4b) usually requires all z_p to vanish. Hence (4.2b) can be satisfied with all $z_p=0$ and

therefore $D(E_j^e)=0$. Conversely if (4.1) is satisfied by a value of E_j^e then for $E^e=E_j^e$ it is possible to find a set of y_q that satisfy (4.2) for all $z_p=0$ and hence a set of ξ^r for (4.4) with all $X^r=0$. Consequently such an E_j^e will also do for (4.5).

The conclusion that (4.2) is a consequence of (4.5) involves the assumption that if all $X^r=0$ then all $z_p=0$. This is not always the case. Thus, for example, if all the $I_n^{(q)}$ should vanish, then all the s_p^r vanish also and hence the $X^r=0$ for arbitrary finite z_p. In this case D does not contain E^e and it is not possible to make it equal to zero by a proper choice of E^e. In this case, however, all $S^{rr'}$ vanish and hence from (4.5) $E_j^e=\mathsf{W}_r$. The determinant D contains, therefore, indeterminate fractions of the form 0/0 for the solutions of (4.5). In general one cannot expect the quantities s_p^r to be such as to make it possible to satisfy an infinite number of equations $\sum s_p^r z_p=0$ with a finite number of unknowns z_p unless all the z_p vanish.

The system of Eqs. (4.5) has as a consequence orthogonality relations between the coefficients ξ_j^r. These follow in the usual manner by subtracting the result of multiplying the kth equation by ξ_j^r from the result of multiplying the equation by ξ_k^r and summing over all r. One finds in this way that

$$\sum_r \xi_j^r \xi_k^r = \delta_{jk}, \tag{4.5a}$$

provided the ξ_j^r are properly normalized. These are conditions characteristic of orthogonal rather than of unitary transformations. In a well-known manner one derives from (4.5a) the similar set of conditions

$$\sum_j \xi_j^r \xi_j^s = \delta_{rs}. \tag{4.5b}$$

With the help of Eqs. (4.5a), (4.5b) one can determine the coefficients c_j in the expansion

$$\xi^r = \sum_j c_j \xi_j^r, \tag{4.6}$$

so as to satisfy Eq. (4.4). One finds

$$\xi^r = \sum_s \left[\sum_j \xi_j^r \xi_j^s/(E_j^e - E)\right] X^s. \tag{4.6a}$$

Here the quantity E^e has been assigned its physically significant value E. One solves next Eqs. (4.4a) for the $\bar{y}_q$ in terms of the ξ^r and determines therefore through (4.6a) and (4.4b) the expression for $\bar{y}_q$ in terms of the z_p. The last of the three formulas (4.2c) determines z_p in terms of $\bar{z}_p$ and gives therefore a formula for $\bar{y}_p$ in terms of the $\bar{z}_q$. A comparison of the form so obtained with Eq. (4.2a) gives

$$B_{qp}/D = w_p \delta_{pq}/i + \sum_{j,r,s} w_p w_q \sigma_q^r \sigma_p^s \xi_j^r \xi_j^s/(E_j^e - E), \tag{4.7}$$

which when substituted into Eq. (3.9) gives with the aid of (4.4a), (4.2c), and (4.5)

$$A_q = w_q \sum_j \left(\sum_r \sigma_q^r \xi_j^r\right)\left(\sum_s \sigma_p^s \xi_j^s\right)/(E_j^e - E). \tag{4.8}$$

This formula represents A_q as a sum of terms, each term having a pole in the complex plane. The quantity E^e has been replaced by E in Eq. (4.8) because the applications of the formula must be made for real values of the energy.

The quantity A_q/w_q is seen to be symmetric in p and q. The amplitude A_q is introduced by Eq. (3.6) in such a way that the number of systems generated in state q per unit incident system in state p is

$$(v_q/v_p)\,|A_q|^2 = (w_p/w_q)\,|A_q|^2 = w_p w_q |A_q/w_q|^2. \tag{4.8a}$$

The right term of this equation shows that this is also the number of systems which are generated in state p per unit incident system in state q. The scattering matrix thus satisfies the requirement of symmetry which is equivalent to detailed balance at high temperatures.

The numerator of every term in the sum representing A_q/w_q in Eq. (4.8) is a product of two terms, one of which depends only on p and the other only on q. This is to be expected from the general form for A_q/w_q given by Eq. (3.9). When the determinant D vanishes all second minors formed by the cofactors B_{pq} vanish and the cofactors can be represented, therefore, in the form $(B_{pp}B_{qq})^{\frac{1}{2}}$. This

situation is very similar to that occurring in the theory of vibrations of classical dynamics and has already been made use of in connection with the present problem.

5. RESONANCE WIDTH

The relations (4.5) determine a connection between the resonance width and the coefficients occurring in the numerators of the terms in the sum representing A_q/w_q. One defines real numbers E_j^R, E_j^I, x_j^r, y_j^r by

$$E_j^e = E_j^R + iE_j^I, \quad \xi_j^r = x_j^r + iy_j^r. \tag{5}$$

One obtains then from the real and imaginary parts of Eq. (4.5) by multiplying by $(-y_j^r, x_j^r)$ and by (x_j^r, y_j^r) and summing over r the relations

$$E_j^I = -\sum_q \Gamma_{qj}; \quad \Gamma_{qj} = w_q |\sum_r \xi_j^r \sigma_q^r|^2 / \sum_r |\xi_j^r|^2, \tag{5.1}$$

$$E_j^R = \sum_r W_r |\xi_j^r|^2 / \sum_r |\xi_j^r|^2, \tag{5.2}$$

and one has

$$A_q = \left(\frac{v_p}{v_q}\right)^{\frac{1}{2}} \sum_j \frac{G_{qj} G_{pj}}{E_j^R - E - i\sum_q \Gamma_{qj}}, \tag{5.3}$$

with

$$G_{qj} = w_q^{\frac{1}{2}} \sum_r \xi_j^r \sigma_q^r, \tag{5.4}$$

so that

$$|G_{qj}|^2 = \Gamma_{qj} \sum_r |\xi_j^r|^2. \tag{5.5}$$

Substitution of the value of ξ_j^r in terms of x_j^r, y_j^r by means of Eq. (5) into the orthogonality relation (4.5a) for $j=k$ gives

$$\sum_r [|x_j^r|^2 - |y_j^r|^2] = 1, \tag{5.6}$$

and one has, therefore,

$$\sum_r |\xi_j^r|^2 = 1 + 2\sum_r |y_j^r|^2 \geqq 1, \tag{5.7}$$

so that in view of Eq. (5.5)

$$|G_{qj}|^2 \geqq \Gamma_{qj}. \tag{5.8}$$

It should be remarked that:

(a) Whenever the equality sign applies in Eq. (5.8) one obtains the relation between the resonance width and the numerators in the dispersion formula which holds for the "one-level" theory[1] or for the "one level with background" theory.[8] The latter theory being somewhat more general, comparison is made with it. One has

$$a_{qp} = -(\delta_{pq} + 2iA_q) \exp\{-L\pi i + 2\delta_q i\}, \tag{5.8a}$$

where a_{qp} is the matrix element of the scattering matrix[8] corresponding to incidence along channel p and emergence along channel q. It was found that close to resonance one can represent

$$a_{qp} \leqq \left(\frac{v_p}{v_q}\right)^{\frac{1}{2}} \frac{C_q C_p}{E - E^e} + d_{qp},$$

where d_{qp} represents the "background matrix" and it was also found that

$$|E^e - E^{e*}| = \sum_q |C_q|^2, \tag{5.1, I}$$

where the C_q are in general complex constants. Identifying the coefficient of $(E-E^e)^{-1}$ in these formulas with that in (5.3) one has

$$4|G_p|^2 |G_q|^2 = |C_q|^2 |C_p|^2$$

for all q, p. One has, therefore,

$$2|G_q|^2 = |C_q|^2, \tag{5.8b}$$

which together with (5.1, I) gives

$$|E - E^{e*}| = 2\sum_q |G_q|^2,$$

which leads to

$$\sum_q \Gamma_{qj} = \sum_q |G_q|^2 \tag{5.9}$$

on account of the first Eq. (5.1) of the present paper. The "one-level" theory is thus seen to correspond to the sign of equality in Eq. (5.8).

(b) It will be seen later that for weak interactions giving small values of the Γ_{qj} one obtains agreement with (5.9) without making any assumption concerning applicability of the "one level with background" approximation. The agreement with (5.9) which one obtains in this case can also be understood as being due to the sharpening of resonances which makes the "one level with background" theory applicable.

6. CROSS SECTIONS

The functions f_q do not have the asymptotic behavior appropriate to regular solutions in the absence of a field. Linear combinations of f_q, g_q are therefore introduced in such a way as to correspond to field-free particles. These combinations will be taken to be F_q, G_q which will be arranged to have asymptotic behaviors.

$$F_q \sim \sin(k_q r - L\pi/2), \quad G_q \sim \cos(k_q r - L\pi/2). \tag{6}$$

In terms of these functions one finds on account of (3.2)

$$\exp[i\delta_p]\varphi_q \sim \delta_{pq}F_p + [\delta_{pq}\exp[i\delta_p]\sin\delta_p + A_q\exp[i(\delta_p+\delta_q)]](G_q+iF_q). \tag{6.1}$$

Remembering that G_q+iF_q is a diverging wave and applying Eq. (6.1) to three-dimensional problems with angular momentum L, the right-hand side of (6.1) can be made to represent the coefficient of $i^L(2L+1)P_L(\cos\theta)/(k_p r)$ in the expression for the qth wave at a large distance. Here θ is the scattering angle and P_L is the Legendre polynomial of order L. The cross section for disintegration *via* mode q due to incidence in mode p is

$$\sigma_{p\to q} = (2L+1)(v_q/v_p)\frac{\Lambda_p^2}{\pi}|\delta_{pq}\exp[-i\delta_p]\sin\delta_p + A_q|^2, \tag{6.2}$$

which becomes in view of Eq. (5.3)

$$\sigma_{p\to q} = (2L+1)\frac{\Lambda_p^2}{\pi}\left|\delta_{pq}\exp[-i\delta_p]\sin\delta_p + \sum\frac{G_{qj}G_{pj}}{E_j^R - E - i\sum_q\Gamma_{qj}}\right|^2. \tag{6.3}$$

This result is very similar to that of Bethe. The main difference is that the quantities $|G_{qj}|^2$ are not exactly the same as the Γ_{qj} but are related to them through Eq. (5.5).

7. AN ISOLATED LEVEL

If one of the levels W_r is located so that the width of other levels does not appreciably overlap it, one can obtain convenient expressions for the A_q directly from Eq. (3.9) without the aid of the secular equations (4.5). The quantities $\beta_{qq'}$ in Eq. (3.8a) depend then critically only on the term involving $1/(\mathsf{W}_r - E)$. The other terms contributing to $\beta_{qq'}$ vary relatively slowly with E and will be lumped into one combination which varies slowly with E. One has thus

$$\beta_{qp} = \sigma_q{}^r\sigma_p{}^r/(\mathsf{W}_r - E) + \epsilon_{qp}, \tag{7}$$

where

$$\epsilon_{qp} = \sum_{s\neq r}\sigma_q{}^s\sigma_p{}^s/(\mathsf{W}_s - E). \tag{7.1}$$

One finds by standard rules for determinants that

$$D = \det|\mu_{qp}| + (\sum M_{qp}\sigma_p{}^r\sigma_q{}^r)/(\mathsf{W}_r - E), \tag{7.2}$$

where

$$\mu_{qp} = i\delta_{pq}/w_p + \epsilon_{qp}, \tag{7.3}$$

and M_{pq} is the cofactor of μ_{pq} in $\det|\mu_{pq}|$. The index p in the present discussion is meant to take on any one of the values 1, 2, $\cdots$, N. Only in the final formulas will it be made to have the value corresponding to the incident state.

One introduces a set of quantities x_q by means of

$$\sum_q \mu_{pq}x_q = \sigma_p{}^r, \tag{7.4}$$

so that

$$x_q=\sum_p M_{qp}\sigma_p{}^r/D', \quad D'=\det|\mu_{pq}|, \tag{7.4a}$$

and one obtains

$$\frac{B_{pq}}{D}=\frac{M_{pq}}{D'}-\frac{x_px_q}{\mathsf{W}_r-E+i\sum_q x_q{}^2/w_q+\sum_{p,q}\epsilon_{pq}x_px_q}, \tag{7.5}$$
$$=\frac{M_{pq}}{D'}-\frac{x_px_q}{\mathsf{W}_r-E+[\sum_{p,q}M_{pq}\sigma_p{}^r\sigma_q{}^r]/D'}.$$

Here the μ_{pq}, x_q, ϵ_{pq} are all complex. For weak coupling (small H_p and $w_qJ_{nm}{}^{(q)}$) the ix_q are approximately real. The first line of Eq. (7.5) is written so as to show the similarity of the result with (4.7) and (6.3). In the second line the denominator is expressed explicitly in terms of the $\sigma_p{}^r$.

It is an interesting fact that

$$\sum_q\frac{|x_q|^2}{w_q}=-Im\{\sum_{p,q}M_{p,q}\sigma_p{}^r\sigma_q{}^r/D'\}. \tag{7.6}$$

This formula means that the sum of disintegration probabilities occurring in the numerator of (7.5) when properly normalized gives the apparent width of resonance. The quantity ix_p takes place in the numerator of (7.5) of the quantity

$$w_p(\sum_s\sigma_p{}^s\xi_j{}^s)_{j=r}$$

in (4.7) and hence according to (5.4)

$$w_p{}^{\frac{1}{2}}(G_{pj})_{j=r}\to ix_p.$$

It becomes reasonable, therefore, to define

$$w_q{}^{\frac{1}{2}}G_{qr}'=ix_q, \tag{7.6a}$$

and

$$\Gamma_{qr}'=|G_{qr}'|^2 \tag{7.6b}$$

in terms of which (7.5) gives

$$\frac{B_{pq}}{D}=\frac{M_{pq}}{D'}+\frac{w_p{}^{\frac{1}{2}}w_q{}^{\frac{1}{2}}G_{pr}'G_{qr}'}{\mathsf{W}_r'-i\sum_q\Gamma_{qr}'-E}, \tag{7:7}$$

where W_r' is W_r corrected for Dirac's energy shift and is obtainable from Eq. (7.8).

The validity of Eq. (7.7) can be seen and the value of the energy can be derived as follows. Equation (7.4) can be written in view of (7.3)

$$ix_p/w_p+\sum\epsilon_{pq}x_q=\sigma_p{}^r. \tag{7.7a}$$

It will be noted that the ϵ_{pq} and the $\sigma_p{}^r$ are real. The complex conjugate of the above equation is, therefore,

$$-ix_p{}^*/w_p+\sum_q\epsilon_{pq}x_q{}^*=\sigma_p{}^r. \tag{7.7b}$$

One has, therefore,

$$\sum_p|x_p|^2/w_p=\sum_p ix_p(-ix_p{}^*/w_p)=i\sum_p\sigma_p{}^rx_p-i\sum_{p,q}x_p{}^*\epsilon_{pq}x_q, \tag{7.7c}$$

where the value of $-ix_p{}^*/w_p$ has been substituted by means of (7.7b). In view of the fact that ϵ_{pq} is real and also symmetric in p, q the quadratic form occurring on the right side of (7.7c) assumes real values only. Taking the real and imaginary parts of both sides of (7.7c) one obtains, therefore,

$$\sum_p|x_p|^2/w_p=-Im\sum_p\sigma_p{}^rx_p, \tag{7.7d}$$

$$Re\sum_p\sigma_p{}^rx_p=\sum_{p,q}x_p{}^*\epsilon_{pq}x_q. \tag{7.7e}$$

It will be noted in addition that on account of (7.4), (7.4a)

$$(\sum_{p,q}M_{pq}\sigma_p{}^r\sigma_q{}^r)/D'=\sum_p\sigma_p{}^rx_p, \tag{7.7f}$$

Eqs. (7.7d), (7.7f) show that (7.6) is true. Equation (7.7e) gives

$$\mathsf{W}_r'=\mathsf{W}_r+\sum_{p,q}x_p{}^*\epsilon_{pq}x_q. \tag{7.8}$$

These relations show also that

$$\begin{aligned}\sum_p \sigma_p{}^r x_p &= i\sum_p x_p{}^2/w_p+\sum_{p,q} x_p\epsilon_{pq}x_q \\ &= -i\sum_p |x_p|^2/w_p+\sum_{p,q} x_p{}^*\epsilon_{pq}x_q.\end{aligned} \tag{7.9}$$

It will be noted in connection with the above formulas that:

(a) They do *not* involve an approximation of supposing that one level is isolated from other levels. They are put into a form, however, which is convenient for the representation of cross sections in situations and energy regions in which the effect of one level W_r is more pronounced than that of other levels. In such cases the quantities ϵ_{pq} vary relatively slowly and to a first approximation the x_q are constants as a result of Eqs. (7.4). Similarly the "background" M_{pq}/D' occurring in Eq. (7.7) is then approximately constant.

(b) The relation between the numerators of the dispersion term and the imaginary part of its denominator is simpler in the form (7.6b) applying to the isolated level representation (7.7) than in the form (4.7) which corresponds to representation by many levels.

(c) The simple relation (7.6b) between the numerators of the dispersion term and the resonance width is in agreement with the relation (5.1, I) previously derived from rather general considerations for the one-level case. The formulas of the present paragraph may be regarded as a verification of the previous work if they are applied to cases in which W_r' and $\sum \Gamma_{qr}'$ are nearly constant.

(d) The quantity W_r' is a function of the energy not only on account of the dependence of the $\sigma_p{}^r$ and W_r on the energy but also on account of the occurrence of E in ϵ_{pq} as well as the x_q. The latter dependence has its origin in the occurrence of E in combinations with W_s-E in the expression for ϵ_{pq} given by Eq. (7.1).

(e) It appears at first sight as though the isolated level form represents the effect of singling out one of the terms in the sum over complex eigenvalues in (4.7) and lumping all other terms into one contribution considered as a background. This is not the case, however. The last term in (7.7) is not equal to any one term in (4.7).

In fact, the quantity E occurring in combinations W_s-E in the ϵ_{pq} enters both W_r' and the Γ_{qr}'. The denominator of the last term of (7.7) does not have, therefore, the simple form $E_f{}^c-E$. A comparison of the denominator of the second term in the last line of Eq. (7.5) with the formula for D given by Eq. (7.2) shows, in fact, that the resonance denominator in the one-level formula vanishes at all the roots of D as E is varied in the combinations W_r-E, W_s-E. Varying E in the latter manner corresponds to the procedure of introducing the quantity E^c. The resonance denominator in the isolated level formula has, therefore, many roots and consequently is not equal to the denominator in any one of the terms in the "interfering level" formulas (4.7), (5.3), (6.3).

(f) The term M_{pq}/D' which represents the "background" is a complex number which is real only in special cases.

(g) Combining Eqs. (3.9), (6.2), (7.7) one obtains a formula for the collision cross section in the "isolated level" form:

$$\sigma_{p\to q}=(2L+1)\frac{\Lambda_p{}^2}{\pi}\left|\delta_{pq}(i+\exp[-i\delta_p]\sin\delta_p)+\left(\frac{v_p}{v_q}\right)^{\frac{1}{2}}\frac{M_{pq}}{D'}+\frac{G_{pr}'G_{qr}'}{\mathsf{W}_r'-i\sum_q \Gamma_{qr}'-E}\right|^2. \tag{7.91}$$

In this formula the potential scattering term containing the δ_p interferes with the constant amplitude i. In the "interfering levels" formula (6.3) for the cross section there is no such interference. There is also a compensation of the term in the above formula through the term in M_{pq}/D'.

(h) It is clear from the comparisons between the "isolated level" and "interfering levels" formulas that cross-section formulas similar in qualitative physical consequences may correspond to different relations between the apparent disintegration probabilities occurring in the numerators of the dispersion terms and the effective resonance widths determined by the imaginary part of the denominators.

8. WEAK COUPLING

In this section it will be supposed that all

$$\left|\frac{S^{sr}}{\mathsf{W}_s-\mathsf{W}_r}\right|\ll 1 \quad (s\neq r), \tag{8}$$

and this condition will be referred to as "weak coupling" because the compound state is coupled to the continuum through the existence of the quantities σ^{rp} which determine the quantities S^{sr} by means of Eqs. (4.2c), (4.3).

The "interfering levels" formula for A_q leads in this case to

$$A_q=(v_p/v_q)^{\frac{1}{2}}\sum_r(\Gamma_{pr}\Gamma_{qr})^{\frac{1}{2}}/(E_r^c-E), \tag{8.1}$$

with

$$\Gamma_{qr}^{\frac{1}{2}}\cong w_q^{\frac{1}{2}}\sigma_q^r, \tag{8.1a}$$

$$E_r^c\cong\mathsf{W}_r-i\sum_q\Gamma_{qr}+\sum_{s\neq r}(\textstyle\sum_p w_p\sigma_p^s\sigma_p^r)^2/(\mathsf{W}_r-\mathsf{W}_s). \tag{8.1b}$$

In the above formulas the notation is consistent with that of Eqs. (5) to (5.3). The quantity $\Gamma_{qr}^{\frac{1}{2}}$ corresponds to G_{qr} of Eq. (5.4). The sign of the $\xi_{qr}^{\frac{1}{2}}$ is chosen so as to have ξ_r^r approximately equal to unity. In view of the weakness of coupling there is only a slight difference between E_r^c and W_r. It is possible, therefore, to label the levels E_j^c consistently by the index r of the parent level.

The intermediate steps in the calculation leading from Eq. (5.3) to Eq. (8.1) consist in working out the first power of the small quantity on the left side of Eq. (8) for the Γ_{qr} and for the real part of $E_r^c-\mathsf{W}_r$. The formula (8.1) for A_q represents, therefore, a result suitable for estimating the damping constants and the energy shift to a first approximation. It will be noted that in this approximation the inequality in Eq. (5.7) can be replaced by an equality.

For the "isolated level" form one finds for

$$\frac{M_{pq}}{D'}\cong-i\delta_{pq}w_q+w_pw_q\sum_{s\neq r}\sigma_p^s\sigma_q^s/(\mathsf{W}_s-E) \tag{8.2}$$

$$G_{qr}'\cong w_q^{\frac{1}{2}}\sigma_q^r, \tag{8.3}$$

$$A_q\cong\left(\frac{v_p}{v_q}\right)^{\frac{1}{2}}\left[\sum_{s\neq r}\frac{(\Gamma_{qs}'\Gamma_{ps}')^{\frac{1}{2}}}{\mathsf{W}_s-E}+\frac{(\Gamma_{pr}'\Gamma_{qr}')^{\frac{1}{2}}}{\mathsf{W}_r'-i\sum_q\Gamma_{qr}'-E}\right]. \tag{8.4}$$

The formulas written above are obtained from Eq. (7.7) combined with Eq. (3.9). The approximations are just like those for Eqs. (8.1), (8.1a), (8.1b) with the additional approximation of supposing that E is close to W_r. It was in fact supposed that quantities of the order $(\sigma_p^r)^2/|\mathsf{W}_s-E|$ are $\ll 1$. It is seen that Eq. (8.4) agrees with Eq. (8.1) within the approximations made.

One also readily verifies Eq. (7.9) by means of the approximate values for the x_p that correspond to Eq. (8.2).

It is seen that the approximation of weak coupling gives one expressions of the same form as those obtained by Bethe and Placzek for weak coupling.

9. RELATION TO THE ONE-BODY PROBLEM

The representation of resonances which has been obtained in the present paper includes the resonance effects of potential wells. It does not necessarily give an explicit representation or listing of these among the resonance terms of Eq. (6.3). Thus, for example, Eq. (6.3) can give values of the scattering cross section varying rapidly with the energy on account of a rapid variation of δ_p corresponding to a resonance in the potential scattering. Under such conditions some of Γ_{qj} will also vary rapidly and an effect on the real part of E_r^c will be present on account of the maximum in the $I_n^{(q)}$ and the rapid variation of the σ_r^s. The latter effect can be seen to be present through an inspection of the last term in Eq. (8.1b). It will be noted, however, that the resonance to the potential well does not bring in a term with a resonance denominator in the present representation and that the resonance

occurs partly through a variation of the phase shift, partly through a variation of the real part of the complex energy rather than through the vanishing of the real part of the resonance denominator.

The many-body point of view of nuclear structure emphasized by Bohr makes resonances to potential wells an uninteresting question and it is, therefore, no inconvenience not to have them explicitly indicated by resonance terms.

10. EXPLICIT SOLUTION FOR A SPECIAL CASE

If $N=2$, and if $V(r)=\infty$ when $a<r<\infty$ while

$$H_1, H_2, V, V_1, V_2 = \text{const.} \quad (0<r\leqq a), \tag{10}$$

the quantities $I_n^{(q)}$, $J_{nm}^{(q)}$ are found to be

$$I_n^{(q)} = i_{qn} w_q^{-\frac{1}{2}}; \quad J_{nm}^{(q)} = j_{qnm}/w_q, \tag{10.1}$$

where the values of the symbols are as follows

$$i_{qn} = (-)^n \left(\frac{2}{k_q a}\right)^{\frac{1}{2}} H_q \frac{(2M)^{\frac{1}{2}} k_n f_q(k_q a)}{\hbar(\kappa_{q0}^2 - k_n^2)}, \tag{10.1a}$$

$$k_n = \frac{\pi n}{a}, \quad \kappa_{q0}^2 = \frac{2M}{\hbar^2}[E - V_q(r)], \quad (0<r<a), \tag{10.1b}$$

$$j_{qmn} = \frac{g_q(k_q a)}{f_q(k_q a)} i_{qn} i_{qm} - \frac{2MH_q^2}{\kappa_{q0}^2 - k_n^2}\delta_{mn}. \tag{10.1c}$$

The quantities i_{qn}, j_{qmn} have the dimensions of $E^{\frac{1}{2}}$, E, respectively, where E is the energy. The common mass is denoted by M.

For incidence in state 1, i.e., for $p=1$, one finds for the coefficients of the asymptotic forms defined by Eq. (3.2)

$$A_2 = -(k_1/k_2)^{\frac{1}{2}} \alpha_{12}/\Delta, \tag{10.2}$$

$$A_1 = -1/b_1 + (1+b_2\alpha_{22})/(b_1\Delta) = [-\alpha_{11} + b_2(\alpha_{12}^2 - \alpha_{11}\alpha_{22})]/\Delta, \tag{10.2a}$$

where

$$\Delta = (1+b_1\alpha_{11})(1+b_2\alpha_{22}) - b_1 b_2 \alpha_{12}^2, \tag{10.2b}$$

$$\alpha_{qq'} = \sum_n i_{qn} i_{q'n}/(E - \hat{E}_n), \tag{10.2c}$$

$$\hat{E}_n = W_n + H_1^2/[E - W_n - V_1(a) + V(a)] + H_2^2/[E - W_n - V_2(a) + V(a)], \tag{10.2d}$$

$$b_q = [g_q(k_q a) + i f_q(k_q a)]/f_q(k_q a). \tag{10.2e}$$

The quantity W_n is the nth energy level of the residual nucleus:

$$W_n = \hbar^2 k_n^2/(2M) = \hbar^2 n^2/(8Ma^2). \tag{10.2f}$$

It should be pointed out in connection with the above results that:

(a) Formulas (10.2), (10.2a) give the quantities A_q for Eq. (6.3) in which the cross sections are expressed in terms of A_q.

(b) Substitution of the symbols involved by means of (10.1a), (10.1b), (10.2c) . . . (10.2f) gives the dependence of the A_q on the energy explicitly through substitution.

(c) The potentials $V_1(r)$, $V_2(r)$ although assumed to be constant in the interval $(0, a)$ are not restricted in any way in the interval (a, ∞). The formulas thus include the influence of potential barriers on the cross sections.

If one assumes that for $r=a$

$$g_2/f_2 \gg g_1/f_1, \tag{10.3}$$

and that

$$b_1 \sum_{n,m} \frac{(i_{2n} i_{1m} - i_{1n} i_{2m})^2}{(\hat{E}_n - \hat{E}_m)(E - \hat{E}_n)} \ll \sum_n \frac{i_{2n}^2}{E - \hat{E}_n}; \tag{10.3a}$$

then it follows from Eq. (10.2) that

$$A_2 \backeq -H_1 f_1/(H_2 g_2). \tag{10.4}$$

The assumption of Eq. (10.3) means that the second mode is bottled in by its barrier much more than the first. The assumption of Eq. (10.3a) means that the coupling energy H_1 of the first mode is kept sufficiently small. The form of A_2 given by (10.4) is interesting in that it contains the irregular function for the final state in the denominator and the regular function for the initial state in the numerator.

For

$$V_1(r)=V_2(r)=V_0 \quad (0<r<a), \tag{10.5}$$

the equations for A_1, A_2 reduce to

$$A_1=-\frac{2H_1^2f_1^2(k_1a)}{k_1a\Delta'}, \quad A_2=-\frac{2H_1H_2f_1(k_1a)f_2(k_2a)}{k_2a\Delta'}, \tag{10.6}$$

where Δ' is given by

$$\Delta'-2b_1H_1^2f_1^2/(k_1a)-2b_2H_2^2f_2^2/(k_2a)=\left[\sum_n W_n\left(\frac{\gamma_1}{E-W_{n1}}+\frac{\gamma_2}{E-W_{n2}}+\frac{\gamma_3}{E-W_{n3}}\right)\right]^{-1}, \tag{10.6a}$$

$$=2(\gamma_1x_1\cot x_1+\gamma_2x_2\cot x_2+\gamma_3x_3\cot x_3)^{-1};$$

with

$$W_{n1}=W_n+V_0/2+[(V_0/2)^2+H_1^2+H_2^2]^{\frac{1}{2}}, \tag{10.7}$$

$$W_{n2}=W_n+V_0/2-[(V_0/2)^2+H_1^2+H_2^2]^{\frac{1}{2}}, \tag{10.7a}$$

$$W_{n3}=W_n+V_0, \tag{10.7b}$$

and

$$\gamma_1=(W_n-W_{n2})^{-1}(W_{n1}-W_{n2})^{-1}, \tag{10.8}$$

$$\gamma_2=(W_n-W_{n1})^{-1}(W_{n2}-W_{n1})^{-1}, \tag{10.8a}$$

$$\gamma_3=(W_{n2}-W_n)^{-1}(W_{n1}-W_n)^{-1}=-(H_1^2+H_2^2)^{-1}, \tag{10.8b}$$

$$x_s=[2Ma^2\hbar^{-2}(E+W_n-W_{ns})]^{\frac{1}{2}}; \quad (s=1, 2, 3). \tag{10.9}$$

One sees from Eqs. (10.6), (10.6a) that the numerators of these formulas for the A_q contain the factors $f_q(k_qa)/(k_qa)^{\frac{1}{2}}$ and that the denominators contain imaginary terms in the combinations $2iH_q^2f_q^2/(k_qa)$ so that the damping constants depend essentially on the regular function and the interaction energy H_q. It is of interest to note that Eq. (10.6a) gives an explicit expression in terms of cotangents with the arguments x_s defined by Eq. (10.9).

The example just considered shows that the representation of the scattering amplitudes as a sum of interfering terms can be far from being the simplest.

PHYSICAL REVIEW VOLUME 69, NUMBERS 9 AND 10 MAY 1 AND 15, 1946

A Note on the Relativistic Problem of Uniform Rotation

E. L. HILL
Department of Physics, University of Minnesota, Minneapolis, Minnesota

(Received January 12, 1946)

A study of uniform rotational motion about an axis is made on the basis of a definition of hydrokinetic character. A solution is found in which the particle speed is linear with distance from the axis of rotation to terms in $(R\omega_0/c)^2$, but approaches the speed of light at great distances. This result is unchanged by the introduction of relativistic accelerated Euclidean axes. Reasons are given for concluding that Ehrenfest's paradox in the problem of the rotating disk, and the question of the "geometry" of the motion, in the sense of general relativity theory, can be answered only on the basis of a theory of the generation of the rotation.

1. INTRODUCTION

THE difficulties presented in the theory of relativity by the "rigid" motion of a body about a fixed axis have been discussed by a number of authors. Among these difficulties, the apparent paradox pointed out by Ehrenfest[1] has received particular attention. For simplicity,

[1] P. Ehrenfest, Physik. Zeits. 10, 918 (1909).

consider any section of the body by a plane perpendicular to the axis of rotation, and any circle in this plane having its center on the axis. Since the elements of the circumference of this circle everywhere move in the direction of their instantaneous velocities, one would anticipate a diminished value for the length of the radius. On the other hand, since the elements of the radii of the circle everywhere move normally to the directions of their velocities, no such contraction would be expected. The ratio of circumference to diameter of the circle would therefore be expected to be smaller than the Euclidean value, and to depend on the radius of the circle. This is the standard argument from which it is usually concluded that the "geometry" of the rotating body ceases to be Euclidean.[2]

Solutions of this paradox have been proposed by Lorentz[3] and Eddington[4] on the basis of the general theory of relativity. In a recent paper Berenda[5] has given a careful summary of this work, and has himself proposed yet another solution.

In this note a different approach will be presented, based on an altered view of the *kinematics* of the motion. Previous discussions generally have started with the classical definition of uniform rotation, according to which each particle seems to the observer to move on the circumference of a circle about the axis of rotation with a speed which is a linear function of the radius of the circle. It does not appear to have been a worrisome point to other writers that this requirement imposes a necessary condition on the size of a body performing such a rotational motion. For if this speed-distance law were to hold at large distances from the axis of rotation, points at a great distance from the axis would have speeds exceeding that of light, which is a violation of the basic principles of relativity theory. Rather than consider that there is such a limitation on the size of a rotating body, the conclusion is drawn that the speed-distance law must be non-linear.

The thesis developed here is that the definition of uniform rotational motion to be used cannot be that of the classical theory. It is anticipated that, with a suitable definition, the speed-distance relation should satisfy two general *a priori* criteria: (a) for *small* distances from the axis of rotation the particle speed should be a (nearly) linear function of the distance, as in the classical theory, and (b) for *large* distances from the axis the particle speed should approach the speed of light.

It will be shown that by a reasonable definition of uniform rotation a consistent solution can be found which satisfies these criteria and which also degenerates into the classical theory in the limit $c \to \infty$, as it must be expected to do.

2. STATEMENT OF THE PROBLEM

In order to simplify the discussion, we consider the motion as that of a system of points, or of a "fluid," in which each particle moves on a circle about the axis of rotation, the particle speed being a function only of the distance from the axis. In the observer's system of coordinates, which is supposed Euclidean, the z axis is taken along the axis of rotation. Figure 1 shows a section perpendicular to the axis of rotation, the observer's system being at rest. If Q is an arbitrary point in this plane, and $v(R)$ is the linear speed of the particles at a distance R from the

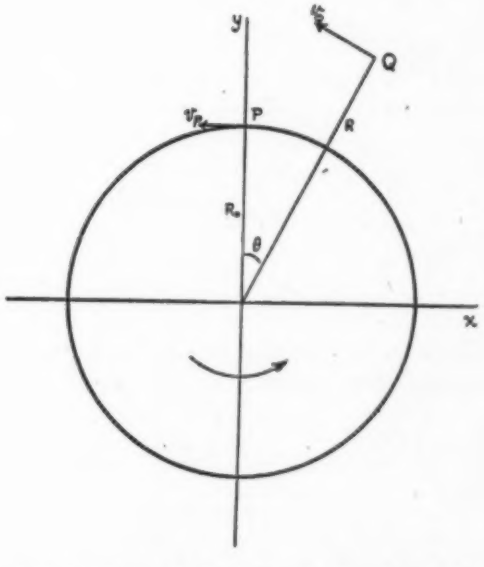

FIG. 1. Kinematical relations in the observer's coordinate system.

[2] For instance in A. Einstein and L. Infeld, *The Evolution of Physics* (Simon and Shuster, New York, 1938), p. 240.
[3] H. A. Lorentz, Nature **106**, 795 (1921).
[4] A. S. Eddington, *The Mathematical Theory of Relativity* (Cambridge University Press, Cambridge, 1924), second edition, p. 112.
[5] C. W. Berenda, Phys. Rev. **62**, 280 (1942). Further references will be found in this paper.

origin, the velocity components of Q are

$$v_x(Q) = -v(R)\cos\theta = -y\xi(R), \quad v_y(Q) = v(R)\sin\theta = x\xi(R), \tag{1}$$

with

$$\xi(R) = v(R)/R, \quad R = (x^2+y^2)^{\frac{1}{2}}.$$

Definition. *The motion of the fluid will be considered to be a uniform rotation with constant angular velocity ω_0 if the relative angular velocity of the material about any point P, as measured in a set of axes with respect to which P is momentarily at rest, has the value ω_0 independently of the choice of the point P.*

No transformations other than those of the special theory of relativity are contemplated in this definition, so that all axis systems used will be Euclidean. It is to be expected on the basis of symmetry considerations that this requirement can be satisfied by a suitable choice of the function $v(R)$, and that at each point the relative angular velocity vector will be parallel to the z axis.

3. DETERMINATION OF THE FUNCTION $v(R)$

We start by choosing a point P which, for convenience, is taken to be on the y axis at the instant considered, at a distance R_0 from the center of rotation. From Eqs. (1) the instantaneous velocity components of P, in the observer's system, are

$$v_x(P) \equiv v_0 = -R_0\xi(R_0), \quad v_y(P) = 0.$$

A set of moving axes, with origin at P and in which P is instantaneously at rest (at time $t = t' = 0$), is now introduced by the Lorentz transformation

$$x' = \frac{x - v_0 t}{(1-v_0^2/c^2)^{\frac{1}{2}}}, \quad y' = y - R_0, \quad z' = z, \quad t' = \frac{t - v_0 x/c^2}{(1-v_0^2/c^2)^{\frac{1}{2}}}, \tag{2}$$

for which the corresponding velocity transformation equations are

$$v_x' = \frac{v_x - v_0}{1 - v_x v_0/c^2}, \quad v_y' = \frac{v_y(1-v_0^2/c^2)^{\frac{1}{2}}}{1 - v_x v_0/c^2}, \quad v_z' = \frac{v_z(1-v_0^2/c^2)^{\frac{1}{2}}}{1 - v_x v_0/c^2}. \tag{3}$$

For the determination of the apparent instantaneous angular velocity of the fluid in the neighborhood of P, as measured in this rest-system of P, it is sufficient to set $t' = 0$, and to expand the relative velocity components of the points about P in power series in x' and y', retaining only linear terms. The angular velocity vector is then computed from the usual hydrokinetic formula

$$\omega' = \tfrac{1}{2}\,\mathrm{curl}'\,\mathbf{v}'. \tag{4}$$

With these conditions we find the coordinate relations

$$x = x'/(1-v_0^2/c^2)^{\frac{1}{2}}, \quad y = y' + R_0, \quad z = z'. \tag{5}$$

Making use of Eqs. (1), (3), and (5) we obtain the following expressions for the instantaneous relative velocity components of the points near P, to first-order terms,

$$v_x' = -y'\left[\frac{\xi + R\,d\xi/dR}{1-v^2/c^2}\right], \quad v_y' = x'[\xi/(1-v^2/c^2)], \quad v_z' = 0. \tag{6}$$

The bracketed expressions are to be given their values at the point P.

The only non-vanishing component of the relative angular velocity vector is now found to be

$$\omega_z' = \frac{1}{2}\left[\frac{2\xi + R\,d\xi/dR}{1-v^2/c^2}\right]. \tag{7}$$

Following our definition of rigid rotational motion, we set

$$\omega_z' \equiv \omega_0 \equiv \text{constant},$$

from which we obtain the differential equation for the speed-distance function

$$\frac{dv}{dR} + \frac{2\omega_0}{c^2}v^2 + \frac{v}{R} - 2\omega_0 = 0. \tag{8}$$

This is a special case of the general Riccati equation for which the solution is

$$v(R) = -ic\frac{J_1(i2R\omega_0/c)}{J_0(i2R\omega_0/c)}, \tag{9}$$

J_0 and J_1 being the usual Bessel functions.

4. DISCUSSION OF THE SOLUTION

The nature of this result is examined most readily by writing out the expansions for the

limiting cases of large and small distances from the axis of rotation. We find

$R\omega_0/c \ll 1$

$$v(R) = R\omega_0[1 - \tfrac{1}{2}(R\omega_0/c)^2 + \tfrac{1}{3}(R\omega_0/c)^4 \cdots], \quad (10)$$

$R\omega_0/c \gg 1$

$$v(R) = c[1 - \tfrac{1}{4}(c/R\omega_0) - \tfrac{1}{32}(c/R\omega_0)^2 \cdots]. \quad (11)$$

Equation (10) shows that, to a high degree of approximation, the velocity distribution in the neighborhood of the axis is that of the classical theory, the speed being a nearly linear function of the distance. Equation (11) shows that, if $\omega_0 \neq 0$, points at a great distance from the axis have speeds approximating that of light. Since this solution degenerates to the classical result for $c \to \infty$, it is entirely consistent with the general criteria laid down in the introductory remarks.

The apparent rate of volume dilatation at the point P is given by

$$d\Sigma'/dt' = \operatorname{div}' \mathbf{v}' = 0,$$

so that our solution is in agreement with the classical result in this test of the "rigidity" of the motion.

On the other hand, there is a divergence from the classical theory in that the tensor giving the apparent rate of the shearing motion about P does not vanish, having the non-zero component

$$\gamma_{xy}' = \tfrac{1}{2}(\partial v_x'/\partial y' + \partial v_y'/\partial x')$$
$$= (1 - v^2/c^2)^{-1} \cdot [-\omega_0(1 - v^2/c^2) + v/R].$$

In the limiting cases we find

$R\omega_0/c \ll 1$

$$\gamma_{xy}' = \omega_0 \cdot \tfrac{1}{2}(R\omega_0/c)^2[1 - \tfrac{1}{3}(R\omega_0/c)^2 \cdots],$$

$R\omega_0/c \gg 1$

$$\gamma_{xy}' = \omega_0 \cdot [1 - \tfrac{1}{2}(c/R\omega_0) \cdots].$$

Near the axis the rate of shear is a small quantity of second-order, but at large distances it approaches the limiting value ω_0. The rotation axis is unique in that it is only on it that the shearing motion vanishes.

5. CONCLUSION

In order to furnish a test of the uniqueness of the definition of uniform rotational motion, a calculation has been made in which the coordinate system used was such that in it the point P was instantaneously at the origin at rest and also without acceleration. The relativistic method of introducing accelerated Euclidean axis systems has been developed in a previous paper.[6] It was found that exactly the same results are obtained as above, so that our solution has a certain claim to uniqueness.

The question naturally occurs whether one could use a set of moving coordinates in which the point P would be *permanently* at rest. If such a set of proper coordinates could be defined in a relativistically significant manner it might be possible to define uniform rotational motion with respect to them in such a way as to satisfy the classical result that the rotation, as observed in the proper coordinate system of *any* point, would appear to be an uniform rotation about an axis through that point. No such system of coordinates is now known.

In conclusion, it is to be noted that this discussion does not anwer the problem posed in Ehrenfest's paradox, since it does not establish a correlation between the particles of the rotating medium with their positions in a non-rotating condition. In order to give an answer, and even a clear meaning, to this question, it seems essential that one give a theory of the generation of the motion from a state of rest, for it is only in this way that one can tell what has happened to any portion of the medium. However, there is no apparent reason why the result of such a theory should be unique. One might, for instance, consider the generation of the motion in a fluid under the action of elastic forces, or one could simulate it by an infinite set of charged particles moving in an electromagnetic field. So long as only the initial state of rest and the kinematics of the final state of motion are given, the correlation found between these states might well depend on the details of the process used. For this reason it is the writer's present belief that Ehrenfest's paradox, as well as the question of the type of "geometry" which is applicable to the motion, are ill-defined questions to which no definitive answers can be given without further specifications of the systems to be discussed.

[6] E. L. Hill, Phys. Rev. **67**, 358 (1945).

Space Charge in Plane Magnetron

LEIGH PAGE AND NORMAN I. ADAMS, JR.
Sloane Physics Laboratory, Yale University, New Haven, Connecticut

(Received February 18, 1946)

The space charge equation for the plane magnetron is solved; the current is obtained as a function of the magnetic field, and the effect of the magnetic field on the distribution of potential and charge is discussed.

BEFORE attempting to apply to the cylindrical magnetron the method employed by the authors to solve the space charge equation of the cylindrical diode,[1] it was felt desirable to develop the theory of the limitation of current by space charge in the plane magnetron. Although the space charge equation of the plane magnetron can be solved in closed form and is of sufficient importance to have merited attention, the authors of this paper have been unable to find its solution in the literature. Following the present paper is an investigation of the more important space charge equation of the cylindrical magnetron.

The plane magnetron consists of two infinite parallel plane electrodes a distance d apart between which is a uniform magnetic field H parallel to the electrodes. Let the ion-emitting electrode or cathode be the plane $y=0$. Then the equation of the anode is $y=d$. The Z axis will be oriented parallel to H, and saturation emission of ions from the cathode with negligible initial velocities will be assumed. Evidently the excess V of the potential of any point above that of the cathode and the volume density ρ of space charge will be functions of y only.

With Heaviside-Lorentz units, the fundamental equations involved in the theory are

$$\dot{x}^2+\dot{y}^2=-\frac{2e}{m}V(y), \tag{1}$$

$$\ddot{x}=\frac{e}{mc}\dot{y}H, \tag{2}$$

$$\frac{d^2V}{dy^2}=-\rho(y), \tag{3}$$

$$\dot{y}\rho(y)=j, \tag{4}$$

where j is the constant current density.

[1] L. Page and N. I. Adams, Jr., Phys. Rev. 68, 126 (1945).

Put $\Phi\equiv-2(e/m)V\geq 0$, $\Omega\equiv eH/mc$. Then, from (1) and (2),

$$\dot{y}^2=\Phi-\Omega^2y^2\equiv U,$$

and, after ρ is eliminated from (3) by means of (4), it is found that U satisfies the differential equation

$$\frac{d^2U}{dy^2}+2\Omega^2=\frac{2J}{U^{\frac{1}{2}}}, \tag{5}$$

where $J\equiv(e/m)j$. The boundary conditions at the cathode require that U and dU/dy vanish at $y=0$. The function U must vanish again at cut-off.

The first integral of (5) subject to these boundary conditions is

$$(dU/dy)=(8JU^{\frac{1}{2}}-4\Omega^2U)^{\frac{1}{2}}. \tag{6}$$

To get the second integral put

$$U\equiv\frac{4J^2}{\Omega^4}\sin^4\theta, \quad y\equiv\frac{J}{\Omega^3}\xi.$$

Then (6) becomes

$$d\xi=4\sin^2\theta d\theta,$$

of which the integral is

$$\xi=2\theta-\sin 2\theta, \tag{7}$$

since ξ and θ vanish together. Evidently the zeros of U corresponding to the cathode and to cut-off come at $\theta=0$ and $\theta=\pi$, respectively. At cut-off, then, $\xi=2\pi$.

From the defining equations for $\sin\theta$ and ξ it follows that

$$\frac{\Omega y}{\Phi^{\frac{1}{2}}}=1\Big/\left(1+4\frac{\sin^4\theta}{\xi^2}\right)^{\frac{1}{2}},$$

$$\frac{Jy^2}{\Phi^{\frac{1}{2}}}=1\Big/\xi\left(1+4\frac{\sin^4\theta}{\xi^2}\right)^{\frac{1}{2}}.$$

Hence, if we calculate corresponding values of θ and ξ from (7), we can plot the ratio of J to $(2/9)\Phi^{\frac{1}{2}}/y^2$ against the ratio of (eH/mc) to $\Phi^{\frac{1}{2}}/y$,

as in Fig. 1. Since the value of J in the absence of a magnetic field is $(2/9)\Phi^{\frac{3}{2}}/y^2$, the ordinate represents the ratio of the current actually existing to that which would exist for the same Φ and y if the magnetic field were not present. Furthermore, since $\Phi=\Omega^2y^2$ is the condition for cut-off, the abscissa represents the ratio of the magnetic field present to that required for cut-off, with the specified Φ and y. In Table I are listed the figures used in plotting the curve. The most interesting feature of the curve is the fact that the current decreases only slightly with increasing magnetic field until cut-off is imminent.

If Φ_D specifies the potential difference between the electrodes when the plane of cut-off $y=D$ coincides with the anode $y=d$, then $\Phi_D=\Omega^2D^2$, and the potential difference between the cathode and a parallel plane at a distance y, is given by

$$\frac{\Phi}{\Phi_D}=\frac{y^2}{D^2}\left(1+4\frac{\sin^4\theta}{\xi^2}\right).$$

Furthermore, the charge density ρ is given by

$$\frac{e}{m}\rho=\frac{\Omega^2}{2\sin^2\theta}=\frac{\Phi_D}{2D^2\sin^2\theta},$$

TABLE I. Dependence of current on magnetic field.

$\frac{eH}{mc}\Big/\frac{\Phi^{\frac{1}{2}}}{y}$	$J\Big/\frac{2}{9}\frac{\Phi^{\frac{3}{2}}}{y^2}$	$\frac{eH}{mc}\Big/\frac{\Phi^{\frac{1}{2}}}{y}$	$J\Big/\frac{2}{9}\frac{\Phi^{\frac{3}{2}}}{y^2}$
0.000	1.000	0.683	0.919
0.070	0.999	0.729	0.905
0.139	0.997	0.771	0.890
0.208	0.993	0.809	0.875
0.275	0.988	0.844	0.860
0.341	0.982	0.901	0.829
0.405	0.974	0.943	0.799
0.466	0.966	0.971	0.771
0.525	0.955	0.993	0.738
0.581	0.944	0.9996	0.720
0.634	0.932	1.0000	0.716

TABLE II. Distribution of potential and charge.

y/D	Φ/Φ_D	$(y/D)^{4/3}$	$P/(\Phi_D/D^2)$	$2/9(y/D)^{-4/3}$	$\frac{(\Phi_d/d^2)}{(\Phi_D/D^2)}$
0.00000	0.00000	0.00000	∞	∞	—
0.00645	0.00097	0.00120	5.237	62.83	23.25
0.0486	0.0145	0.0177	1.447	1.668	6.12
0.1486	0.0655	0.0787	0.764	0.792	2.96
0.3065	0.1768	0.2066	0.553	0.489	1.88
0.5000	0.3513	0.3969	0.500	0.353	1.41
0.6936	0.5639	0.6139	0.553	0.284	1.17
0.8514	0.7682	0.8069	0.764	0.247	1.06
0.9514	0.9172	0.9357	1.447	0.230	1.013
0.9936	0.9880	0.9914	5.237	0.223	1.0008
1.0000	1.0000	1.0000	∞	0.222	1.00000

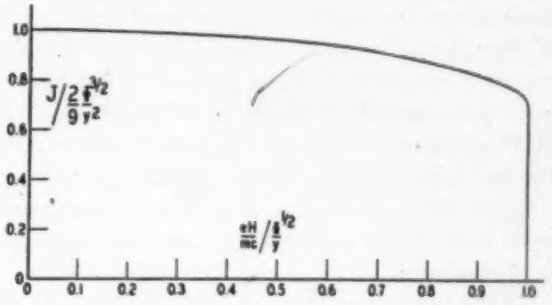

FIG. 1. Variation of relative current density with magnetic field, potential, and distance.

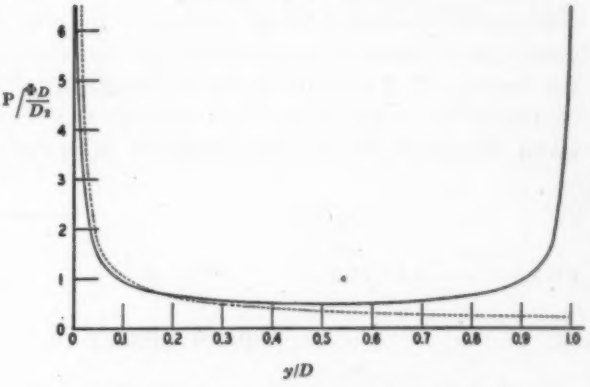

FIG. 2. Charge density with magnetic field (solid curve) and without magnetic field (broken curve) as a function of relative distance.

or, if $P\equiv(e/m)\rho$,

$$\frac{PD^2}{\Phi_D}=\frac{1}{2\sin^2\theta}.$$

In Table II are given both Φ/Φ_D and $P/(\Phi_D/D^2)$ for values of y/D ranging from 0 to 1, that is, from the surface of the cathode to the plane of cut-off. Since the first of these ratios is equal to $(y/d)^{4/3}$ when no magnetic field is present, values of $(y/D)^{4/3}$ are listed for comparison with Φ/Φ_D. The striking feature of the table is that the potential distribution is so little affected by the magnetic field. The charge density becomes infinite at the plane of cut-off as well as at the surface of the cathode, as expected. At both ends, however, nearly the entire rise takes place in a very narrow layer close to the limiting plane. As

$$\frac{Pd^2}{\Phi_d}=\frac{2}{9}\left(\frac{y}{d}\right)^{-1},$$

when no magnetic field is present, values of $(2/9)(y/D)^{-1}$ are given in the fifth column for

comparison. In addition, the ratio of P to Φ_D/D^2 is plotted against y/D in Fig. 2 for both the case where a magnetic field is present (solid curve) and the case where there is no magnetic field (broken curve). The total charge per unit area on the anode is twice that which would be present on a condenser at the same potential as compared with four-thirds as much in case the magnetic field is absent.

In the preceding discussion the plane of cut-off has been supposed to coincide with the anode. Suppose, now, that the potential or charge distribution is desired for a case where the distance d of the anode from the cathode is less than the distance D of the cut-off plane. The potential of the anode being known, Φ_d as well as d is given. Hence, in the specified magnetic field, the quantity

$$M \equiv \Phi_d/\Omega^2 d^2$$

is a *known quantity*. By use of the cut-off relation $\Phi_D = \Omega^2 D^2$,

$$M \equiv \frac{\Phi_d}{\Phi_D}\frac{D^2}{d^2}.$$

Values of this quantity are given in the last column of Table II. From the value of M can be determined the ratio d/D and hence the potential and charge distribution everywhere between the electrodes. For example, if M is found to be 2.96, then $d/D = 0.1486$ from the first column in the table, or the distance between the electrodes is only 14.86 percent of the distance from the cathode to the (virtual) plane of cut-off.

PHYSICAL REVIEW VOLUME 69, NUMBERS 9 AND 10 MAY 1 AND 15, 1946

Space Charge in Cylindrical Magnetron

LEIGH PAGE AND NORMAN I. ADAMS, JR.
Sloane Physics Laboratory, Yale University, New Haven, Connecticut
(Received February 18, 1946)

The space charge equation for the cylindrical magnetron is solved, the current is obtained as a function of the magnetic field, and the effect of the magnetic field on the distribution of potential and charge is determined.

THE object of this paper is to apply the methods employed in discussing the space charge equation of the diode[1] to the cylindrical magnetron consisting of two coaxial cylindrical electrodes of radii a and b ($a<b$) in a uniform magnetic field H parallel to their common axis. The inner electrode or cathode emits ions (electrons) with negligible initial velocities. These ions are accelerated toward the outer electrode or anode by a radial electric field because of a difference of potential between the electrodes. Saturation emission of ions from the inner electrode is assumed.

While Brillouin[2] has discussed the particular solution of the space charge equation corresponding to circular paths of the ions, very little progress seems to have been made in solving the space charge equation for the more important case of ions originating on the inner electrode.

With polar coordinates r, θ in a plane at right angles to the common axis of the electrodes, the fundamental equations required are, in Heaviside-Lorentz units,

$$\ddot{r}^2 + r^2\dot{\theta}^2 = -\frac{2e}{m}V(r), \tag{1}$$

$$\frac{d}{dt}(r^2\dot{\theta}) = -\frac{e}{mc}Hr\dot{r}, \tag{2}$$

[1] L. Page and N. I. Adams, Jr., Phys. Rev. 68, 126 (1945).
[2] L. Brillouin, Phys. Rev. 60, 385 (1941); Elec. Comm. 20, 112 (1941).

$$\frac{1}{r}\frac{d}{dr}\left(r\frac{dV}{dr}\right)=-\rho(r), \tag{3}$$

$$r\dot{r}\rho(r)=\frac{j_l}{2\pi}, \tag{4}$$

where $V(r)$ is the excess of the potential at distance r from the axis over that of the cathode, $\rho(r)$ is the space charge per unit volume, and j_l is the constant current per unit length of the electrodes.

Put $\Phi\equiv-2(e/m)V\geqslant 0$, $\Omega\equiv eH/mc$. Then, from (1) and (2),

$$\dot{r}^2=\Phi-\tfrac{1}{4}\Omega^2a^2\left(\frac{r}{a}-\frac{a}{r}\right)^2\equiv U(r), \tag{5}$$

and, when ρ is eliminated from (3) by means of (4), it is found that U must satisfy the differential equation

$$\frac{d}{dr}\left(r\frac{dU}{dr}\right)+\Omega^2a\left(\frac{r}{a}+\frac{a^3}{r^3}\right)=\frac{(e/m)(j_l/\pi)}{U^{\frac{1}{2}}} \tag{6}$$

subject to the boundary conditions that U and its derivative with respect to r vanish at the cathode $r=a$. Evidently U vanishes again at cut-off.

Next put

$$p\equiv(r/a)^{\frac{1}{2}},\quad U\equiv Kp\psi^2(p),$$

where K is a constant coefficient, getting

$$p\frac{d}{dp}\left(p\frac{d\psi^2}{dp}\right)+2p\frac{d\psi^2}{dp}+\psi^2+\frac{9}{4}\frac{\Omega^2a^2}{K}\left(p^2+\frac{1}{p^4}\right)=\frac{9}{4\pi}\frac{e}{m}\frac{j_la}{K^{\frac{1}{2}}}\frac{1}{\psi}.$$

We take $K^{\frac{1}{2}}\equiv(9/4\pi)(e/m)j_la$, so as to make the coefficient of $1/\psi$ on the right-hand side equal to unity. Then

$$\psi=\frac{1}{p^{\frac{1}{2}}}\frac{U^{\frac{1}{2}}/a}{\left(\frac{9}{4\pi}\frac{e}{m}\frac{j_l}{a^2}\right)^{\frac{1}{2}}},\quad \frac{\Omega^2a^2}{K}=\frac{\Omega^2}{\left(\frac{9}{4\pi}\frac{e}{m}\frac{j_l}{a^2}\right)^{\frac{1}{2}}}\equiv s^2, \tag{7}$$

and the equation for ψ becomes

$$\psi\left[p\frac{d}{dp}\left(p\frac{d\psi^2}{dp}\right)+2p\frac{d\psi^2}{dp}+\psi^2+\frac{9}{4}s^2\left(p^2+\frac{1}{p^4}\right)\right]=1. \tag{8}$$

If we make $s=0$ to pass to the case of the simple cylindrical diode in the absence of a magnetic field, it is easily seen that the function ψ of this paper becomes the cube root of the function g (equivalent to Langmuir's β^2) of the earlier paper.[1]

Following the method employed in that paper we shall seek a solution of (8) in the form of a "near formula" which converges rapidly in the neighborhood of $p=1$ and which satisfies the boundary conditions at the surface of the cathode. Then we shall look for a complete solution in the form of a "far formula" which converges rapidly for large values of p and the two arbitrary constants of which we can determine so as to make the two formulas fit in the region where both converge satisfactorily. Of course p is limited to values less than cut-off. We shall aim for an accuracy of one percent or better in our expansions in series.

NEAR FORMULA

To get the near formula satisfying the boundary conditions at the cathode, we change the independent variable in (8) to x, where $x^3\equiv 1-1/p$. Then x is zero at the cathode, increasing as r

increases. In the new variable the differential equation takes the form

$$\psi\left[\frac{(1-x^3)^4}{9x^6}\left\{x\frac{d}{dx}\left(x\frac{d\psi^2}{dx}\right)-3x\frac{d\psi^2}{dx}\right\}+\frac{(1-x^3)^3}{3x^3}x\frac{d\psi^2}{dx}+(1-x^3)^2\psi^2+\frac{9}{4}s^2\{(1-x^3)^6+1\}\right]=(1-x^2)^2. \quad (9)$$

The solution satisfying the boundary conditions is of the form

$$\psi=(9/4)^{\frac{1}{2}}x^2[\Phi_0-s^2x^2\Phi_1-s^4x^4\Phi_2-s^6x^6\Phi_3-\cdots],$$

where $\Phi_0, \Phi_1, \Phi_2, \Phi_3\cdots$ are series in integral powers of $z\equiv x^3$. Evidently

$$\psi^2=(9/4)^{\frac{1}{2}}x^4[\chi_0-s^2x^2\chi_1-s^4x^4\chi_2-s^6x^6\chi_3-\cdots],$$

where

$$\chi_0=\Phi_0^2, \quad \chi_1=2\Phi_0\Phi_1, \quad \chi_2=2\Phi_0\Phi_2-\Phi_1^2, \quad \chi_3=2\Phi_0\Phi_3-2\Phi_1\Phi_2, \quad \cdots.$$

Substituting in (9) we find for $\Phi_0, \Phi_1, \Phi_2, \Phi_3$,

$$\Phi_0\left[\tfrac{1}{4}(4+4z+z^2)\chi_0+\tfrac{3}{4}(1-z)(5-2z)z\frac{d\chi_0}{dz}+\frac{9}{4}(1-z)^2z\frac{d}{dz}\left(z\frac{d\chi_0}{dz}\right)\right]=1,$$

$$\Phi_1(1-z)^2+\Phi_0^2\left[(1-z)^2\left\{\tfrac{1}{4}(18-18z+9z^2)\chi_1+\tfrac{3}{4}(1-z)(9-6z)z\frac{d\chi_1}{dz}+\frac{9}{4}(1-z)^2z\frac{d}{dz}\left(z\frac{d\chi_1}{dz}\right)\right\}-\left(\frac{9}{4}\right)^{4/3}\{(1-z)^6+1\}\right]=0,$$

$$\Phi_1^2+\Phi_0\Phi_2+\Phi_0^3\left[\tfrac{1}{4}(40-56z+25z^2)\chi_2+\tfrac{3}{4}(1-z)(13-10z)z\frac{d\chi_2}{dz}+\frac{9}{4}(1-z)^2z\frac{d}{dz}\left(z\frac{d\chi_2}{dz}\right)\right]=0,$$

$$\Phi_1^3+2\Phi_0\Phi_1\Phi_2+\Phi_0^2\Phi_3+\Phi_0^4\left[\tfrac{1}{4}(70-110z+49z^2)\chi_3+\tfrac{3}{4}(1-z)(17-14z)z\frac{d\chi_3}{dz}+\frac{9}{4}(1-z)^2z\frac{d}{dz}\left(z\frac{d\chi_3}{dz}\right)\right]=0,$$

and continuing in this manner we obtain the near formula

$$\begin{aligned}\psi=1.3104x^3[&\{1-0.06667z-0.04139z^2-0.02719z^3-0.01916z^4-0.01420z^5-0.01091z^6\\&-0.00862z^7-0.00697z^8-0.00572z^9-0.00476z^{10}-0.00402z^{11}-0.00342z^{12}\cdots\}\\&-0.5897s^2x^2\{1+0.0238z+0.7452z^2+0.7781z^3+0.9224z^4+1.0675z^5+1.2136z^6+1.361z^7\\&+1.508z^8+1.656z^9+1.805z^{10}+1.955z^{11}+2.108z^{12}\cdots\}-0.1490s^4x^4\{1+0z+1.622z^2\\&+1.791z^3+2.794z^4+3.894z^5+5.272z^6\cdots\}-0.0749s^6x^6\{1-0.076z+2.528z^2+2.833z^3\cdots\}\\&-0.0472s^8x^8\{1\cdots\}-0.0334s^{10}x^{10}\{1\cdots\}-0.0263s^{12}x^{12}\{1\cdots\}-\cdots].\end{aligned} \quad (10)$$

The leading coefficients in this expression (i.e., the coefficients of s^2x^2 and its powers) check with the expression for U in the theory of the plane magnetron,[3] as should be the case, since, when $z\to 0$, the formula (10) becomes applicable to the plane magnetron. Of course, accurate computations cannot be made from (10) for the case where the magnetic field is so strong that cut-off occurs for a value of z very small compared with unity. That case, however, is provided for, to a sufficient degree of accuracy, by the theory of the plane magnetron.[3] Hence we limit the use of the near formula (10) to cases where cut-off occurs at a distance from the axis some ten or more times the radius a of the cathode.

FAR FORMULA

Now we must look for a complete solution of (8) valid for large values of p. We shall neglect the term in $1/p^4$ as compared with the term in p^2 in the coefficient of s. This introduces an error of only one-seventh of one percent even when p is as small as three. Physically this approximation amounts

[3] L. Page and N. I. Adams, Jr., Phys. Rev. 69, 492 (1946).

to neglect of the magnetic flux through a cross section of the cathode as compared with the magnetic flux through a circle of radius r.

Following the method used with the cylindrical diode[1] we find that solutions exist in power series of

$$Cp^{-1\pm i/2^{\frac{1}{2}}}=\frac{1}{p}e^{\pm i\theta}, \quad \theta\equiv\frac{1}{2^{\frac{1}{2}}}\log p+\alpha.$$

Substituting a power series in these variables in the differential equation, we obtain the solution

$$\psi=1+\frac{2c}{p}\cos\theta-\frac{2c^2}{p^2}\left\{\frac{6}{11}\cos 2\theta+\frac{2(2)^{\frac{1}{2}}}{11}\sin 2\theta\right\}+\frac{2c^3}{p^3}\left\{\frac{1}{2}\cos 3\theta+\frac{7(2)^{\frac{1}{2}}}{24}\sin 3\theta+\frac{5}{44}\cos\theta\right.$$
$$\left.+\frac{29(2)^{\frac{1}{2}}}{88}\sin\theta\right\}-\cdots-\frac{9}{76}s^2p^2\left[1-\frac{2c}{p}\left\{\frac{3}{4}\cos\theta-\frac{(2)^{\frac{1}{2}}}{8}\sin\theta\right\}\right.$$
$$\left.+\frac{2c^2}{p^2}\left\{\frac{17}{11}\cos 2\theta-\frac{17(2)^{\frac{1}{2}}}{22}\sin 2\theta-1\right\}-\cdots\right]-\frac{81}{12{,}274}s^4p^4\left[1-\frac{2c}{p}\left\{\frac{1121}{512}\cos\theta\right.\right.$$
$$\left.\left.-\frac{175(2)^{\frac{1}{2}}}{512}\sin\theta\right\}+\cdots\right]-\frac{60{,}831}{82{,}088{,}512}s^6p^6\left[1-\cdots\right]-\cdots. \quad (11)$$

This is a complete solution since it contains the two arbitrary constants c and α. The numerical coefficients were verified by substituting the solution back in the differential equation after it had been expressed in trigonometrical form.

Now when $s=0$ (i.e., no magnetic field present), ψ must reduce to the cube root of the function g calculated for the cylindrical diode in the earlier paper.[1] Let C_{10} and C_{20} be the coefficients of the pair of variables appearing in ψ in that case. If, then, C_1 and C_2 are the coefficients when $s\neq 0$, it is evident from the form of the near formula (10) that

$$C_1=C_{10}+C_{12}s^2+C_{14}s^4+\cdots, \quad C_2=C_{20}+C_{22}s^2+C_{24}s^4+\cdots.$$

Consequently the terms in (11) involving all coefficients C_{ij} other than C_{10} and C_{20} are of higher order in $1/p$ than any we have retained, and therefore will be neglected. Hence we obtain at once from the theory of the diode,[1]

$$c=-0.3260, \quad \theta=93°.288\log_{10}p+22°.83, \quad (12)$$

as the proper values of the constants required to satisfy the assumed boundary conditions at the cathode, giving for the final form of ψ,

$$\psi=1-\{0.65200\cos\theta\}\frac{1}{p}-\{0.11594\cos 2\theta+0.05466\sin 2\theta\}\frac{1}{p^2}-\{0.03465\cos 3\theta+0.02858\sin 3\theta$$
$$+0.00787\cos\theta+0.03229\sin\theta\}\frac{1}{p^3}-\cdots-0.11842s^2p^2\left[1+\{0.48900\cos\theta-0.11526\sin\theta\}\frac{1}{p}\right.$$
$$\left.+\{0.32850\cos 2\theta-0.23229\sin 2\theta-0.21256\}\frac{1}{p^2}+\cdots\right]-0.006{,}599s^4p^4\left[1+\{1.4275\cos\theta\right.$$
$$\left.-0.3152\sin\theta\}\frac{1}{p}+\cdots\right]-0.000{,}741s^6p^6\left[1+\cdots\right]-\cdots. \quad (13)$$

As a test we have calculated ψ from both the near formula (10) and the far formula (13) for $p=3$ ($z=\frac{2}{3}$, $r=5.196a$) through terms in s^4. From the first we get

$$\psi=0.9215-1.016s^2-0.34s^4-\cdots,$$

although little confidence can be placed in the coefficient of s^4 since the coefficients involved in this

term in (10) have been computed only through s^6 as against coefficients computed through s^{12} in the first two terms. On the other hand, from (13) we obtain

$$\psi = 0.9214 - 1.023s^2 - 0.49s^4 - \cdots.$$

Evidently the magnetic field must be such as to make s somewhat less than one-half in order to make the two calculations of ψ agree to within one percent. This is a rather severe test, however, particularly of the near formula, which was designed for small values of s and which we have applied to a value two-thirds of its upper limit unity.

The far formula (13) will give values of ψ accurate to better than one percent for $p \geqslant 4 (r/a \geqslant 8)$ provided only that the magnetic field is small enough so that sp is not much greater than unity. This means that the formula cannot be used close to cut-off.

CUT-OFF FORMULA

In order to apply the far formula (11) in the neighborhood of cut-off, where $\psi = 0$, we need far more of the leading terms (i.e., those in s^2p^2 and its powers) than have been computed so far. Therefore we turn back to (8) and calculate to twenty-one terms the particular solution corresponding to $c=0$ in (11). In this calculation we have included the contribution to the first four terms of the series of the previously neglected term in $1/p^4$ in (8), mainly for the purpose of showing how utterly negligible is the contribution of this term for all except the very smallest values of p. The terms in c in (11) can be added to this particular solution if needed, but they are negligible if cut-off occurs at large p.

In order to avoid many zeros between the decimal point and the first significant figure of the coefficients, it will be convenient to put

$$q \equiv \frac{9}{38} s^2 p^2 = 0.23684 s^2 p^2.$$

Then we find for the desired particular solution

$$\psi = 1 - 0.50000q\left\{1 + \frac{1}{p^6}\right\} - 0.11765q^2\left\{1 + \frac{0}{p^6} + \frac{1.030}{p^{12}}\right\} - 0.05578q^3\left\{1 - \frac{2.241}{p^6} + \frac{0.891}{p^{12}} + \frac{1.064}{p^{18}}\right\}$$
$$- 0.03324q^4 - 0.02227q^5 - 0.01602q^6 - 0.01209q^7 - 0.00944q^8 - 0.00757q^9 - 0.00620q^{10}$$
$$- 0.00516q^{11} - 0.00435q^{12} - 0.00371q^{13} - 0.00319q^{14} - 0.00277q^{15} - 0.00242q^{16}$$
$$- 0.00213q^{17} - 0.00189q^{18} - 0.00168q^{19} - 0.00150q^{20} - \cdots. \quad (14)$$

It should be noted that, although ψ is a function of the two independent parameters p and s for small or moderate p, it becomes a function of the single variable $(sp)^2$ for sufficiently large p.

From this series can be obtained the value of q at cut-off for large r/a. A few trials show that ψ vanishes for a value of q a little greater than unity. In order to secure greater accuracy, a correction is made to the computed value of $\psi(q)$ for values of q in this neighborhood by adding to (14) a geometrical series with ratio equal to that of the last few terms. The justification for this procedure lies in the fact that the last few terms in (14) in such cases have a nearly constant ratio, and, furthermore, the correction is small. The results are given in Table I.

TABLE I. Values of $\psi(q)$ near cut-off for large p.

q	$1-\psi(q)$ (uncorrected)	$1-\psi(q)$ (corrected)
1.03	0.872	0.907
1.05	0.921	0.988
1.06	0.948	1.047
1.08	1.007	1.257

The uncorrected values of $\psi(q)$ obtained from the twenty-one terms of (14) show that q is certainly less than 1.08 at cut-off, and the corrected values indicate that its value lies between 1.05 and 1.06, and closer to the first than the second. Therefore we infer that, for large p, cut-off occurs at $q=1.05$ with an error not greater than one percent.

CALCULATIONS AND GRAPHS

We are now in a position to plot curves from the formulas derived. We can cover all cases except that in which cut-off occurs close to the cathode. First we calculate ψ as a function of s for various values of p, although, in order to avoid large numbers of zeros after the decimal point, we shall use $q \equiv (9/38)s^2p^2$ as variable instead of s itself. In Table II are listed formulas for ψ for values of p covering the entire range from 1 up. To and including $p=2$ the near formula (10) is used, for $p=3$ and greater ψ is calculated from the far formula (13). In the region $2 \leqslant p \leqslant 4$ the accuracy is least, as neither formula converges very well in this range. This is indicated in the table by giving fewer terms in the expressions for ψ in this region. For $p \geqslant 9$ terms from (14) may be added as cut-off is approached, the accuracy becoming greater the larger p. From the last series we have already found that cut-off comes at $q=1.05$ for very large p. By the same method we find that cut-off comes at $q=1.06$ for $p=25$.

The most important family of curves is that giving the current plotted against the magnetic field for a given Φ and p. From Eq. (7) defining s we have

$$q=\frac{9}{38}p^2\frac{\Omega^2}{\left(\frac{9}{4\pi}\frac{e}{m}\frac{j_l}{a^2}\right)^{\frac{1}{2}}},$$

and the square of Eq. (7) defining ψ, if we eliminate U by means of (5), becomes

$$\psi^2=\frac{\Phi-\frac{1}{4}\Omega^2a^2(r/a-a/r)^2}{a^2p\left(\frac{9}{4\pi}\frac{e}{m}\frac{j_l}{a^2}\right)^{\frac{1}{2}}}.$$

Eliminating j_l from these equations we find

$$\frac{\Omega r}{\Phi^{\frac{1}{2}}}=\frac{2.05480(q)^{\frac{1}{2}}}{[\psi^2+1.05556q(1-a^2/r^2)^2]^{\frac{1}{2}}}, \qquad (15)$$

TABLE II. Formulas for ψ for various values of $p=(r/a)^{\frac{1}{2}}$.

p	r/a	$\psi(q)$ where $q=(9/38)s^2p^2$
1.000	1.000	0
1.250	1.398	$0.4413-0.2547q-0.062q^2-0.029q^3-0.015q^4-\cdots$
1.333	1.540	$0.5098-0.3092q-0.079q^2-0.038q^3-0.02q^4-\cdots$
1.500	1.837	$0.6122-0.3814q-0.100q^2-0.05q^3-\cdots$
2.000	2.828	$0.7851-0.463q-0.11q^2-\cdots$
3.000	5.196	$0.9214-0.480q-0.11q^2-\cdots$
4.000	8.000	$0.9745-0.479q-0.12q^2-\cdots$
9.000	27.000	$1.0284-0.4822q-0.107q^2-0.056q^3-\cdots$
16.000	64.000	$1.0291-0.4867q-0.109q^2-0.056q^3-\cdots$
20.000	89.443	$1.0265-0.4885q-0.1098q^2-0.0558q^3-\cdots$
25.000	125.000	$1.0232-0.4904q-0.1110q^2-0.0558q^3-\cdots$
Very large	Very large	$1.0000-0.5000q-0.1177q^2-0.0558q^3-\cdots$

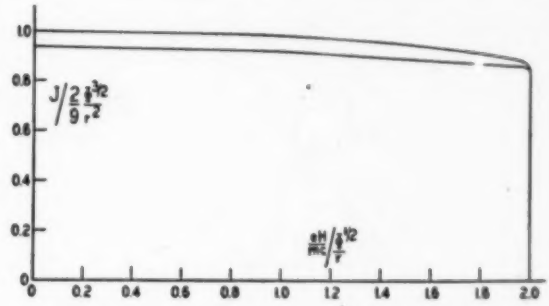

FIG. 1. Variation of relative current density with magnetic field, potential and distance. Upper curve r/a very large, lower curve $r/a=125$.

and eliminating Ω

$$\frac{J}{\frac{2}{9}\frac{\Phi^{\frac{1}{2}}}{r^2}}=\frac{1}{\left[\psi^2+1.05556q\left(1-\frac{a^2}{r^2}\right)^2\right]^{\frac{1}{2}}}, \qquad (16)$$

where we have put $j_l \equiv 2\pi r j$ and then substituted J for $(e/m)j$. Evidently j is the current density at distance r from the axis.

TABLE III. Current as function of magnetic field for r/a very large.

q	ψ	$\frac{eH}{mc}\Big/\frac{\Phi^{\frac{1}{2}}}{r}$	$J\Big/\frac{2}{9}\frac{\Phi^{\frac{1}{2}}}{r^2}$
0.00	1.000	0.000	1.000
0.10	0.949	0.648	0.992
0.20	0.895	0.914	0.983
0.30	0.838	1.115	0.973
0.40	0.776	1.284	0.964
0.50	0.710	1.430	0.953
0.60	0.638	1.560	0.942
0.70	0.557	1.678	0.930
0.80	0.464	1.785	0.917
0.90	0.349	1.883	0.901
1.00	0.177	1.971	0.883
1.05	0.000	2.000	0.857

TABLE IV. Current as function of magnetic field for $r/a=125$.

q	ψ	$\frac{eH}{mc}\Big/\frac{\Phi^{\frac{1}{2}}}{r}$	$J\Big/\frac{2}{9}\frac{\Phi^{\frac{1}{2}}}{r^2}$
0.00	1.023	0.000	0.934
0.10	0.973	0.633	0.926
0.20	0.920	0.893	0.919
0.30	0.864	1.091	0.912
0.40	0.804	1.257	0.904
0.50	0.740	1.401	0.897
0.60	0.670	1.530	0.889
0.70	0.591	1.649	0.882
0.80	0.499	1.758	0.875
0.90	0.386	1.860	0.868
1.00	0.217	1.957	0.864
1.06	0.000	2.000	0.845

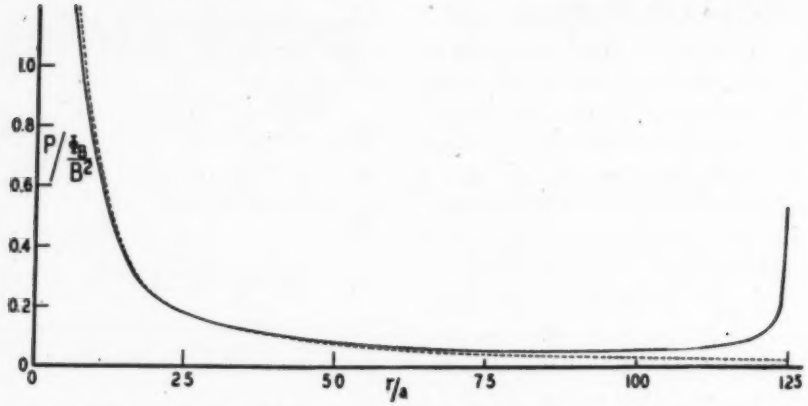

FIG. 2. Charge density with magnetic field (solid curve) and without magnetic field (broken curve) as a function of r/a.

We have plotted two curves of the family under consideration in Fig. 1. The upper one is for p very large, and the lower one for $p=25$ $(r/a=125)$. In both cases we have neglected $(a/r)^2$ as compared with unity in (15) and (16). The calculated values for the two curves are given in Tables III and IV. Only for $q \gtrsim 1$ has it been necessary to add a small correction to (14) to account for the effect of additional terms beyond the one in q^{20}. It will be noted that both curves are very nearly horizontal, the second even more so than the first. This is quite in accord with the experimental measurements of Hull,[4] who used a ratio of anode to cathode radius not very different from 125.

Next we consider the distribution of potential and of space charge for the case where the anode $r=b$ coincides with the surface $r=B$ of cut-off, limiting ourselves to the case where $a/b \ll 1$. Then (5) gives $\Phi_B=\frac{1}{4}\Omega^2B^2$ at cut-off. Since, in general,

$$\Phi=\tfrac{1}{4}\Omega^2r^2\left[\left(1-\frac{a^2}{r^2}\right)^2+\frac{18}{19}\frac{\psi^2}{q}\right],$$

it follows that the distribution of potential is given by

$$\frac{\Phi}{\Phi_B}=\left(\frac{r}{a}\right)^2\left(\frac{a}{B}\right)^2\left[\left(1-\frac{a^2}{r^2}\right)^2+0.94737\frac{\psi^2}{q}\right]. \quad (17)$$

Furthermore, if we put $P\equiv(e/m)\rho$, it follows that $P=J/U^{\frac{1}{2}}$, and the distribution of space charge is given by

$$\frac{P}{\Phi_B/B^2}=\frac{4}{19q\psi}=\frac{0.21053}{q\psi}. \quad (18)$$

In Table V are given, in the third and fourth columns, respectively, the values of Φ/Φ_B and $P/(\Phi_B/B^2)$ corresponding to the values of p as given in the first column or of r/a as given in the second, for $b/a=125$. The values these two quantities would assume if no magnetic field were present, are given in the fifth and sixth columns. It is to be noted that the potential distribution is not greatly affected by the magnetic field. The charge density, on the other hand, rises very abruptly in the immediate vicinity of cut-off when a magnetic field is present, becoming infinite at the surface of cut-off. In Fig. 2 the graph of $P/(\Phi_B/B^2)$ plotted against r/a is shown by the solid curve. The broken curve represents the same quantity when no magnetic field is present.

TABLE V. Distribution of potential and of space charge when anode coincides with cut-off surface.

p	r/a	$[\Phi/\Phi_B]_H$	$[P/(\Phi_B/B^2)]_H$	$[\Phi/\Phi_B]_0$	$[P/(\Phi_B/B^2)]_0$
1.000	1.000	0.000	∞	0.000	∞
1.250	1.398	0.009	180.3	0.009	192.3
1.333	1.540	0.012	137.2	0.013	146.3
1.500	1.837	0.020	90.4	0.022	96.4
2.000	2.828	0.044	39.7	0.047	42.3
3.000	5.196	0.091	15.09	0.097	16.00
4.000	8.000	0.136	8.07	0.145	8.51
9.000	27.000	0.343	1.596	0.364	1.592
16.000	64.000	0.620	0.613	0.647	0.504
20.000	89.443	0.781	0.505	0.805	0.323
22.000	103.189	0.863	0.533	0.883	0.267
24.000	117.576	0.946	0.804	0.961	0.225
25.000	125.000	1.000	∞	1.000	0.207

[4] A. W. Hull, Phys. Rev. **18**, 31 (1921).

Impedance Representation of Tangential Boundary Conditions[1]

GLEN D. CAMP
University of California, Division of War Research, San Diego, California
(Received February 18, 1946)

The importance of tangential boundary surface forces in some systems is noted. The tensor formulation of a generalized impedance boundary condition, involving a tangential as well as a normal impedance, is given. The tangential impedance, seen by a plane working into a viscous fluid, is calculated.

INTRODUCTION

IN the study of the steady-state motion of continuous elastic systems, a well-known and valuable theoretical procedure consists in replacing the inert parts of a system, outside a conveniently chosen bounding surface, by an impedance boundary condition. A suitable approximation to the solution of the resultant impedance-terminated boundary value problem, with the specific impedances appearing as parameters, then frequently yields a satisfactory understanding of the system even with very rough values of the impedances. Furthermore, one may then separately attack the problem of experimentally or theoretically determining the impedances, often in a simpler system.

Tangential boundary surface forces appear to be very important in certain systems and the impedance representation of these forces therefore becomes attractive. The purpose of this paper is to formulate the boundary conditions corresponding to a tangential, as well as normal, impedance. The solution of boundary value problems involving this generalized impedance boundary condition, by a direct variational method, is discussed elsewhere.[2]

GENERALIZED IMPEDANCE BOUNDARY CONDITION

Let the displacement of an elastic system have components[3] u_p $(p=1, 2, 3)$. The normal and tangential components of the displacement at any point on the boundary surface are

$$u_{np}=n_pn_qu_q, \tag{1}$$

$$u_{tp}=u_p-u_{np}=(\delta_{pq}-n_pn_q)u_q, \tag{2}$$

in which $\mathbf{n}$ is the unit normal to the surface.[4]

The force acting on an element of boundary surface dS is

$$-(Z_n\dot{u}_{np}+Z_t\dot{u}_{tp})dS=-Z_{pq}\dot{u}_qdS, \tag{3}$$

$$Z_{pq}=Z_nn_pn_q+Z_t(\delta_{pq}-n_pn_q). \tag{4}$$

Thus the boundary surface forces are generated by a second rank, symmetric, complex tensor Z_{pq}, having only two distinct[5] characteristic values, namely Z_n and Z_t.

It is frequently convenient to use boundary quantities which act on the displacement rather than the velocity. One may define the quantities S_{pq}, S_n, and S_t by the relations

$$Z_{pq}\dot{u}_q=S_{pq}u_q, \tag{5}$$

$$S_{pq}=i\omega Z_{pq}=S_nn_pn_q+S_t(\delta_{pq}-n_pn_q). \tag{6}$$

These new quantities will be called *stiffances*, S_{pq} being the stiffance tensor with characteristic values S_n and S_t.

In terms of the stiffance tensor, the generalized impedance boundary condition becomes

$$-T_{pq}n_q-S_{pq}u_q+F_p=0, \tag{7}$$

in which T_{pq} is the stress tensor at surface points, F_p is the surface force, per unit area, arising from active external agencies, and $\mathbf{n}$ points outward for the convention which makes a tension positive.

[1] This work represents one of the results of research carried out by the University of California, Division of War Research, under contracts with the Office of Scientific Research and Development, Section 6.1, National Defense Research Committee, and with the Bureau of Ships, Navy Department.

[2] Glen D. Camp, Phys. Rev. 69, 516 (1946).

[3] Cartesian coordinates (x_1, x_2, x_3) are used throughout; however, all results are expressed in tensor form and hence the generalization to any coordinate frame is straightforward.

[4] The Einstein summation convention, according to which the sum over all repeated indices is understood without writing a sum sign, is used throughout.

[5] If the environment is tangentially anisotropic, the tangential degeneracy is removed, and Z_{pq} then has three distinct characteristic values.

TANGENTIAL STIFFANCE FOR A PLANE VISCOUS SHEAR WAVE

As a simple example, one may express the well-known tangential force, corresponding to a plane shear wave in a viscous fluid, in terms of a tangential stiffance. Let the $+z$ half of space be filled with a viscous fluid driven in the x direction with amplitude $u(0)$ by a uniform tangential motion of the $z=0$ plane. The Stokes-Navier equation for this case is

$$(\rho\omega^2+i\omega\mu d^2/dz^2)u(z)=0, \tag{8}$$

in which μ is the viscosity of the fluid.

The solution of this equation, and the tangential stiffance, are

$$u(z)=u(0)\exp(-ikz), \tag{9}$$

$$k=(\rho\omega/i\mu)^{\frac{1}{2}}, \tag{10}$$

$$S_t=-T_{zz}/u=-(\mu(du/dz)/u)_{z=0}=(i\mu\rho\omega)^{\frac{1}{2}}. \tag{11}$$

If the smallest dimension of a flat surface is several shear wave-lengths, a common case, the plane-wave stiffance is a good approximation.

The writer desires to express his appreciation to the administration of the University of California, Division of War Research, and particularly to Dr. G. P. Harnwell, Director, and Dr. F. N. D. Kurie, Associate Director, for making this and other work possible and for constant encouragement in its execution; and to the Bureau of Ships, United States Navy, for its enlightened policies toward research, and for permission to publish.

PHYSICAL REVIEW VOLUME 69, NUMBERS 9 AND 10 MAY 1 AND 15, 1946

A Variational Method for Linear Dissipative Anisotropic Elastic Systems[1]

GLEN D. CAMP
University of California, Division of War Research, San Diego, California

(Received February 18, 1946)

A boundary value problem, governing a quite general elastic system, is defined. Although limited to steady-state drive (or free vibrations), it is applicable to transient drives by the usual method of Fourier superposition. A variational principle, rigorously equivalent to this boundary value problem, is given. It is amenable to the *direct* or *semi-direct* method, and thus takes advantage, in the choice of trial functions, of any qualitative or semi-quantitative knowledge of the system. It furnishes practically useful approximations, with reasonable labor, to the solution of problems which have not been treated successfully by other methods. An example is worked out in detail and the solution is interpreted physically.

INTRODUCTION

DISSIPATION plays an essential role in many elastic systems, either as true losses within a system, or as energy flow into a bounding system regarded for convenience as external.

The formulation of the boundary value problems governing linear dissipative elastic systems is straightforward, but it is well known that satisfactory approximations to the solutions of these problems have been found in only the simplest cases. This circumstance makes a direct variational approach very attractive, since this method takes advantage, in the choice of trial functions, of any qualitative or semi-quantitative understanding of the system.

The first steps toward developing a variational method for dissipative systems were taken by Bateman, who succeeded in deriving field equations, generated by non-self-adjoint operators, from a variational principle.[2] However, this development is not yet complete because it is not clear how to take account of the all-important boundary conditions. In the meantime, it is the

[1] This work represents one of the results of research carried out by the University of California, Division of War Research, under contracts with the Office of Scientific Research and Development, Section 6.1, National Defense Research Committee, and with the Bureau of Ships, Navy Department.

[2] H. Bateman, Phys. Rev. **38**, 815 (1931); Nature **131**, 472 (1933).

purpose of this paper to present a variational method which is restricted to free vibrations or steady-state drive. These cases have great importance for themselves and can also be used to solve transient problems by Fourier integral superposition, if the spectral breadth of the driving forces is not too great.

Subject to the above limitations on time dependence, this variational principle is equivalent to the *complete* boundary value problem (boundary conditions, as well as propagation equations) governing a quite general type of linear dissipative elastic system, to be described below.

BOUNDARY VALUE PROBLEM

System

The system considered here is contained within a finite region R bounded by a surface S. According to the method of terminating a radiative system so widely used in acoustics, all interactions of the system with the medium outside R are assumed to occur across the surface S and to be representable by a specific impedance, which may be any reasonable function of position on S, and of frequency. In acoustics, it has been customary to use only a normal specific acoustic impedance but here the possibility of a tangential[3] impedance is included since this makes it possible to take some account of systems in which shear waves may be important, e.g., the reflection-conversion of longitudinal to shear waves at the boundary between a solid and a viscous liquid, cemented joints, etc., and does not appreciably complicate the boundary value problem or the equivalent variational principle. While in many cases it may be difficult or impossible to calculate or measure these impedances with much precision, their use is nevertheless often very valuable because they enable the general character of a system to be determined theoretically and thus suggest significant experiments and provide a framework for interpreting experimental results which might otherwise be completely unintelligible.

Within R there may be regions R_1', R_2',—excluded from R, each bounded by an impedance surface similar to S; these might represent pieces of rubber, etc., used as dampers or for other purposes in a vibrating system. Also, the included part of R need not necessarily be a homogeneous medium, but may be broken into sub-regions R_1'', R_2''—each occupied by a linear, homogeneous (but not necessarily isotropic) dissipative medium. The bounding surface of any one of these sub-regions R'' may consist partly of the impedance surfaces bounding regions of type R' and partly of the bounding surfaces of other R'' regions. Thus the elastic system consists of the region R–R' bounded externally by S and perhaps internally be impedance surfaces and perhaps containing certain surfaces of discontinuity separating different elastic media.

Stress and Propagation Equations

The displacement is a vector $u_p(x_1, x_2, x_3, t)$,[4] $p=1, 2, 3$, and the strain is the second-rank symmetric tensor

$$s_{pq}=(u_{p,q}+u_{q,p})/2.^{5} \tag{1}$$

The stress is assumed to have the form[6]

$$T_{pq}=c_{pqrs}s_{rs}+\mu_{pqrs}\dot{s}_{rs}, \tag{2}$$

$$c_{pqrs}=c_{qprs}=c_{rspq}, \tag{3}$$

$$\mu_{pqrs}=\mu_{qprs}=\mu_{rspq}. \tag{4}$$

The coefficients form fourth-rank tensors because of the tensor character of all other quantities. Aside from the general symmetry conditions satisfied by both, to be discussed below, and a condition of positive-definiteness, they are arbitrary phenomenological constants.

The first term is the well-known form for a conservative anisotropic elastic system, in tensor notation. Only the general symmetry conditions[7] are assumed for the c-tensor, and hence there may be as many as 21 distinct elastic moduli. This generality in no way complicates the present discussion, and makes it possible to treat anisotropic materials.

---

[3] Glen D. Camp, Phys. Rev. **69**, 515 (1946). The formulation of boundary conditions involving tangential impedances is given.

[4] Cartesian coordinates are used throughout; all results are given in tensor form, so that the generalization to any coordinate system is straightforward.

[5] The notation $u_{p,q}$ is an abbreviation for du_p/dx_q.

[6] For convenience, the Einstein summation convention is used throughout, i.e., all summation signs are deleted and summation is to be carried out over all *repeated* indices, such as r and s in Eq. (2).

[7] W. Voigt, *Lehrbach der Kristallphysik* (B. G. Teubner, Leipzig), 1928, p. 793.

The second term is the obvious tensor generalization of the Stokes-Navier terms for a viscous fluid. The symmetry conditions assumed to be satisfied by the μ-tensor, Eq. (4), have interesting physical interpretations. The symmetry under exchange of the first and second indices follows from the well-known requirement that the stress be symmetric; that for exchange of the third and fourth indices from the symmetry of the strain-velocity tensor.

The symmetry under exchange of the pairs of indices is quite another matter, and systems in which this is not the case are conceivable; however, such systems would not satisfy the reciprocity principle. It is readily shown that Eq. (2) leads to a dissipation of energy within the medium, per unit of time and volume, of amount

$$D=\dot{\delta}_{pq}\mu_{pqrs}\dot{\delta}_{rs}. \tag{5}$$

This quadratic form in the strain-velocity rejects any part of μ which is not symmetric under exchange of the pairs of indices and hence any such part, like the magnetic deflection of a charge, dissipates no energy and therefore corresponds to a *conservative velocity-dependent* stress. Such stresses are excluded from the present discussion.

Since the time variation of all quantities is restricted to $\exp(i\omega t)$, with ω real for a steady-state drive and complex for free vibrations, the stress equation takes the form

$$T_{pq}=\mathfrak{c}_{pqrs}S_{rs}, \tag{6}$$

$$\mathfrak{c}=c+i\omega\mu. \tag{7}$$

The propagation equation, which expresses Newton's second law applied to an arbitrary element of volume, is

$$\rho\ddot{u}_p=-\rho\omega^2u_p=T_{pq,q}+B_p, \tag{8}$$

in which B_p is any body force density arising from external sources.

The external body force is usually zero but it is convenient to retain it as a means of estimating the error in an approximate solution, since it gives the fictitious body force required to maintain any assumed displacement. If this fictitious force is small compared to the kinetic reaction, $\rho\omega^2u_p$, one has a good approximation.

Boundary Conditions

Across the interface between two elastic media, the surface force must be continuous (Newton's third law),

$$(T_{pq}^{(2)}-T_{pq}^{(1)})n_q=0, \tag{9}$$

in which $\mathbf{n}$ is the unit vector normal to the interface.

At an impedance surface, the boundary condition is

$$-T_{pq}n_q-S_{pq}u_q+F_p=0, \tag{10}$$

in which $\mathbf{n}$ points outward for the convention which makes a tension positive and S_{pq} is the stiffance[3] tensor. In the general theory, no assumption need be made concerning the dependence of this tensor upon position or frequency.

Boundary Value Problem

Collecting Eqs. (8)–(10), we find the boundary value problem under consideration is

$$\rho\omega^2u_p+T_{pq,q}+B_p=0 \quad \text{in } R-R', \tag{8}$$

$$(T_{pq}^{(2)}-T_{pq}^{(1)})n_q=0 \quad \text{on interfaces,} \tag{9}$$

$$-T_{pq}n_q-S_{pq}u_q+F_p=0$$

$$\text{on impedance surfaces,} \tag{10}$$

$$u_p \text{ continuous throughout } R-R' \tag{11}$$

in which Eq. (11) means that the system does not rupture at any point.

EQUIVALENT VARIATIONAL PRINCIPLE

The above boundary value problem, complete except of course for Eq. (11) which must be appended, is rigorously and reciprocally equivalent to the variational principle

$$\delta I=0, \tag{12}$$

$$I=\int dV(u_p\rho\omega^2u_p/2-u_{p,q}\mathfrak{c}_{pqrs}u_{r,s}/2+B_pu_p)$$

$$+\int dS(-u_pz_{pq}u_q/2+F_pu_p) \tag{13}$$

for arbitrary variations of the displacement. The integration is over the region R–R' and all external and internal bounding surfaces. In the "potential energy" term in the volume integral, the change from the strain to the (unsymmetrical) derivative of the displacement is permissible because of the symmetry of the tensor $\mathfrak{c}$, Eqs. (3), (4), and (7).

To verify this equivalence, we need only take the first variation and do one partial integration on the variation of the "potential energy." The

resultant volume integral, exclusive of the exact divergence, then gives Eq. (8). The exact divergence, with the aid of the Gauss flux-divergence theorem, then gives contributions at all interfaces and impedance surfaces. At the interfaces, the integrand of the surface integral is the dot product of the variation of the displacement by the discontinuity in the flux of T_{pq}, and this discontinuity must therefore be zero, yielding Eq. (9). Finally the integral over the impedance surfaces yields Eq. (10).

The vanishing of δI does not yield an extreme value of I, since the latter is a complex number, but only a stationary value. A helpful geometric interpretation is obtained by imagining a one-(complex) parameter family of displacements $u_p(x_1, x_2, x_3; \alpha)$ which includes the solution for the value α_0 of the parameter. Then I becomes a function of α and the solution corresponds to a saddle point at α_0; in this case, therefore, the real and imaginary parts of I are extrema, one a maximum and the other a minimum.

To illustrate one way of using this variational principle, an example is worked out in the next section by what may be called the semi-direct method. This example, a rod of finite lateral dimensions with impedance loads on the lateral and end faces, is chosen because the 0th approximation is well known and because the corrections deduced are readily interpreted physically.

EXAMPLE

Let us consider a system which is a component of many vibrating systems and which, although admitting a simple qualitative description, is sufficiently involved to give some indication of the practical value of the method. A homogeneous isotropic rod of uniform rectangular[8] cross section, several times longer than its larger lateral dimension, is driven by uniform forces at its two ends where it also sees given normal stiffances S_1 and S_2. It is imbedded in a medium which presents to its lateral faces uniform normal and tangential stiffances S_n and S_t.

It will be shown that the present treatment yields a fair approximation even up to the frequency at which the larger lateral dimension becomes of the same order of magnitude as the longitudual wave-length, and that this approximation is better the smaller the Poisson ratio, as would be expected. Depending upon the shape ratios and Poisson ratio, the approximation obtained may be valid through several resonances.

Taking the $z(=x_3)$-axis along the axis of the rod, one may expand the displacement in any plane normal to this axis in powers of x and y ($=x_1$ and x_2), the coefficients being functions of z. All x and y integrations may then be done explicitly and we have thus replaced a variational principle involving the three field quantities u_p, which are functions of three independent variables, by one involving infinitely many field quantities which are, however, functions of z only. The integral I then becomes an expansion in the moments of all orders of the cross section of the rod; in the present example, however, all odd-order moments drop out because of the symmetry of the section.

Thus, if we apply the semi-direct method in any physically reasonable case, the variational principle automatically weights the successive terms in I and this weighting furnishes a simple basis for making a consistent approximation.

In the present case, all intrinsic terms up to second-order moments will be retained, while impedance terms will be retained only to the lowest order in which each occurs.

Rather than a power series, it is more convenient to use functions, the first three of which are simply related to the Legendre polynomials, satisfying

$$X_\alpha = 1,\ x,\ \tfrac{1}{2}(x^2-\langle x^2\rangle_M),\ \tfrac{1}{6}(x^3-3x\langle x^2\rangle_M);\quad \alpha=0 \text{ to } 3 \qquad (14)$$

$$dX_\alpha/dx = X_{\alpha-1} \quad \text{with} \quad X_{-1}=0 \qquad (15)$$

in which $\langle x^2\rangle_M$ is the average of x^2 over the section. A similar set of functions of y are used.

The displacements in the present problem satisfy the following symmetry conditions: u is odd in x, even in y; v is odd in y, even in x; and w is even in x and y. We therefore have

$$u = u_{10}X_1 + u_{30}X_3 + u_{12}X_1Y_2 + \cdots, \qquad (16)$$

$$v = v_{01}Y_1 + v_{21}X_2Y_1 + v_{03}Y_3 + \cdots, \qquad (17)$$

$$w = W + w_{20}X_2 + w_{02}Y_2 + \cdots. \qquad (18)$$

[8] A circular cross section could be readily treated by going over to cylindrical coordinates, but this would introduce irrelevant discussions of the transformation of the various tensors.

All terms up to third order in the lateral dimensions have been saved so that, upon differentiating to get the strains, and calculating I, the latter will be correct to second-order moments. However, we now see that the third-order terms in Eqs. (16), (17) can be dropped because, after differentiating, the resultant second-order terms have zero average values. Thus only the first terms of Eqs. (16), (17) need be saved.

The "potential energy" density in the volume integral of I, for the present isotropic system, is

$$\lambda s_{pp}s_{qq}/2+\mu s_{pq}s_{pq}, \tag{19}$$

in which λ and μ are complex if there is internal dissipation. The volume integral in I therefore becomes

$$\tfrac{1}{2}A\int dz\{\rho\omega^2(\langle x^2\rangle_{Av}u_{10}^2+\langle y^2\rangle_{Av}v_{10}^2+W^2)$$
$$-\lambda(u_{10}+v_{01}+W')^2-2\mu(u_{10}^2+v_{01}^2+W'^2)$$
$$-\mu[(u_{10}'+w_{20})^2\langle x^2\rangle_{Av}+(v_{01}'+w_{02})^2\langle y^2\rangle_{Av}]\}. \tag{20}$$

The lateral stiffance integral is

$$-\tfrac{1}{2}A\int dz\{S_n(au_{10}^2+bv_{01}^2)$$
$$+S_t(a^{-1}+b^{-1})W^2\}, \tag{21}$$

in which a and b are the half-dimensions in the x and y directions, respectively.

Finally, the integration over the ends yields the boundary terms

$$A(-S_1W_1^2/2-S_2W_2^2/2+F_1W_1+F_2W_2). \tag{22}$$

Adding Eqs. (20)–(22) and setting the first variation to zero, we obtain the following results after doing a partial integration on the term in $\delta W'$:

$$u_{10}'+w_{20}=0, \tag{23}$$
$$v_{01}'+w_{02}=0. \tag{24}$$
$$(\lambda+2\mu)u_{10}+\lambda v_{01}$$
$$=-\lambda W'+(\rho\omega^2\langle x^2\rangle_{Av}-S_na)u_{10}, \tag{25}$$
$$\lambda\mu_{10}+(\lambda+2\mu)v_{01}$$
$$=-\lambda W'+(\rho\omega^2\langle y^2\rangle_{Av}-S_nb)v_{01}, \tag{26}$$

together with a propagation equation for W and two boundary conditions, to be given below.

The shear component s_{12} vanishes identically after we drop the third-order terms in Eqs. (16), (17), and Eqs. (23), (24) assert that the other two shears vanish. Thus there are no shear strains in the present order.

Equations (25) and (26) are the Poisson contraction equations, with corrections for the kinetic reaction associated with the lateral motion and for the normal stiffance on the lateral faces. Neglecting these corrections, their zero-order solution is

$$u_{10}=v_{01}=-\sigma W', \tag{27}$$
$$\sigma=\lambda/2(\lambda+\mu). \tag{28}$$

It should be noted that, if there is internal dissipation, the Poisson ratio σ is complex. Putting these 0th-order solutions into the correction terms, one can express u_{10} and v_{01} as slightly different multiples of W'.

Only one combination of u_{10}, v_{01}, and W' appears in the propagation equation for W and the boundary conditions, and these equations therefore become

$$[\rho\omega^2-S_t(a^{-1}+b^{-1})]W+YW''=0, \tag{29}$$
$$-YW_1'+S_1W_1-F_1=0, \tag{30}$$
$$YW_2'+S_2W_2-F_2=0, \tag{31}$$
$$Y=Y_0-\sigma^2\rho\omega^2R^2-S_n(a+b), \tag{32}$$
$$Y_0=\mu(2\mu+3\lambda)/(\lambda+\mu), \tag{33}$$

in which R is the radius of gyration of the cross section.

The boundary value problem, Eqs. (29)–(31), is formally identical with that governing an infinitely thin conservative rod, the difference lying entirely in the altered value of the constants. We may therefore take over intact the well-known and valuable electric circuit analogy whereby this system is equivalent to a four-terminal network driven by F_1 and F_2 at each pair of terminals.[9]

The physical interpretation of the correction terms in Eq. (29) is interesting. This equation may be put into the form

$$\rho\omega^2(1+\sigma^2k^2R^2)W+[Y_0+\sigma^2S_n(a+b)]W''$$
$$=S_t(a^{-1}+b^{-1})W, \tag{29'}$$

in which k is the propagation number for longi-

[9] See, for example, W. P. Mason, *Electromechanical Transducers and Wave Filters*, D. Van Nostrand Company, Inc., New York, 1942. The circuit shown in Fig. 6.7, p. 205, is applicable if the piezoelectric drive is shorted out.

tudinal waves. Ignoring the imaginary parts of k, Y_0, σ, and S_n, a rod of finite lateral dimensions with normal and tangential impedance loads on its lateral faces therefore transmits longitudinal waves, in the present approximation, like an infinitely thin rod with a density larger by the frequency dependent parathesis in the first term, a Young's modulus increased by a uniform distribution of springs on its lateral faces, and with a body force density proportional to the tangential stiffance.

Various aspects of the lateral inertia correction have been studied by Pockhammer, Chree, and Rayleigh.[10] The body force proportional to S_t is readily deduced by considering the motion of a slab normal to the longitudinal axis as if it were rigid. And the correction to the Young's modulus can be deduced by regarding the Poisson motion as rigidly coupled to the longitudinal, like a pantograph. However, one must be extremely cautious in these deductions to avoid saving terms of a given order while neglecting others of the same order. Furthermore, the deduction of the boundary conditions is extremely involved. While one will prefer to deduce a result from direct mechanistic arguments wherever possible, this type of argument becomes hopelessly obscure if one needs higher order terms and a formal method, with *a posteriori* physical interpretation, becomes more satisfactory.

In conclusion, it is interesting to estimate the highest frequency at which the foregoing approximation may be safely used. For this purpose, let all impedances be set to zero, whereupon the Rayleigh formula for the resonant frequencies emerges,

$$f_n \simeq n f_1 (1 - \tfrac{1}{2} n^2 \pi^2 \sigma^2 R^2 / L^2), \qquad (34)$$

in which f_1 is the lowest resonant frequency of the infinitely thin rod and n is any odd integer. Equation (34) is in error by terms proportional to the fourth-order moments, and we may therefore expect that it is a good approximation so long as the second term in the parenthesis is small compared to one. For a square rod of steel ($\sigma \simeq 0.3$), twice as long as its lateral dimensions, the correction term becomes one at $n=7$, the fourth resonance, and is only about $\frac{1}{2}$ at the third resonance. If the rod is three times as long as its lateral dimensions, the correction term is less than $\frac{1}{2}$ at the fourth resonance. These are rather stubby rods, so that in many cases one will have a much better approximation.

[10] A. H. Love, *Theory of Elasticity* (Dover Publications, New York, 1944), p. 287, *et seq.* and p. 428.

FURTHER APPLICATIONS

The variation principle here discussed has been extended to deal with free and driven piezoelectric crystals where, in addition to the three displacements, there is a fourth field quantity, the electrostatic potential. It is hoped to present these results shortly.

The possibility of obtaining a related variation principle, suitable for studying high frequency cavity resonators and radar antennae, is being studied.

ACKNOWLEDGMENTS

The writer desires to express his appreciation to Drs. G. P. Harnwell and F. N. D. Kurie, former and present Director of this Laboratory, for policies which made this work possible and for their constant encouragement during its execution; to Drs. R. Courant, K. Friedrichs, and J. K. L. MacDonald of the Applied Mathematics Panel at New York University and to Dr. C. Eckart, Associate Director of this Laboratory, for valuable discussions; to Dr. H. Feshbach of Massachusetts Institute of Technology and to Drs. L. Foldy and H. Primakoff, formerly of Columbia University, Division of War Research, for valuable criticisms; and to the Bureau of Ships, United States Navy, for its enlightened policies toward research, and for permission to publish.

Finally, the writer wishes to acknowledge his great indebtedness to the late Dr. H. Bateman of California Institute of Technology. His pioneer work on variational principles for systems governed by operators which are not self-adjoint, which appears to have been largely overlooked, was the starting point of this work; and the generous spirit in which he gave his time and his wide knowledge in discussing this and other problems will always be remembered.

Conduction and Dispersion of Ionized Gases at High Frequencies

H. MARGENAU*
*Radiation Laboratory,** Massachusetts Institute of Technology, Cambridge, Massachusetts*
(Received January 7, 1946)

The distribution in energy of electrons in a high frequency electromagnetic field is derived by kinetic theory methods. By use of the distribution law, the current density and hence the (complex) conductivity are calculated as functions of electron density, pressure, and frequency of the field. The real part of the conductivity has a maximum for gas pressures, or frequencies, such that the mean free time of an electron is approximately equal to the period of the field. From the conductivity, the dielectric constant of the medium, its index of refraction, and its extinction coefficient are deduced. The results are applicable in microwave researches and in ionosphere problems.

IN several phases of microwave work and in the analysis of ionosphere problems[1] it is necessary to know the conductivity of an ionized gas as a function of electron density, pressure of the gas, and frequency of the waves. Two limiting cases of the conductivity problem are well understood: for low frequencies and high pressures, the current density set up by an alternating field strength $E\cos\omega t$ is given by Langevin's mobility formula

$$I=\frac{4}{3}\frac{e^2E\lambda n}{(2\pi mkT)^{\frac{1}{2}}}\cos\omega t; \tag{1}$$

it is in phase with the field strength. For high frequencies and low pressures, on the other hand, the current is in quadrature with the field and is represented by the formula characteristic of free electrons,

$$I=(e^2En/m\omega)\sin\omega t. \tag{2}$$

The symbols here have their usual significance; λ is the mean free path of the electrons and n their volume concentration.

Under conditions intermediate between the two extremes described by Eqs. (1) and (2) it becomes necessary to consider the effect of electron collisions upon the forced oscillations which the field imposes on them. This is usually done[2] by including in the equation of motion of the electron a friction term of the form $g(dx/dt)$ which has the result of converting Eq. (2) into

$$I=\frac{e^2Em\omega n}{m^2\omega^2+g^2}\sin\omega t. \tag{2'}$$

When this formula is compared with experiment, g is frequently treated as an empirical parameter, and the use of (2′) has led to considerable success.[2] Hulburt[3] and others have used a suggestion of Lorentz to the effect that $g=2m$ times the collision frequency of the electrons, and Childs[4] has discussed some of the shortcomings of this procedure. Aside from its artificiality, it may be criticized primarily for ignoring the distribution-in-energy of the electrons and hence for failing to provide a proper average over electron speeds.

Avoiding these approximations and using kinetic theory methods, we describe in the present note a compact way of obtaining formulas for the conductivity and dispersion of an ionized gas at all pressures and frequencies.

I. DISTRIBUTION FUNCTIONS

We assume that, owing to agencies other than the electromagnetic waves dispersed, a concentration of n electrons per cc is maintained in the gas. At present it will be assumed that they have two sources of energy only, elastic collisions and the external electric field. The case in which the waves are themselves capable of ionizing or exciting the molecules will be treated in a later paper; it cannot be handled with the same precision as the one where the electrons make only elastic collisions.

* Now at Yale University.

** This paper is based on work done for the Office of Scientific Research and Development under contract OEMsr-262.

[1] See Lee H. R. Mimno, Rev. Mod. Phys. 9, 1 (1937).

[2] See K. K. Darrow, Bell System Tech. J. 11, 576 (1932); 12, 91 (1933).

[3] E. O. Hulburt, Phys. Rev. 29, 706 (1927).

[4] E. C. Childs, Phil. Mag. 13, 873 (1932).

Of the n electrons per cc, $f(v_x, v_y, v_z)dv_x dv_y dv_z$ have velocity components about v_x, v_y, v_z. The function f satisfies the Boltzmann "transfer equation" which reads

$$\frac{e}{m}\mathcal{E}\frac{\partial f}{\partial v_x}+\frac{\partial f}{\partial t}=\left(\frac{\partial f}{\partial t}\right)_c, \tag{3}$$

provided the field $\mathcal{E}$ is applied in the X direction. Here $\partial f/\partial t$ represents the local time rate of change caused in f by variations of $\mathcal{E}$, and $(\partial f/\partial t)_c$ that due to encounters with gas molecules. Collisions between electrons will be neglected, and a term involving the magnetic field strength need not be included in Eq. (3) because the velocity of the electrons is small when compared with that of light. Now let

$$\mathcal{E}=E\cos\omega t, \tag{4}$$

and put

$$\gamma=eE/m. \tag{5}$$

The distribution function $f(\mathbf{v})$ will be expanded as usual in spherical harmonics of the components of $\gamma\mathbf{v}$, and all harmonics beyond the first will be neglected. Thus

$$f(\mathbf{v})=f_0(v)+\gamma v_x[f_1(v)\cos\omega t+g_1(v)\sin\omega t], \tag{6}$$

and the functions f_0, f_1, and g_1 depend only on the magnitude of $\mathbf{v}$. It may be shown[5] that

$$\left(\frac{\partial f_0}{\partial t}\right)_c=\frac{1}{v^2}\frac{m}{M}\frac{\partial}{\partial v}\left(\frac{v^4 f_0}{\lambda}\right)+\frac{kT}{Mv^2}\frac{\partial}{\partial v}\left(\frac{v^2}{\lambda}\frac{\partial f_0}{\partial v}\right), \tag{7}$$

$$\left(\frac{\partial(v_x f_1)}{\partial t}\right)_c=-\frac{v_x v}{\lambda}f_1, \tag{8}$$

$$\left(\frac{\partial(v_x g_1)}{\partial t}\right)_c=-\frac{v_x v}{\lambda}g_1, \tag{9}$$

where λ is the mean free path of the electrons and M the mass of a gas molecule. On inserting these expressions in (3) and equating coefficients of γv_x we have

$$\frac{\cos\omega t}{v}\frac{\partial f_0}{\partial v}-\sin\omega t\cdot\omega f_1+\cos\omega t\cdot\omega g_1 = -\cos\omega t\cdot\frac{v}{\lambda}f_1-\sin\omega t\cdot\frac{v}{\lambda}g_1. \tag{10}$$

Terms even in v_x yield, after averaging over directions,

$$\frac{\gamma^2}{3v^2}\cos^2\omega t\cdot\frac{\partial}{\partial v}(v^3 f_1) +\frac{\gamma^2}{3v^2}\cos\omega t\sin\omega t\cdot\frac{\partial}{\partial v}(v^3 g_1)=\left(\frac{\partial f_0}{\partial t}\right)_c,$$

and this, when averaged over a period of the wave becomes, with the use of (7),

$$\frac{\gamma^2}{6}\frac{\partial}{\partial v}(v^3 f_1)=\frac{m}{M}\frac{\partial}{\partial v}\left(\frac{v^4 f_0}{\lambda}\right)+\frac{kT}{M}\frac{\partial}{\partial v}\left(\frac{v^2}{\lambda}\frac{\partial f_0}{\partial v}\right). \tag{11}$$

Equation (10), on the other hand, resolves itself on equating coefficients of sine and cosine terms into the following two:

$$g_1=\frac{\omega\lambda}{v}f_1, \tag{12}$$

$$\frac{1}{v}\frac{\partial f_0}{\partial v}=-\frac{v}{\lambda}f_1-\omega g_1, \tag{13}$$

so that

$$f_1=-\frac{\lambda}{v^2+\omega^2\lambda^2}\frac{\partial f_0}{\partial v}. \tag{14}$$

This may be put into Eq. (11), which becomes after integration (the constant of integration being 0),

$$-\frac{\gamma^2}{3}\frac{\lambda v^4}{v^2+\omega^2\lambda^2}\frac{\partial f_0}{\partial v^2}=\frac{m}{M}\frac{v^4 f_0}{\lambda}+\frac{2kT}{M}\frac{v^4}{\lambda}\frac{\partial f_0}{\partial v^2},$$

hence

$$\log f_0=-\int_0^{v^2}\frac{(m/2)d(v^2)}{kT+[M\gamma^2\lambda^2/6(v^2+\omega^2\lambda^2)]}. \tag{15}$$

If γ is so small that kT outweighs the second term in the denominator, f is Maxwellian. If the second term is dominant, we obtain a distribution function similar to Druyvesteyn's,[5] though differing from it by the presence of the term in ω:

$$f_0=A\exp\left[-\frac{3m(v^4+2\omega^2\lambda^2v^2)}{2M\gamma^2\lambda^2}\right]. \tag{16}$$

In arriving at this result λ has been treated as constant.

A more convenient way of expressing f_0 as well as the subsequent results is by introducing two energy parameters

$$\epsilon_1=\tfrac{1}{2}m(\omega\lambda)^2 \quad\text{and}\quad \epsilon_2=eE\lambda \tag{17}$$

[5] S. Chapman and T. G. Cowling, *The Mathematical Theory of Non-Uniform Gases* (Cambridge University Press, New York, 1939), pp. 348 *et seq.* P. M. Morse, W. P. Allis and E. S. Lamar, Phys. Rev. **48**, 412 (1935).

characteristic of the distribution. In terms of them and of $\epsilon=\frac{1}{2}mv^2$, Eq. (16) reads

$$f_0=A\exp\left[-\frac{6m}{M\epsilon_2^2}(\epsilon^2+2\epsilon_1\epsilon)\right]. \qquad (16')$$

It is clear that for sufficiently large ϵ_1 the distribution differs appreciably from Druyvesteyn's formula even in the limiting case ($\epsilon_2\to\infty$) here under consideration. On integrating (15) without approximation one obtains the accurate distribution law

$$f_0=Ae^{-\epsilon/kT}\left(1+\frac{\epsilon/kT}{(\epsilon_1/kT)+\alpha}\right)^{\alpha}, \qquad (18)$$

with

$$\alpha\equiv\frac{M}{12m}\left(\frac{\epsilon_2}{kT}\right)^2. \qquad (19)$$

To determine the constant A we use the relation

$$n=4\pi\int_0^\infty f_0v^2dv=2\pi\left(\frac{2kT}{m}\right)^{\frac{3}{2}}A\int_0^\infty e^{-x}\left(1+\frac{x}{x_1+\alpha}\right)^{\alpha}x^{\frac{1}{2}}dx$$

$$=\left(\frac{2\pi kT}{m}\right)^{\frac{3}{2}}A\left\{1+\frac{3}{2}\frac{\alpha}{\alpha+x_1}+\sum_{j=2}^{\infty}\frac{\alpha(\alpha-1)\cdots(\alpha-j+1)}{j!}\cdot\frac{1\cdot3\cdot5\cdots(2j-3)}{(\alpha+x_1)^j}\cdot\frac{4j^2-1}{2^j}\right\},$$

where

$$x_1\equiv\frac{\epsilon_1}{kT}=\frac{m(\omega\lambda)^2}{2kT};\quad x\equiv\frac{\epsilon}{kT}. \qquad (20)$$

In this report our interest is confined chiefly to the condition

$$x_1\gg\alpha, \qquad (21)$$

which is satisfied for most high frequency electromagnetic waves with intensity below the level of ionization. If we consider as an example 3-cm waves passing through He gas at a pressure of 20 mm, x_1 is about 100 provided T is room temperature. Condition (21) then requires that $E\ll7$, E being measured in volts/cm. For shorter waves and lower pressures E is allowed to be greater.

Wishing to approximate the parenthesis in Eq. (18) by an exponential, we expand

$$\log\left(1+\frac{x}{x_1+\alpha}\right)^{\alpha}-\log e^{\alpha x/x_1+\alpha}=\alpha\sum_{j=2}^{\infty}\left(-\frac{1}{j}\right)\left(\frac{x}{x_1+\alpha}\right)^j$$

and thus obtain

$$f_0=A\exp\left[-\frac{x_1}{x_1+\alpha}x-\frac{1}{2}\frac{\alpha x^2}{(x_1+\alpha)^2}+\frac{1}{3}\frac{\alpha x^3}{(x_1+\alpha)^3}-\cdots\right]. \qquad (22)$$

In the direct-current case, the first term in the exponent is zero, and the second represents the Druyvesteyn distribution. For alternating currents, and under condition (21), the first term alone is important and leads to a Maxwellian distribution

$$f_0=A\exp\left[-x_1/(x_1+\alpha)\right]x, \qquad (23)$$

corresponding to a temperature

$$T'=T(1+\alpha/x_1). \qquad (24)$$

In the present instance this is essentially T.

Because of the great convenience afforded by the use of the Maxwell formula which, perhaps somewhat unexpectedly, presents itself as a valid approximation in the a.c. case even for values of the field strength that calls for the use of the Druyvesteyn formula under d.c. conditions—it seems important to know whether condition (21)

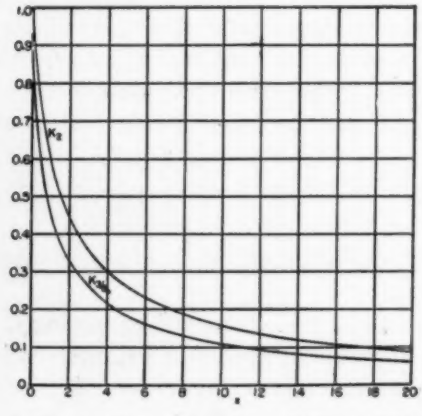

FIG. 1. K_2 and $K_{3/2}$ as functions of $X\equiv m\omega^2\lambda^2/2kT$.

is *necessary* for this approximation to hold. We first note that, if *both* x_1 and α are small, Eq. (22) to be sure becomes nugatory, but Eq. (15) clearly shows that f_0 is Maxwellian. Finally, to investigate the situation for larger values of α, numerical computations have been made. The results indicate that for practical purposes (18) and (23) may be regarded as identical in the part of the velocity range where f_0 is sufficiently large to matter, so long as x_1 is not smaller than α. Zeroth and first moments of the energy, when computed with (23), differ by less than 3 percent from their correct values based on (18). Condition (21) may therefore be replaced for most purposes by

$$x_1 \geq \alpha. \tag{21'}$$

II. CONDUCTIVITY OF THE MEDIUM WHEN DISTRIBUTION FUNCTION IS MAXWELLIAN

The current density through the gas is

$$I = ne\bar{v}_z = e\gamma \int v_z^3 (f_1 \cos\omega t + g_1 \sin\omega t) v^2 dv \sin\theta d\theta d\phi$$

because of (6). Hence in view of Eq. (12),

$$I = \frac{4\pi}{3} e\gamma \int_0^\infty f_1 \left(\cos\omega t + \frac{\lambda\omega}{v} \sin\omega t \right) v^4 dv. \tag{25}$$

In accordance with our assumption (21) Eq. (23) leads to

$$f_0 = Ae^{-\epsilon/kT}, \quad A = n(m/2\pi kT)^{\frac{3}{2}}, \tag{26}$$

so that (14) takes the form

$$f_1 = \frac{\lambda m v}{v^2 + \omega^2\lambda^2} f_0. \tag{27}$$

Using the definition

$$\int_0^\infty \frac{x^p e^{-x}}{x_1 + x} dx \equiv K_p(x_1), \tag{28}$$

we obtain (cf. Eq. (20) for the meaning of x_1) from (25), (26), and (27)

$$I = \frac{4}{3} \frac{e^2 E\lambda n}{(2\pi mkT)^{\frac{1}{2}}} [K_2(x_1) \cos\omega t + x_1^{\frac{1}{2}} K_{3/2}(x_1) \sin\omega t]. \tag{29}$$

This formula is equivalent to the following one for the complex conductivity:

$$\sigma_{\text{complex}} = \frac{4}{3} \frac{e^2\lambda n}{(2\pi mkT)^{\frac{1}{2}}} [K_2(x_1) - ix_1^{\frac{1}{2}} K_{3/2}(x_1)], \tag{30}$$

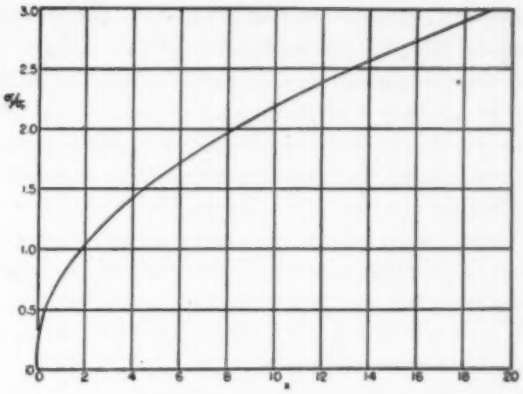

FIG. 2. Ratio of imaginary ("out of phase") to real ("in phase") part of the conductivity as a function of X. When this ratio is much larger than 1, formula (2) is applicable.

which is defined by the relation $I = \sigma_{\text{complex}} E e^{i\omega t}$. To exhibit the analytic nature of this formula we record that it may also be written

$$\sigma_{\text{complex}} = \frac{8}{3} \frac{e^2\lambda n}{(2\pi mkT)^{\frac{1}{2}}} \int_0^\infty \frac{t^4 \exp[-t^2] dt}{t + i\lambda(m/2kT)^{\frac{1}{2}}\omega}. \tag{30'}$$

The functions K_2 and $K_{3/2}$ can be expressed in terms of the exponential integral $Ei(-x_1)$ and the error function erf $[(x_1)^{\frac{1}{2}}]$ (both defined as in Jahnke-Emde, *Funktionentafeln*), respectively:

$$K_2(x_1) = 1 - x_1 - x_1^2 \exp[x_1] E_i(-x_1),$$

$$K_{3/2}(x_1) = (\tfrac{1}{2} - x_1)\pi^{\frac{1}{2}} + \pi x_1^{\frac{1}{2}} \exp[x_1]\{1 - \text{erf}[(x_1)^{\frac{1}{2}}]\}.$$

Graphs of these are shown in Figs. 1 and 2. We note that

$$\lim_{x_1 \to 0} K_2 = 1, \quad \lim_{x_1 \to 0} K_{3/2} = \tfrac{1}{2}\pi^{\frac{1}{2}},$$

$$\lim_{x_1 \to \infty} K_2 = \frac{2}{x_1}, \quad \lim_{x_1 \to \infty} K_{3/2} = \frac{3\pi^{\frac{1}{2}}}{4x_1}.$$

Thus Eq. (29) has the following two limiting forms:

$$\lim_{x_1 \to 0} I = \frac{4}{3} \frac{e^2 E\lambda}{(2\pi mkT)^{\frac{1}{2}}} n \cos\omega t + \frac{\omega e^2 E\lambda^2}{3kT} n \sin\omega t, \tag{31}$$

$$\lim_{x_1 \to \infty} I = \frac{16}{3} \frac{e^2 E}{m\omega^2\lambda} \left(\frac{kT}{2\pi m} \right)^{\frac{1}{2}} n \cos\omega t + \frac{e^2 E}{m\omega} n \sin\omega t. \tag{32}$$

The first term on the right of (31) represents the

Langevin mobility formula, Eq. (1); the second term in (32) is the familiar expression for the current (in quadrature with the applied e.m.f.) due to entirely free electrons, Eq. (2). In problems involving the passage of cm waves through ionized gases, the limiting form (32) is usually applicable.

This applies *a fortiori* to the positive ions. Because of their large mass, x_1 is very large, and (29) describes their contribution to the conductivity, which is seen to be very small and can be neglected for most purposes.

The real and imaginary parts of σ_{complex} are functions of λ, and hence of the pressure of the gas. The imaginary part, being proportional to $x_1 K_{3/2}(x_1)$, is a monotonically increasing function of x_1: for a given frequency ω it starts with the value $e^2n/m\omega$ at low pressures and goes to zero as $\omega e^2\lambda^2/3kT$ at high pressures. The real part, however, which is proportional to $x_1^{\frac{1}{2}}K_2(x_1)$, has the value zero at both ends of the range of x_1 and passes through a maximum.

On differentiating, it is seen that this point is fixed by the condition

$$K_2(x_1)+2x_1K_2'(x_1)=0,$$

which leads to $x_1=2.1$. Thus maximum conductivity occurs when

$$\omega\lambda=6.8\times10^{13}(kT)^{\frac{1}{2}}. \tag{33}$$

This equation places the maximum of conductivity nearly at that value of the pressure for which the mean free time τ_1 of an electron between impacts equals τ_2, the "period" of the light wave. For if we take the period as the time per radian, $\tau_2=1/\omega$, while $\tau_1=\lambda/v=\lambda(m/3kT)^{\frac{1}{2}}$. Equality of τ_1 and τ_2 then implies $x_1=3/2$ or

$$\omega\lambda=5.75\times10^{13}(kT)^{\frac{1}{2}}, \tag{34}$$

a result not very different from (33).

In some experiments[6] high frequency waves are sent through gases maintaining an independent electrical discharge, and their dispersion and attenuation are measured. If the energy distribution of the electrons is Maxwellian, formula (29) may be shown to be applicable, and T appearing therein (also implicitly in x_1) refers to the temperature of the electrons sustaining the discharge.

III. EXACT THEORY OF CONDUCTIVITY

Starting with Eq. (18) and using the abbreviations (19) and (20), we obtain with the use of (14) and (15)

$$f_1=2A\left(\frac{m}{2kT}\right)^{\frac{1}{2}}\lambda\frac{(x+x_1+\alpha)^{\alpha-1}}{(x_1+\alpha)^{\alpha}}e^{-x}x^{\frac{1}{2}}. \tag{35}$$

When this is inserted in Eq. (25) there results, after an appropriate change of variable,

$$I=\frac{8\pi}{3}\frac{e^2E\lambda}{m^2}AkT\left\{\int_0^\infty\frac{(x+x_1+\alpha)^{\alpha-1}}{(x_1+\alpha)^{\alpha}}e^{-x}x^2dx\cdot\cos\omega t\right.$$
$$\left.+x_1^{\frac{1}{2}}\int_0^\infty\frac{(x+x_1+\alpha)^{\alpha-1}}{(x_1+\alpha)^{\alpha}}e^{-x}x^{\frac{1}{2}}dx\cdot\sin\omega t\right\}. \tag{36}$$

The remaining integrals, as well as A, may be expressed in terms of confluent hypergeometric functions[7] in the form

$$I=\frac{e^2E\lambda n}{(2\pi mkT)^{\frac{1}{2}}}(W_{[(\alpha-1/2)/2],\,[(\alpha+3/2)/2]}(x_1+\alpha))^{-1}\{\tfrac{2}{3}(x_1+\alpha)^{\frac{1}{2}}W_{[(\alpha-3)/2],\,[(\alpha+2)/2]}(x_1+\alpha)\cdot\cos\omega t$$
$$+(\pi x_1)^{\frac{1}{2}}W_{[(\alpha-5/2)/2],\,[(\alpha+3/2)/2]}(x_1+\alpha)\cdot\sin\omega t\}. \tag{37}$$

For small integral values of α the integrands in Eq. (36) can be expanded easily and the integrals become sums of Γ-functions. When this procedure is possible it is far less laborious than the use of Eq. (37).

IV. DIELECTRIC CONSTANT, INDEX OF REFRACTION

For ready reference we compile here a few facts that are well known and indicate how the foregoing results may be used in the computation of the optical properties of an ionized medium.

Ampere's law, for an isotropic medium without space charge and with permeability unity, has the form

$$\nabla\times\mathbf{H}=\frac{1}{c}\dot{\mathbf{D}}+\frac{4\pi}{c}\mathbf{I}.$$

[6] A. Szekely, Ann. d. Physik [5], **3**, 112 (1929). E. V. Appleton and F. W. Chapman, Proc. Roy. Soc. London **44**, 246 (1932).

[7] Whittaker and Watson, p. 340.

If we introduce the "ordinary" dielectric constant $\epsilon_0 = D/\mathcal{E}$ and the conductivity $\sigma = I/\mathcal{E}$, this equation when written for field strengths proportional to $e^{i\omega t}$ reads

$$\nabla \times \mathbf{H} = \frac{i\omega}{c}\epsilon_0 \mathcal{E} + \frac{4\pi\sigma}{c}\mathcal{E}.$$

If σ is real, the current density in phase with $\mathcal{E}$ is $\sigma\mathcal{E}$, that out of phase is $(\omega/4\pi)\epsilon_0\mathcal{E}$. But if σ is complex, that is $\sigma = \sigma_r - i\sigma_i$, then ϵ_0, the measure of the current in quadratature with $\mathcal{E}$, must be replaced by the new dielectric constant

$$\epsilon = \epsilon_0 - (4\pi\sigma_i/\omega), \tag{38}$$

while the dissipative current density is $\sigma_r\mathcal{E}$. For the present problem, σ_r and σ_i may be identified from Eqs. (30) [or (36), (37)].

The index of refraction, N, of the medium is defined by

$$\mathcal{E} = Ee^{i\omega(t-(N/c)\mathbf{K}\cdot\mathbf{r})}, \tag{39}$$

$\mathbf{K}$ being a unit vector in the direction of propagation. When Maxwell's equations are solved with insertion of this form of $\mathcal{E}$, it is seen that

$$N^2 = \epsilon - (4\pi i\sigma_r/\omega). \tag{40}$$

If, as usual, we introduce the "ordinary" index of refraction n and the extinction coefficient k, such that

$$N = n - ik, \tag{41}$$

we obtain from (40)

$$n^2 - k^2 = \epsilon = \epsilon_0 - (4\pi\sigma_i/\omega),$$
$$nk = 2\pi\sigma_r/\omega;$$

whence

$$n^2 = \frac{\epsilon}{2}\{1 \pm [1 + (4\pi\sigma_r/\epsilon\omega)^2]^{\frac{1}{2}}\},$$
$$k^2 = \frac{\epsilon}{2}\{-1 \pm [1 + (4\pi\sigma_r/\epsilon\omega)^2]^{\frac{1}{2}}\}. \tag{42}$$

Here the positive sign is to be taken when $\epsilon \geqslant 0$, the negative sign when $\epsilon \leqslant 0$, (see Eq. (35)) the reason being that n and k are real. For waves in the cm region ϵ becomes negative at electron concentrations of $10^{12}/\text{cm}^3$. Detailed applications of these results will be given in another communication.

The author wishes to express his indebtedness to Dr. C. G. Montgomery for suggesting this problem to him and for helpful comments.

PHYSICAL REVIEW VOLUME 69, NUMBERS 9 AND 10 MAY 1 AND 15, 1946

Some Properties of Very Intense Shock Waves

R. G. SACHS
Ballistic Research Laboratory, Aberdeen Proving Ground, Maryland
(Received February 12, 1946)

Conditions have been obtained for the existence of a steady shock wave of such an intensity that radiation pressure plays a role in determining the properties of the shock. These conditions are completely analogous to the Rankine-Hugoniot equations for ordinary shocks; they are obtained by consideration of the conservation of mass, momentum, and energy. The results are applied to hydrogen and other very light gases. The application to other media requires a much more complicated discussion of the equation of state and specific heat under extremely high pressures and temperatures. In the light gases, the thickness of the shock front is extremely large because the radiation free path, which is determined by Compton scattering, is very large. The velocity of sound in a medium under very high pressures and temperatures is also discussed, and it is found that this velocity continues to increase with increasing pressure, a condition that is necessary for the shock to be stable.

1. INTRODUCTION

THE conditions for the existence of a steady shock wave in matter are well known. These conditions, which may be called the Rankine[1]-Hugoniot[2] equations, relate the pressure, density, and material velocity behind the shock to those in front of the shock for a given velocity of the shock front. They are simple consequences of the conditions for conservation of mass, momentum, and energy across the shock front, as well as of the equation of state of the medium through which the shock is moving.

The Rankine-Hugoniot equations have served to treat problems concerned with any shocks that can be produced in the laboratory. However, it may be of interest, for example in the study of stellar explosions, to consider shocks which are so intense that radiation pressure plays an important role in determining their properties. It is the purpose of this discussion to indicate the changes in the Rankine-Hugoniot relations that are necessary to take account of the radiation pressure, and to derive some of the consequences of these new relations.

Since the derivation of the Rankine-Hugoniot relations will serve as a guide for our purpose, it will be recalled in the next section. The radiation problem will then be treated in subsequent sections.

[1] W. J. M. Rankine, Trans. Roy. Soc. London, **A160**, 277 (1870).
[2] H. Hugoniot, J. Ecole Poly. **58** (1889).

2. THE RANKINE-HUGONIOT EQUATIONS

In the derivation of these equations, a shock wave is assumed to be represented by a discontinuity in pressure, density, and temperature which moves through the medium with a velocity, V. This discontinuity exists as such only on the macroscopic scale. On the molecular scale, the changes in pressure, etc., must necessarily take place over a distance of several mean free paths in order to maintain equilibrium in the transition. It has recently been shown by Thomas[3] that this condition is satisfied for quite intense shock waves in gases.

Instead of considering the medium to be initially at rest and the shock moving with speed V, it is more convenient to observe the phenomenon from a coordinate system in which the shock is at rest and the material is being fed into the shock front with the speed V. This condition

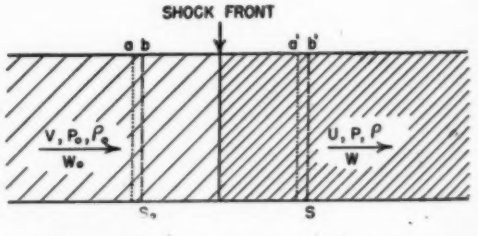

FIG. 1. Schematic representation of shock in coordinate system moving with the shock front. S_0 and S are planes fixed with respect to the shock front. The slab ab of material of thickness Vdt moves into the section S_0S in time dt, and the slab $a'b'$ of thickness Udt moves out of that section in the same time.

[3] L. H. Thomas, J. Chem. Phys. **12**, 449 (1944).

is indicated in Fig. 1. Material at pressure P_0 and density ρ_0 is being fed into the shock with velocity V (from left to right)—and material at pressure P and density ρ is leaving the front with a velocity $U(U<V)$.

Consider now the section S_0S of the material between the vertical dashed lines,[4] which are taken to be at rest in this coordinate system. Since the shock is assumed to be steady, the mass, momentum, and energy of the material in this section must be conserved during the infinitesimal time dt.[5] The mass that flows into S_0S in this time is the mass of the slab ab of material or $\rho_0 V dt$, and the mass that flows out is the mass of the slab $a'b'$ or $\rho U dt$, so conservation of mass requires that

$$\rho_0 V = \rho U. \tag{1}$$

Since the mass $\rho_0 V dt$ has a velocity V, it imparts a momentum $\rho_0 V^2 dt$ to the section. Similarly, a momentum $\rho U^2 dt = \rho_0 V U dt$ leaves the section. Since the section is under a pressure P_0 on the left and P on the right, it also acquires a momentum toward the right of $(P_0 - P)dt$, in this time. The condition that the momentum be conserved is, then:

$$\rho_0 V(V-U) = P - P_0. \tag{2}$$

Similarly, the slab ab carries in with it a kinetic energy $\frac{1}{2}\rho_0 V^3 dt$, and the slab $a'b'$ carries out a kinetic energy $\frac{1}{2}\rho_0 V U^2 dt$. In addition, the material that moves into the section in time dt must move a distance Vdt against a pressure P_0 while that moving out moves a distance Udt against a pressure P, so an amount of work $(P_0 V - PU)dt$ is done on the section. Finally, the internal energy (E_0) of unit mass of the material at pressure P_0 and density ρ_0 is different from that (E) at pressure P and density ρ. Thus the section ab carries in an energy $\rho_0 V E_0 dt$, and the section $a'b'$ carries out an energy $\rho_0 V E dt$. The condition that all of these changes in energy lead to no over-all change in the total energy of the section S_0S is:

$$\rho_0 V[\tfrac{1}{2}(V^2 - U^2) + E_0 - E] = PU - P_0 V. \tag{3}$$

The Eqs. (1)–(3) are the Rankine-Hugoniot equations. Taken along with the equation of state, they provide the necessary relations for determining the physical conditions existing behind a shock front which is moving with a known velocity. For a perfect gas, the equation of state is

$$E = P/(\gamma-1)\rho, \tag{4}$$

where γ is the ratio of specific heats. Equation (4) may be used to eliminate E and E_0 from Eq. (3). Then the Eqs. (1)–(3) give three independent relations between the four unknown quantities P, ρ, U, V.

It is generally convenient to deal with the dimensionless quantities $p = P/P_0$, $x = \rho/\rho_0$, $u = U/V$, $v = V(\rho_0/P_0)^{\frac{1}{2}}$, and $\epsilon = E\rho_0/P_0$. In terms of these quantities, the Eqs. (1) to (4) become

$$ux = 1, \tag{5}$$

$$v^2(1-u) = p - 1, \tag{6}$$

$$\tfrac{1}{2}v^2(1-u^2) + \epsilon_0 - \epsilon = pu - 1, \tag{7}$$

$$\epsilon = p/(\gamma-1)x. \tag{8}$$

These equations, which now in virtue of (8) refer to a perfect gas, may easily be solved to give p, x, and u in terms of v. One consequence of them which we will use is that, as the pressure becomes infinitely great, the density ratio x approaches the finite value $(\gamma+1)/(\gamma-1)$.

3. THE STEADY SHOCK CONDITIONS FOR VERY INTENSE SHOCKS

If the shock pressure is very high, that is of the order of 10^5 atmospheres, the temperature is correspondingly high, so the energy density of radiation is comparable with the internal energy density of the material. Similarly, the radiation pressure is comparable with the material pressure. Under this condition, the Eqs. (5)–(8) can no longer be correct. It is necessary to introduce terms in them that will take account of the momentum and energy transferred by the radiation.

If the radiation energy density is W, the radiation pressure is

$$P_{\text{rad}} = \tfrac{1}{3}W. \tag{9}$$

The radiation density and pressure at every point is determined by the temperature at that point

[4] If the shock front is not plane, the distances S_0S, ab, and $a'b'$ must be small compared to the radius of curvature.

[5] It is necessary that ab and $a'b'$ be large compared to a mean free path so dt must be large compared to the mean free path divided by V.

by the relation

$$W=a(kT)^4 \tag{10}$$

where $a=2.23\times10^{49}$ erg^{-3} cm^{-3}.

Turning now to Fig. 1, a radiation energy density W must be included on the right side of the shock. For generality we include an energy density W_0 on the left side (in front of the shock) although this quantity is negligibly small in the usual case of a shock advancing into a medium at nearly standard conditions.

In discussing ordinary shocks, it was pointed out that the changes represented as discontinuous in Fig. 1 must actually take place over a distance which is large compared to a molecular mean free path. An equivalent condition applies to the present case. The thickness of the shock front is large compared to some length λ' where λ' must obviously be at least as great as the mean free path, λ, for the scattering or absorption of radiation. However, λ' is not to be set equal to λ because the velocity of light, c, is so great compared to the shock velocity that an appreciable amount of radiation can be lost by diffusion even if the thickness of the shock front is large (but not large enough) compared to the mean free path. Thus for a shock front which is initially very sharp, the radiation will diffuse through the front and raise the temperature of the medium just ahead of the shock. The front is continually broadened by this process. The broadening eventually ceases to be important, however, because the time required for the diffusion of the radiation through a given distance is proportional to the square of the distance while the time required for the shock to negotiate the same distance is linear in the distance. Thus as the shock becomes thicker, a stage is reached in which only a negligible fraction of the radiation gets ahead of the shock.

A rough estimate of the thickness, λ', at which the broadening process virtually ceases is obtained by taking it to be that distance for which the average velocity of diffusion is equal to the velocity, V, of the shock. The average diffusion velocity over a distance λ' is roughly $c\lambda/\lambda'$. Setting this equal to V, the estimate

$$\lambda'=c\lambda/V$$

is obtained for the minimum thickness of a steady shock.

In the following considerations, it is assumed that the distance S_0S (Fig. 1) is large compared to λ'. On the other hand, the time interval dt which will be considered need only be so large that the thickness of each of the slabs ab and $a'b'$ in Fig. 1 is large compared to λ. The path length λ' does not enter in this case because each slab is cut from a region of uniform radiation density, and diffusion need not be considered in such a region.

The first of the conditions given in Section 2, that is, the conservation of mass, is not changed by the presence of radiation since shock waves so intense as to require a relativistic treatment will not be considered.[6] This condition is expressed in dimensionless form by Eq. (5).

The condition for conservation of momentum must be modified to include the effect of the radiation pressure. Since the thickness of the section S_0S of material is large compared to the radiation free path, the radiation pressure will transfer momentum to the section in the same degree as that transferred by the particle pressure. Thus Eq. (2) is to be changed by adding the corresponding radiation pressure to each of the particle pressure terms. Since the radiation pressure is $\frac{1}{3}W$, the equation to be substituted for Eq. (2) is:

$$\rho_0V(V-U)=P+\tfrac{1}{3}W-(P_0+\tfrac{1}{3}W_0). \tag{11}$$

In dimensionless form, this equation becomes:

$$v^2(1-u)=p+w-1-w_0, \tag{12}$$

where

$$w=\tfrac{1}{3}W/P_0. \tag{13}$$

Consideration of the conservation of energy leads to the result that Eq. (3) must be modified by the addition of a radiation pressure term and a radiation energy term, as would be expected. As a consequence of the condition that the thickness of the material ab or $a'b'$ flowing into or out of the section S_0S in time dt is large compared to the radiation free path, the slabs ab and $a'b'$ absorb the full radiation momentum P_{rad}. They thereby do an amount of work $\frac{1}{3}W_0Vdt$ and $-\frac{1}{3}WUdt$ on

[6] In the relativistic case, the conservation of mass would appear as part of the energy conservation equation, but an additional condition would be required for conservation of particles or for conservation of electric charge if pair production is taken into account.

the section S_0S. It follows that $\frac{1}{3}W$ and $\frac{1}{3}W_0$ are to be added to the corresponding particle pressures on the right side of Eq. (3).

In addition to this change in the pressure term, there is a corresponding change in the internal energy term in Eq. (3). It is to be remembered that that term was due to the internal energy carried into and out of the section S_0S by the material in ab and in $a'b'$, respectively. In order to obtain the corresponding contribution of the radiation, let us imagine that perfectly reflecting, double faced mirrors which move along with the material are placed at a, b, a', and b'. These have no effect on the radiation equilibrium, so between the mirrors the radiation density is W (or W_0).[7] The total radiation energy between the mirrors ab is carried into the section S_0S, and the radiation energy between $a'b'$ is carried out of the section in time dt. The consequent increase in the energy of the section is $W_0Vdt-WUdt$, so a term W_0V-WU must be added to the left side of Eq. (3). With both of the necessary changes, Eq. (3) is replaced by

$$\rho_0V[\tfrac{1}{2}(V^2-U^2)+E_0-E]+VW_0-UW = (P+\tfrac{1}{3}W)U-(P_0+\tfrac{1}{3}W_0)V. \quad (14)$$

In dimensionless form, this is

$$\tfrac{1}{2}v^2(1-u^2)+\epsilon_0-\epsilon+4(w_0-uw)=pu-1. \quad (15)$$

Equations (5), (12), and (15) provide the necessary description of the shock phenomenon. Since these equations are useful primarily for very intense shock waves, some simplification of them can be secured by neglecting the quantities w_0 and 1 which are small compared with w, and the quantity ϵ_0 which is small compared to ϵ, if the shock wave is advancing into a medium at nearly standard conditions. The resulting equations are:

$$ux=1, \quad (16a)$$

$$v^2(1-u)=p+w, \quad (16b)$$

$$\tfrac{1}{2}v^2(1-u^2)-\epsilon=(p+4w)u. \quad (16c)$$

[7] If the mirrors (assumed to be penetrable by the material) move with a velocity different from the material, they disturb the radiation energy equilibrium because the reflected intensities on the two sides are different from the incident intensities and different from each other as a consequence of the Doppler effect. This point was called to the author's attention by Professor J. E. Mayer.

4. THE EQUATIONS OF STATE

The Eqs. (16) must be augmented by the equation of state for the material and the equation of state for the radiation. The latter is simply given by Eq. (10), or, in terms of the dimensionless w,

$$w=a(kT)^4/3P_0. \quad (17)$$

When the equation of state for the material is given, the temperature, T, in (17) can be expressed in terms of the material pressure and density. Then these conditions, along with Eqs. (16), are sufficient to determine all of the variables of the system as a function of one of them, which is the desired result. However, under the conditions to be considered, the equation of state of the material cannot always be expressed in simple form. The temperatures are so high that molecules and solids are dissociated into a gas of highly ionized ions and electrons. Many of the free electrons have sufficiently high thermal energy to be treated as a non-degenerate classical gas, but there are additional electrons in the excited ionic states which will make a somewhat complicated contribution to the specific heat, and therefore to the thermodynamic equation of state.

The problem is complicated further if we are dealing with a material which is initially liquid or solid because although the atomic structure is destroyed by the high temperature, the density is very high, so the material behaves more like a liquid with a very high vapor pressure than a gas. This liquid is highly ionized, so there are free electrons throughout. The higher atomic levels are split into bands because of the high density, and these bands may be only partially occupied, as if the liquid were a metallic conductor. The electrons in these partially occupied bands behave very much like free electrons.[8] These free and almost-free electrons contribute to the equation of state as if they constituted a perfect monatomic gas. The contribution to the equation of state made by the liquid consisting of atomic ions cannot be obtained without a detailed investigation of the material under consideration.

In order to avoid the difficulty of obtaining the

[8] The really free electrons have energies greater than the ionization potential or, speaking in terms of a metal, their energies are greater than the work function.

equation of state and yet still obtain a qualitative picture, the properties of a shock wave in a perfect monatomic gas containing Z free (nondegenerate) electrons per atom will be considered. The contribution of the bound electrons to the specific heat will be included by taking the value of γ, the ratio of specific heats, to be temperature dependent. It will introduce no serious complication to admit that Z is temperature dependent. Then these assumptions yield a reasonable approximation for a shock in a light gas. However, for the more interesting case of a shock in a dense medium, the approximations are poor and the results will indicate only the qualitative behavior of the shock.

The thermodynamic equation of state can be formally written as

$$E=P/(\gamma-1)\rho, \tag{18}$$

where now γ is assumed to be temperature dependent to take account of the contribution of bound electrons to the specific heat. In dimensionless form, this is

$$\epsilon=p/(\gamma-1)x. \tag{19}$$

The equation of state for a gas containing an effective number Z of free electrons per atom is given by

$$P/\rho=(Z+1)N_0kT/A, \tag{20}$$

where A is the atomic weight and N_0 the Avogadro number. It follows that

$$kT=Ap/\rho(Z+1)N_0. \tag{21}$$

Inserting this in Eq. (10) gives the relation between the radiation energy density and the particle pressure and density:

$$W=a[AP/\rho(Z+1)N_0]^4. \tag{22}$$

In terms of the dimensionless $w=\frac{1}{3}W/P_0$, this becomes

$$w=\alpha^4(p/x)^4, \tag{23}$$

with

$$\alpha=\left(\frac{a}{3P_0}\right)^{\frac{1}{4}}\frac{AP_0}{(Z+1)N_0\rho_0}$$

$$=5.23\times10^{10}\frac{AP_0}{(Z+1)N_0\rho_0}, \tag{24}$$

where the numerical factor is in units of erg^{-1}. It is to be remembered that Z, and therefore α, may be temperature dependent.

Equations (19) and (23), when used in conjunction with Eqs. (16), completely determine the properties of an intense shock wave in a medium of the type under discussion. That is, the properties are determined in terms of the functions $\alpha(T)$ and $\gamma(T)$. It will be shown in the next section that the essential results can be obtained in such a way that the rather insensitive function $\alpha(T)$ can be inserted as a last step.

5. FORMAL SOLUTION OF THE EQUATIONS

The Eqs. (16), (19), and (23) can now be solved to give p, u, and w in terms of x. The relation between u and x is, according to Eq. (16a)

$$u=1/x. \tag{25}$$

Substituting this in Eq. (16b):

$$v^2=x(p+w)/(x-1). \tag{26}$$

Inserting Eq. (25), (26), and (19) in Eq. (16c) yields after straightforward algebraic operations:

$$p=(7-x)w/(x-X_0), \tag{27}$$

where

$$X_0=(\gamma+1)/(\gamma-1). \tag{27a}$$

Using the expression Eq. (23) for w, the relation between p and x is found to be

$$p=\left(\frac{x}{\alpha}\right)^{4/3}\left(\frac{x-X_0}{7-x}\right)^{1/3}. \tag{28}$$

From Eq. (27) the expression for w is

$$w=\left(\frac{x}{\alpha}\cdot\frac{x-X_0}{7-x}\right)^{4/3}; \tag{29}$$

and from Eq. (26), that for v is

$$v=\left[\frac{(7-X_0)}{(7-x)}\frac{xp}{x-1}\right]^{\frac{1}{2}}, \tag{30}$$

where p can be obtained from (28).

It is to be remembered that the Rankine-Hugoniot equations lead to a limit for the density ratio of $X_0=(\gamma+1)/(\gamma-1)$ for very high pressures. Now we find that, with radiation, the density ratio becomes greater than X_0 (where, it is to be remembered, the value of X_0 depends on the temperature) but reaches a limiting value of 7. It is seen that these equations do not apply for

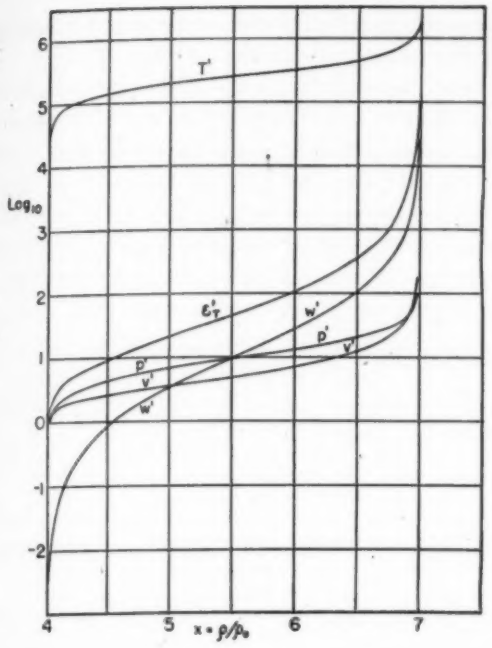

FIG. 2. Log curves of reduced pressure, velocity, etc., as a function of density ratio in shock. The scale for hydrogen is: $p, w, \epsilon_T = 9.2\times10^{13}$ atmos., $T = 9.8$°K, $V = 2.7\times10^{4}$ meters/sec.

$x \leq X_0$. To obtain the correct results for such values of x, it is necessary to retain the terms of the order of 1 which were neglected in arriving at Eqs. (16).

A quantity that is of interest is the total internal energy per unit volume, that is, the sum of the particle energy density and the radiation energy density. The energy per unit volume due to matter is $E\rho$, which, if measured in units of P_0, becomes $\epsilon x = p/(\gamma-1)$, according to Eq. (19). The radiation energy density in units of P_0 is $3w$, so the total energy density, ϵ_T, is given by

$$\epsilon_T = p/(\gamma-1)+3w. \tag{31}$$

This quantity is probably the best measure of the intensity of the shock wave, and, as such, will simply be called the intensity of the shock.

It will also be of interest to know the temperature behind the shock front. This can easily be obtained as a function of w from Eq. (17). The result is:

$$T = 1.41\times10^{5}w^{\frac{1}{2}}\ °\text{K}, \tag{32}$$

for $P_0 = 10^6$ ergs/cm^3 = 1 atmos.

It is convenient to express the equations obtained in this section in terms of the new dependent variables $p' = \alpha^{4/3}p$, $w' = \alpha^{4/3}w$, $\epsilon_T' = \alpha^{4/3}\epsilon_T$, $v' = \alpha^{\frac{1}{2}}v$, $T' = \alpha^{\frac{1}{2}}T$. The primed quantities are obtained from the unprimed by a change of scale, the scale factor in general depending on the temperature and therefore, on the independent variable x. In these terms, the equations become

$$p' = x^{4/3}\left(\frac{x-X_0}{7-x}\right)^{1/3}, \tag{33a}$$

$$w' = \left(x\frac{x-X_0}{7-x}\right)^{4/3}, \tag{33b}$$

$$\epsilon_T' = p'/(\gamma-1)+3w', \tag{33c}$$

$$v' = \left[\frac{7-X_0}{7-x}\,\frac{xp'}{x-1}\right]^{\frac{1}{2}}, \tag{33d}$$

$$T' = 1.4\times10^{5}w'^{\frac{1}{2}}. \tag{33e}$$

6. QUANTITATIVE RESULTS FOR HYDROGEN AND OTHER VERY LIGHT GASES

The Eqs. (33) could be solved to give the desired dependence of pressure, velocity, etc., on density if the functions $\alpha(T)$ and $X_0(T)$ were known. These functions depend in detail on the particular gas under consideration. The function $\alpha(T)$ can be treated to a fair approximation without great difficulty because it does not appear explicitly in Eqs. (33). $X_0(T)$, on the other hand, is an unpleasant function which will show rapid changes whenever kT is equal to the energy of an excited state of an ion in the gas. Therefore, the treatment of the problem for most gases would be tedious. One gas for which this is not true is hydrogen. It will be shown that the temperature is high enough so that the hydrogen is ionized over the entire region of interest. Therefore, the gas consists of (unexcitable) ions and free electrons. In this case $\gamma = 5/3$, so $X_0 = 4$.

With this value of X_0, the values of p', w', v', etc., have been computed from Eqs. (33), and their logarithms have been plotted in Fig. 2. To obtain the corresponding values of p, w, v, etc., it is necessary to determine α, and thereby the scale factors p/p', v/v', etc. Since in this case $Z = 1$, Eq. (24) gives for α

$$\alpha = 2.61\times10^{10}\,AP_0/N_0\rho_0 = 2.61\times10^{10}\,kT_0,$$

where $T_0 = 300$°K. Thus

$$1/\alpha = 940. \tag{34}$$

The factor by which T' is to be multiplied to obtain T in °K is

$$1/\alpha^{\frac{1}{2}}=9.8, \tag{35a}$$

and that by which p', w', ϵ_T' are to be multiplied to obtain p, w, ϵ_T in atmospheres is

$$1/\alpha^{4/3}=9.2\times10^3. \tag{35b}$$

The factor by which v' is to be multiplied to obtain the velocity of the shock in units of $(P_0/\rho_0)^{\frac{1}{2}}=280$ m/sec. is

$$1/\alpha^{\frac{1}{2}}=96. \tag{35c}$$

It can be seen in Fig. 2 that the radiation ceases to play an important role in the shock for $x\leq4.01$. This then is the lowest value of x which is of interest for this discussion. At $x=4.01$, Eqs. (33) with $X_0=4$ give $T'=3.36\times10^4$. Therefore, $T=3.3\times10^5$ °K, which corresponds to a value of kT of 28 electron volts or over twice the ionization potential of hydrogen. It can be seen from Fig. 2 that the temperature increases rapidly as x increases beyond the value 4.01, so for almost all values of x in the region between $x=4$ and $x=7$, the thermal energy is far greater in magnitude than the potential energy, which can then be neglected. It follows that the assumption that the gas consists of free electrons and protons with its consequent values of $X_0=4$ and $1/\alpha=940$ is a reasonable approximation over most of the region of interest. The properties of the shock in hydrogen are therefore given by Fig. 2 in the following units:

$$\begin{array}{ll} p, w, \epsilon_T & 9.22\times10^5 \text{ atmospheres,} \\ T & 9.8\text{°K,} \\ v & 2.7\times10^4 \text{ meters/sec.} \end{array} \tag{36}$$

The curves in Fig. 2 can also be used to determine the properties of an intense shock in other light gases as long as the intensity of the shock is so great that kT is large compared to the total ionization potential of the gas. The ionization potential for the last electron of an atom of atomic number Z is Z^2 times greater than that of hydrogen, while the temperature for the same value of x is only $[(Z+1)/2]^{\frac{1}{2}}$ times greater than that for hydrogen. Therefore, the range of intensities over which our approximation applies narrows rapidly with increasing Z, and even for air, it is only to the very highest shock intensities considered that Fig. 2 can be applied. It should be pointed out that there is an upper limit to the intensity that can be considered on the basis of the equations used here since at $x=6.99$, the velocity of the shock in hydrogen is about 5×10^8 cm/sec. or 2 percent of the velocity of light. Above this intensity, relativistic effects would become appreciable, and our considerations would have to be modified as indicated in footnote 6.

In the range of intensities to which Fig. 2 applies for light gases other than hydrogen, the units are, of course, different from those given in (36). According to Eqs. (24) and (34), they may be obtained from Eqs. (35) by setting

$$1/\alpha=940(Z+1)/2.$$

7. CONDITION FOR THE FORMATION OF THE SHOCK

Up to this point, it has been assumed that a steady shock can exist, and some consequences of this assumption have been derived. The question naturally arises as to whether the steady shock will ever be formed under reasonable conditions. For ordinary shocks, the answer to this question is usually given by pointing out that the velocity of sound increases with increasing pressure of the medium through which the sound wave is traveling. Therefore, a pressure pulse that has a smooth rather than a discontinuous change in pressure will change form by the high pressure region moving faster than the low pressure region in front of it. The ultimate form of the pulse will then be that of a shock. It will now be shown that a similar process does occur in a medium at extremely high pressure.

For this purpose, it is necessary to write down the hydrodynamic equations for such a medium and thereby determine the velocity of sound. In doing so, it will be assumed that there are only negligible changes in pressure, temperature, etc., over distances of the order of $\lambda''=\lambda c/C$, where C is the velocity of sound. This assumption is made to avoid treating the effects of diffusion of radiation in obtaining the sound velocity. It will be shown that this "non-diffusion" velocity, C, increases with increasing pressure. Therefore, a large amplitude sound pulse which satisfies the non-diffusion condition stated above will become steeper at the front as it progresses. Ultimately,

the thickness of the front will reduce to a distance of the order of λ'', whereupon diffusion of the radiation becomes important, and the simple hydrodynamic theory does not apply. The diffusion process sends more energy forward than backward since the pulse has, at this stage, a steeper gradient toward the front than toward the back. Thus, the added effect of diffusion is to sharpen the front of the pulse even further. This process of sharpening continues until the thickness is of the order of $\lambda'=\lambda c/V$, as shown in Section 3. It is to be noted that $\lambda'\ll\lambda''$ since $C\ll V$.

It appears then that a sufficiently broad, large amplitude sound pulse will eventually take the form of a shock of the type discussed in the foregoing sections. However, a pulse of thickness less than λ'' will broaden by diffusion until it becomes so broad that the non-diffusion, hydrodynamic effects take control. Then it will proceed to form a shock, but the peak of the shock would be expected to have a smaller intensity than the maximum in the original pulse.

We now consider the hydrodynamic theory under the non-diffusion conditions described above, in order to show that C increases with pressure. Methods analogous to those described in Section 3, show that the equation of continuity has the usual form:

$$\text{div } \rho\mathbf{U}=-\partial\rho/\partial t. \tag{37}$$

The equation for conservation of momentum now takes the form

$$\rho d\mathbf{U}/dt=-\text{grad } (P+\tfrac{1}{3}W), \tag{38}$$

and conservation of energy yields

$$\rho\frac{d}{dt}(E+\tfrac{1}{2}U^2)+\rho\frac{d(W/\rho)}{dt}=-\text{div } [(P+\tfrac{1}{3}W)\mathbf{U}]. \tag{39}$$

The latter equation, with the help of the other two, may be written as

$$\frac{dE}{dt}+\frac{1}{\rho}\frac{dW}{dt}=\frac{(P+4W/3)}{\rho}\frac{d\rho}{dt}, \tag{40}$$

that is, just the condition for constant entropy.

From the form of the Eqs. (37) and (38), it is apparent that the velocity of sound is given by

$$C=\left[\frac{\partial(P+\frac{1}{3}W)}{\partial\rho}\right]_S^{\frac{1}{2}} \tag{41}$$

as would be expected. The constant entropy condition, which is indicated by the subscript S, is expressed by Eq. (40). Since the radiation energy density is given by Eq. (23) or

$$W=3\beta(P/\rho)^4 \tag{42}$$

with

$$\beta=\frac{a}{3}\left[\frac{A}{(Z+1)N_0}\right]^4,$$

the velocity of sound becomes

$$C=\left[\left(\frac{\partial P}{\partial\rho}\right)_S^{\frac{1}{2}}\left[1+\frac{4}{3}W\left(\frac{1}{P}-\frac{1}{\rho}\left(\frac{\partial\rho}{\partial P}\right)_S\right)\right]^{\frac{1}{2}}\right]. \tag{43}$$

In the case that $W\ll P$, that is, for negligible radiation pressure, this reduces to the normal expression for the velocity of sound, as it should.

The derivative, $(\partial P/\partial\rho)_S$ may be evaluated with the help of Eq. (40), the thermodynamic equation of state, Eq. (18), and Eq. (42). Straightforward manipulation leads to

$$\left(\frac{\partial P}{\partial\rho}\right)_S=\frac{\gamma P+16(\gamma-1)W/3}{P+4(\gamma-1)W}\cdot\frac{P}{\rho}, \tag{44}$$

which reduces to the usual expression when $W\ll P$. For $W\gg P$, this becomes

$$(\partial P/\partial\rho)_S=4P/3\rho,$$

and Eq. (43) becomes

$$C=\tfrac{2}{3}(W/\rho)^{\frac{1}{2}}. \tag{45}$$

Under all conditions, the coefficient of P/ρ in Eq. (44) is larger than one. Consequently, the coefficient of W in Eq. (43) is positive. Therefore, the velocity of sound, C, is a steadily increasing function of the pressure, which is the required condition for the formation of a shock, as expressed in the beginning of the section.

The equation for the velocity of sound obtained in this section could also have been derived by applying Eqs. (1), (11), and (14) to the case of a very weak shock in a medium at high pressure (P_0, W_0 large).

8. CONCLUSION

It has been shown that the conditions prevailing in very intense steady shocks can be

obtained by a direct generalization of the Rankine-Hugoniot equations. These conditions yield simple quantitative results for a shock in a very light gas such as hydrogen. For other media, the equation of state and dependence of specific heat on temperature under extremely high temperature conditions are required. Because of this added complication, they have not been treated here.

The results obtained for the light gases are applicable only to plane shock waves of very long duration since the radius of curvature[4] and the length of the shock must be large compared to the thickness of the shock front. In turn, the thickness of the shock front is large compared to λ' and therefore to the free path for radiation, as shown in Section 3. Since the radiation free path is determined by Compton scattering for the gas of free electrons and unexcitable ions under consideration, it will be of the order of[9] 10^4 cm, which is undesirably large.

For the more practical case of a heavy gas, the greater part of the radiation frequency distribution will fall in the neighborhood of the absorption lines of the excited ions, so the radiation free path will be very short. However, the medium will still be nearly transparent to the high frequency tail of the distribution, so there will be a continual degradation of the energy in the shock front due to the loss of radiation of high energy. In a solid or liquid, the free path for almost the entire range of frequencies will be short, i.e., of the order of a millimeter, due to Compton scattering, since the density of electrons is very high. In this case, the medium is appreciably transparent only to the extremely high energy x-rays. Since the frequency of occurrence of such energetic quanta is extremely small, their escape should have only a small effect on the properties of the shock.

One further point is worth mentioning before concluding. In all of these considerations, it has been assumed that the shock wave is passing through a stable medium. However, at the temperatures prevailing in very intense shock waves, very ordinary media may undergo nuclear reactions. The existence of these reactions would lead to an added internal energy term in Eq. (14) and subsequent equations. If the reaction were sufficiently exothermic and the reaction rate were high enough,[10] a detonation wave rather than a shock wave would pass through the medium.

[9] See W. Heitler, *The Quantum Theory of Radiation* (Oxford University Press, New York, 1936), p. 157.

[10] *High enough* means that an appreciable fraction of the material must undergo a nuclear transformation within the duration of the shock wave. Reaction rates are usually quite slow even at the temperatures considered here because of the Coulomb potential barrier, so the duration of the shock would need to be quite long.

Influence of Polarized Light on the Falling-Off Effect of the Limiting Potential of Einstein's Photoelectric Law

ERICH MARX
*Rensselaer Polytechnic Institute, Troy, New York**

(Received April 26, 1944)

The investigation reported here deals with a special photoelectric effect which was discovered in 1929. It consists of the following phenomenon: If light of two different frequencies is incident on an insulated metal electrode the limiting potential of the electrode is determined not only by the light of higher frequency but also by the light of lower frequency. The light of lower frequency causes a drop in the value of the limiting potential. This effect, called here the "falling-off effect," was explained by an extension of the work function in Einstein's law to include the work necessary to overcome the space charge which is generated by the photons of lower frequency. This space charge is composed of electrons of insufficient energy to reach the range of the electrons generated by the photons of higher frequency. It seemed desirable to investigate the effect under varied experimental conditions, in particular with polarized light. In this case preliminary observations of Marx and Meyer seemed to show results which were not covered by the space charge theory. This new research, however, shows for the case of polarized light the quantitative correctness of the law of the falling-off effect as obtained before for unpolarized light. The theoretical dependence of the effect on the intensities and frequencies of the two components of the beam is verified experimentally. It was evident that the falling-off effect was conditioned more by the value of the intensities of the components than by their frequencies (cf. Fig. 8). It was shown, moreover, that certain unexpected results with polarized light were accounted for by the same space charge theory which explained the first observations.

1. INTRODUCTION

THE plan of the experimental investigation of which the first part is published here was developed in a lecture delivered at a meeting of the Texas Academy of Science.[1]

In several experimental papers[2-6] it has been pointed out that the potential to which an electrode charges itself when irradiated with light is lowered when light of a lower frequency is added to the original beam. Such an influence is not provided for by Einstein's fundamental law:

$$\epsilon V = h\nu - P, \tag{1}$$

where ϵ and h are the elementary charge and Planck's constant, V, the limiting potential of the photoelectrode; P the work function, and ν the highest frequency of the incident light. The law of decrease, called here the "falling-off effect," has been shown to be valid[4] for electrodes of K, Na, Rb, Cs, and theory shows that it will be valid for every photoelectric effect in vacuum.[6] This law is:

$$R = R_0 \frac{n_2\nu_1/\nu_2(\nu_1-\nu_2)h/\epsilon}{n_1 - bn_2}. \tag{2}$$

It represents the amount by which the Einstein potential is reduced when a radiation of lower frequency is added to the original beam. The expression shows the dependence of this reduction in potential, R, on the frequencies, and intensities, n_1, n_2, of the component radiations.

If $-dV/dx$ is the electric field near the photoelectrode which charges itself to a positive potential V and if x, the normal coordinate, is measured from the surface of the electrode, the work A which is done by the electron is given by

$$A = 4\pi\epsilon \int_{-\infty}^{+\infty} dx \int_{-\infty}^{x} \rho dx, \tag{3}$$

where ρ represents the density of the space charge.

Equation (3) shows that the work A to be done by the electron increases with increasing space charge. Therefore, whenever a space charge is present the work to be done by the electron will be evident in the limiting potential which will appear to be smaller than without the space

* This investigation was carried out at Trinity University, San Antonio, Texas, 1941–1942. The work was supported by a grant-in-aid from the Penrose Fund of the American Philosophical Society.

[1] E. Marx, Proc. Trans. Texas Acad. Sci. **26**, 33–38 (1943).
[2] E. Marx, Naturwiss. **17**, 806 (1929).
[3] E. Marx and A. E. Meyer, Physik. Zeits. **31**, 357 (1930).
[4] A. E. Meyer, Doctors Dissertation, Leipzig. Ann. d. Physik **9**, 787 (1931).
[5] E. Marx, Phys. Rev. **35**, 1059 (1930).
[6] E. Marx and A. E. Meyer, Physik. Zeits. **32**, 153–163 (1931).

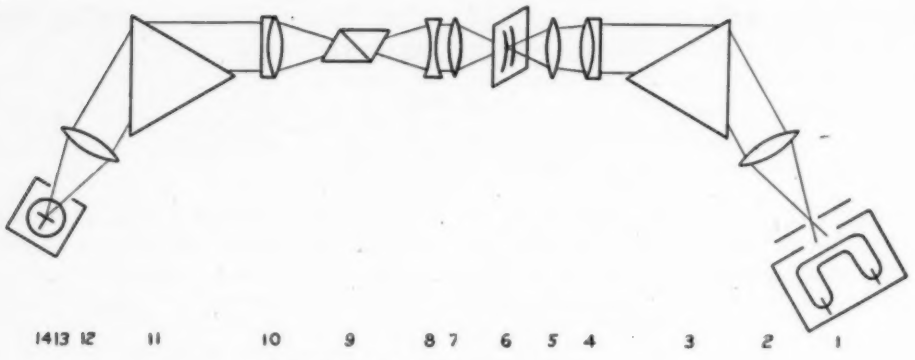

FIG. 1. Optical arrangement.

charge. This, however, is the case for every photoelectric effect, on account of the following fact:

Ramsauer[7] showed that the electrons liberated by monochromatic light are distributed over a rather extended range of velocities. All electrons which do not reach the distance of the fastest electrons return in a vacuum to the photoelectrode from which they started and build a space charge which is largest at the very point where they reach the velocity zero.

Let ρ be the density of electrons in the direction of propagation of the electrons; k, the coordinate of the maximum density corresponding to the maximum of the distribution of electron velocities; a, a constant of the dimension of ρ. The Ramsauer distribution of the electron velocities is described by the same curve for all spectral lines, if we set either the most frequent velocity or the maximal velocity equal to unity. If, therefore, we introduce instead of the x coordinate the coordinate x/k, we attach to every limiting potential unit value. The distribution of velocities coincides, however, as explained above, with the distribution of space charges at the photoelectrode. For this distribution we have

$$\rho=f(x)=a(x/k)^4(\exp[2x^2/k^2]-1)^{-1}, \quad (4)$$

where a has the dimension of charge density.

On account of this space charge distribution a part of the kinetic energy of the fastest electrons is lost and, therefore, the limiting potential is decreased. Integration of Eq. (3), if we substitute in it (4) and if we refer with a' and k' to the interior of the photoelectrode on the negative x axis, gives the work A to be done by the fastest electrons

$$A=4\pi\epsilon Cak(k+k'). \quad (5)$$

But this work A done by the electron, in passing a space charge is really the same work as that reduction in potential which is measured by R in formula (2) above. This was proved by physical and mathematical considerations developed in the earlier paper.[8]

It should be noted that even with strictly monochromatic light those electrons which have not the highest velocity return to the photoelectrode and are effective as a space charge especially at the point of return. This reduction of potential energy is, however, independent of the frequency and of the intensity* and will, therefore, not affect the linearity of the Einstein law.

The reduction of the limiting potential V in the case of a mixture of two frequencies represents an increase in the potential P/ϵ in Einstein's law which is generally denominated "work-function." The influence of the space charge on the limiting potential in this case is, however, of a new type. The phenomenon may be explained as due to a quasicondenser with the space charge as one side and the induced plus-charge on the photoelectrode as the other side. The maximum space charge due to the added frequency determines the law of decrease of potential.[8]

This extension of Einstein's photoelectric law has been discussed in some detail in the well-

[7] C. Ramsauer, Ann. d. Physik **45**, 961 (1914).

[8] E. Marx and A. E. Meyer, Physik. Zeits. **32**, 158 (1931).

* Cf. reference 6 Physik. Zeits. **32**, 153 (1931), ff. This was shown by formulating the differential equation of the equilibrium when the limiting potential was reached.

known textbook of Hughes and Du Bridge[9] in connection with their report of the experiments which deal with the falling-off effect.

The suggestion of these authors to investigate the effect further has been followed in the present investigation.

2. THE EXPERIMENTAL ARRANGEMENT

We wish to measure the limiting potential, when two monochromatic, polarized spectrum lines of known and variable intensity are combined on a potassium electrode, while no light falls on the counter electrode.

(a) Optical Arrangement

The light source for the measurements was a mercury arc of the Hanovia Chemical Manufacturing Company. The optical arrangement was a double monochromator, i.e., an arrangement of two spectroscopes in series. Figure 1 shows the diagram. The double slits[6] transmitted either the blue line $\lambda = 4358$A together with blue-green $\lambda = 4916$A or $\lambda = 4358$A together with green $\lambda = 5461$A or $\lambda = 4358$A together with yellow $\lambda = 5791/70$A. The whole arrangement was protected against light from other sources.

In most cases the images of the two lines were very approximately united on the same spot of the potassium electrode.

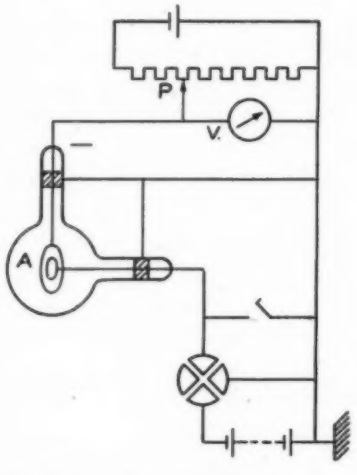

FIG. 2. Wiring diagram for measuring limiting potentials.

[9] A. L. Hughes and L. A. Du Bridge, *Photoelectric Phenomenon* (McGraw-Hill Book Company, Inc., New York and London, 1932), p. 505: Chapter, "The Marx Effect."

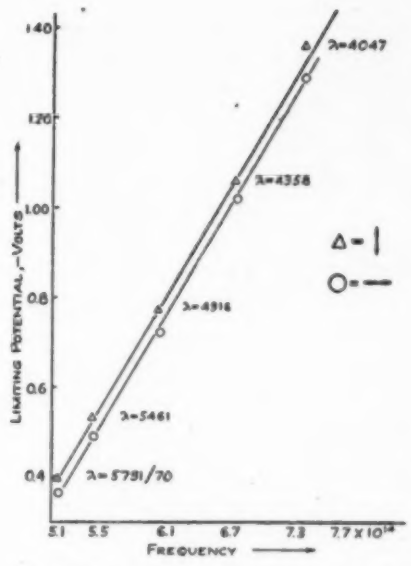

FIG. 3. Limiting potentials for various polarizations.

Directly behind the exit slit 13 was the cell shown in Fig. 4. Instead of it, 14 could be put, a technical Cs-cell from Pressler in Leipzig which measured relative intensities.

(b) Measurement of Limiting Potentials with Polarized Light at Normal Incidence

The photo-cell was irradiated with linearly polarized light at normal incidence and the limiting potential determined. The Nicol was then rotated through 90 degrees and the limiting potential again determined. Varying mixtures of frequencies and intensities were used. The potentials were measured as before by a compensation method. This compensation is obtained by applying a negative potential to the counter electrode such that the potential of the photo-electrode, connected with the electrometer, is the same during irradiation as it was without irradiation. Figure 2 gives the electrical connections. In the earlier investigations it was shown that this method gives extremely satisfactory results. The standard test for the correctness of the measurements is the linear dependence of V on ν and the value of the slope of V over ν.

Figure 3 shows the measurements for two mutually perpendicular directions of polarization of the incident light. The points are obtained as averages of about 12 series of measurements

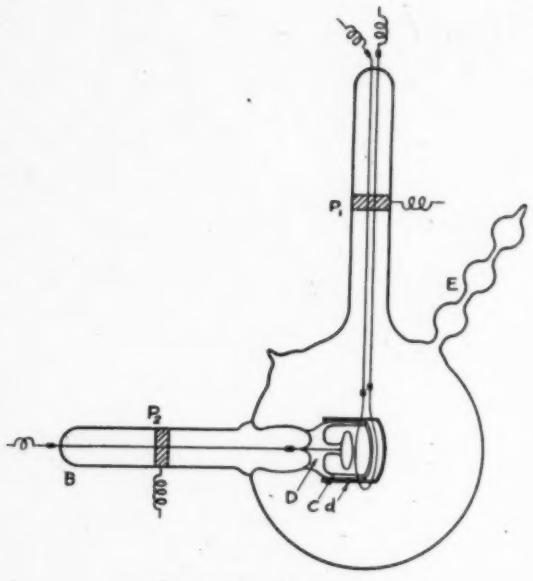

FIG. 4. The photo-cell.

with the same photoelectric tube. These graphs show clearly a linear dependence of V on ν.

The accuracy of the measurements with polarized light is not inferior to earlier measurements with unpolarized light. The slopes correspond to values of h/ϵ of about 4.16×10^{-15}- and 4.15×10^{-15}-volt seconds for the two different states of polarization. It is not easy to find the explanation as to why the limiting potentials (*L.P.*) of the polarized light in the two positions of the Nicol should not be the same. In both cases the light had normal incidence and the electrical vector of the beam was situated in the plane of the photoelectrode.

This same difference was found, however, with different tubes, not only of the construction described below, but even with the technical Cs-tube that was used (cf. below under *c*) for the measurement of relative intensities. In this case the Cs-electrode was connected with the electrometer and the limiting potential was compensated at the anode.

The explanation of the divergence of the absolute values of *L.P.* for the two orientations of the Nicol is the following: The requirement of enough light through the system to generate a *L.P.* at the photoelectrode which is independent of the intensity of the incident beam was attained by the arrangement of Fig. 1. The lenses 7 and 8 concentrate the light of the vertical slit 6 on the entrance plane of the Nicol 9. By this device the whole entrance plane of the Nicol is intensively illuminated. The lens system 10 and 12 formed an elongated strip-like image of the entrance plane of the Nicol on the photoelectrode of the tube 14. As a consequence when the Nicol was rotated the elongated spot of light on the electrode also rotated.

Now theory shows that the arrangement is very sensitive with regard to any displacement of the maximum k of the space charge, i.e., with the velocity distribution of the electrons which build up the space charge. As an indication of the correctness of the absolute values in both cases it should be noted that the slope of the two straight lines is the same. This indicates the correct value of h/ϵ. The supposition is, therefore, that the measured difference is real and that at different orientations of the Nicol the space charge distribution was such that the absorption of the fastest electrons was different in the two cases.

It seems possible and plausible that the influence of the earth's magnetic field in the laboratory generated different displacements for the electrons which were liberated by the two beams of light polarized perpendicular to each other, both having normal incidence on the photoelectrode. The electrons emerge from the electrode in a preferably normal direction with a maximum speed corresponding to one electron volt. The most frequent electron velocity corresponds in this case to about 0.4 electron volt or 2.38×10^{7} c.g.s.u. Let us suppose that the vertical component of the earth's magnetic field of 0.3 c.g.s.u. was acting on the electrons emitted from the illuminated strip. If the strip is horizontally orientated and the magnetic field vertical most of

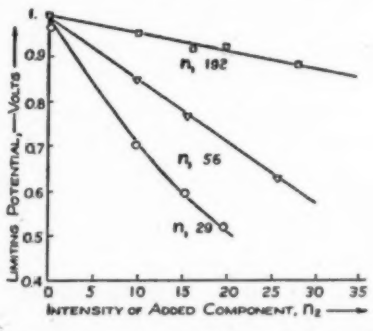

FIG. 5. Dependence of the limiting potential V upon the intensities of the components of a beam of polarized light composed of two wave-lengths.

the electrons with smaller speed will be deflected with a radius of curvature of 4.5 cm. This vertical deflection brings the electrons with smaller speed from amongst those of higher speed so that the course of the fastest does not cross the same amount of space charge as for the case of no magnetic field. When the Nicol is turned 90°, however, the magnetic field acts so that the deflection of the electrons is in the direction of the long dimension of the illuminated strip. The slow electrons will hence not be as effectively cleared from the beam as before. This results in an increase in space charge and a decrease in limiting potential. The observed difference in the limiting potential in both orientations is in this case of no principal interest but the explanation accounts fully for the influence of space charges on the value of the measured limiting potential for the two polarized rays.

(c) Measurement of the Intensities

The intensity of the incident light was measured with the same photo-cell which was used in my earliest measurements and in those of A. E. Meyer.[4] It is described in the doctor's dissertation of the latter.[4] The characteristics of the tube had not changed during the intervening time. It was a cesium cell with helium at about 1/100-mm pressure.

The reasons for measuring the intensity with a cesium cell of technical design rather than with the experimental cell or a thermopile were as follows: The experimental cell used here (Fig. 4) was not designed to measure currents but to measure potentials. Its field was non-linear. On the other hand, the cesium cell had approximately a linear field and indicated immediately and with great sensitivity an electronic current which was proportional to the incident intensity. The tube-current was measured with a galvanometer of sensitivity of 1.4×10^{-8} amp. per mm deflection. The mercury lamp (cf. 2a) was more constant than that used in earlier experiments.

This cesium cell was in turn calibrated in absolute units by a special Eppley bismuth silver thermopile with 24 junctions and a length of 35 mm. The light was concentrated on the junctions by a cylindrical lens. The galvanometer for the thermopile had the same resistance as the thermopile, about 23 ohms. The sensitivity was

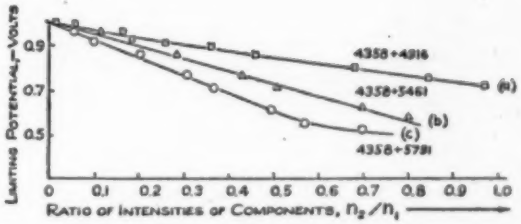

FIG. 6. Dependence of the *L.P.* upon the ratio of the intensities of the components n_2, n_1, for one intensity level of the primary component, n_1, and for different combinations of colors.

3.75×10^{-9} amp. per mm, but it permitted readings to 0.1 mm of the scale by reading at night.

This sensitivity was, however, not sufficient for determining the intensity of the violet line 4047A in ergs per sec. Therefore, this line was not used.[10] The current sensitivity of the cesium cell was much higher than that of the cell graphed in Fig. 4. If i_t is the current in the technical cell, i_p that in the potassium cell, then the values of i_t/i_p for the different wave-lengths 4358, 4916, 5461, and 5791A were 7.25, 18.9, 17, 8.75, respectively.

The limiting potential to which the photoelectrode Fig. 4 was brought by blue light of 4358 was independent of the intensity between the values of 4 ergs/sec. and 26.6 ergs/sec. The time to reach it was of course shorter in the second case.[11]

(d) Description of the Photo-Cell

The tubes used were of Pyrex glass and were skilfully blown by Mr. Charles Klump in San Antonio. They were evacuated by a Cenco diffusion pump. Figure 4 shows the tube.

The photoelectrode was a plate of sheet platinum, 2 cm in diameter, covered with potassium. This platinum electrode was attached to a platinum wire sealed into a narrow glass tube. A screw connected the electrode with a chromnickel wire carrying a platinum extension which was sealed at *B*. The chromnickel wire passed a grounded platinum cylinder P_2. This grounded cylinder was located two inches from the end of the tube.

This distance was necessary because this end had to be heated by a burner so strongly that

[10] For the method of performing such measurements refer to Ann. d. Physik 9, 795 (1931).

[11] With regard to the theory of this independence of the limiting potential on intensity see Physik. Zeits. 31, 3, 156 (1931).

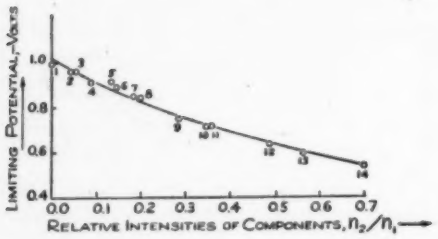

FIG. 7. Dependence of the *L.P.* upon the ratio of the intensities of the components, n_2, n_1, for all intensity levels of the primary component, n_1, and for a given combination of colors.

every trace of a potassium deposit which might form a shunt to the photoelectrode would be removed from it. This had to be done before each measurement, if checking by an electroscope in the dark showed incomplete insulation. The short tube *C*, sealed on the handle *D* of the electrode support, carried a cylinder *d* of red glass which was fixed on *C* by mica sheets. This method of fixing the red cylinder, which had to shield the anode against light, had to be used because at that time red glass which could be sealed on Pyrex glass was not available.

The anode consisted of a thin platinum wire loop which was arranged around the red cylinder so that the wire did not touch the glass. This anode could be heated through a Chromel lead and reached yellow heat at 2 amp. Heating before each measurement was necessary in order to make sure that no trace of potassium deposit would be on the anode. The side tube which held the anode was provided with a grounding cylinder which was in contact with the deposit on the inner wall, but not with the anode wire itself. The anode had to show insulation, even if checked by an electroscope.

The tube itself was thoroughly evacuated under heating to about 400 degrees C before the potassium was deposited. This had to be done in three stages using the three glass bulbs at *E*. The inside of the tube was covered with a thin potassium deposit which was grounded by the two grounding cylinders P_1 and P_2.

3. DEPENDENCE OF THE LIMITING POTENTIAL V UPON THE INTENSITIES OF THE COMPONENTS OF A BEAM OF POLARIZED LIGHT COMPOSED OF TWO WAVE-LENGTHS

Figure 5 shows for three different intensity levels of primary blue light, 4916A, the manner in which the *L.P.*, is affected by different additions of yellow light, 5791A.

It can be seen from the slopes of the curves that the higher intensity levels of the primary blue light permit a proportionately greater amount of the added secondary light for a given reduction in *L.P.*

The law of dependence of the *L.P.* on intensity and frequency is easier to recognize from Fig. 6. The curves show that for the addition of a second radiation of varied intensity and frequency the *L.P.* depends only on the intensity ratio, n_2/n_1, and that the drop in *L.P.* or the falling-off effect increases with the difference between the frequencies of the primary and added beam. The influence observed here is completely accounted for by formula 2 given by the theory.

This formula also contains the factor b which explains the deviation of the *L.P.* from linearity which is particularly apparent in curve *c*. Note that this is also more apparent when the added component has a frequency widely different from the primary light and then at relatively high n_2/n_1.

This dependence of the *L.P.* on the ratio of the intensities and its independence of the absolute levels of the intensities becomes more evident if we plot n_2/n_1 against *L.P.* in a single curve for different levels of n_2 (5791A) and n_1 (4358A). This is shown by Fig. 7. The particular points which build up the curve are obtained by combining different intensity levels of the same colors. Point (2) and (3) are obtained from $n_2/n_1 = 1.48/29$ and $10.9/192$; Point (6), (7), and (8) from $n_2/n_1 = 27.8/192$, $10.9/56$, and $37.7/192$; Point (9), (10), and (11) from $16.5/56$, $10.9/29$, $20.5/56$; Point (12), (13), (14) from $27/56$, $16.5/29$, and $20.5/29$.

Figure 7 can be used to determine the numerical constants of formula 2. This can be done in the following way. If we put (2) in the form

$$R=\frac{h}{\epsilon}-R_0\frac{(\nu_1-\nu_2)\nu_1}{\nu_2}\frac{n_1}{n_2}\frac{1}{1+bn_2/n_1}\text{ volts},$$

we get for blue and yellow light

$$(\nu_1-\nu_2)\nu_1/\nu_2=2.19\times10^{14};\quad h/\epsilon=0.4115\times10^{-14}.$$

To determine R_0 we choose a point on the linear part of the curve. Thus we obtain $R_0=0.913$.

To determine $\mathfrak{b}$ we choose a point from the non-linear part of the curve and find $\mathfrak{b}=0.378$. With these constants we obtain

$$R=0.82n_2/n_1\frac{1}{1+0.378n_2/n_1} \qquad (2')$$

which shows the dependence of R on the intensities n_1 and n_2 for this particular combination of blue and yellow light. This is the curve given in Fig. 7.

We can now see the important factors that condition the drop in the *L.P.* or the falling-off effect, namely, that while for monochromatic light the *L.P.* is independent of intensity, for non-monochromatic light the *L.P.* is dependent on the ratio of the intensities of the components. Both are results of the theory of the space charge interference given before by Meyer and the author.[12] This theory is now shown to be also valid for polarized light. If we restrict the observations that are graphed in Figs. 5, 6, and 7 to such relatively small additions of (n_2), to the primary beam, (n_1), that they produce no deviation from the linear slope of the *L.P.*, we can show that all observations given in Figs. 5, 6, and 7 for the combined colors of 4358A, 4916A, 5461A, and 5791/70A result in a general law for the falling-off of the *L.P.*, namely:

$$R=NR_0 \ (2''),$$

where

$$N=n_1/n_2\times(\nu_1-\nu_2)/\nu_2\times\nu_1h/\epsilon \text{ volts}$$

is the factor which determines the falling-off effect of the *L.P.* through the parameters n_1, n_2 and ν_1, ν_2.

Figure 8 demonstrates the general dependence of the limiting potential for all used colors and intensities for the numerous observations registered before. The identity of the particular points of this curve with those registered above in Fig. 6 is easy to see from the different symbols of the colors and the reference given for this graph. All colors and intensities now appear arbitrarily

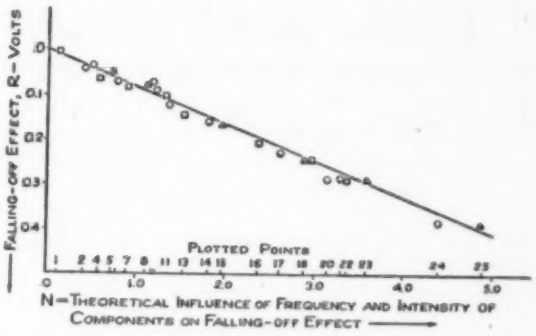

FIG. 8. General dependence of R on the simultaneous variation of the frequency and intensity of the components showing the preponderant effect of the ratio of the intensities over that of the frequencies. The symbols of the points in the figure are: □ bluegreen (4916A) component at 1, 4, 7, 11, 13, 16, 19, 22 (all taken from Fig. 6a); △ green (5461A) at 5, 8, 15, 18, 23 (all taken from Fig. 6b); ○ yellow (5791/70A) at 2, 3, 6, 9, 10, 12, 14, 17, 20, 24 (all taken from Fig. 6c).

distributed but all follow the rule derived from the theory of the falling-off effect developed for non-polarized light, and extended here for the case where the incident light is polarized and brought in the simple form (2″).

Values at the end of curves 6*a*, 6*b*, and 6*c* were not plotted in Fig. 8 because they show deviations of linearity corresponding to theory and can therefore not prove the simple law given by (2″).

The N's which correspond to the observation-numbers 1 through 25 vary from 0.14 to 4.82 showing the combined influence of varying n_1, n_2, ν_1, ν_2 upon the falling-off effect. The influence of the frequency appears less significant than that of the intensity ratio.

This investigation was carried out at Trinity University, San Antonio, Texas. It was made possible by a grant-in-aid from the Penrose Fund of the American Philosophical Society in Philadelphia.

I was supported in the experimental work by Mr. Werner Guthry of Trinity University, San Antonio. Dr. Max Delbrueck of Vanderbilt University and Dr. G. Howard Carragan of Rensselaer Polytechnic Institute were kind enough to read the manuscript before printing. I am especially indebted to Dr. Carragan for his kind help in the final edition of the paper.

[12] Erich Marx and A. E. Herbert Meyer, Physik. Zeits. 31, par. 3, 156 (1931).

Letters to the Editor

PROMPT publication of brief reports of important discoveries in physics may be secured by addressing them to this department. The closing date for this department is the third of the month. Because of the late closing date for the section no proof can be shown to authors. The Board of Editors does not hold itself responsible for the opinions expressed by the correspondents. Communications should not in general exceed 600 words in length.

Some Aspects of Meek's Sparking Equation

LEON H. FISHER
Department of Physics, University of California, Berkeley, California
March 5, 1946

IN his paper, "A Theory of Spark Discharge," Meek[1] formulated a quantitative criterion for sparking by means of the streamer mechanism. This criterion led to Meek's equation for sparking. In the above paper, Meek compares values of sparking potentials for air as calculated from his equation with data given by Whitehead.[2] Meek found his calculated values to be in good agreement with those experimentally observed for values of $p\delta$ (pressure $\times$plate distance) from 10,000 to about 100 mm$\times$cm. According to Meek, the calculated values are higher than the observed ones for $p\delta$ less than 100 mm$\times$cm, and the deviation increases steadily with decreasing $p\delta$. Below this value of $p\delta$, it is assumed that the discharge proceeds by means of the Townsend type of mechanism, the positive ion density becoming too low to insure adequate photo-ionization for streamer formation.

In connection with some recent measurements of sparking potentials, the writer has had occasion to examine in some detail the nature of the departure of the theoretical from the experimental curve at small values of $p\delta$. In an attempt to reproduce Meek's curve, the pressure was taken as 760 mm, and the gap length was varied to obtain varying values of $p\delta$. The original value of $K=1.0$ in Meek's equation has been replaced subsequently by the value $K=0.1$. Recent measurements by the author[3] show that the proper value of K is much less than 0.1. Using this small value of K, with constant pressure (760 mm), Meek's equation was used to calculate sparking potentials down to 10 mm$\times$cm. Excellent agreement (to within a few percent) was obtained down to this value of $p\delta$ with the data given by both Whitehead[2] and Schumann.[4] Changing K to 0.1 gave values which were 20 percent higher than the experimental values at $p\delta=10$ mm$\times$cm. (Changing K from 0.1 to 1.0 has very little effect.) Meek's curve (with $K=1.0$) calls for a departure of about 70 percent at $p\delta=10$ mm$\times$cm.

It is apparent that Meek's curve was not obtained by the procedure outlined here. Quite probably he used a constant gap distance (near one centimeter) with varying pressure. Using a lower value of K he would not have found so much deviation at low $p\delta$. It has been pointed out by Meek that his equation does not obey Paschen's law. It particularly fails to do so at low $p\delta$ when $p\delta$ remains constant and δ varies by a factor of one hundred.

If one examines Whitehead's summary of data at low $p\delta$, one finds variations as great as 50 percent among various observers. Therefore existing experimental data taken over a long time with poorly controlled conditions cannot be used to support Meek's claim that his equation fails at low $p\delta$ or the possibility pointed out by the writer that at high pressures no deviation occurs at all. Indeed, both conclusions may be correct for, as has been pointed out,[5] Paschen's law has never been verified over an extended pressure range. To answer the question, a set of carefully controlled experiments are needed in which $p\delta$ is varied by changing first pressure, then gap length. These experiments should be carried out in a single laboratory.

There is some basis for believing that both Meek's and the writer's contentions are true. For constant δ, the positive ion concentration decreases with decreasing $p\delta$, and the streamer mechanism probably does become inoperative at low $p\delta$. At constant pressure, the positive ion density *increases* with decreasing $p\delta$. Thus it may be that the streamer mechanism continues to be effective at high pressures and low $p\delta$.

[1] J. M. Meek, Phys. Rev. **57**, 722 (1940).
[2] S. Whitehead, *Dielectric Phenomena* (D. Van Nostrand Company, Inc., New York, 1927), p. 42.
[3] L. H. Fisher, Phys. Rev. **65**, 153 (1944).
[4] W. O. Schumann, *Durchbruchfeldstärke durch Gasen* (Verlagsbuchhandlung Julius Springer, Berlin, 1923), p. 25.
[5] Reference 4, p. 115.

Synthesis by Nuclear Recoil*

ALLEN F. REID
Columbia University, New York, New York
March 18, 1946

THIS is an investigation in the use of nuclear recoils in specific synthesis to afford efficient methods of producing radioactive isotopes in high specific activity either in the synthesized compound or a derivative or decomposition form; it was primarily started in an attempt to synthesize a highly radioactive compound for medical use. The Szilard-Chalmers' technique[1] makes use of these recoils to break selectively the chemical bonds of activated atoms; in the experiments recorded here the purpose was to utilize this energy for synthesis. The choice of reactants used was a matter of convenience and ease of manipulation. The synthesis attempted was

$$I^{127}+n\rightarrow I^{128}+\gamma$$
$$C_5H_{12}+I^{128}\text{ (on recoil)}\rightarrow C_5H_{11}I^{128}+H.$$

A solution (A) of 0.103 g I_2 in 40 cc normal pentane was made up. This, along with the same amount of undissolved I_2, was irradiated with slow neutrons from the Columbia cyclotron; then the I_2 was dissolved in 40 cc normal pentane (solution (B)). The solutions were then resolved to determine distribution of the I^{128} activity. The I_2 was quantitatively removed with 0.08M $Na_2S_2O_3$ solution; n-amyl iodide was added as a carrier and the amyl iodide and pentane separated by distillation. Activities were measured by means of a Geiger-Mueller counter. In B, <0.5 percent of the I^{128} activity was found in the amyl

iodide and pentane fractions. In A, 38±3 percent of the activity followed the n-amyl iodide, the remainder was in the elementary I_2 form. The organic I^{128} probably was distributed among all amyl iodides but no attmpt was made to resolve the amyl iodide fraction further. Removal of most of the I_2 in A from the pentane was accomplished within 15 minutes after the end of the 5-minute irradiation period, so little amyl iodide-iodine exchange was probable.

In two subsequent runs in which the slow neutron source arrangement was different and in which longer time intervals elapsed between separation of the I_2 and amyl iodide, >23 percent of the I^{128} activity of the irradiated solutions was found with the amyl iodide, as against <3 percent of the activity in the amyl iodide fractions from the controls.

The results of these experiments show that nuclear recoils may be used in specific synthesis furnishing compounds with very high specific radioactivity, though no satisfactory estimate can be made at this time of the extent of the application. Further exploration along these lines is planned.

* Publication assisted by the Ernest Kempton Adams Fund for Physical Research at Columbia University, New York.
[1] L. Szilard and T. A. Chalmers, Nature **134**, 462 (1934).

The East-West Asymmetry of Cosmic Radiation at a Geomagnetic Latitude of 28°31′ and an Estimation of the Difference of the Exponents of the Absorption Law for the Polar and the Equatorial Regions

FRANCIS OSTER, SHENG-LIN CH'U,* AND LIEH-YANG LO
The Catholic University, Peiping, China
March 15, 1946

WITH a conventional triple coincidence G-M counter arrangement, the east-west asymmetry of cosmic radiation was measured in Peiping, China, which is at a longitude 116°20′E and a latitude 39°56′N. The geomagnetic latitude of the city was calculated[1] to be 28°31′. The result of the measurement is given in Table I and shown in Fig. 1. The asymmetry is represented by $A=(I_W-I_E)/[(I_W+I_E)/2]$, which is plotted as ordinate in the graph, I_W and I_E being the counting rates for the west and the east incident rays, respectively.

TABLE I. Measurements showing east-west asymmetry at Peiping, China.

Zenith angle θ	$A=\frac{I_W-I_E}{\frac{I_W+I_E}{2}}$	Δr_e	$A'=A\frac{0.15}{\Delta r_e}+1$	$h=10\sec\theta$	$\log A'$	$\log h$
15°	0.033±0.014	0.046	1.108	10.35	0.0444	1.015
30°	0.059±0.018	0.098	1.090	11.55	0.0375	1.063
45°	0.067±0.019	0.16	1.063	14.14	0.0264	1.151
50°	0.074±0.021	0.18	1.062	15.56	0.0258	1.192
55°	0.059±0.027	0.20	1.044	17.43	0.0187	1.241
60°	0.036±0.031	0.22	1.024	20.00	0.0103	1.301

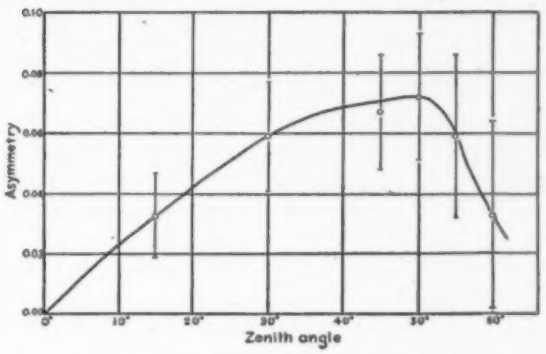

FIG. 1. East-west asymmetry against zenith angle.

It was suggested by Johnson[2] that the difference of the exponents of the absorption law $I=A/h^n$ for the polar and the equatorial regions can be more precisely determined from the analysis of the asymmetry measurements. In the present calculation the range of the threshold energies, by which the value of A was to be divided, was obtained by interpolation of Lemaitre and Vallarta's function[3] for the latitudes 0°, 20°, and 30°; thus, curves were drawn with the threshold energy against the latitude for different zenith angles both in the east and the west directions, then the ranges of the threshold energies for different zenith angles at our latitude 28°31′ were read from these curves. As there are only three points for each curve, the estimation cannot be very accurate; yet as our latitude 28°31′ is very close to 30°, for which the threshold energies were given by Lemaitre and Vallarta, the error cannot be large. Figure 2, a logarithmic plot of $A(0.15/\Delta r_e)+1$ against the atmospheric path h, shows that the points lie nearly on a straight line, the slope of which gives the value $\delta(=\Delta n)$, which was found to be 0.12.

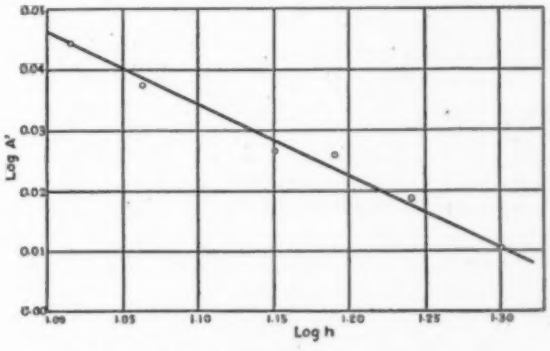

FIG. 2. Logarithmic plot of $A(0.15/\Delta r_e)+1$ against the atmospheric path h.

* Now at Yenching University, Peiping, China.
[1] A. H. Compton, Phys. Rev. **43**,387 (1933).
[2] T. H. Johnson, Rev. Mod. Phys. **10**, 193 (1938).
[3] G. Lemaitre and M. S. Vallarta, Phys. Rev. **50**, 493 (1936).

Remarks on the Fine Structure of "Positronium"

GUIDO BECK
Observatorio Astronómico, Córdoba, Argentina
March 14, 1946

IN a recent letter Dr. Ruark* has pointed out the importance of using positron beams, now available with sufficient intensity, in order to study the spectrum of the system electron-positron, which he calls "positronium." Dr. Ruark states that none of these lines can be found in necular spectra, in agreement with what Dr. Gaviola pointed out to me some time ago.

The purpose of this letter is to emphasize the importance which Dr. Ruark's suggestion would have, if the fine structure of the positronium spectrum could be measured. The theory of this spectrum has been discussed in detail by Mr. Jean Pirenne in Lyon (France), but his paper, printed in France during the war, has not yet reached us. I have to refer, therefore, to the part of his manuscript which I was able to bring with me in 1942.

According to Mr. Pirenne's calculations, the annihilation probability of positronium depends considerably on the characteristics of the different levels and does not exclude the possibility of obtaining the fine structure of the spectrum, which, in its turn, depends on features of quantum field theory which present actual interest:

(*a*) Positronium represents only one part of the general problem of interaction of two Dirac electrons: electron-electron, electron-positron, positron-positron. It obeys Pauli's principle if one considers the charge sign as an additional bivalent variable, similar to the spin.

(*b*) Apart from trivial interaction terms, we find two short range (δ-function) interaction terms. The first of these terms

$$V_\sigma = -q\mu^3({}^1\sigma^2\sigma)\delta(r_{12}), \qquad (1)$$

(q=numerical constant, μ=Bohr's magneton) appears even in the case of like particles and is already known from Fermi's hyperfine-structure formula for the interaction between two spins.

The second term,

$$V_a = -q'\mu^3\tau\{1+\tfrac{1}{2}(1+{}^1\sigma^2\sigma)\}\delta(r_{12}) \qquad (2)$$

(q'=numerical constant, τ=electron-positron exchange operator) refers only to unlike particles. This term has been found, for the first time, by Bhabha** and can be considered as resulting from an annihilation of the pair, followed by a reproduction of a pair with different momentum direction.

(*c*) Both terms influence the fine structure of the positronium spectrum, which could determine the numerical values of q and q', the magnitude of which is doubtful. Quantum electrodynamics, as used by Møller and Bhabha, represents the singular field functions by their Fourier decompositions and leads to the values

$$q=4\pi,\ q'=4\pi$$

while Fermi's semi-classical treatment leads to

$$q=8\pi/3.$$

* A. E. Ruark, Phys. Rev. **68**, 278 (1945).
** Bhabha, Proc. Roy. Soc. **A154**, 195 (1936); see also G. Beck, Phys. Rev. **64**, 374 (1943).

Thermal Recrystallization of Quartz

D. D'EUSTACHIO AND S. GREENWALD
Bliley Manufacturing Corporation, Erie, Pennsylvania
March 30, 1946

IN a previous study,[1] it was reported that thin wafers prepared from single crystals of quartz are no longer single crystals. The present writers have continued to study the phenomenon. A better and more rapid method of preparing the wafers has been developed. Improved technique has also made possible the use of filtered radiation. The results of the new work show that the wafers are composed of polycrystalline material, each crystal being slightly disoriented with respect to its neighbor. The range of disorientation observed in etched wafers varied from one to two degrees. For any given setting of the wafers, only a small portion (10–30 percent) of the irradiated area reflected monochromatic radiation. The areas from which reflection occurred changed as the plate was rotated. After the quartz had been heated, the observed x-ray reflections resembled those obtained with normal, thick, single crystals. The range through which reflection occurred decreased to 5′–15′, while the area contributing to a reflection increased to 70–90 percent. The temperatures required to produce this effect were surprisingly low. Approximately 100 hours at 500°C, 40 hours at 600°C, 20 hours at 700°C, and less than 9 hours at 800°C were required to change the quartz so that it was again reasonably good crystal. Figure 1 is a plot of the logarithm of the time required for "recrystallization" *versus* the reciprocal of the absolute temperature. The points lie very nearly on a straight line.

If a thin plate, after being heated, was bent 25 to 50 times around a cylinder 3 to 4 cm in diameter, the quartz returned to the "polycrystalline" state. The process was

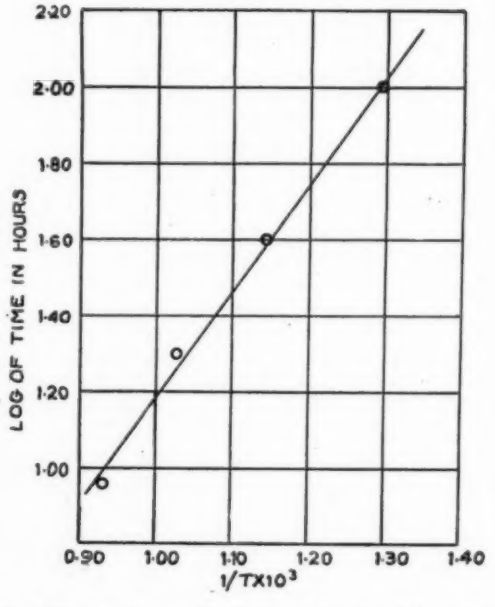

FIG. 1. Time for "recrystallization" as a function of temperature.

reversible, the crystal reverting to the "single crystal" condition after it was heated again.

The wafers used in these experiments were from 25 to 30 microns thick. They were cut so that the major surface formed an angle of $12°\pm20'$ with the $10\bar{1}1$ plane. The plates were lapped to a thickness of about 40 microns and then etched to the required thickness. Care was taken in all cases to use the same area of the wafer for successive pictures. Since the area irradiated was 3 mm×10 mm this could be done with great accuracy. In Fig. 2 are reproduced

a b c

FIG. 2. CuKα reflection from $10\bar{1}1$ plane in quartz. (a) Before heating, (b) after heating to 600°C for 40 hr., (c) after bending 50 times around a cylinder 3 cm in diameter.

photographs of the Bragg reflection from the $10\bar{1}1$ plane obtained with a plate 27 microns thick.

The degree of recovery observed suggests that the material cannot be truly polycrystalline, but is rather composed of a series of slightly disoriented crystals connected with regions of badly distorted material. This view of good crystal surrounded by badly stressed or even glassy material is further supported by Laue photographs taken with an x-ray beam about eight microns in diameter. The spots obtained from the unheated "polycrystalline" material are sharper than those obtained either from heat-treated material or thick specimens.

A more detailed report is in process of preparation.

[1] D. D'Eustachio and S. B. Brody, Paper presented at the American Physical Society, January, 1946.

Angular Correlation of Successive γ-Rays

G. GOERTZEL* AND I. S. LOWEN
Washington Square College, New York University
Washington Square, New York
April 1, 1946

THE correlations between the directions of emission of successive γ-rays from an atomic nucleus have been investigated both theoretically[1] and experimentally.[2] The writers have extended these calculations to take into account the effect of reorientation of the nuclear angular momentum caused by the interaction of the nuclear magnetic moment with the moment of the external electrons. Formulae have been derived for angular correlations valid for all multipole orders both in Hamilton's approximation, where interaction with the external electrons is omitted, and in the case where such interactions are taken into account.

For the purpose of this calculation, the state of the atom is specified by quantum numbers I, J, F, m, representing, respectively, nuclear spin, electronic angular momentum, total angular momentum, and the component of the total angular momentum on the Z axis. When the hyperfine structure splitting of the energy levels can be neglected, I, J, F, m, may be replaced by the quartet I, J, m_I, m_J. Since J and m_J do not change, one need consider I and m_I only.[1]

For the angular distribution in the I, J, F, m scheme, the following is obtained

$$W=\Sigma_{nn'lpe'e''}|(A_l|H(\mathbf{k}\cdot\mathbf{e}')|B_n)|^2 S_{nn'}|(B_{n'}|H \times(\varkappa_0''\cdot\mathbf{e}'')|C_p)|^2,\ l=n\pm1,$$

where

$$S_{nn'}=\Sigma_{FF'rqm}\frac{(IJFm|IJn'q)(IJn'q|IJF'm)(IJF'm|IJnr)(IJnr|IJFm)}{1+(2\pi\tau_B\nu_{FF'})^2}.$$

The notation used here in specifying the matrix elements is identical with that of reference 1. In the expression for $S_{nn'}$, I and J are the nuclear and electronic angular momentum quantum numbers of state B; n and n' are possible values of the projection of I on the Z axis; r and q bear the same relation to J. $(IJFm|IJn'q)$ represents the well-known transformation coefficient.[3] τ_B is the life time of the state B and $\nu_{FF'}$ is the hyperfine structure separation of levels of state B characterized by F and F'. It follows from the unitary properties of the transformation coefficients that, if $2\pi\tau_B\nu_{FF'}\ll1$, $S_{nn'}=(2J+1)\delta_{nn'}$, which then gives Hamilton's results for the angular distribution.

In order to obtain a formulation for the solution of the angular distribution problem for a general case, the expansion of the radiation field in terms of spherical eigenwaves was used.[4] One then obtains for the angular distribution in a case in which the first transition corresponds to a $2^{l'}$ pole and the second to a 2^l pole

$$W=\Sigma_n(g^{l'}{}_{n+1,n}+g^{l'}{}_{n-1,n})[G^l{}_{nn}f_{l0}(\vartheta)+\sum_{m=1}^{l}(G^l{}_{n,n+m}+G^l{}_{n,n-m})f_{lm}(\vartheta)],$$

where

$$f_{lm}(\vartheta)=E^*{}_{lm}E_{lm}+E^*{}_{l,-m}E_{l,-m},$$

$$E_{lm}=\tfrac{1}{2}e^{-i\varphi}(1+\cos\vartheta)[(l+1-m)(l+m)]^{\frac{1}{2}}Y^{-m+1}{}_l+m\sin\vartheta\,Y^{-m}{}_l-\tfrac{1}{2}e^{i\varphi}(1-\cos\vartheta)[(l+1+m)(l-m)]^{\frac{1}{2}}Y^{-m-1}{}_l,$$

$$g^{l'}{}_{n\pm1,n}=|(A_{n\pm1}|Y^{\pm1}{}_{l'}|B_n)|^2,$$

$$G^l{}_{n,n\pm m}=|(B_n|Y^{\mp m}{}_l|C_{n\pm m}|^2.$$

The $Y^m{}_l$ are spherical harmonics with Condon and Shortley's definition of phases.[3] The values of the f's, g's, and G's for $l=1$ or 2 are of course identical with those used by Hamilton.

Specific calculations with these formulae indicate that, as the hyperfine structure separation of the intermediate level increases, the angular correlation grows less. Some such effect as this may be partly responsible for the small angular correlation observed experimentally by Beringer.[2]

Finally, the writers wish to point out that correlations analogous to those of the γ-rays may be expected for the electrons emitted in the internal conversion of successive

γ-rays. Calculations now under way confirm this expectation. Owing to the higher efficiency of counters for electrons than γ-rays, such correlations may be easier to observe experimentally.

* This work was carried out while one of us (G.G.) held a fellowship from the Radio Receptor Company, Inc., of New York.
[1] D. R. Hamilton, Phys. Rev. **58**, 122 (1940).
[2] R. Beringer, Phys. Rev. **63**, 23, (1943); Y. Watase, Proc. Phys. Math. Soc. Japan **23**, 618 (1941); S. Kikuchi, Y. Watase, and J. Itoh. Zeits. f. Physik **119**, 185 (1942).
[3] E. U. Condon and G. H. Shortley, *Theory of Atomic Spectra* (The Cambridge University Press, New York, 1935).
[4] W. Heitler, Proc. Camb. Phil. Soc. **32**, 112 (1936).

Effect of Absorption on Decay of Infra-Red Sensitive Phosphors*

R. T. Ellickson and W. L. Parker
Polytechnic Institute of Brooklyn, Brooklyn, New York
April 1, 1946

THERE have been different opinions expressed regarding the order of the process involved in the decay of infra-red sensitive phosphors.[1] Urbach and Ward presented some evidence from excitation and exhaustion curves that the process was of the second order for alkaline earth sulfides and selenides. Fonda reported that there was evidence that the decay of the natural phosphorescence of ZnS was according to a second-order process while the decay of the phosphorescence due to infra-red stimulation was according to a first-order process.

By taking into account the absorption of the incident infra-red and the emitted visible light, we have derived an equation for the decay curve under infra-red stimulation. The derivation is based on a second-order process and is similar to one made by de Groot[2] for the decay of the luminescence of ZnS. The usual expression for a second-order process is $B=B_0(1+\alpha t)^{-2}$ where B is the brightness, B_0 is the initial brightness, and α, in our case, is proportional to the infra-red intensity, the infra-red absorption coefficient, and the quantum efficiency. Because of absorption, α has a different value at different depths in the phosphor and the simple equation above should be replaced by

$$B(t)=B_0\int_0^\infty \frac{\exp[-(\mu_1+\mu_2)x]}{(1+\alpha t\exp[-\mu_1 x])^2}dx, \qquad (1)$$

where μ_1 and μ_2 are the absorption coefficients for infra-red and visible light. By a simple change of variable, Eq. (1) becomes

$$B(t)=B_0\frac{P+1}{(\alpha t)^{P+1}}\int_0^{\alpha t}\frac{y^P}{(1+y)^2}dy, \qquad (2)$$

where $p=\mu_2/\mu_1$.

It is easily shown that the slope of a logarithmic plot of the decay curve at large values of the time is $-(p+1)$ if $p\leqslant 1$. This explains the failure of our decay curves to give the value of -2 for this slope as required by the simple theory.

Figure 1 shows the decay in brightness of a strontium selenide-samarium-europium phosphor under infra-red stimulation. The curve is calculated from Eq. (2) with $B_0=13{,}800$, $\alpha=1.30$, and $p=0.25$ for which Eq. (2) becomes

$$B=13{,}800\frac{1.25}{(1.3t)^{1.25}}\left[\frac{1}{4\sqrt{2}}\ln\frac{(1.3t)^{\frac{1}{4}}+\sqrt{2}(1.3t)^{\frac{1}{4}}+1}{(1.3t)^{\frac{1}{4}}-\sqrt{2}(1.3t)^{\frac{1}{4}}+1}+\frac{1}{2\sqrt{2}}\tan^{-1}\frac{\sqrt{2}(1.3t)^{\frac{1}{4}}}{1-(1.3t)^{\frac{1}{2}}}-\frac{(1.3t)^{\frac{1}{4}}}{(1+1.3t)}\right].$$

No precise measurements of the absorption coefficients have been made, so it is not possible for us to check the value of 0.25 obtained here for p. The excellent agreement with the experimental data leads us to believe that the form of the equation is essentially correct.

The details of the calculation will be submitted for publication in the very near future.

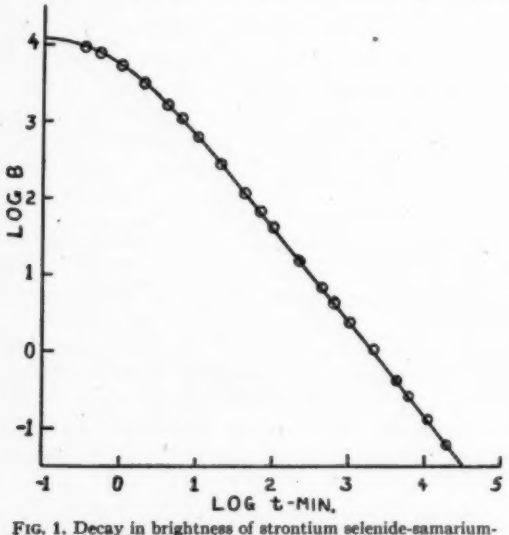

Fig. 1. Decay in brightness of strontium selenide-samarium-europium phosphor under infra-red stimulation.

* The work described in this letter was carried out under Contracts OEMsr 982 and NObs 28370 between the Polytechnic Institute of Brooklyn and the Office of Scientific Research and Development, and the Bureau of Ships, respectively.
[1] See the reports of Urbach, Ward, Fonda, *et al.*, Report of the March, 1946 meeting of the Optical Society of America at Cleveland, Ohio.
[2] W. de Groot, Physica **7**, 432 (1940).

The Origin of the Synchrotron

Edwin M. McMillan
Radiation Laboratory, Department of Physics, University of California, Berkeley, California
April 18, 1946

A RECENT letter by Veksler[1] has made me aware of the fact that the failure to refer to his previously published work in my letter on the synchrotron[2] may have created an unfortunate impression. The reason for this failure is simply that I was entirely ignorant of his work until it was pointed out to me near the end of October, after my letter had appeared.

This seems to be another case of the independent occurrence of an idea in several parts of the world, when the time is ripe for the idea. The present great interest in very high energy particles furnished the need for new methods of acceleration, and the principle of phase stability applied to cyclotron-like devices is a promising solution. Since my first thoughts on the subject occurred near the beginning of July, 1945, it is clear that Veksler's discovery of the principle was earlier.

[1] V. Veksler, Phys. Rev. **69**, 244 (1946).
[2] E. M. McMillan, Phys. Rev. **68**, 143 (1945).

Radii of the Nuclei of Natural α-Emitters

M. A. PRESTON*
Department of Mathematics, University of Toronto, Toronto, Canada
April 22, 1945

THE standard theories[1] of α-radioactivity based on the one-body rectangular hole potential appear to obtain only one relation between λ, the decay constant, E, the energy of the α-particle, and r_0, the radius of the nucleus. However in the course of their arguments, all these writers make an assumption involving the potential of the hole, *viz.*:

$$\mu k r_0 = \pi, \tag{1}$$

where $\mu=(1-U/E)^{\frac{1}{2}}$, U=constant potential for $r<r_0$, $k=(2mE)^{\frac{1}{2}}/\hbar$, m=mass of α-particle.

Sexl[2] has shown that a more rigorous treatment yields the following two formulae.

$$\mu = -\tan\alpha_0 \tan(\mu k r_0), \tag{2}$$

$$\lambda = \frac{2v}{r_0}\cdot\frac{\mu^2\tan\alpha_0}{\mu^2+\tan^2\alpha_0}\cdot\exp\{-\kappa(2\alpha_0-\sin 2\alpha_0)\}, \tag{3}$$

where $\alpha_0=\arccos(Er_0/2e^2Z)^{\frac{1}{2}}$, $\kappa=4e^2Z/\hbar v$, v=velocity of α-particle, and Z=charge number of product nucleus. Equation (2) replaces (1) and accurate calculations using (2) and (3) show that $\mu k r_0$ is always less than π by about 0.2 radian, raising the values found for r_0 by about 5 percent.

Equations (2) and (3) hold only for zero spin difference between original and product nuclei. Sexl also gives formulae for $l\neq 0$, but they appear to be based on inaccurate approximations. The same holds true for all other formulae for $l\neq 0$.

It will be shown elsewhere that Sexl's result can be obtained in a simpler and more rigorous way and also generalized correctly for $l\neq 0$. In the meantime the results of calculations for some r_0's are given here.

The most recent calculations of nuclear radii are those given by Bethe.[1] The following criticisms can be raised against them. Firstly, they are derived from the less accurate theories. Secondly, they are not based on the new values of the fundamental physical constants.[3] Thirdly, in the case of an α-ray spectrum of more than one line, Bethe employs the total decay constant. But the λ used should refer to the probability of decay with the one energy E only; the error is often appreciable. Such cases are indicated by an asterisk in Table I where I have used the partial decay constants.

Table I compares the new values of r_0 with Bethe's and gives also the deepness B of the potential hole, calculated from (2) and (3). $B=(2Ze^2/r_0)-U$. The table contains only those α-rays for which nuclear spin difference is almost certainly zero. Values of λ and E are those found generally in tables,[4] except where indicated by a note. Birge's[5] values of e, m, h, etc., were used.

I wish to thank Professor L. Infeld for his generous guidance in this work.

* Holder of National Research Council of Canada Studentship.
[1] G. A. Gamow, *Constitution of Atomic Nuclei and Radioactivity* (Cambridge, 1937); H. A. Bethe, Rev. Mod. Phys. **9**, 161 (1937); F. Rasetti, *Elements of Nuclear Physics* (Prentice-Hall, Inc., New York, 1936); von Weizsäcker, *Die Atomkerne* (Akad. Verlagsgesellschaft, Leipzig, 1937).
[2] Sexl, Zeits. f. Physik **81**, 163 (1933).
[3] R. T. Birge, Rev. Mod. Phys. **13**, 233 (1941).
[4] Feather, *Nuclear Physics* (The Cambridge University Press, New York, 1936); Curie, *Radioactivité* (Hermann, Paris, 1935), Vol. II; Hoag, *Electron and Nuclear Physics* (D. Van Nostrand Company, Inc., New York, 1938); Stranathan, *The "Particles" of Modern Physics* (The Blakiston Company, Philadelphia, 1942); Lewis and Bowden, Proc. Roy. Soc. **145**, 235 (1934); International Commission, J. de phys. et rad. **2**, 273 (1931).

TABLE I. Values of r_0 and B. (The letters refer to the remarks below.)

Nuclei	Radii ×10¹³ cm New	Bethe	Total decay energy-Mev New	Bethe	λ-per sec. New	Bethe	B-Mev	$R=r_0A^{-1/3}$ New	Bethe
UI-UXI	9.3₇	9.8	4.31[a]	4.15	4.82×10^{-18}[c]	5.0×10^{-18}	23.9	1.52	1.59
	9.3₄		4.32[b]				23.9	1.52	
UII-Io	9.2₆	9.6	4.89[a]	4.76	8.14×10^{-14}[c]	7×10^{-14}	25.6	1.51	1.57
	9.2₁		4.91[b]				25.7	1.51	
Io-Ra	9.2₆	9.5	4.80[d]	4.67	2.6×10^{-12}[e]	2.9×10^{-12}	23.1	1.52	1.56
*Ra-Rn	9.2₉	9.0	4.879	4.88	1.35×10^{-11}	1.42×10^{-11}	22.3	1.53	1.49
Rn-RaA	9.2₈	9.0	5.589	5.59	2.097×10^{-6}	2.10×10^{-6}	21.0	1.54	1.50
RaA-RaB	9.1₄	9.0	6.112	6.11	3.78×10^{-3}	3.8×10^{-3}	20.3	1.53	1.51
RaF-RaG	8.2₇	8.2	5.410[f]	5.40	5.886×10^{-4}[f]	5.7×10^{-4}	23.8	1.40	1.39
Th-MThI	9.9₂	8.7	3.99[g]	4.34	1.2×10^{-6}	1.2×10^{-6}	22.0	1.62	1.42
	10.0₁				1.7×10^{-6}[h]		21.8	1.64	
*RdTh-ThX	9.3₁	8.8	5.517	5.52	9.7×10^{-3}	1.15×10^{-3}	22.1	1.54	1.45
ThX-Thn	9.2₉	9.0	5.786	5.79	2.20×10^{-6}	2.20×10^{-6}	21.4	1.54	1.49
Thn-ThA	9.2₈	9.1	6.400	6.40	1.27×10^{-2}	1.27×10^{-2}	20.2	1.55	1.52
ThA-ThB	9.1₂	8.9	6.904	6.90	4.95	5.0	19.5	1.53	1.49
*ThC-ThC''	7.5₇	7.0	6.1607	6.20	4.65×10^{-3}	6.7×10^{-6}	25.4	1.28	1.18
Pa-Ac	8.1₈	8.6	5.24[d]	5.16	6.7×10^{-12}[i]	6.9×10^{-12}	27.2	1.34	1.41
*An-AcA	8.7₀	8.5	6.953	6.95	1.22×10^{-1}	1.77×10^{-1}	21.5	1.45	1.42
AcA-AcB	8.9₉	8.8	7.508	7.51	3.47×10^{2}	3.5×10^{2}	19.3	1.51	1.48
*AcC-AcC''	7.9₀	7.3	6.739	6.74	4.48×10^{-3}	5.3×10^{-3}	24.3	1.33	1.23

[a] Feather, see reference 4.
[b] From values of range given by Sizoo, Physica **4**, 791 (1937) and graphs of range against energy given by M. S. Livingston and H. A. Bethe, Rev. Mod. Phys. **9**, 266 (1937). Value then corrected to include recoil energy, since the tabulated value is total energy.
[c] A. O. Nier, Phys. Rev. **55**, 150 (1939).
[d] Obtained as in (*b*), using range given by Mme. Curie, reference 4.
[e] Hernegger, Akad. Wiss. Wien **143**, 367 (1934).
[f] W. Y. Chang, Phys. Rev. **69**, 60 (1946).
[g] Obtained as in (*b*), using range given by G. H. Henderson and G. C. Laurence, Phys. Rev. **52**, 46 (1937).
[h] 1.7×10^{-6} is given by Feather reference 4 and by Stranathan, reference 4.
[i] Stranathan, reference 4.

The Synchro-Betatron, Electron Accelerator Guide Fields

H. F. KAISER AND E. C. GREANIAS
U. S. Naval Research Laboratory, Washington, D. C.
February 18, 1946

THE idea of modifying the Kerst form of betatron for operation as a synchrotron brings with it a number of interesting possibilities.

The first of these is that the betatron may be allowed to function as a conventional betatron, the electrons being accelerated by induction up to some desired point in the acceleration cycle and then completing their acceleration by application of oscillatory potential to the synchrotron dees within which the electrons are bunched and accelerated by the method described by Veksler[1] and by MacMillan.[2] This idea has been evolved independently and recently published by Pollock[3] who considered it as a means for starting the electrons in the synchrotron.

The second interesting possibility is that the energy of the accelerated particles need not be limited to the maximum energy that is possible in the conventional betatron since the synchrotron operation may be automatically synchronized with a field pulsing operation to provide in the betatron at the moment in which synchrotron operation begins, a rapidly increasing and powerful guide field which increases in strength with the energy of the particle. The obvious advantage is that now much higher energies can be obtained with a given orbital radius and thus makes possible use of smaller apparatus for a given maximum energy.

The questions that arise in connection with this idea are: (1) Will the synchrotron acceleration proceed satisfactorily and rapidly enough for the rates of field increase possible by use of special auxillary coils placed in the betatron either on the pole faces or around the guide poles (large ampere-turns outside of the poles will saturate the central field and increase the guide field)? (2) What are the practical limitations on the production of the necessary guide fields?

As shown by Veksler[1] the conditions for the magnetic field and the accelerating voltage may be so chosen that there is an equilibrium accelerating voltage V_R determined by arbitrary constants and the electron injection voltage. assuming that 4 kv per turn is a practical possibility we shall have in a betatron operating at 180 cycles per second a quarter-period of approximately 1400 microseconds. In much less than a fourth of this time relativistic speeds $v \to c$ may be obtained by induction acceleration. Assuming that synchrotron operation is begun at 350 microseconds, the possible energy increase in the next 1000 microseconds will be about $0.001c/2\pi r \times 4$ kv or about 955 Mev for $r=20$ cm, neglecting losses by radiation. (If these are not compensated by shielding, the maximum energy possible for so small a radius will be below 500 Mev.) If the guide field can be increased in correspondence to the energy increase to 955 Mev, a rate of field increase of $\dot{H}=1.5\times10^8$ gauss per sec. is required. Although large, this value is still small compared to Veksler's limitation: $\dot{H} \ll 4\pi V_0/T_\lambda^2 c$. V_0=accelerating potential; c=velocity of light; T_λ=period of electric field.

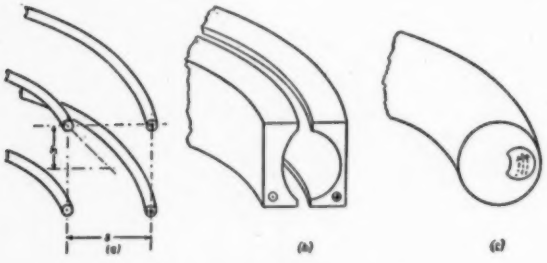

FIG. 1. Conductor guide systems.

The practical possibility of producing such a guide field may now be examined. Considering for simplicity the pulsing coils as a set of two pairs of closely spaced concentric conductors arranged, as shown in (*a*) of Fig. 1, above and below the orbital plane, the field at the center of this group is:

$$H_s=\frac{8Is}{2(h^2+s2/4)}=0.564I \text{ amperes for } h=s/2=0.707 \text{ cm.}$$

Note that the directions of the currents are such that field is small outside of the coil system. For an electron energy $E\sim10^3$ Mev and $r=20$ cm. $H_s\sim10^3/3\times10^{-4}\times20 \sim1.7\times10^5$ gauss and the required current $I=3\times10^5$ amperes. The ohmic resistance of one of these conductors is about

$$R=\frac{2\pi\times20\times1.72\times10^{-6}}{1}=2.16\times10^{-4}$$

ohms for 1 cm² cross section. The inductance of a conductor pair is approximately:

$$L=\frac{\pi(20.7^2-19.3^2)\cdot1.7\times10^5}{3\times10^5\sim10^8}\leqq1 \text{ microhenry.}$$

The time constant

$$T=\frac{10^{-6}}{4\times2.16\times10^{-4}}=1.15\times10^{-3} \text{ sec.}$$

for parallel connection, is quite consistent with the time available for acceleration. The driving voltage, assuming an approximately linear current rise will then be about $10^{-6}\times3\times10^5/10^{-3}$ or 300 volts per pair. The conditions for producing a super guide field in a betatron of ordinary size are such as may be met with current pulsing transformers or by direct short circuit on a large direct current source. The pulse power is about 45 megawatts and the heat generated per pulse in a conductor is about 1160 calories giving a temperature rise of 11.3°C for a conductor of 1120 g weight. Intermittant operation is thus indicated. Mechanical stresses are very large and require special attention.

From the above it may be noted that even more powerful guide fields may be produced by reducing the sectional dimensions of the coil system. This suggests that the best location for the coil system is the immediate vicinity of the equilibrium orbit and as close as practicable to it. Furthermore it is obvious that the necessary field "shaping" for focusing and orbital stability may be obtained by special shaping of the conductors or even by allowing the inner

conductors to carry a larger current. Continuity and smoothness of the field must be preserved by careful joining of current inlets and outlets to avoid disturbing effects at these points. There is also the interesting possibility of so arranging the conductor system that it will form the dee system itself. A possible system having only the disadvantage that the particle must travel a short linear path each half turn on crossing the dee gap is under consideration.

A further interesting possibility related to the above is a modification of a field-producing scheme first described by Rabi[4] in which a uniform transverse magnetic field is produced in a cylindrical cavity, within and parallel to, but not concentric with, a larger conductor of circular cross section. While considered by Rabi as a long straight conductor, it may obviously be applied to the case of an annular torus of fairly large diameter. A departure from circular section in the cavity (or of the main conductor) as shown in (*c*) is required for field law and shaping. By use of such conductors it is possible that the conventional magnetic yoke of the betatron may be partly or completely dispensed with. These conductors may also be regarded as electromagnetic wave guides which may be exicted in various ways for particle acceleration.

The authors wish to express their appreciation to Dr. A. E. Ruark and Dr. B. F. Salzberg for review and helpful discussion of this material.

[1] V. Veksler, J. Phys. U.S.S.R. **9**, 153 (1945).
[2] E. M. McMillan, Phys. Rev. **68**, 143 (1945).
[3] H. C. Pollock, Phys. Rev. **69**, 125 (1946).
[4] I. I. Rabi, Rev. Sci. Inst. **5**, 78 (1934).

On the Theory of the Electrostatic Beta-Particle Energy-Spectrograph. IV

F. T. Rogers, Jr.*
Indianapolis, Indiana
April 5, 1946

CALCULATIONS in an earlier paper[1] of the same general title developed the basic differential equation,

$$\left.\begin{aligned} &d^2\delta/d\phi^2+R(d\delta/d\phi)^2+Q\delta-qr_0=0,\\ &0\leqslant R=-C/4r_0\ll 1,\end{aligned}\right\} \tag{1}$$

for the focusing action of the electrostatic analyzer (concentric-cylinder form) on particles moving with relativistically significant speeds. In that paper the $R\delta'^2$-term was merely neglected so that a "first-order" theory could be worked out. Since this first-order theory indicated an appreciable ("chromatic") dependence of the back-focal length of the system (considered as a "particle-lens") upon particle energy, it is of interest to have explicit information bearing upon the justification for neglecting the $R\delta'^2$-term.

Although the same general result appears if Eq. (1) be studied either by approximate "equivalent linearization," or by series methods, or by obtaining from Eq. (1) an approximate "correction" to the previous solution,[1] perhaps the most satisfactory demonstration can be had by treating Eq. (1) as a "quasi-linear" differential equation. If one seeks a solution in the form (here $x=Q^{\frac{1}{2}}\phi$)

$$\delta=qr_0/Q+A_1(\phi)\sin x+A_2(\phi)\cos x, \tag{2a}$$

yet requires that

$$d\delta/d\phi=A_1(\phi)Q^{\frac{1}{2}}\cos x-A_2(\phi)Q^{\frac{1}{2}}\sin x, \tag{2b}$$

then clearly $A_1(\phi)$ and $A_2(\phi)$ must satisfy

$$\left.\begin{aligned} dA_1/d\phi&=-RQ^{\frac{1}{2}}(A_1\cos x-A_2\sin x)^2\cos x,\\ dA_2/d\phi&=RQ^{\frac{1}{2}}(A_1\cos x-A_2\sin x)^2\sin x;\end{aligned}\right\} \tag{3}$$

Eqs. (3) do not appear to be readily soluble in exact, closed form. But the functions,

$$\left.\begin{aligned} A_1(\phi)&=r_0\delta_i/Q^{\frac{1}{2}}l'\\ &\quad-R\delta_i^2[(H+J)\sin x-\tfrac{1}{4}I\cos^3 x-\tfrac{3}{4}J\sin^2 x],\\ A_2(\phi)&=(\delta_i-qr_0/Q)\\ &\quad-R\delta_i^2[(H-J)\cos x-\tfrac{3}{4}I\sin^3 x+\tfrac{3}{4}J\cos^2 x],\end{aligned}\right\} \tag{4a}$$

where

$$\left.\begin{aligned} H&=\tfrac{1}{2}(r_0^2/Ql'^2-1),\\ I&=-r_0/Q^{\frac{1}{2}}l',\\ J&=\tfrac{1}{2}(r_0^2/Ql'^2+1),\end{aligned}\right\} \tag{4b}$$

appear to afford a very good approximate solution to Eqs. (3); this can be seen directly by substituting Eqs. (4) into Eqs. (3) and noting that $R\delta_i$ is negligible in comparison with unity in a first-order theory.

Clearly the effects of the $R\delta'^2$-term in Eq. (1) appear in Eqs. (2) and (4), essentially as terms in the second order of δ_i which are further multiplied by the small quantity R. To this extent, therefore, that term is properly negligible in a first-order theory.

* Address: Laboratory, U. S. Naval Ordnance Plant.
[1] F. T. Rogers, Jr. and C. W. Horton, Rev. Sci. Inst. **14**, 216 (1943)

The Production of High Centrifugal Fields

J. W. Beams and J. L. Young, III
Rouss Physical Laboratory, University of Virginia, Charlottesville, Virginia
April 11, 1946

THE maximum stress in a spinning homogeneous metal rotor is approximately proportional to the square of the peripheral speed. That is, the maximum stress the rotor will stand without bursting is proportional to $(2\pi N)^2R^2$, where N is the number of revolutions per sec. and R is the radius of the rotor. On the other hand the centrifugal acceleration at the periphery of the rotor is $(2\pi N)^2R$. Therefore, in order to produce high centrifugal fields the rotor should have a small radius R and a high rotational speed N.

A method of spinning rotors in a high vacuum previously developed in this laboratory[1] has been improved and used to spin small steel rotors up to their bursting speeds. The rotor speeds were measured by a calibrated photoelectric pick-up. The highest peripheral speed so far attained was with a 3.97-mm steel, ball-shaped rotor which burst at a peripheral speed of 9.6×10^4 cm/sec. The smallest rotor so far used was a 1.59-mm ball-shaped rotor (ball bearing with a small flat ground on top). It was spun at 166,000 r.p.s. without bursting which produced a centrifugal field of 8.8×10^7 times gravity on its periphery. With still smaller rotors it is hoped to produce correspondingly higher fields.

[1] See MacHattie, Rev. Sci. Inst. **12**, 429 (1941).

A Spherical Shell Nuclear Model

H. A. WILSON
Rice Institute, Houston, Texas
April 19, 1946

A DISCUSSION of the energies of the beta-, gamma-, and alpha-rays from the naturally radioactive elements led the writer[1] in 1933 to suggest that the nuclei of these elements may have sets of equally spaced energy levels with spacings of 0.387 Mev.

Recently Wiedenbeck[2] has reported equally spaced levels in Au, Ag, In, Cd, and Rh with spacings between 0.36 and 0.50 Mev. Equally spaced levels with separations about 0.4 Mev. are also found with N, Be, Al, and Co. It seems probable therefore that most atomic nuclei have a set of equally spaced levels with separations near to 0.4 Mev.

An account of a simple classical mechanical model of a nucleus, which has nearly equally spaced levels with spacings equal to about 0.4 Mev for all nuclei from beryllium to uranium, follows.

The model is a thin spherical shell which is supposed to be flexible, inextensible, and uniformly charged with positive electricity. The possible frequencies of vibration of the shell assuming its area to remain constant are equal to $(Ze/4\pi r)(Amr)^{-\frac{1}{2}}[n(n+1)-2]^{\frac{1}{2}}$ where Z=atomic number, A=mass number, r=radius of the shell, and $n=2, 3, 4, 5 \ldots$. The vibration with $n=2$ would not be excited by x-rays. m=mass of one nuclear particle.

This gives nearly equally spaced frequencies with spacing $(Ze/4\pi r)(Amr)^{-\frac{1}{2}}$ for large values of n.

Letting $r=r_1A^{\frac{1}{3}}$ and putting in the numerical values of e and m we get

$$r_1=2.46\times10^{-13}(Z/A\Delta E)^{\frac{1}{2}},$$

where ΔE is the energy level separation in Mev corresponding to the frequency spacing for large values of n.

The values of $(Z/A\Delta E)$ with ΔE about 0.4 Mev are nearly equal to unity so that $r=2.46\times10^{-13}A^{\frac{1}{3}}$ approximately.

Table I gives values of ΔE and r for several elements. The third column gives values of $1+2.3A^{\frac{1}{3}}$ which agree nearly with the values of r in most cases.

The value of r for uranium given by Gamow's theory is 9×10^{-13} and the value given by the target area for fast neutrons is 10×10^{-13}. Gamow's theory gives the radius of the potential hole inside the nucleus. On the shell model the radius should be equal to Gamow's radius plus the radius of the alpha-particle which may well be about 4×10^{-13}. This makes the shell radius 13×10^{-13} which agrees as well as could be expected with 15×10^{-13}. The value 10×10^{-13} for uranium from the target area for fast neutrons was obtained by putting the target area equal to $2\pi r^2$. Classically the target area would be πr^2 so the classical radius would be 14×10^{-13} which is nearly equal to 15×10^{-13}.

TABLE I.

Element	ΔE	$r\times10^{13}$	$(1+2.3A)^{1/3}\times10^{13}$
Uranium	0.387	15.25	15.25
Silver	0.39	12.6	11.95
Aluminum	0.43	7.9	7.9
Beryllium	0.388	5.8	5.8

The threshold levels for x-ray excitation for Au, In, Cd, Ag, and Rh were measured by Wiedenbeck[2] and found to be nearly equal with an average value of 1.2 Mev. According to the shell model the threshold should be $(10)^{\frac{1}{3}}\Delta E$ which is about 1.3 Mev.

The formation of a shell instead of a sphere may be caused by saturation of the nuclear forces. Thus if we suppose each particle cannot be strongly attracted by more than four nearby particles, it is easy to see that the electrostatic forces should pull out a sphere into a shell.

The area of the shell $S=4\pi r^2$ must be determined by the number N of neutrons and the number Z of protons in it. We may suppose, for example, that $S=aZ-bN$ where a and b are positive quantities which vary slowly with $A=N+Z$.

[1] H. A. Wilson, Phys. Rev. **44**, 858 (1933); Proc. Roy. Soc. **144**, 280 (1934).
[2] M. L. Wiedenbeck, Phys. Rev. **68**, 237 (1945).

β-Ray Spectrum of K^{40}

B. DŽELEPOW, M. KOPJOVA, AND E. VOROBJOV
The University of Leningrad, Leningrad, U.S.S.R.
April 15, 1946

FOR the theory of β-decay the highly forbidden transmutations are of the greatest importance. From this point of view the investigation of β-decay $K^{40}\rightarrow Ca^{40}$ must be very interesting, as the spin K^{40} is 4^1 and the spin Ca^{40} is 0. A large half-period of decay (1.4×10^9 years[3]) with relatively great hardness of β-spectrum also indicates that the third-or the fourth-order exclusion takes place here.[3] The β-spectrum investigation is difficult because of the low activity of natural potassium: one cm³ of potassium emits about 0.6 electron/sec. For this reason the shape of the β-spectrum K^{40} has not yet been investigated; only rough determinations of upper limit have been made. The results were obtained in a wide region of 0.7 to 1.3 Mev.[4]

We have investigated the β-spectrum K^{40} with a magnetic spectrometer of special design (Fig. 1). The apparatus placed in a box corresponded to six general β-spectrometers of the Danysz-type. The central counter was common for all the spectrometers, six other counters being situated each near their own potassium source. The number of coincidences between the central counter and the six other counters was measured with different magnetic fields. The counters were made of Al foil 20μ thick. $K_2C_2O_4$ powder 69mg/cm² thick, plated to a celluloid strip, served as the source of electrons. It is possible that our β-spectrum was distorted in the region of low energies, because of electrons scattering in the source, in the first counter or in the gas. To correct this inaccuracy, the spectrum of RaE was obtained by us under the same conditions. For this pur-

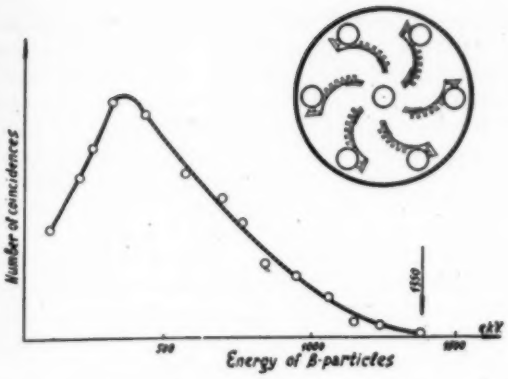

FIG. 1. Above—magnetic spectrometer with 7 counters. Below—β-ray spectrum of K^{40}.

pose RaE was mixed in the required proportions with $CaCO_3$ (60 mg/cm²). The comparison of β-spectrum of RaE as found by us with those obtained by Neary and Alichanow, Alichanian, and Dželepow[5] showed that the distortions existed only in the region lower than 400 kev, and reached 60 percent at 100 kev. The suitable corrections having been made, the β-spectrum K^{40} (shown in Fig. 1) was obtained. The spectrum upper limit is 1350 ± 50 kev. As to its shape the β-spectrum K^{40} is similar to a spectrum belonging to the allowed transmutations.

[1] J. Zacharias, Phys. Rev. **60**, 168 (1941).
[2] A. Bramlay and A. Brewer, Phys. Rev. **53**, 502 (1938).
[3] E. Konopinski, Rev. Mod. Phys. **15**, 209 (1943).
[4] W. S. Henderson, Phys. Rev. **55**, 238 (1939); W. Libby and D. Lee, Phys. Rev. **55**, 245 (1939); C. Anderson and S. Neddermeyer, Phys. Rev. **45**, 653 (1934).
[5] G. Neary, Proc. Roy. Soc. **A175**, 71 (1940). A. Alichanow, A. Alichanian, and B. Dželepow, Physik. Zeits. Sowjetunion **11**, 204 (1937).

The Inversion Spectrum of Ammonia

WILLIAM E. GOOD
University of Pittsburgh and Westinghouse Research Laboratories, East Pittsburgh, Pennsylvania
April 20, 1946

THE strong absorption band[1] of NH_3 at 0.8 cm^{-1} has been resolved into 28 sharp, widely separated lines. The necessary high resolution was obtained by using a continuous wave source. The gas sample is held in a section of waveguide two and one-half meters long, which is arranged in a balanced system with two crystal detectors.

At a pressure of about 0.1 mm Hg it is possible to observe each fine structure line (see Fig. 1) on an oscilloscope by synchronizing the horizontal sweep of the oscilloscope with the frequency sweep of the oscillator tube. Identification of the lines was accomplished by using a calibrated absorption type wavemeter.

Preliminary measurements of the frequencies and the intensities of the various lines are graphed in Fig. 2. Every line is completely resolved. In fact, the half-widths of the lines at this pressure are less than the width of the inked lines on the graph.

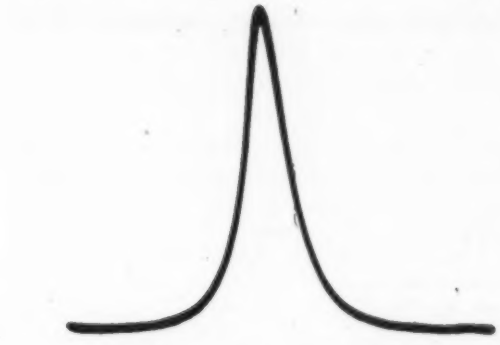

FIG. 1. One of the absorption lines for NH_3.
$f=23{,}878$ mc/sec.; $p\simeq0.1$ mm Hg;
Intensity$\simeq0.18$ db/m;
full scale frequency sweep $=22$ mc/sec. $=0.00073$ cm^{-1}.

Each line can be associated with the molecule being in a definite rotational state. The centrifugal distortion caused by being in a particular rotational state slightly affects the inversion frequency.

The theoretical expression that Hsi-Yin Sheng, E. F. Barker, and D. M. Dennison[2] derive for this case is

$$\frac{\nu}{hc}\,(\mathrm{cm}^{-1})=\frac{\nu_0}{hc}-0.0011(J^2+J-K^2)+0.0005K^2,$$

however, their infra-observations gave -0.00_8 for the coefficient of (J^2+J-K^2). The preliminary expression that we obtain from our experimental data is

$$\frac{\nu}{hc}\,(\mathrm{cm}^{-1})=0.7932-0.0048(J^2+J-K^2)+0.0020K^2.$$

The observed intensity of the lines agrees well with the population of the various rotational levels for thermal equilibrium at 300°K.

As the pressure of the NH_3 is reduced, the lines are observed to become sharper and at a pressure of about 10^{-2} mm Hg a hyperfine structure is resolved. The investigation is being continued using improved equipment.

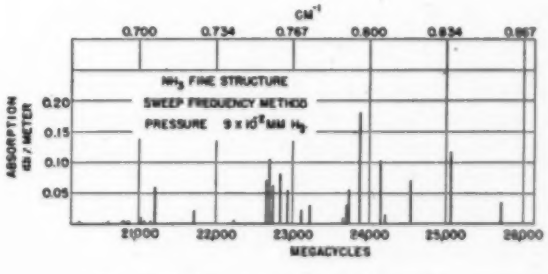

FIG. 2. The inversion spectrum of ammonia.
$T=24$°C.

Addendum: After preparation of this letter we received the March 16, 1946 issue of Nature in which we note the excellent work of Bleaney and Penrose on this same subject.

[1] C. E. Cleeton and N. H. Williams, Phys. Rev. **45**, 234 (1934).
[2] Hsi-Yin Sheng, E. F. Barker, and D. M. Dennison, Phys. Rev. **60**, 786 (1941).

Detection of Rapidly Moving Ionospheric Clouds

H. W. WELLS, J. M. WATTS, AND D. E. GEORGE
Department of Terrestrial Magnetism, Carnegie Institution of Washington, Washington, D. C.
April 2, 1946

RAPIDLY moving ionospheric clouds were detected in the earth's outer atmosphere (ionosphere) during the magnetic storm March 25–26, 1946, at the Kensington Ionospheric Laboratory, Department of Terrestrial Magnetism, Carnegie Institution of Washington. The clouds move in from long to short range or out again in intervals of few minutes. They are first detected at maximum ranges of 800–900 km. They are tracked inward at velocities of 1 to 2 km per second to *F*-layer levels (300–400 km). Occasionally they are seen to move out again at about the same rate. They are observed both during the night when background ionization is low and during the day when background ionization is high. Angle of arrival of the signals cannot be ascertained by the method employed.

These clouds were observed repeatedly during the interval 15^h00^m, March 25, to 07^h00^m, March 27, 1946—the first opportunity for application of the new recording technique to observation of magnetic-ionospheric storms. The observations were made with the new "panoramic" ionospheric recorder, developed with support of the United States Signal Corps which sweeps over the range, 1.5 to 20.0 Mc/sec. at adjustable intervals of 5 to 30 seconds. Repetition at such short intervals registers ionospheric fluctuations of short duration which have been missed by earlier instrumentation. The technique has been perfected to the extent that successive records can be projected as motion pictures. Compression of the time-scale as a result of projection provides a sense of continuity which simplifies visualization and interpretation of an otherwise long succession of events.

The panoramic sweep is displayed on a cathode-ray tube and records are made automatically by successive exposures of single frames of film for each sweep. Examples of normal records with 15-second sweep at 30-second intervals for three minutes are illustrated in Fig. 1 while rapidly changing disturbed conditions are illustrated in Fig. 2. Although illustration of a cloud tracking is not immediately feasible, Fig. 2 serves to demonstrate the rapid changes which may occur in a 30-second interval between exposures. Both figures are enlarged from 16-mm film. The parallel horizontal lines are height-markers at 50-km intervals upward from the base-line at 0-km and the "pips" at top of record are frequency-markers at 1-Mc/sec. intervals with increasing frequency from left to right. In the figures the visible range is from 1.5 to 14 Mc/sec. The total elapsed interval in each case is three minutes with time progressing downward from top to bottom.

The principal effects of influx of the clouds are: (1) sudden changes in *F*-layer ionization; (2) rapid changes in *F*-layer heights indicating turbulence which is often progressive from high to low heights and from high to low frequencies; (3) rapid fluctuations of echoes at the lower frequencies with occasional temporary disappearance indicating high absorption.

We are inclined to attribute these clouds to an inflow of corpuscles which are bombarding the atmosphere in an irregular manner during magnetic disturbance. These probably are the first direct quantitative observations of such bombardment. They are interpreted as establishing that corpuscular radiation contributes to the net ionization of the *F*-region. The equivalent maximum electronic density is estimated from magneto-ionic theory to be 2 to 4×10^5 electrons per cc. Much of the uninterpreted scatter of the disturbed *F*-region previously seen on slow recorders can doubtless be traced to chance registration of various aspects of rapidly moving clouds. It is considered probable that other higher velocity cloud movements exist which will be detected by even faster recordings.

The new technique of ionospheric recording and presentation provides a very powerful tool for study of special ionospheric features which occur during magnetic storms,

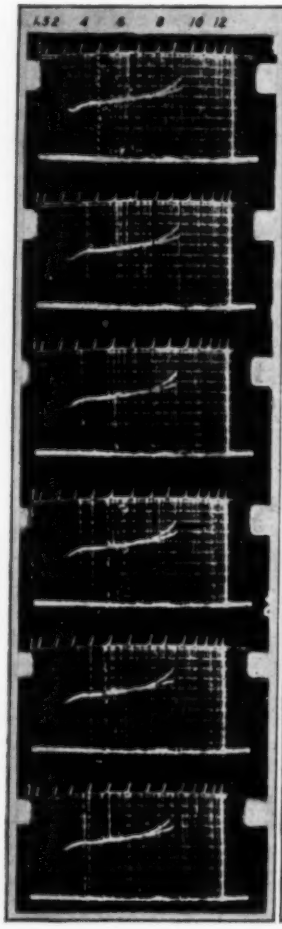

FIG. 1.

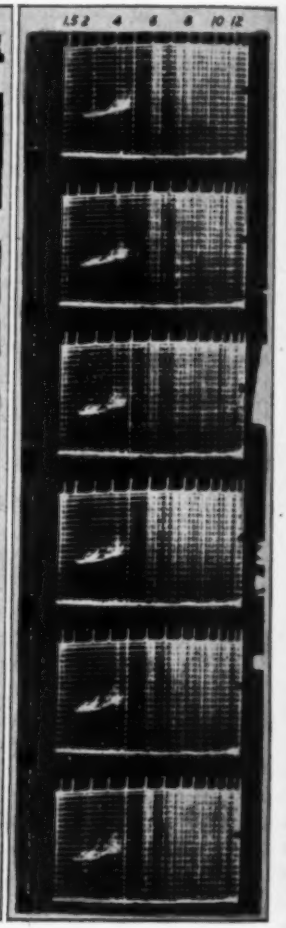

FIG. 2.

FIGS. 1 and 2. (1) Six successive normal ionospheric 15-sec. records during three minutes afternoon March 19, 1946; (2) six successive disturbed ionospheric 15-sec. records during three minutes of magnetic storm, March 25, 1946, showing rapid changes. (Records are reproduced from original 16-mm film; height-markers are at 50-km intervals, frequencies are indicated from 1.5 to 14 Mc/sec.)

eclipses, radio fade-outs, sporadic *E*, *F*2 scatter, and abnormal stratifications. Projection makes possible quick scanning of an enormous wealth of data, selection of portions for critical study, and visualization of dynamic events of short duration.

Lowering of Electrical Breakdown Field Strength at Microwave Frequencies Due to Externally-Applied Magnetic Field

D. Q. Posin
Radiation Laboratory, Massachusetts Institute of Technology, Cambridge, Massachusetts
April 12, 1946

THE following effects have been observed in connection with 3-cm microwave breakdown studies[1] conducted on air gaps in wave guide:

(1) An approach of a permanent magnet to a gap which is on the verge of microwave sparking can make the gap spark over. In one favorable experiment 35 spark-overs took place out of 36 approaches with a magnet.

(2) A magnet of pole-face cross section smaller than the patch of wave guide over which it is poised may lower the breakdown field strength by 20 percent or more, depending on certain conditions, such as strength of the magnetic field and height of the breakdown gap.

(3) When the magnet is swept along on the outside of the vertically-narrowed wave guide (which encloses the breakdown gap) the gap may spark at a field strength lower by as much as a factor of 2 or more than when the magnet is absent. The sweeping magnet must remain upright, for the effect mentioned.

(4) No sparking effect can be reliably reported when the magnetic field is applied at right angles to the microwave electric vector, either along the direction of propagation, or crosswise to it.

(5) When broadface permanent magnets are used, the poised (stationary) effect and the sweep effect are much diminished.

The following possible explanations have been considered: (a) Vertical magnetostriction of the wave guide, including the possibility of interaction between the applied magnetic field and the currents in the wave guide surface. (b) Magnetic spiral-focusing in the gap (oscillating helices) leading to more intense concentrated ionization. (c) Larmor precession resonance with accompanying increase of gas conductivity.[2] For various reasons, and the fact that the lowering of breakdown peak power by a factor of 4 (Poynting vector proportional to field squared) in the sweep cases is equivalent in violence to the shrinking of the height of the gap[3] by the same factor 4, none of the mentioned possible explanations seems at the moment to be adequate. However, further investigation of both the effect and the possible causes is being continued.

[1] D. Q. Posin, Bull. Am. Phys. Soc. **21**, No. 2, April, abstract L6.
[2] Appleton and Childs in experiments cited by K. K. Darrow, Bell Sys. Tech. J. 11, No. 4, 605.
[3] D. Q. Posin, Ina Mansur and H. Clarke, Radiation Laboratory Report 731.

The Two-Body Problem in Einstein's and Birkhoff's Theories

T. F. Morris
Department of Mathematics, University of Toronto, Toronto, Canada
March 27, 1946

C. GRAEF[1] has obtained the solution of the two-body problem according to Birkhoff's theory.[2] After the substitution $x_1 \to \eta_1$, $x_2 \to \zeta_1$, $y_1 \to \eta_2$, $y_2 \to \zeta_2$, and after the correction of some obvious typographical errors his equations may be written as follows

$$\ddot{\eta}_i/m_2 = +(\eta_i-\zeta_i)/r^3[3/2r^2\{(\eta_k-\zeta_k)\dot{\zeta}_k\}^2 - 2\dot{\zeta}_k\dot{\zeta}_k - \dot{\eta}_k\dot{\eta}_k + 4\dot{\eta}_k\dot{\zeta}_k - 1] + (\eta_k\zeta_k)(\dot{\zeta}_k - 2\dot{\eta}_k)(\dot{\zeta}_i - \dot{\eta}_i)/r^3, \quad (1)$$

where

$$r^2 = (\eta_k-\zeta_k)(\eta_k-\zeta_k).$$

The repetition of an index implies summation from one to two. Another set, for $\ddot{\zeta}_i$ is obtained by replacing η with ζ and m_2 with m_1. Let $\alpha_i = M^{-1}(m_1\eta_i + m_2\zeta_i)$ be the coordinates of the center of gravity where $M = m_1 + m_2$. Then

$$\ddot{\alpha}_i = m_1m_2(\eta_i-\zeta_i)/Mr^3[3/2r^2(\{(\eta_k-\zeta_k)\dot{\zeta}_k\}^2 - \{(\zeta_k-\eta_k)\dot{\eta}_k\}^2) - \dot{\zeta}_k\dot{\zeta}_k + \dot{\eta}_k\dot{\eta}_k] + m_1m_2(\eta_k-\zeta_k)(\dot{\eta}_k-\dot{\zeta}_k)(\dot{\eta}_i-\dot{\zeta}_i)/Mr^3. \quad (2)$$

Einstein, Infeld, and Hoffman[3] have obtained the equations for the two-body problem on the basis of the general theory of relativity. The equations that correspond to (2) are

$$\ddot{\alpha}_i = m_1m_2(\eta_i-\zeta_i)/Mr^3[3/2r^2(\{(\eta_k-\zeta_k)\dot{\zeta}_k\}^2 - \{(\zeta_k-\eta_k)\dot{\eta}_k\}^2) - \dot{\zeta}_k\dot{\zeta}_k + \dot{\eta}_k\dot{\eta}_k + (m_1-m_2)/r] + m_1m_2(\eta_k-\zeta_k)(\dot{\eta}_k-\dot{\zeta}_k)(\dot{\eta}_i-\dot{\zeta}_i)/Mr^3. \quad (3)$$

Thus, as far as motion of the center of gravity is concerned, the only difference between (2) and (3) is the term

$$(Mr^4)^{-1}m_1m_2(\eta_i-\zeta_i)(m_1-m_2) \text{ in (3).} \quad (4)$$

Robertson[4] has shown that the average value of $\ddot{\alpha}_i$, $\langle\ddot{\alpha}\rangle_{Av} = \frac{1}{T}\int_0^T \ddot{\alpha}_i dt$ over a period of the classical motion, is zero for Eq. (3); i.e., there is no secular change in the velocity of the center of gravity. The average value of (4) however, is not zero, and for Eq. (2) this leads to the result that $\langle\ddot{\alpha}_1\rangle_{Av} = m_1m_2(m_2-m_1)\epsilon/2Ma^{3/2}p^{3/2}$ and $\langle\ddot{\alpha}_2\rangle_{Av} = 0$ where $r^{-1} = p^{-1}[1+\epsilon\cos w]$. This acceleration is in the direction of the periastron of the minor component of a double star. Levi-Civita[5] has given an example of a binary star for which such an acceleration might be detected.

Berenda[6] has suggested that the difference in the results of the two theories, may be caused by different methods of approximation. This remark would not apply to the result deduced above, since the extra term in (3) is an interaction term which arises on account of the nonlinear character of the field equations.[7]

I wish to thank Dr. Infeld for suggesting this problem to me.

[1] C. Graef, Boletin Sociedad Mat. Mexicana 1, Nos. 4 and 5, 25.
[2] G. Birkhoff, Boletin Sociedad Mat. Mexicana 1, Nos. 4 and 5, 1.
[3] Einstein, Infeld, and Hoffman, Ann. Math. [1] 39, 65.
[4] H. P. Robertson, Am. Math. [1], 39, 101.
[5] T. Levi-Civita, Am. J. Math. 59, 225. Oddly enough the magnitude of the acceleration is the same as that obtained by Levi-Civita from relativity theory through a mistake in the calculation.
[6] C. W. Berenda, Phys. Rev. 67, 56 (1945).
[7] H. P. Robertson, reference 4, p. 103 footnote.

The Racetrack: A Proposed Modification of the Synchrotron*

H. R. CRANE
Randall Laboratory of Physics, University of Michigan, Ann Arbor, Michigan
April 20, 1946

EXPERIMENTS are being carried on at the University of Michigan on an electron accelerator which, we believe, contains enough novel features to warrant a brief description at this time. Basically, the machine employs the principle of the adiabatic acceleration of electrons by a radiofrequency electric field, in a slowly changing magnetic field, a principle which was discovered by Veksler[1] and by McMillan.[2] The vacuum tube is in the form of two half-circles connected by straight sections. That there are no essential difficulties in regard to the stability of the orbits in this shape of field is shown by D. M. Dennison and T. H. Berlin in an accompanying letter. One of the straight sections of the tube connecting the half-circles contains the injection apparatus and target, and the other contains the accelerating cavity. In order to maintain a nearly constant radius for the equilibrium orbit, the radiofrequency is modulated so that throughout the acceleration cycle it is proportional to the velocity of the electron. The electron beam is initially bent into the orbit by means of a pair of electrostatic deflection plates.

The sketch in Fig. 1 and the data given in the table below are the result of measurements on several scale-model magnets, and constitute the approximate specifications for the full scale machine which is now under construction.

Orbit radius = 100 cm
Length of straight section = 60 cm
Geometrical cross section of magnet gap, 7½ × 17½ cm
Injection energy, 500 kev ($\beta = 0.86$)
Maximum frequency modulation, 14 percent
Maximum field, 8000 oersteds at center of each magnet
Final energy, 200 Mev
Weight of iron, 7 tons
Condenser kva, 9000 at 60 cycles
Power loss at 60 cycles continuous; copper 18 kw, condensers 27 kw, iron 10 kw.

Our preliminary investigations have not given us much information on the important question of current yield, but some of the differences between the racetrack and the betatron (or the synchrotron with betatron injection) which affect the yield can be pointed out. In order to keep the amount of frequency modulation within reasonable limits, say 14 percent, the injection energy of the electrons must be high, about 500 kev. This has several consequences. 1. The injected beam is quite "stiff," which may increase the difficulty of filling the tube at the beginning of the acceleration cycle. 2. Space charge effects in the initial electron cloud will be smaller, but it is difficult to say whether this will be an advantage or a disadvantage. 3. Scattering by the residual gas in the tube will be smaller than it is in the betatron.

The advantages of the racetrack are mainly of an engineering and economic nature. 1. The type of magnet used is efficient in regard to both weight of iron and condenser kva. 2. The injection box and the accelerating cavity may be made of solid metal, in spaces that are free from the magnetic field. 3. Since the r-f accelerating

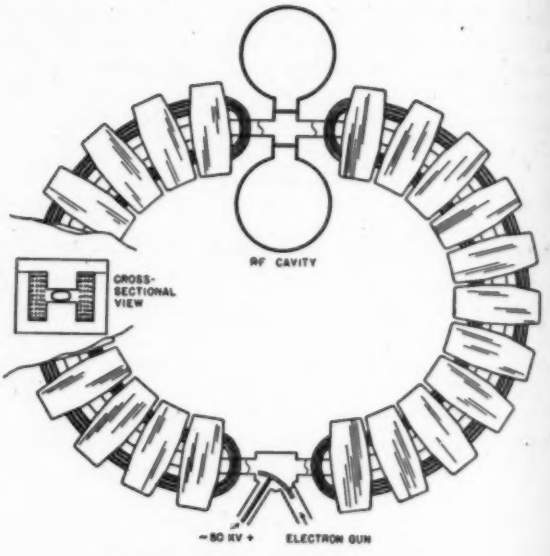

FIG. 1. Sketch of proposed accelerator.

device does not occupy space within the magnet gap, practically all of the volume of magnetic field which has the proper "fall-off" is available for electron orbits. 4. The energy output can be increased by enlarging the half-circles, with an increase in cost which is not far from linear.

While the advantages mentioned may not be decisive in the intermediate energy range, we believe that they will take on real importance when voltages above a billion are contemplated, and it is with this prospect in view that we intend to test the feasibility of the method.

[1] V. Veksler, J. Phys. U.S.S.R. **9**, 153 (1945).
[2] E. M. McMillan, Phys. Rev. **68**, 143 (1945).
* The work described in this Letter has been supported by the Bureau of Ordnance, U. S. Navy, under contract NOrd-7924.

The Stability of Orbits in the Racetrack*

D. M. DENNISON AND T. H. BERLIN
Randall Laboratory of Physics, University of Michigan, Ann Arbor, Michigan
April 20, 1946

IN the preceding letter by H. R. Crane, a modification of the synchrotron has been described in which the magnetic field is contained in two semicircular regions joined by two regions in which the magnetic field is absent or very small. The equilibrium orbits resemble an oval racetrack. It would be very awkward, analytically, to treat the stability of the orbits of the problem just described. The essential question, however, is whether an azimuthal variation in the magnetic field which is periodic in $\theta/2$ produces any elements of instability and this problem may be readily solved by the method of successive approximations.

The orbits of the circular synchrotron have been studied[1] and it is known that the radial coordinate of the electron may oscillate harmonically with the two frequencies ω_1 and ω_2 while the z coordinate oscillates with the single frequency ω_3. If the magnetic field in the median

plane varies as r^{-n} and if the frequency of the r-f field is ω_0, then $\omega_1=(1-n)^{\frac{1}{2}}\omega_0$ and $\omega_3=n^{\frac{1}{2}}\omega_0$. The remaining frequency, ω_2, depends upon the magnitude of the r-f potential and upon the energy of the electron. In general, it is much smaller than ω_0 and in a reasonable numerical example, ω_2 varies from $\omega_0/30$ at ½Mev to $\omega_0/400$ at 150 Mev. In zeroth and first orders of approximation the orbits are stable and the amplitudes of the oscillations decrease slowly as the magnetic field increases.

The azimuthal variation in the magnetic field may be introduced by assuming that the z component of the field has the form

$$H_z=\sum_{p=0}\frac{\lambda^p A_p\cos 2p\theta}{r^n}.$$

λ is the parameter of smallness, and shows that a development of the equations of motion is contemplated. The quantities A_p are even functions of z and the median plane is defined by $z=0$. The remaining field components may be derived from H_z in the usual way.

Since we are interested in discovering any elements of instability due to the introduction of the azimuthal field variation, it will be sufficient to examine the case where the magnetic field is constant in time. The first-order solution resembles that for the circular synchrotron except that the r coordinate is harmonic in the three frequencies, $2\omega_0$, ω_1, and ω_2, while z oscillates with the single frequency ω_3. In still higher order of approximation no new fundamental frequencies occur but there appear overtones and combination tones of the oridinal four frequencies. A commensurability, or near commensurability, between the frequencies, may, in some cases, lead to a vanishing resonance denominator and a consequent instability in the motion. Our analysis has been carried through the fourth order of approximation.

The results may be summarized as follows. The sharpness of resonance is defined by

$$\epsilon=\frac{2j\omega_0+k\omega_1+l\omega_2+m\omega_3}{\omega_0},$$

where j, k, l, and m are positive or negative integers (including zero). High order resonances may develop large amplitudes but only after many turns. When $\epsilon\lesssim 1/N$, the amplitude of the motion will grow to the value C after N turns. If r_0 is the mean radius of the orbit, A is some average of the initial r and z amplitudes due to the ω_1, ω_2, and ω_3 oscillations, and B is the amplitude of the r motion due to the azimuthal variation of the field, we find that,

$$N\sim\frac{Cr_0^{|j|+|k|+|l|+|m|-2}}{B^{|j|}A^{|k|+|l|+|m|-1}}.$$

Reasonable numerical values would be $A=C=2$ cm, $B=20$ cm, and $r_0=\frac{1}{2}10$ cm.

In Table I the harmful resonances through fourth order are listed. The fourth row of the table gives N, the number of turns necessary to produce a catastrophe (also the sharpness of the required resonance), while the last row gives the value of the magnetic fall-off which would produce that resonance. [It will be noted that resonances where $l\neq 0$ are not listed. These resonances do occur and have been studied but since ω_2 is small compared with ω_0 and since it changes as the electrons acquire energy, they are never dangerous. The resonances leading to values of $n\geq 1$ or $n\leq 0$ have been omitted since for these, the motion is unstable even in first order.]

TABLE I. Harmful resonances.

2nd order		3rd order			4th order			
j	0	0	−1	−1	0	0	−1	−1
k	−1	2	1	3	1	3	4	0
m	2	−2	2	0	−4	−2	0	4
N	50	3000	300	300	170,000	170,000	17,000	17,000
n	0.20	0.50	0.36	0.56	0.06	0.69	0.75	0.25

It is clear from Table I that for a magnetic fall-off of $n=0.56$ to 0.75 the orbits will be stable. The resonance at $n=0.69$ is so sharp as to be innocuous and for orders above the fourth, the resonances will be still sharper.

We therefore conclude that for suitable values of n the racetrack orbits will be stable. The reasoning has been based upon a perturbation treatment. The deviation of the racetrack from the circular synchrotron represents a rather large perturbation and hence the calculated values for N may be somewhat in error. The method is completely adequate, however, for it rigorously predicts all the values of magnetic fall-off for which instabilities may occur. Analogous calculations have been made for other types of periodic azimuthal variations and it is interesting to note that the stability is improved by going to a racetrack with four rather than two straight sections.

[1] For example, see D. M. Dennison and T. H. Berlin, Phys. Rev. (in print).

* The work described in this letter has been supported by the Bureau of Ordnance, U. S. Navy, under contract NOrd-7924.

Elastic Deficiency and Color of Natural Smoky Quartz

CLIFFORD FRONDEL
Department of Mineralogy, Harvard University, Cambridge, Massachusetts
April 25, 1946

IN a recent paper,[1] the writer has drawn attention to the fact that the elastic properties of quartz are altered by exposing the substance to radiation. The effective radiations include electron beams, deuterons, alpha-particles and x-radiation over the region from gamma-rays of radioactive origin up to at least 2.28A. The effect is conveniently investigated by means of peizoelectric quartz oscillator-plates. These offer a coupled electro-mechanical system that is sensitive to minute variations in the density and elasticity of the medium. During the irradiation of a quartz oscillator-plate, the frequency of oscillation decreases according to an exponential law until a saturation value is reached. This value appears to be independent of the type of radiation, but varies by a factor of at least 20 among different specimens of quartz. The quartz concomitantly becomes smoky in color, and the depth of color is proportional to the change in frequency. The several elastic moduli are affected unequally with the C_{14} modulus relatively highly responsive.[2] Baking the irradiated plates at temperatures over *ca.* 180°C or exposing them to short

wave ultraviolet radiation bleaches the color and restores the frequency of the plate to the original value.

It has now been found that natural smoky quartz possesses an elastic deficiency associated with the color analogous to that of artificially colored smoky quartz. When oscillator-plates fashioned from a natural smoky quartz crystal are decolorized by baking, the frequency of oscillation is found to increase, as in artificially irradiated plates, and the increase is proportional to the original depth of color. Natural colorless quartz is not so affected. The effect is small and not easily measured in pale smoky crystals. To cite a specific instance, a number of 8900 Kc BT-cut oscillator-plates were made from a single, black and almost opaque raw quartz crystal. These plates increased in frequency by 1000 cycles when decolorized by baking. Control plates of the same frequency cut from various colorless, water-clear, raw crystals, and identically manufactured by the etch method, changed randomly in frequency, when baked, in amounts up to +50 cycles. This change is believed caused by unloading of films of water. If the smoky plates were irradiated before baking, the color somewhat darkened and the frequency decreased by 800 cycles; and when these plates were baked, they increased in frequency by 1800 cycles. Similarly, the baked and decolorized plates when re-irradiated decreased by 1800 cycles, and this amount of change could be thereafter repeatedly effected upwards and downwards by successive baking and irradiation. The original smoky color is thus equivalent to 1000 cycles of frequency, so to speak; or alternatively the frequency-thickness constant, K, can be said to increase by an amount (0.011 percent) equivalent to 1000 cycles in a 8900-kc plate when the color is bleached out by baking. The absolute value of K in this case and its relation to that of ordinary colorless quartz is not known.

These observations are of interest in connection with the generally held theory of origin of natural smoky quartz, which ascribes the color to natural radiations of radioactive origin.[3] Several points of difference exist, however, between the effects of the artificial and supposed natural irradiation. The natural smoky color does not begin to bleach until about 225°C, as compared to *ca.* 180° for the artificial color. The rate of bleaching at these temperatures is extremely slow, requiring months for completion, but increases rapidly with increasing temperature. Natural smoky quartz also shows a relatively weak thermo-luminescence during heating, but this effect may luminescence during heating, but this effect may not be related to the color[4] or elastic deficiency. It is also observed that natural smoky quartz usually is unevenly pigmented and contains adjoining and often alternating bands of smoky and colorless or nearly colorless material. When such specimens are irradiated, the colorless or relatively light colored bands always are observed to be the more deeply affected, and this is true whether the sample has first been decolorized by baking or not. The natural smoky zones themselves always are further deepened in color by artificial irradiation and hence are not saturated in terms of these radiations. The few specimens measured were from one-half to two-thirds saturated. The depth of color in the darkest colored natural smoky quartz crystals observed, which were jet black and opaque except on thin edges, is only about one-tenth the maximum and one-half the average depth of color, as measured by the associated frequency change in oscillator-plates, observed in artificially irradiated quartz. The effects of the artificial and presumed natural irradiation thus seem to differ in several respects, although the smoky color produced in both instances has an identical absorption spectrum[5] and is associated with an elastic deficiency.

[1] C. Frondel, Am. Min. **30**, 432 (1945).
[2] V. E. Bottom, and V. Nowicki, Long Branch Signal Lab., Eng. Memo. No. 1 (Sept. 1945).
[3] E. F. Holden, Am. Min. **10**, 203 (1925).
[4] S. P. Choong, Proc. Phys. Soc. London **57**, 49 (1945).
[5] N. Mohler, Am. Min. **21**, 258 (1936).

Erratum: Bose-Einstein Condensation of Trapped Electron Pairs. Phase Separation and Superconductivity of Metal-Ammonia Solutions

[Phys. Rev. **69**, 243 (1946)]

RICHARD A. OGG, JR.
Department of Chemistry, Stanford University, California

ON page 244, lines 12 to 14 should read, "but at a concentration small enough to lower the degeneracy temperature to the prevailing temperature."

Proceedings of the Southeastern Section of the American Physical Society

MINUTES OF THE ATLANTA, GEORGIA MEETING ON APRIL 12–13, 1946

THE twelfth annual meeting of the Southeastern Section of the American Physical Society was held in the Atlanta Biltmore Hotel, Emory University, and the Georgia School of Technology, Atlanta, Georgia, on Friday and Saturday, April 12–13, 1946. Approximately 175 members and guests attended. Local arrangements were made by a committee headed by F. E. Lowance.

The regular program consisted of fourteen papers, abstracts for eleven of which are appended hereto. Abstracts of the other papers will be found in the May-June issue of the *American Journal of Physics*.

Additional features of the program were: invited papers, "The Development of Atomic Energy," by F. G. Slack and "The Periodical Literature of Physics—History, Characteristics, and Trends," by Duane Roller; an address, "New Opportunities and New Responsibilities for Scientists," by M. D. Whitaker; and a demonstration-symposium on microwave techniques, by members of the Georgia Tech Physics Department.

At the business meeting the election of the following officers for the Section was announced: Chairman, Rose C. L. Mooney; Vice-Chairman, J. H. Howey; Secretary, Eric Rodgers; Treasurer, C. B. Crowley; and Member of the Executive Committee, E. Scott Barr.

The time and place for the 1947 meeting are to be announced later.

E. SCOTT BARR, *Retiring Secretary*

ABSTRACTS

1. The Kentucky Electrostatic Generator. L. A. PARDUE AND CLYDE B. CRAWLEY, *University of Kentucky.*—A description of the construction and operating characteristics of the Kentucky electrostatic generator is given. The generator is the Van der Graaff pressure type producing a voltage of 300 to 400 kv at atmospheric pressure and about 1.4 mv under several atmospheres of pressure. Provision is made for completely drying the air before admitting it to the tank. A target assembly with magnetic analyzer is a part of the equipment and such auxiliary equipment as cloud chambers, counters, electroscopes, etc. are under construction. The voltages mentioned above are calculated from the deflection of a hydrogen beam in the known magnetic field of the magnetic analyzer.

2. The Geiger Counter as an X-Ray Dosimeter. WALLACE F. FULLER AND A. A. BLESS, *University of Florida.*—The possibility of using a Geiger counter as an x-ray dosimeter has been investigated. The frequency of counts is directly proportional to the *r* output of a tube as measured by a standard *r* meter. The counter will give results reliable to a few percent when used in the verification of the inverse square law, or the laws of absorption. While the accuracy of the counter is not as high as that of FP-54, for example, it is entirely sufficient for the measurements of the dosage in biological experiments and, when properly calibrated, can be used in place of more expensive *r* meters. The sensitivity of the counter is very high. It can measure with fair accuracy weak intensities of scattered radiation of the order of $10^{-5}r$ per minute.

3. New Measurements on the Infra-red Spectrum of $C^{13}O^{16}$ and $C^{13}O^{18}$. R. T. LAGEMANN,* A. H. NIELSEN,† AND F. P. DICKEY,‡ *Mendenhall Laboratory of Physics, The Ohio State University, Columbus, Ohio.*—In repeating the measurements of Whitcomb and Lagemann[1] on the infra-red spectrum of CO, Lagemann,[2] using a 2887 line-per-inch grating, was able to resolve the rotation lines of $C^{13}O^{16}$ as well as those of $C^{12}O^{18}$. As these measurements were not completed, the problem was again undertaken using a 7200 line-per-inch replica grating in the same prism-grating spectrometer. Both the fundamental vibration region at 4.65μ and the first overtone vibration region at 2.35μ are being completely remeasured. Most of the rotation lines of the normal and isotopic CO are well resolved. Combination relations are being applied to this data and new values of the vibrational and rotational constants for these molecules are being computed.

* Emory University, Emory University, Georgia.
† The University of Tennessee, Knoxville, Tennessee.
‡ The Ohio State University, Columbus, Ohio.
[1] S. E. Whitcomb and R. T. Lagemann, Phys. Rev. 55, 181 (1939).
[2] R. T. Lagemann, J. Chem. Phys. 10, 193 (1942).

4. Plasticity *Versus* Elasticity in Stretched Rubber as Indicated by Creep Interference with the Joule Effect. MILTON L. BRAUN, *Catawba College.*—Both rubber and neoprene bands have been stretched with constant loads up to six times their original length, and maintained under these stresses for several years. No deterioration is detectable. Changes in length have been observed as a

function of time and of temperature by a method previously described.[1] The comparatively high gradient of produced temperatures has consistently given rise to normal Joule effects, but for the slower diurnal or seasonal temperature changes the Joule effect has been masked, suppressed, eliminated, or completely reversed by the phenomenon of creep. This masking and reversal of the negative rate of expansion may be interpreted as caused by a plastic property of rubber. With the slowly rising temperature of the approach of each summer, there was a marked elongation whose absolute magnitude is of the same order as that of the usual contracting Joule rate. With seasonal lowering of temperature there was a continuation of the lengthening process, but of somewhat reduced magnitude, a phenomenon usually accounted for by drift or creep, but now considered as caused by a restricted plasticity. This simultaneous presence of both elastic and plastic properties in rubber-like substances is in keeping with the network theory of the structure of rubber as stated by Guth and his fellow workers.

[1] Milton L. Braun, J. App. Phys. 8, 138 (1937).

5. Balancing Sedimentation by Electrophoresis in High Centrifugal Fields. J. W. BEAMS, *University of Virginia.*—The maximum mass "resolving power" of an analytical ultracentrifuge used in the standard rate of sedimentation method for determining molecular weights is very roughly proportional to the maximum strength of the rotor. This limitation can be removed in at least two ways. First, by maintaining the sedimentation boundary under investigation at a constant radius by flowing the solvent from periphery to axis at the same rate as the sedimentation or, second, by balancing the rate of sedimentation with electrophoresis. The first method has been used previously,[1] and in this paper apparatus utilizing the second method is described. The sector-shaped centrifuge cell has crystal quartz windows for optical observations and special electrodes for passing current in an approximately radial direction through the cell. Special precautions were taken to allow as much heat conduction from the cell as possible. Centrifugal fields from 2×10^5 gravity to 2.5×10^5 gravity were used.

[1] Science 543, 89 (1939). Science in Progress 2.

6. Absorptive Effects Relating to Fine Structure in the Angular Distribution of Cosmic-Ray Intensity. D. COOPER, *Georgia School of Technology.**—The results of studies[1-4] of fine structure in the directional intensity of cosmic rays indicate, in terms of Schremp's[2] theoretical analysis, that the observed fine structure arises from range absorption of lines or bands in the energy spectrum of the primary radiation. A study of the detailed shape of the absorption curve for lead has been made with a triple coincidence Geiger counter apparatus.[1] This curve does not provide fine structure that can be correlated with the fine structure in the zenith-angle curves. This apparent discrepancy between experiment and theory may be explained if certain conditions are imposed on the production or decay of the meson component.

* Experimental work done at the University of Missouri, Columbia, Missouri.
[1] D. Cooper, Phys. Rev. 58, 288 (1940).
[2] E. J. Schremp and H. S. Ribner, Rev. Mod. Phys. 11, 149 (1939).
[3] E. J. Schremp and Alfredo Banos, Jr., Phys. Rev. 59, 614(L), (1941).
[4] M. L. Yeater, Phys. Rev. 67, 74 (1945).

7. Ceramic Dielectrics. D. C. SWANSON, *University of Florida.*—A study of the dielectric properties of certain alloys prepared as ceramic dielectrics was carried on by the University of Florida Engineering and Industrial Experiment Station during the war period in connection with the Office of Scientific Research and Development. The materials studied have dielectric constants of several thousand and specific resistances ranging from 10^6 to 10^{13} ohm-cm. These materials show marked change in electrical properties with change in temperature and applied voltage. With proper choice of the alloys almost any desired dielectric behavior can be obtained.

8. Static Direction Finder. H. L. KNOWLES, *University of Florida.*—The Static Direction Finder developed at the Engineering and Industrial Experiment Station at the University of Florida for the Army Signal Corps is described. The apparatus makes use of the conventional crossed loops of the radio direction finder feeding into two identical amplifiers whose outputs energize the vertical and horizontal deflecting plates of a cathode-ray oscillograph. The azimuth of the incoming signal may be determined visually or photographically from the angular orientation of the flash on the face of the scope. The method of determining the position of the storm area by synchronized observations with a three-station network is discussed.

9. Integration of $\sin^2 x\,dx/x$.* SCHUYLER M. CHRISTIAN, *Agnes Scott College.*—A table is being prepared, giving values of the definite integral, $\int_0^x \frac{\sin^2 x}{x}dx$, which is needed in solving some physical problems. Typical values are:

x	Integral
0.5	0.119,906
1.0	0.423,691
2.0	1.052,246
3.	1.218,513
4.	1.267,080
5.	1.462,628
6.	1.555,950
7.	1.573,438
8.	1.683,106
9.	1.748,135
10.	1.764,305
11.	1.833,071

* Read by title.

10. Multi-Element X-Ray Tube for Diffraction Studies.* R. PEPINSKY, *Physics Department, Alabama Polytechnic Institute, Auburn, Alabama.*—Details are given of the

construction and operation of an x-ray tube for crystal diffraction studies, the usual diode being modified by introduction of a simple electron gun and a control grid. Following the technique of Guinier and Devaux,[1] electrostatic focusing is obtained through application of a voltage between the filament and a focusing cylinder, so that the latter is several hundred volts negative with respect to the former. A control grid is inserted within the focusing cylinder, to permit monitoring of tube current as previously described.[2] An auxiliary focusing voltage is applied to a reflecting cup just behind the filament. The target is at high positive potential, and the tube body and focusing cylinder are grounded. Other electrode voltages are introduced by means of the cut-off base of a metal radio tube, soldered onto the cathode structure.[3] The very fine focal spot obtained permits use of a single pinhole near the diffracting specimen, affording considerable saving in tube current. Characteristic curves for the various control and focusing elements are presented.

* Read by title.
[1] A. Guinier and J. Devaux, Comptes rendus **217**, 682 (1943).
[2] R. Pepinsky, Phys. Rev. **67**, 308 (1945).
[3] A. Hemmendinger, Rev. Sci. Inst. **10**, 389 (1939).

11. The Modulus of Elasticity and Column Action as Applied to the Structure of the Giant Reed (*Arundo Donax*). OTTO STUHLMAN, JR., *The University of North Carolina.*— The changes in mass, length, diameter, and modulus of elasticity were determined for the internodes of the reed in ascending order. Changes in growth are correlated with these quantities. Starting at the base, grasses display increases in length, followed by a converging series of decreases in length of the internodes, until the flowering stem is reached. This stem shows a characteristic accelerated growth. The data will show how changes in mass, volume, and modulus of rigidity of the internodes all point to the same locus of the origin of the rate of change in growth, as simulated by the change in linear dimensions of the plant stalk. The structural relations indicate that the locus of the energy supply of the fruit stalk is a prime contributing factor in modifying the growth of the internodes forming the column structure. The modulus of elasticity is about 400,000 pounds per square inch. (White cedar 910,000 lb./sq. in.) Southern industries are probably not aware of the economic value and the strength of this material.